

IntechOpen

Non-woven Fabrics

Edited by Han-Yong Jeon



NON-WOVEN FABRICS

Edited by **Han-Yong Jeon**

Non-woven Fabrics

<http://dx.doi.org/10.5772/60468>

Edited by Han-Yong Jeon

Contributors

Haoyi Li, Weimin Yang, Radostina A. Angelova, Osman Babaarslan, Nazan Kalebek, Nesrin Karaduman, Nedim Erman Bilisik, Kadir Bilisik, Hiroaki Akasaka, Sachiko Inubushi, Tianyuan Wang, Takumi Fukumoto, Yusuke Demizu, Ryohei Sasaki, Izabella Krucinska, Houman Borouchaki, Abel Cherouat, Masoud Haghi Kashani, Abbas Milani, Burçak Karagüzel Kayaoğlu, Sanjoy Debnath, Jean-Yves Drean, Omar Harzallah, Han-Yong Jeon, Bipin Kumar

© The Editor(s) and the Author(s) 2016

The moral rights of the and the author(s) have been asserted.

All rights to the book as a whole are reserved by INTECH. The book as a whole (compilation) cannot be reproduced, distributed or used for commercial or non-commercial purposes without INTECH's written permission.

Enquiries concerning the use of the book should be directed to INTECH rights and permissions department (permissions@intechopen.com).

Violations are liable to prosecution under the governing Copyright Law.



Individual chapters of this publication are distributed under the terms of the Creative Commons Attribution 3.0 Unported License which permits commercial use, distribution and reproduction of the individual chapters, provided the original author(s) and source publication are appropriately acknowledged. If so indicated, certain images may not be included under the Creative Commons license. In such cases users will need to obtain permission from the license holder to reproduce the material. More details and guidelines concerning content reuse and adaptation can be found at <http://www.intechopen.com/copyright-policy.html>.

Notice

Statements and opinions expressed in the chapters are those of the individual contributors and not necessarily those of the editors or publisher. No responsibility is accepted for the accuracy of information contained in the published chapters. The publisher assumes no responsibility for any damage or injury to persons or property arising out of the use of any materials, instructions, methods or ideas contained in the book.

First published in Croatia, 2016 by INTECH d.o.o.

eBook (PDF) Published by IN TECH d.o.o.

Place and year of publication of eBook (PDF): Rijeka, 2019.

IntechOpen is the global imprint of IN TECH d.o.o.

Printed in Croatia

Legal deposit, Croatia: National and University Library in Zagreb

Additional hard and PDF copies can be obtained from orders@intechopen.com

Non-woven Fabrics

Edited by Han-Yong Jeon

p. cm.

ISBN 978-953-51-2271-5

eBook (PDF) ISBN 978-953-51-5773-1

We are IntechOpen, the world's leading publisher of Open Access books Built by scientists, for scientists

3,800+

Open access books available

116,000+

International authors and editors

120M+

Downloads

151

Countries delivered to

Our authors are among the
Top 1%

most cited scientists

12.2%

Contributors from top 500 universities



WEB OF SCIENCE™

Selection of our books indexed in the Book Citation Index
in Web of Science™ Core Collection (BKCI)

Interested in publishing with us?
Contact book.department@intechopen.com

Numbers displayed above are based on latest data collected.
For more information visit www.intechopen.com



Meet the editor



Han-Yong Jeon is a Professor of geosyntheics and technical organic materials. He achieved Ph.D. from the Hanyang University, Korea (1989). As a professor, he has worked since 1982 and now works for the Inha University, Korea (South). He worked in the International Geosynthetic Society as Council member (2006-2012) and he was the 6th president of the Korean Geosynthetic Society (2011–2013). Also, he was the 32nd President of the Korean Fiber Society (2014-2015). He has published more than 782 papers in domestic and international conferences. He wrote 18 textbooks including “Geosynthetic” and also published 118 papers in domestic and international journals. He has awards of Marquis Who’s Who - Science and Engineering in 2003-2015 and Top 100 Scientists in the World: 2005/2011 of IBC (International Biographical Centre, UK).

Contents

Preface XI

- Chapter 1 **Fiber Selection for the Production of Nonwovens 1**
Nazan Avcioglu Kalebek and Osman Babaarslan
- Chapter 2 **Electrospinning Technology in Non-Woven Fabric Manufacturing 33**
Haoyi Li and Weimin Yang
- Chapter 3 **Variance Analysis and Autocorrelation Function for 2D Fiber Lap Statistical Analysis 55**
Jean-Yves Drean and Omar Harzallah
- Chapter 4 **3D Fabrics for Technical Textile Applications 81**
Kadir Bilisik, Nesrin Sahbaz Karaduman and Nedim Erman Bilisik
- Chapter 5 **Geometrical Draping of Nonwoven Fabrics 143**
Abel Cherouat and Houman Borouchaki
- Chapter 6 **Nonwoven Padding for Compression Management 163**
Bipin Kumar
- Chapter 7 **Non-Woven Textiles in the Indoor Environment 187**
Radostina A. Angelova
- Chapter 8 **Medical Application of Nonwoven Fabrics - Intra-abdominal Spacers for Particle Therapy 205**
Ryohei Sasaki, Hiroaki Akasaka, Yusuke Demizu, Sachiko Inubushi, Tianyuan Wang and Takumi Fukumoto
- Chapter 9 **Plasma Surface Treatments of Nonwovens 215**
Burçak Karagüzel Kayaoğlu

- Chapter 10 **Damage Prediction in Woven and Non-woven Fabric Composites 233**
Masoud Haghi Kashani and Abbas S. Milani
- Chapter 11 **Technologies Involved in the Manufacture of Smart Nonwoven Fabrics 263**
Izabella Krucińska, Ewa Skrzetuska, Beata Surma and Eulalia Gliścińska
- Chapter 12 **Design, Development, Characterization, and Application of Jute-based Needle-Punched Nonwoven 277**
Sanjoy Debnath
- Chapter 13 **Nanotechnology Formulations and Modeling of Hydraulic Permeability Improvement for Nonwoven Geotextiles 297**
Han-Yong Jeon

Preface

Non-woven fabrics are known as the best-characterized embedded materials which can be applied to manufacture the composites in the convergent industry field and manufacturing process is highly specified and differentiated with raw fibers, manufacturing process, characteristics and performance evaluation, end-use etc.

Especially, application range of non-woven fabrics is extended to all the industrial fields needless to say apparel, such as ICT (information and communication technology), bio- and medicals, automobiles, architectures, construction and environmental. This is due to the various and special manufacturing technology of non-woven fabrics to adopt diversified fiber selection and grafting of high-convergence technology.

For outlook of non-woven fabrics, it is possible that cultural-creative consumers think before and after the “point of consumption” if LOHAS (Lifestyles of Health And Sustainability) is linked to eco-environmental concept and design. Non-woven fabrics with thin film can be applied to make the hybrid and convergence products which have a functionalized and tailor-made performance for biomimetics application. Besides this, non-woven fabrics can take charge of a green climate environmental constitution that can be practicable to control micro mechanism and establishment of nature circulation system, including pollution-purification-recollection process by using nanofibers.

In this text, overall stream from raw fibers to final products is included to features of manufacturing and finish process with specialized application end use. Every chapter is related to the important and convergent fields with the technical application purpose from downstream to upstream fields. Also, applicability of non-woven fabrics is introduced to be based on the structural analysis of dimensional concept and various non-woven fabrics as a state-of-art embedded convergent material are emphasized in all industry fields by using nanofibers and carbon fibers.

Finally, we expect the meaningful role of this text as a part of convergence materials and sincerely thank to all authors who wrote the precious manuscripts. Also, we deeply appreciate the effort of Publishing Process Manager Ms. Sandra Bakic and to whom it may concern in the InTech.

Professor Han-Yong Jeon
GeoSynthetics Research Laboratory (GSRL),
Technical Organic Materials Research Laboratory (TOMRL),
Department of Applied Organic Materials Engineering,
Inha University,
South Korea

Fiber Selection for the Production of Nonwovens

Nazan Avcioglu Kalebek and Osman Babaarslan

Additional information is available at the end of the chapter

<http://dx.doi.org/10.5772/61977>

Abstract

The most significant feature of nonwoven fabric is made directly from fibers in a continuous production line. While manufacturing nonwovens, some conventional textile operations, such as carding, drawing, roving, spinning, weaving or knitting, are partially or completely eliminated. For this reason the choice of fiber is very important for nonwoven manufacturers. The commonly used fibers include natural fibers (cotton, jute, flax, wool), synthetic fibers (polyester (PES), polypropylene (PP), polyamide, rayon), special fibers (glass, carbon, nanofiber, bi-component, superabsorbent fibers). Raw materials have not only delivered significant product improvements but also benefited people using these products by providing hygiene and comfort.

Keywords: Fiber, natural fibers, synthetic fibers, nonwoven fabrics, polypropylene (PP)

1. Introduction

The term “nonwoven” became popular more than half a century ago when nonwovens were regarded as low-price substitutes for traditional textiles. However, today, the nonwoven fabric technology is the most modern method used in the branch of textile industry. Nonwoven technology exists to approximate the appearance, texture, and strength of conventional woven and knitted fabrics due to their simple production stages, high efficiency of production, lower cost, and disposability. Multi-layer nonwoven composites, laminates, and three-dimensional nonwoven fabrics are commercially produced. Nonwovens combined with other materials have different chemical and physical properties. Therefore, nonwovens can be used a wide variety of industrial engineering, consumer, and health-care goods [1-7].

Among the textiles applications, nonwovens are one of the fastest-growing segments of the textile industry and constitute roughly one third of the fiber industry. The latest estimates, taking into account the official INDA (Association of Nonwoven Fabrics Industry) figure 1

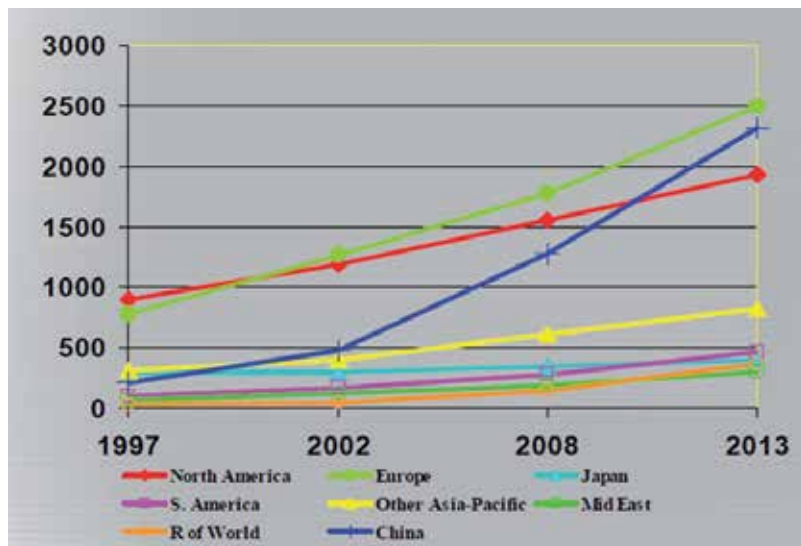


Figure 1. World Nonwoven Production by Region [8]

(Figure 1), put the global nonwovens production at over 1,500,000 tons in North America, over 2,000,000 tons in China, and around 2,500,000 tons in Europe.

2. Fibrous materials

Nonwovens have three key features and are as follows:

- The fabrics are composed of textile fibers.
- The basic structural element of textile fabrics is fibers, rather than yarns or threads.
- The fabrics are held together by means other than the interlacing or interloping characterizing traditional woven or knit fabrics [1].

While manufacturing nonwovens some conventional textile operations, such as carding, drawing, roving, spinning, weaving, or knitting, are partially or completely eliminated. For this reason, the choice of fiber is directly related to fabric quality [1-6, 8-11].

All kinds of fibers can be used to produce nonwoven fabrics. The selection of fibers is based on the following features[1,6]:

- the cost-effectiveness,
- the ease of processability, and
- the desired end-use properties of the web.

The commonly used fibers include natural fibers (cotton, jute, flax, wool), synthetic fibers (polyester (PES), polypropylene (PP), polyamide, rayon), special fibers (glass, carbon, nano-fibers, bicomponent, superabsorbent fibers), etc [1,6,8-10,12-15,16].

Two or more types of fibers are typically utilized. The fibers are usually blended or mixed in order to improve performance properties of nonwovens, such as strength and other properties. The fiber blend or mix can be natural/natural, synthetic/synthetic, or natural/synthetic [6,8-10].

Man-made fibers are the most widely used in the nonwoven industry. Owing to impurities and higher costs, natural fibers are of minor importance for the production of nonwovens.

Fiber characteristics influence not only nonwoven fabric properties but also processing performance. Web cohesion, fiber breakage, and web weight uniformity are the key quality parameters and are influenced by fiber diameter, fiber length, fiber tensile properties, fiber finish, and crimp. The properties of nonwoven fabrics are largely dependent on fiber properties and fabric structural geometry.

2.1. Natural fibers

2.1.1. Cotton

Cotton is the most important vegetable fiber used to produce nonwoven bonded fabrics. The oldest textiles made from cotton originated around 5800 B.C. At present, cotton is cultivated in about 75 countries on 79 million acres of land, which represents about 0.8 % of all agricultural areas worldwide. Cotton plants grow in shrub-or tree-like forms to heights o from 25 cm to 2 m, depending on origin, soil, climate, and cultivation conditions. It grows fruit the size of walnuts which contain seeds that burst open and the cotton swells out in thick white flocks. The process of sowing to harvesting takes 175-225 days. Hand picking is advantageous compared to machine picking, as only fibers from completely mature capsules are being collected. After the harvest, the seeded cotton is ginned. Among the plant-derived fibers, cotton has the highest percentage of cellulose and is free of wooden particulates [1-4,6].

Raw cotton contains the following substances:

- cellulose (80-90%),
- water (6-8%),
- hemicellulose and pectin (4-6%),
- ash (1-10%),
- waxes and fats (0.5-1.0%), and
- proteins (0-1.5%) [6].

The quality of cotton depends on the following parameters:

- length of fiber (10-60 mm),
- fineness of fiber (1.0-4 dtex),

- linear density (1.50-1.54 g/cm³),
- color,
- maturity degree (75-85%),
- purity (trash and dust),
- tensile strength (25-50 cN/tex),
- elongation (7-10%),
- moisture absorption (7-8%), and
- moisture regain (7.1-8.5 %).

Cotton, as a natural cellulosic fiber, has many characteristics, such as:

- comfortable,
- good absorbency,
- good color retention,
- well printable,
- machine-washable,
- dry-cleanable,
- good strength,
- well drapeable and
- easy to handle and sew.

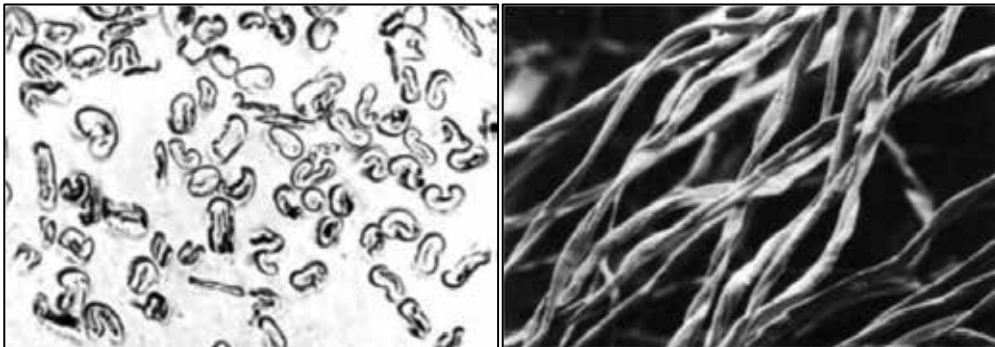


Figure 2. Microscopic View of Cotton Fiber [6]

Figure 2 shows a vertical view, revealing the convolutions typical for a cotton fiber and the cross section of cotton fibers. Cotton's shape and structure make it suitable for the production of nonwoven bonded fabric: cotton has a ribbon-shaped cross-sectional form, spiral twist, a

hollow structure, a high wet strength for a hollow structure, a high wet strength for a high module, and it is hygroscopic.

Cotton fiber was used extensively during the early development period of nonwoven business. Cotton mills in USA tried to find ways to upgrade the waste cotton fibers into saleable products. The first method was bonding the short cotton fibers with latex and resin. These products were used in industrial wipes. Over the past decade, bleached cotton fiber has been used for producing fabrics on conventional nonwoven equipment. These products were used in medical and health-care applications, wiping and wiper markets, and some apparel markets. At the same time, cotton fiber has physical properties like fiber length, strength, and resilience, which is important particularly to its process-ability. For example, long cotton fiber is suitable for producing nonwovens. The fiber has excellent absorbency and feels comfortable for the skin. The wet and dry strengths are good. Dimensional stability and resilience recovery are moderate. The spunlace process is usually utilized in producing medical and health-care fabrics, especially in Japan and the Asian region [14].

2.1.2. *Jute*

After cotton, jute is the natural fiber with the second highest production volume. Chemically, the jute is a highly lignified fiber, which consists of [6,9,11] the following:

- cellulose (60%),
- hemicellulose (26%),
- lignin (11%),
- proteins (1%),
- waxes and fats (1%), and
- ash (1%).

Producing of a compound with the substances cellulose and bastose is differ from bast fibers. Jute is a significant fiber for special applications of nonwoven bonded fabrics. It is mostly used because of its inexpensiveness and good physical properties:

- floor coverings in basic materials,
- base and intermediate layer of tufted floor coverings, and
- upholstery filling pieces.

2.1.3. *Flax*

Flax is the one of the oldest cultivated plants with a cultural importance dating to prehistorical periods. Linseed was first found in the former Mesopotamia. Fragments, linseed, and capsules are estimated to be from the eighth millennium. Flax was discovered during the excavation of Ali Kosh in Iran. In old Egyptian graves and seaside settlements in Switzerland, linen fabrics and mummification bandages were found. They originated around 5000-3000 B.C. The oldest fabric fragment found to date is from a settlement in ancient Egypt [9,11,16].

Flax belongs to the family Linaceae, and the type considered here is from the genus *Linum*. There are wild-growing, small herbaceous perennials and cultivated annual flax plants. Flax is cultivated worldwide in tropical and cold climate zones. Fiber flax grows in humid, moderate climates, whereas oil flax grows in dry, warm areas. The harvest reaps approximately 4000 kg/ha. The fibers are embedded in the parenchyma of the stem in a high concentration and are freed by retting. Then the flax is washed, dried, and broken to loosen the brittle wood from the bast and to separate the fibers from each other. The wooden parts are removed by means of scotches [6]. Finally, the fibers are combed by means of hackles. The properties of technical fibers and single fibers have to be distinguished. The technical fiber is 200-800 mm in length and composed of a fiber bundle. It has a fineness of about 10-40 dtex. The single fiber has a length of 7-42 mm depending on its location in the stem, its diameter is about 15-37 μm , and the density lies between 1.43 (raw) and 1.52 g/cm^3 (bleached). The maturity of the fiber is determined by harvesting time. Good fiber profit with good fiber quality may be obtained at the time of yellow maturity. The relative strength fluctuates between 30 and 55 cN/tex. For all these properties, flax fiber is used for nonwoven bonded fabrics, mostly for the fabrication of filling pieces [11,16].

2.1.4. Wool

Wool is the most important animal fiber used in manufacturing nonwoven bonded fabrics. It is used mainly as reclaimed wool or cuttings because of its high price. The variation in quality and the impurities in reclaimed wool as well as the chemical and physical properties determined by its provenance impose restrictions on its use [17].

Wool is a suitably stiff and permanently crimped bi-component fiber. The distinct variations in thickness are in most cases favorable to produce nonwovens [16]. Wool fiber is initially used to make felt. The wool fibers are then pressed into a flat sheet and subjected to moisture, heat, and agitation. The scaly structure of the wool fiber causes the fibers to interlock and mat. Weaving or knitting in the production of such felts and simple mechanical interlocking of fibers in the production of such felts and simple mechanical interlocking of fibers in a batt structure is capable of producing a dimensional stable fabrics with densities, up to 0.7 g/cm^3 . Animal felts have been used since ancient times. Traditional felting method is still used for producing clothing item such as hats, slippers, interlinings and handbags. In addition to traditional felting method, modern pressed felting techniques are used in a wide range of industrial applications. These products are used for polishing metals, optical surfaces plastics, and jewelry, and in manufacturing seals, gaskets, washers, felt nibs and markers, air and liquid filters, oil wicks, piano cushion felts, shoes, toys, pennants, table covers, notice boards, bookbinding, furniture components and orthopedic appliances. [11,18,19].

Wool is not only used for producing felts but also used for producing needle-punched, hydroentangled, thermally and chemically bonded fabrics. In recent years, the production of serviceable, lightweight wool fabrics of 70-150 g/m^2 for apparel applications using a process known as hydroentanglement has been commercialized. Man-made fibers such as polyester, polypropylene, viscose rayon, and blends containing cotton, wood pulp, and other fibers can

be used for producing hydroentangled bonded fabrics in the medical and hygiene industries. However, in recent years, wool is used hydroentanglement process [20].

For example, while producing hydroentangled fabrics, at firstly the web is transported by a porous belt or a drum is passed below a series of injector heads (typically 6-8 heads in total depending on requirements), which produce single or multiple rows of closely spaced, fine columnar water jets of about 60-140 μm diameter as required. Commercially, these jets operate at pressures of about 25-250 bar, although much higher pressures up to 1000 bar are now possible depending on the machine design. The jet pressures used depend on web weight line speed and fiber properties, and normally, the pressure is profiled so that it tends to increase as the web passed toward the machine exit. Usually, the web is treated face and back to achieve a homogeneously bonded structure, although single-sided treatments are possible using lightweight webs [20]. At each injector, suction is applied from below to remove excess water from the surface of the conveyor. The design and surface structure of the conveyor belt influence the resulting fabric structure. Bonded fabric is taken away from the belt and is dried, wound, and slit according to the required width. Chemical and thermal bonding can be done before and after drying. While producing nonwoven fabrics by the hydroentanglement method, a large volume of water is used. Water has to be recirculated and filtered to remove particulates before entering to the injectors. Recirculation and filtration account for a considerable part of the total cost of a hydroentanglement facility [20].

2.2. Man-made fibers

2.2.1. Polyester

As its name indicates, this type of fiber consists of macromolecules of esters which are chemicals made of acids and alcohol (Figure 3). If many of these basic molecules are combined, they will form polyesters [6].

The earliest study on polyester was conducted by W.H. Carothers at DuPont in the early 1930s, which is comparable to the present-day studies on condensation polymers. Even though a great number of polyesters have been evaluated by now, only a few of them are around that can create good fibers and are crystalline with a melting point between 220 and 280°C, and only three of them gained significance in fiber production [21,22].

Physical properties of polyester fibers are important while producing nonwoven materials. For example, the lengths of cut are adapted to the respective manufacturing procedure. Fibers are also available in different of luster and cross-sectional forms (Figure 4).

They are inexpensive, easily produced from petrochemical sources, and have a desirable range of physical properties. They are strong, lightweight, easily dyeable and wrinkle resistant, and have very good wash wear properties. Therefore, it is mostly used in nonwoven production. Cross-sectional polyester fibers are used in the following three major areas [14]:

- Apparel: Every form of clothing;

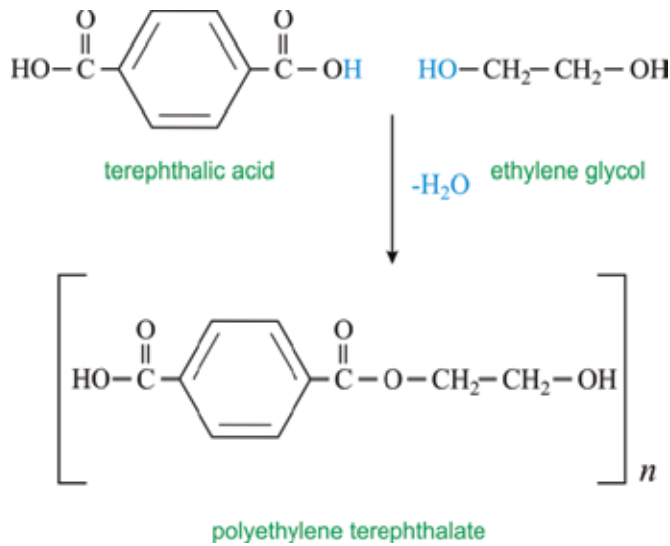


Figure 3. Polyester Fibers [6]

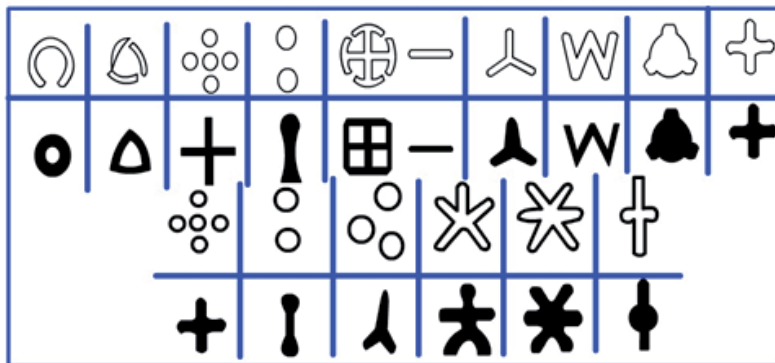


Figure 4. Cross-sectional View of Polyester Fibers [23]

- Home Furnishings: Carpets, curtains, draperies, sheets and pillowcases, wall coverings, and upholstery; and
- Other Uses: Hoses, power belting, ropes and nets, threads, tire cords, auto upholstery, sails, floppy disk liners, and fiberfill for various products including pillows and furniture.

Surgeons' gowns, for example, were once woven from linen but are now for the most part made from repellent-treated entangled polyester fiber pulp composites on spun-bond melt-blown laminates. These new gowns are far superior to the older material in providing a breathable barrier between the surgeon and the patient, which serves to significantly reduce hospital infections. Spun-lace mattress pad facing (100% polyester) continues to be the replacement for spun-bonded material because of the textile-like character of entangled fiber fabrics. Polyeth-

lene terephthalate (PET) has become the most important polymer type of fibrous prostheses. It is reasonably inert, biocompatible, flexible, and resilient and has an appropriate level of tissue acceptance. However, polymerization initiators, antioxidants, titanium dioxide, and other impurities should be minimized to improve its biocompatibility [14].

Polyester is less flammable than cellulosic fibers because it melts while coming in contact with the flame. Crystar, a DuPont trade name, is used to produce as a polyester spunbonded fabrics [14].

Among the bi-component fibers, polyester is the most used fiber. Because of its increasing strength and soft hand of the nonwoven fabric, polyester is used in continuous bi-component filaments having a sheath component made of linear low-density polyethylene (PE) and a core component made of polyester. The tensile strength of the fabrics is improved remarkably by the bi-component filaments and depends on the linear low-density polyethylene /polyester ratio. The ultrasonically bonded polyester/polypropylene blend like Matarh's Ultraskin, the protective clothing, is said to protect wearers from rain while offering the breathability needed to provide comfort [24].

Most of the insulation and industrial products are manufactured from synthetic and inorganic fibers by dry- and wet-laid methods. Nonwoven polyester fiber mats are used to produce electrical insulation laminates and electrical tape backing appliances. Polyester and high-temperature-resistant m-aramid nonwoven mats are used as a cost-efficient interchange for aramid paper for insulation composites [25].

Polyester fiber composites are widely used as filtration media. The layers of composite structure give excellent tear strength, a smooth, fiber-free surface, and edge stability. These products supply higher filtration efficiencies than calendared spun-bonded media [26].

Polyester fibers are used inside seat cushions, back pillows, mattresses and waterbeds, decorative and throw pillows, outdoors furniture, and even hand-stuffed custom upholstery in fiberfill applications [27].

2.2.2. Polypropylene

The fibers from polypropylene were introduced to the textile arena in the 1970's and have become an important member of the rapidly growing family of synthetic fibers.

Polypropylene is generally available as chips or granules which are white in color and are semicrystalline. Polypropylene fibers are produced by a larger variety of processes than any other melt-spun fibers. The general physical properties of polypropylene fibers are shown in Table 1.

Polypropylene has established itself as a very useful industrial and household fiber. However, it has not made a very significant impact in the apparel sector mainly due to its hydrophobicity, lack of dyeability and slightly waxy handle. Polypropylene nonwovens are increasingly being used as filter fabrics for wet filtration in the chemical and pharmaceutical industries. Industrial applications also include medical and surgical disposables [14,28].

Moisture Regain (%)	<0.1
Refractive Index	1.49
Thermal Conductivity (Btu-in/ft.hr.°F)	0.95
Coefficient of Linear Thermal Expansion (°F)	4.0×10^{-5}
Heat of Fusion (cal/g)	21
Specific Heat (cal/g.c)	0.46
Heat of Combustion (Btu/lb)	19400
Oxygen Index	17.4
Decomposition Temperature Range (°C)	328-410
Dissipation Factor (0.1 MHz)	<0.0002
Dielectric Constant (0.1 MHz)	2.25
Specific Volume Resistivity (Ω Cm)	$>10^{16}$

Table 1. Polypropylene physical properties [14]

Advantages of PP fibers for nonwoven fabrics are [12,14] as follows:

- surface smoothness and hardness,
- resistance to micro-organisms,
- chemical resistance,
- inherent hydrophobicity that can be modified using fiber finishes and other treatments,
- high tenacity,
- high shrinkage,
- low melting point leading to significant energy conservation,
- low density and specific gravity enabling lightweight fabrics to be produced,
- good abrasion resistance,
- good resilience,
- good bulk and cover, and
- good stain and soil release.

Disadvantages of polypropylene fibers [14] are as follows:

- difficult to dye after manufacturing,
- high crystallinity and poor thermal conductivity,
- poor UV and thermal stability (requires expensive UV stabilizers and antioxidants to overcome this problem,

- poor resilience compared to PET and nylon,
- poor adhesion to glues and latex, and
- Flammable and melts and burns like wax.

There are only half-dozen manufacturers of polyester spunbonded fabrics in the world, and the bulk of such fabrics are made from both isotactic polypropylene polymers. This is due to the cost and ease of procedure of polypropylene. Polypropylene spunbonded fabrics are used in a variety of end uses, which include absorbent product coverstock markets, home furnishing and automotive markets because of lowest cost, and in low polypropylene non-woven fabric applications [29].

Polypropylene is also used extensively in sheath-core configuration to take advantage of the lower melting point of the former in thermally bonded spunbonds; the polypropylene core fiber retains its fibrous character and excellent physical properties. Even though there is only a very small window of temperature at which polypropylene will melt for bonding purposes, the fabrics made in this manner do not suffer any appreciable loss of fiber properties [29].

2.2.3. Polyamide

Synthetic man-made fibers account for the largest part of the raw material used in manufacturing nonwoven bonded fabrics. Polyamide fibers are the oldest ones that are used in production, and they also increase the serviceability of the product. This improved quality is of importance for various purposes (see Ref. [17]):

- where nonwoven bonded fabrics are subjected to frequent folding as in the case of paper reinforced with synthetic fibers, and
- where they are subjected to exceptional resistance to abrasion, as is the case with needled floor coverings.

The pioneering work of Wallace Carothers of the DuPont Company in the USA led to the discovery of nylon 66 in the 1930s. This polymer was melt-spun to give to the world the first synthetic fiber. The fiber was introduced commercially by DuPont in 1939 using a patent of W.H. Carothers granted in 1938. The success of nylon 66 led to the vigorous growth of the synthetic fiber industry. Subsequently, Paul Schlack in Germany discovered nylon 6, which was produced through another method, in 1939. Both these fibers now occupy an important place among the commodity fibers and have had a far-reaching impact on the international fiber front [30].

Only a few of the many known polyamides have reached large-scale significance for production. Only polyamide 6 (PA6) and polyamide 6.6 (PA66) came to large-scale production. Polyamide 6 is known as perlon and polyamide 6.6, which is generally called nylon to distinguish it from perlon. The numbers after the word "polyamide" indicate the number of carbon atoms in each molecule that make up the polyamide [17]. The structural units of a polyamide are combined by an amide (-NH-CO-) group. A polyamide manufactured from aliphatic monomer(s) is commonly designated as nylon. However, the US Federal Trade

Commission has defined nylon as a manufactured fiber where the fiber-forming substance is a long-chain synthetic polyamide in which less than 85 % of a amide linkages are attached directly to two aromatic rings, while a polyamide in which at least 85 % of the amide links are attached to two aromatic groups is known as an aramid [30].

Polyamide Fibers	Maximum Tensile Strength (cN/tex)	Maximum Elongation (%)	Relative Wet Strength (%)	Water Retention Value (WRV) (%)	Water Content at 20 °C and 65 % Rel.Humidity (%)
1.6 dtex/40 mm bright	50-60	45-55	80-90	10-15	4
3.0 dtex/40 mm semi-dull	45-55	50-60	80-90	10-15	4
17 dtex/ 80 mm semi-dull	40-50	65-75	80-90	10-15	4
22 dtex/80 mm semi-dull	40-50	55-65	80-90	10-15	4
35 dtex/100 mm bright prof	30-40	70-80	80-90	10-15	4

*Fibre does not have the usual round crosssection

Table 2. Typical values for normal polyamide fiber properties [6]

The most important values for the physical properties of normal spun polyamide fibers are listed in Table 2, which covers various fiber thickness, degrees of luster and cross-sectional forms. The term “normal” is of great importance for nonwoven bonded fabrics, because:

- co-polyamide fibers can also be used;
- the filaments used in spun-laid methods are produced under different conditions than the textile or technical man-made methods with regard to their production conditions;
- very strong and excellent tear strength fibers are not used in nonwoven bonded fabrics, whereas they are used in tarpaulins, conveyor belts, and tires,
- fibers which react differently when dyed can be used together, for example, in needle floor coverings;
- nylon fibers are used as nonwovens separators in Ni/H and Ni/Cd batteries;
- these fibers find application in high-performance wipes, synthetic suede, heat insulators, battery separators and specialty papers [14];
- fibers have excellent physical properties like polyester fiber, and it has a high melting point, which conveys good high-temperature performance [14];

- these fibers are more water sensitive than polyester despite the fact that nylon is not considered a comfortable fiber in contact with the skin;
- its toughness makes it a major fiber of choice in carpets, including needle-punched floor covering products. Because it is more expensive than polyester, polypropylene, or rayon, nylon has somewhat limited use in nonwoven products; and
- the resiliency and wrinkle recovery performance of a nonwoven produced from nylon are not as good as that from PET fiber [14].

2.2.4. Rayon

Rayon, which is one of the oldest manufactured fibers, is a regenerated cellulose fiber with a wide spectrum of properties. Historically, rayon faced a strong challenge from synthetic fibers like nylon, polyester, and acrylics, which came much later, but in spite of this competition, it has retained its place as a major textile fiber. The important considerations in favor of rayon are that the essential raw material for its production, namely cellulose, is abundantly available and a renewable source. Moreover, its hydroscopicity and easy dyeability characteristics are additional assets. Furthermore, rayon fibers can be produced with a wide range of properties, particularly mechanical properties, so far unmatched by any other fiber, natural or manufactured [31].

Dissolved cellulose method was first explored at the end of the 19th century. The first fibers were produced by dissolved cellulose in cuprammonium hydroxide solvent and tiny orifices were dissolved into a bath containing reagents. Regenerated filaments form cellulose and break tiny orifices into a reagent bath to remove solvent [31].

Some of the advantages of rayon fibers based on their properties are as follows:

- It is bulky to handle and create bulky fabrics.
- A flame-retardant compound may be mixed with viscous solution prior to spinning or after producing web as coating.
- It has high absorbency and purity. These properties make rayon fiber to produce surgical dressing, sanitary protection, swabs, tampons, and disposable nonwovens [11]. Disposable nonwovens are designed to be discarded after a single use or, sometimes, after a few uses. Examples of disposable nonwovens include medical garments, filters, tea-bag, covers, and disposable diapers.
- It is highly absorbent; that is, it is being produced in order to obtain higher water capacity. These fibers are used in surgical nonwovens.
- It is easy to dye.
- It is a soft material and comfortable to wear and thus used in making bedspreads, blankets, curtains, tablecloths, blouses, dresses, jackets, etc.

2.3. Other fibers

2.3.1. Glass

Glass fiber is an inorganic nonmetallic man-made fiber. Generally, the glass is defined as the frozen state of a supercooled and thus solidified liquid. It results from the suppression of the crystallization of melt. Initial materials for producing glass are different mineral substances largely found in nature (quartz sand, chalk, dolomite, feldspar, and others).

Glass fibers are produced from different compositions (%) of glass (Table 3).

Silica (SiO ₂)	54.0-56.0
Alumina (Al ₂ O ₃)	12.0-14.5
Boron anhydride(B ₂ O ₃)	5.0-10.0
Calcium oxide (CaO)	15.5-16.5
Magnesium oxide (MgO)	4.0-4.2
Sodium oxide (Na ₂ O)	0.7-1.0
Iron oxide (Fe ₂ O ₃)	Up to 0.3

Table 3. Glass fiber composition

Nonwovens of glass fibers are classified as follows:

- A-glass: close to window glass with regard to its composition.
- C-glass: shows better resistance to chemical impact.
- E-glass: combines the characteristics of C-glass with very good insulation to electricity.
- AE-glass: alkali resistant glass [6].

In general, textile glass fibers have a high tenacity at a low elongation combined with extremely low density. This results in favorable tenacity or modulus values relative to their weight. Glass fiber is brittle, but in drawing very thin fibers (with a diameter of several micron) from molten glass, a fibrous material is obtained, having a flexibility sufficient for textile processing and utilization as a finished product.

Glass fiber mats are excellent heat and noise insulation materials. They are capable of withstanding temperatures above 150°C. Textile glass as a mineral material is naturally inflammable and does not release steam or poisonous gases when subjected to heat.

Glass fabrics are highly efficacious for filtering various liquids; filters of glass fibers used for filtering corrosive chemical reagents have a life 10 or 15 times longer than those made of usual materials (cotton, metal web etc). Glass staple fibers are used for the reinforcement of plastics and building materials for insulation and so forth [32].

2.3.2. Carbon

Although first produced for electric lamp filaments from cupro-cellulose by Pauly, Fremery, Bromert and Urban at Oberbruch near Aachen, Germany, in 1898, carbon fibers only gained significance after 1963. In recent years, carbon fibers have found much attention. They are made by means of thermal degradation of viscose fibers or polyacrylonitrile fibers at temperatures up to 1000°C or even 1500°C. The fibers contain between 95 and 98 % carbon. Additional thermal treatment of the pyrolyzed polyacrylonitrile fibers at temperatures between 2000 and 3000°C converts them into graphite, which shows an excellent grid-like structure, where carbon contents amount to 99% [6].

Among the exceptional properties of carbon fibers are their high tenacity, high modulus of elasticity, high brittleness, low creeping tendency, chemically inert behavior, low heat-expansion, and good electrical conductivity. Using their unique properties, the application of carbon fiber is most pronounced in the superfiber category. The high modulus of carbon fibers makes them best suitable for application in composite materials used in high- performance functions. Carbon fiber is not used on its own, but mixed with resin as fiber reinforced materials. This is called a composite material and is now one of the most important structural and heat-resistant materials. The composite material made of glass fiber and plastic is distinguished as glass fiber-reinforced plastics (G-FRP) from that made of carbon fiber and plastic (carbon fiber-reinforced plastic, C-FRB) [14,33].

Such composites are mainly used in:

- aircraft cabin structural materials, such as floor, other internal sections and operations systems;
- aircraft: vertical tail, tail cone, main wing, floor beams, floor panels, composite material for cockpit, and body;
- wind power generations;
- ski-poles;
- natural gas storage tank;
- fishing rod;
- golf shafts; and
- tennis racket [15,21].

In recent years, some new applications of carbon fibers have been found, such as rehabilitation of a bridge in building and construction industry. Others include decoration in automotive, marine, general aviation interiors, general entertainment and musical instruments and after market transportation products. Conductivity in electronics technology provides additional new application [34].

2.3.3. Nanofiber

In fiber diameter, the range from 0.1 to 1 nm is of angstrom size, that from 1 to 10 nm is of nano size, that from 100 to 1000 nm is of sub-micron size, and that from 1000 to 10 000 nm is of micron size. Fibers with an angstrom size diameter are effectively the molecular chain. Nanometer size and sub-micron size fibers can be classed as nanofiber. A micron-size fiber is called a micro-fiber. Fibers with a diameter more than a few micrometers are the conventional fibers, including those with millimeter, centimeter, or meter-order diameter [35].

The nonwoven industry generally considers nanofibers as having a diameter of less than $1\mu\text{m}$, although the National Science Foundation (NSF) defines nanofibers as having at least one dimension of 100 nm or less. The name derives from the nanometer, a scientific measurement unit representing a billionth of an ammeter, or there to four atoms wide.

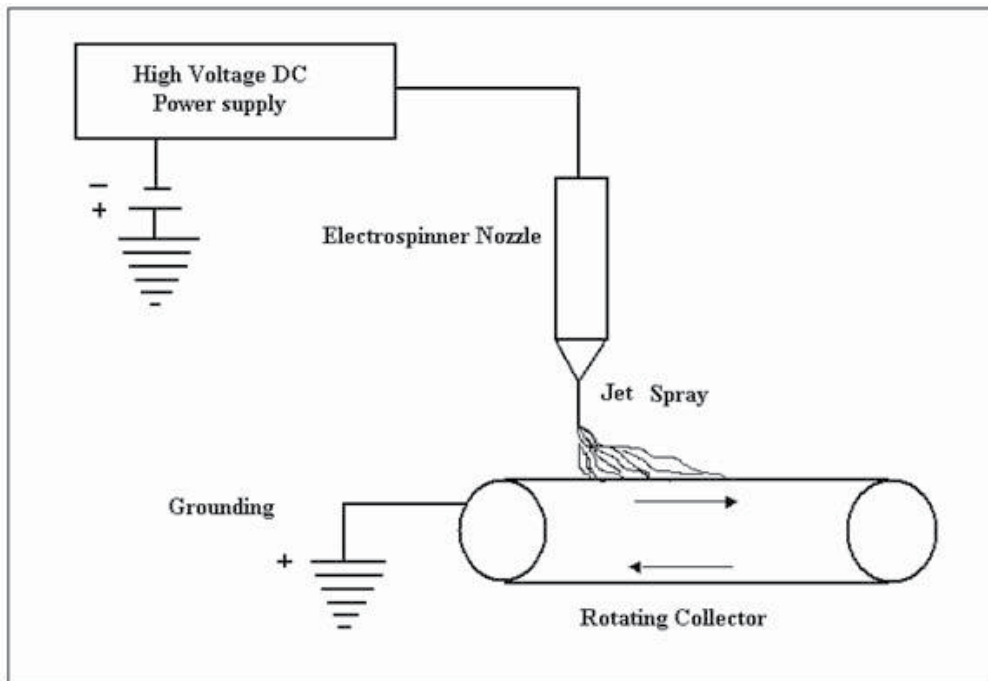


Figure 5. Schematic Diagram of Electrospinning Process [14]

Generally, polymeric nanofibers are produced by an electrospinning process. A schematic diagram of electrospinning is shown in Figure 5. Electrospinning is a process that spins fibers of diameter ranging from 10 nm to several hundred nanometers. This method has been known since 1934 when the first patent on electrospinning was filed. The process makes use of electrostatic and mechanical forces to spin fibers from the tip of affine orifice or spinneret. The spinneret is maintained at positive or negative charge by a DC power supply. When electrostatic repelling force overcomes the surface tension force of the polymer solution, the liquid

spills out of the spinneret and forms an extremely fine continuous filament. These filaments are collected onto a rotating or stationary collector with an electrode beneath the opposite charge to that of the spinneret where they accumulate and bond to form a nanofiber fabric [36].

In this method, polymer and solvents are used. Nanofibers in the range of 10-2000 nm diameter can be achieved by choosing the appropriate polymer solvent system. Table 4 gives a list of some of the polymer solvent systems used in electrospinning [14,37].

Polymer	Solvent
Nylon 6 and nylon 66	Formic acid
Polyacrylonitrile	Dimethyl formaldehyde
PET	Trifluoroacetic acid/dimethyl chloride
PVA	Water
Polystyrene	DMF/toluene
Nylon 6 co polyamide	Formic acid
Polybenzimidazole	Dimethyl acetamide
Polyramide	Sulfuric acid
Polyimides	Phenol

Table 4. Polymer solvent systems for electrospinning [14]

Nanofibers exhibit special properties mainly due to extremely high surface to weight ratio compared to conventional nonwovens. Nonwoven products such as aerosol filters, facemasks, and protective clothing are used mostly in filtration applications because of low density, large surface area to mass, high pore volume, and tight pore size. At present, military fabrics under development designed for chemical and biological protection have been enhanced by laminating a layer of nanofiber between the body side layer and carbon fibers. Nanofibers are also used in medical applications, which include drug and gene delivery, artificial blood vessels, artificial organs, and medical face masks. For example, carbon fiber hollow nano-tubes, smaller than blood cells, have potential to carry drugs into blood cells [14].

2.3.4. Bicomponent

There has been a trend in the polymer industry since the midsixties to apply polymer blends and mixtures for the modification of material properties. In the man-made fiber industry, this trend is realized in the manufacture of fibers consisting of two or more components [38].

Bicomponent fibers can be defined as “extruding two polymers from the same spinneret with both polymers contained within the same filament.” A close relative is “co-spun fiber,” which is a group of filaments of different polymers, but a single component per filament, spun from the same spinneret [39]. Bicomponent fibers are commonly classified by the structure of their cross-section as side-by-side (S/S), sheath core, island in the sea, or

segmented pie. Of these, the side-by-side and sheath core arrangements are relevant for thermal bonding applications [40].

2.3.4.1. Side-by-side

Two components are arranged side by side and are divided along their length into two or more distinct regions (Figure 6). The geometrical configuration of side-by-side bi component fibers, particularly asymmetry, makes it possible to achieve an additional three-dimensional crimp during thermal bonding by differential thermal shrinkage of the two components, for example. This latent crimp gives rise to increased bulk stability and a softer fabric handle [40].

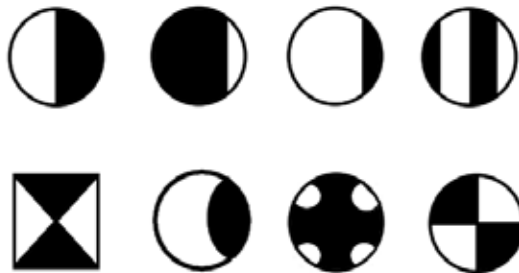


Figure 6. Cross Sections of Side-by-Side Bicomponent Fibers

2.3.4.2. Sheath core fibers

In sheath core bicomponent fibers (Figure 7), one of the components (the core) is fully surrounded by another component (the sheath). The arrangement of the core is either eccentric or concentric depending on the fabric properties required. If high fabric strength is required, the concentric form is selected, whereas if bulk is required, the eccentric type is used. One advantage of sheath core fibers is the ability to produce a surface with the required luster, dyeability, and handle characteristics while having a core that dominates the tensile properties. The core sheath structure also provides a means of minimizing the cost by engineering the relative proportions of the two polymer components. Commercially, the ratio of the polymer components is typically 50:50 or 30:70, but in some cases, a ratio of 10:90 is used [40].



Figure 7. Cross Sections of Sheath Core Bicomponent Fibers

The first industrial exploitation fiber involved the use of Co-PET/PET or PE/PP fibers for hygiene applications as well as high-loft batting, wiping cloths, medical wipes, and filters. The

difference in the sheath core melting temperature in PE/PP is about 40°C. In Co-PET/PET bicomponents, the sheath melts at 100-110°C while the core melts at 250-265°C [40]. Bicomponent fibers are generally used in blend ratios of 10-50% depending on the application and process parameters. A useful experimental guide is given in Table 5.

Parameter	Nonwoven Fabric Handle		
	Soft	Medium	Harsh
Bicomponent Fiber Content (%)	10-20	15-30	">30
Bonding Temperature (°C)	140-150	150-160	160-180
Fiber Fineness (dtex)	1.7-3.3	3.3-6.7	>6.7

Table 5. A practical guide for producing nonwoven fabrics with different handle characteristics from Co-PET/PET bicomponent fibers [8]

2.3.4.3. *Island in the sea or segmented pie*

Island in the sea is one type of bicomponent fiber whereby many fibrils of one polymer are dispersed in the matrix of another polymer. The fibrils are known as islands and the matrix is the sea. The island in the sea fibers have excellent tensile properties, and provide good feel, softness, and bursting and tearing strength for the nonwoven fabrics.

Bicomponent filaments can be used to produce a bonded fabric, with one of the components being thermoplastic to facilitate heat bonding and the other component having properties that will enhance the quality of the final fabric [4]. Bicomponent fibers are also used for spunlaced nonwoven products like medical disposable textiles, filtration products and air-laid nonwoven structures as absorbent cores in wet wipes [14].

2.3.5. *Superabsorbent fibers*

Superabsorbent (also known as superabsorbent polymers or SAP) consists of a material which can absorb many times its own weight in aqueous fluids. Superabsorbent fibers absorb 50-150 times their own weight while the diameter increases. The small diameter of the fiber, which is about 30 µm, gives a very high surface area for contact with the liquid. Viscose rayon or cotton without load only absorbs about 30 times, wool 17 times, and polyester 3 times their own weight [14]. The advantage that fibers offer compared to powders is due their physical form, or dimensions, rather than their chemical nature [18]. Also, the fiber surface is not smooth. It has a crenulated structure with longitudinal grooves. These are beneficial in transporting moisture to the surface. The lubricant has also been selected to enhance this wetting effect and results in a very high rate of moisture absorption. Typically, the fiber will absorb 95% of its ultimate capacity in 15 seconds [35]. They are therefore an ideal material for use in products which are designed to contain fluids such as baby diapers/nappies, incontinence products, and feminine hygiene pads and liners [21,22,38] (Figure 8).

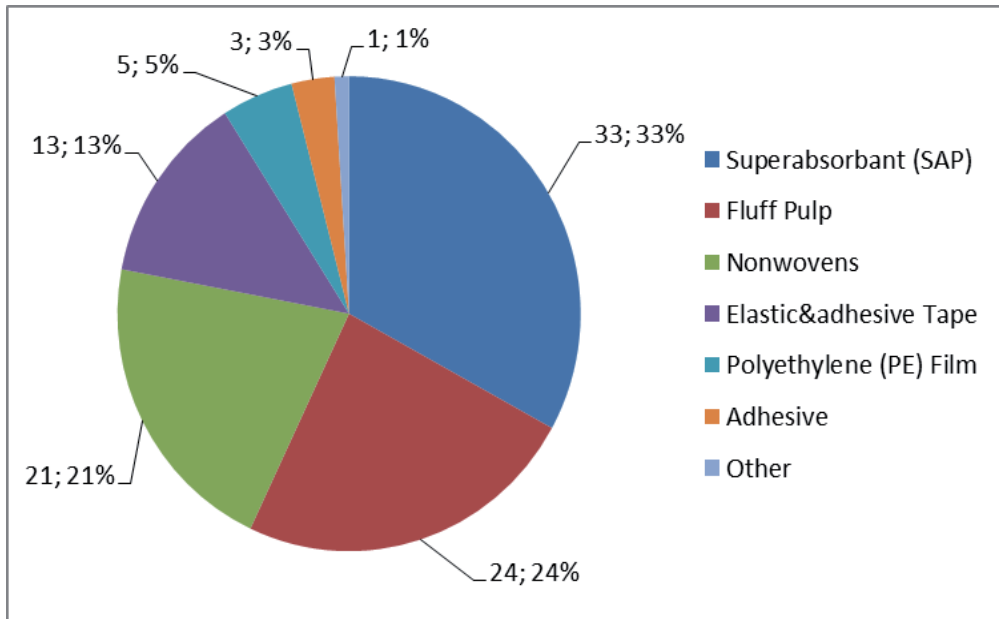


Figure 8. Composition of Baby Diaper [41]

Superabsorbent material was first produced in the early 1970s in Japan and USA. It was introduced into baby diapers in the early 1980s and later that decade into adult incontinence pads. By the early 1990s, superabsorbent material had become widely used in disposable baby diapers/nappies and incontinence products [41]. The use of superabsorbent materials in fiber form has now become a commercial reality. The majority of superabsorbent material available for today's absorbent hygiene products market is sold in granular form; some superabsorbent material is also available as a fiber. The granular material is a polymer made up of millions of identical units of sodium acrylate formed into a chain fence like structure. These are then linked to make the material into a three dimensional network. In their dry state, the long polymer chains are coiled. When they absorb liquid, they uncoil and the network expands. The liquid is then stored in the spaces in the molecular network and the material forms a gel which locks the liquid in [41].

The advantages of super absorbent fibers [41] are as follows:

1. **They help keep the skin dry.** This is done by drawing the liquid away from the skin and absorbing and retaining it in the core of the product. This creates greater comfort for the user.
2. **They help protect against skin irritation in diaper users by reducing skin wetness.** If skin becomes too wet, it is more vulnerable to irritation because the natural balance of the skin, which helps protect against harmful bacteria, can be compromised.
3. **They help prevent the spread of infections.** The containment of fluid in the superabsorbent core reduces leakage. It also reduces the risk of urine mixing with other material

and becoming contaminated with microorganisms which can cause the spread of diseases such as gastroenteritis.

4. **They offer improved quality of life and personal dignity.** Many people suffer from a lack of bladder or bowel control as a result of illness, disability, or age. Disposable products with superabsorbents help many of these individuals, and their care givers maintain a quality of life with greater mobility and independence.

3. Experimental

This chapter focuses on the effects of fiber type, applied force, mass per unit area, contact surface, and fabric direction on the friction behavior of % PP and PES spunbond nonwoven fabrics. These samples have been used in medical packages, aprons, cleaning cloths, make up cleaning pads, protective cloths, wet towels, and home textiles. Therefore, it is important to evaluate friction behavior of nonwoven fabrics. Spunbonded nonwoven fabric samples (100 % polypropylene (PP) and polyester (PES)) were tested. While evaluating samples, Textile-Test Methods For Nonwoven-Part 3: Determination of Tensile Strength and Elongation and Textile-Test Methods For Nonwoven-Part 2: Determination of Fabric Thickness, ISO 9073-2, 1995 standards are used under standard test conditions. Some of the physical characteristics of nonwoven fabrics are given in Table 6. Before friction tests, a digital stereo microscope connected to computer (Figure 9) is used to examine surface view of samples [42].

Weight (g/m ²)	Raw Material	Thickness (mm)	Tensile Strength (N/5 cm)		Elongation (%)	
			MD	CD	MD	CD
12	Polypropylene (PP)	0.10	23.0	11.0	40.0	40.0
	Polyester (PES)	0.07	20.0	10.0	15.0	19.0
17	Polypropylene (PP)	0.11	45.0	40.0	65.0	65.0
	Polyester (PES)	0.09	30.0	14.0	18.0	21.0
100	Polypropylene (PP)	0.49	200.0	163.0	70.0	71.0
	Polyester (PES)	0.75	114.0	150.5	45.3	21.4

Table 6. Physical properties of nonwoven fabrics

Frictional properties of nonwoven fabrics have been tested by using horizontal working principle device. This device is named as “horizontal platform experiment device.” The mechanism is developed which is shown in Figure 10 by designing and extra changes upon conventional universal tensile tester in order to perform friction experiments. The designed and manufactured device consists of anti friction rollers (3,4), non-stretch yarn (5), a sled (6), and a sled bed (7). A non-stretch yarn (5) is passed through rollers (3,4) to upper carrier claw

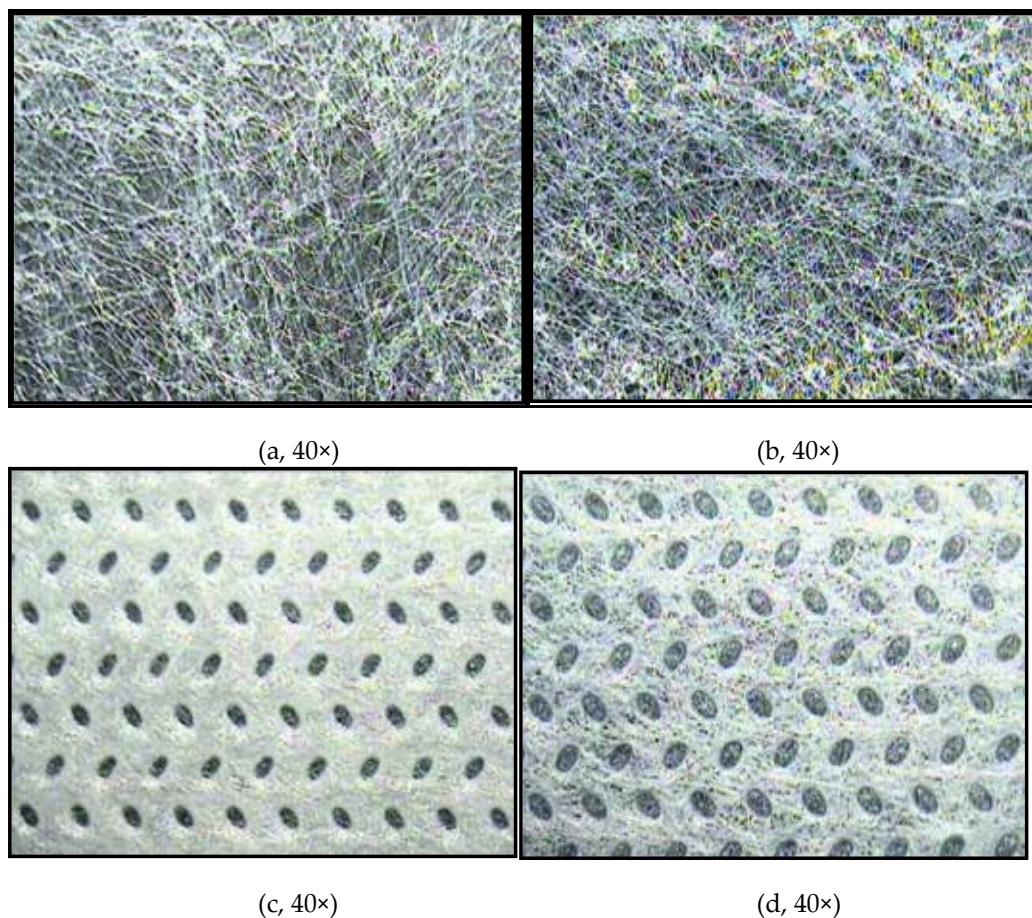
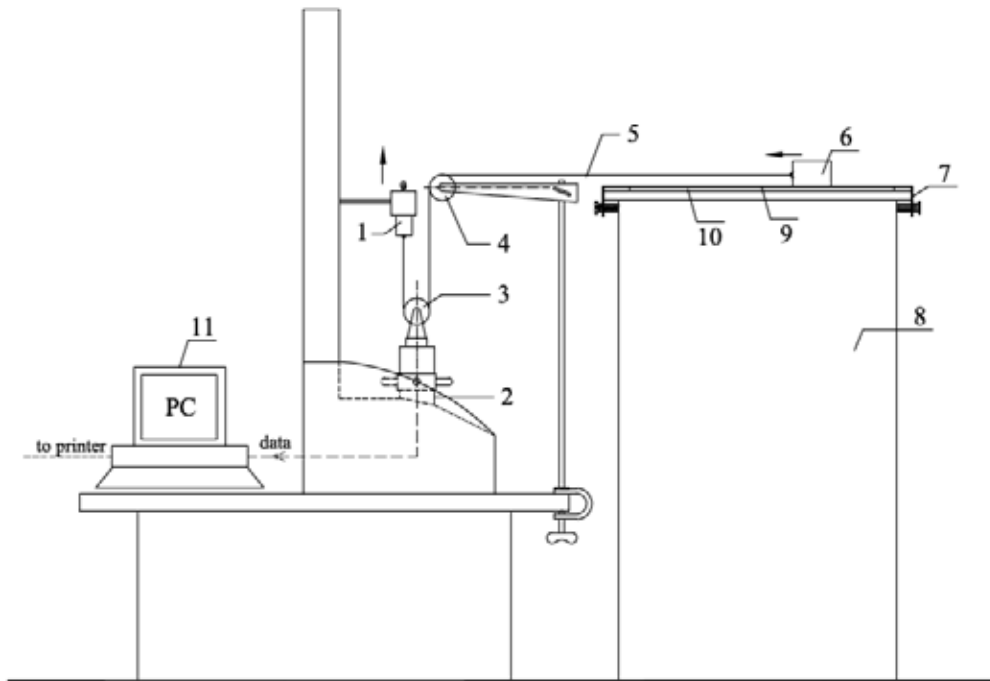


Figure 9. Microscope Views of Nonwoven Fabrics: (a) 12 g/m² Polypropylene, (b) 12 g/m² Polyester, (c) 100 g/m² Polypropylene, (d) 100 g/m² Polyester

(1) of tensile tester. Fastening the sample to the circular sled (6) made of circular 50mm diameter Delrin material is ensured by using a clip in proper dimensions. Nonwoven fabric (10) sample which is covered on sled (6) is lay out in the same direction (MD and CD) with horizontal platform [42].

Sled bed (7) is designed with the aim of stretching the fabric (10) on experiment table (8) so as to hold it stable and to prevent slipping, curling, twisting, or folding during the experiment. While the upper carrier claw (1) of developed device is moving at a specific speed, it also pulls Delrin sled (6), and as a result, a friction occurs between two surfaces. At the same time, the load changes stemming from fabric surface structure created during the movement are perceived by load cell (2) and created in graphical and numerical values by the computer (42).

All nonwoven samples were conditioned according to ISO139 before tests, and tests were performed in the standard atmosphere of $20\pm 2^{\circ}\text{C}$ temperature, and $65\pm 5\%$ relative humidity.



(1. Upper Carrier Claw, 2. Load Cell, 3,4. Anti friction Roller, 5. Non-stretch Yarn, 6. Sled, 7. Sled Bed, 8. Experiment Table, 9. Sponge, 10. Fabric, 11. Computer)

Figure 10. Horizontal Platform Experiment Device [42,43]

Design Expert 6.01 statistical package program is used to analyze data obtained by experimental works according to variance analysis at $\alpha = 0.05$ significance. Obtained analysis of variance (ANOVA) table is summarized in the following section, where *p value* less than 0.05 means that mentioned assessed factor has significant impact. Regression models were formed to define the relationship between independent variables (mass per unit area, fiber type, applied force, contact surface, and fabric direction), and response variables (static and kinetic friction coefficient).

While conducting statistical analysis, fiber type, contact surface, and fabric direction were accepted as categorical, whereas fabric mass per unit area and applied force were accepted as numerical factors. The frictional behavior of samples was used to analyze the general factorial design. The analysis of variance, lack of fit tests, and residual analysis were performed to select the proper model for the friction behavior.

3.1. Results and discussion

Friction tests were conducted under five loads (7.4, 10.2, 14.5, 17.3, and 20.2 N) and from three points of the fabric for machine direction (MD) and cross direction (CD) of samples and under three friction environment (fabric-abrasive wool fabric, wood, and metal). At the end of friction

tests, the highest value for the movement at its start was accepted as static friction resistance, whereas the average of values read thereafter were accepted as kinetic friction resistance. Attention was paid to ensure that the sample attached to Delrin part which was placed on horizontal platform was slightly strained and rubbed to different parts of the fabric. Figures obtained using the test results of friction behavior of nonwoven fabric obtained in the tests are given Figures 11-14 [42].

In Figures 11 and 12, the change against applied force (load) of static friction forces obtained as a result of friction tests conducted at machine direction (MD) and cross direction (CD) under three friction platforms of 100% PP- and PES-based nonwoven surfaces of three weights is shown [42].

When these figures are examined, it can be observed that when the force in normal direction (vertical direction) applied on the sample increased, static friction coefficient values tended to decrease. The result for this effect is interpreted to be the more uniform fabric surface created by fabric friction interaction as load increased, as a result of which friction coefficient tended to decrease [42].

When the impact of fiber type on friction coefficient is viewed, it can be seen that friction coefficient values of polypropylene (PP)-based nonwoven fabrics had much lower values than those of polyester (PES)-based samples. This is believed to have been caused by the fact that polypropylene-based samples had a tougher surface. As the surface is smoother, less force is required for sliding action so as to move when compared to polyester-based nonwoven fabrics, in which case friction coefficient values were measured much lower [42].

In addition, we can see that fabric mass per unit area has a significant impact on friction values. As the fiber orientation of nonwoven fabrics with low weight is not smooth, they showed fluctuations in behaviors, and it has been seen that they had higher friction coefficient. However, it has been found out that as weight increases, friction coefficient values started to decrease as fiber orientation on nonwoven fabric surface was more stable. When one looks at microscope views in Figure 9a and 9b belonging to fabric samples, it can be seen that fiber orientation distributed irregularly, and that as fabric weight increased (Figure 9c and 9d), surface smoothness deteriorated. This structure of the used samples helps us in understanding the obtained findings [42].

When these figures are examined, it can be observed that kinetic friction coefficient values in CD direction of samples at different friction surfaces (abrasive wool fabric, wood and metal) are slightly higher when compared to MD direction. The reason for this result can be the fact that fiber orientation in CD direction is more preventive for friction movement in the formation of samples [42].

When each load group of same type of sample is examined in itself, it can be observed that as the force in applied normal direction (vertical direction) increases, kinetic friction coefficient values tend to decrease. The result for this effect is interpreted to be the more uniform fabric surface created by fabric friction interaction as load increased, as a result of which friction coefficient tended to decrease [42].

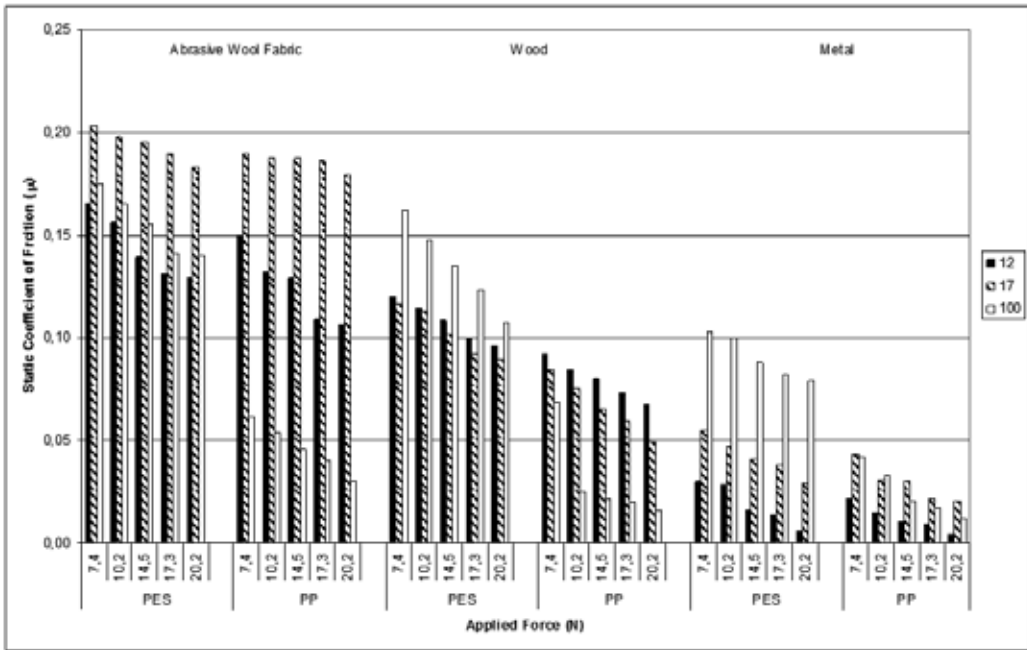


Figure 11. MD Static Friction Coefficient

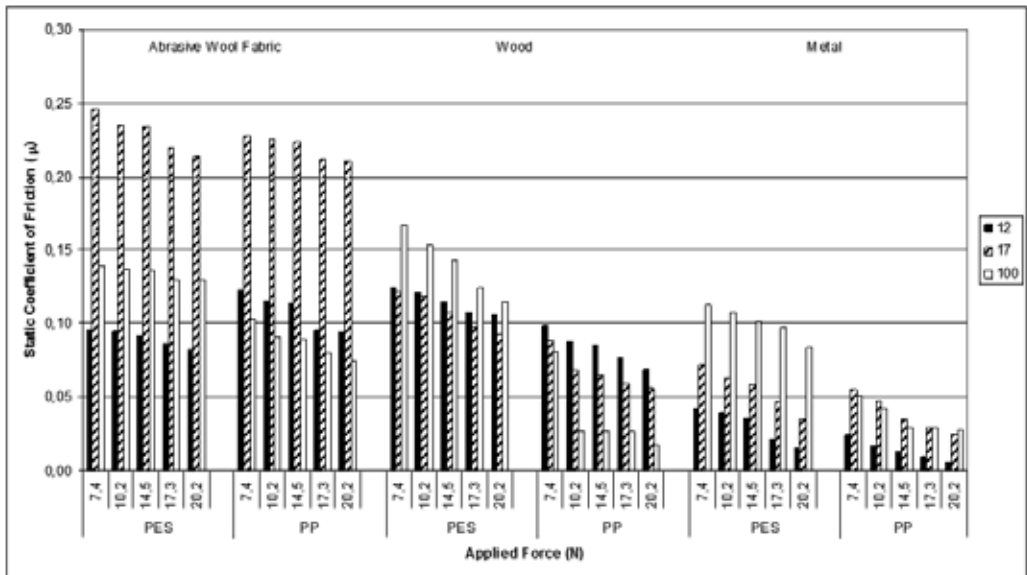


Figure 12. CD Static Friction Coefficient In Figures 13 and 14, the change against applied force (load) of kinetic friction forces obtained as a result of friction tests conducted at machine direction (MD) and cross direction (CD) under three friction platforms of 100% PP- and PES-based nonwoven surfaces of three weights is shown [42].

When we look at the impact of different friction environments on friction behavior, the lowest friction coefficient values were witnessed in fabric-metal friction environment, and the highest friction coefficient values were obtained in abrasive wool fabric friction environment. As metal surface is more smooth and slippery compared to wooden and abrasive wool fabric, it is observed that metal showed smaller resistance to friction, hence lower values for friction of metal in this interaction. In addition, in fabric-abrasive fabric friction environment, as a result of the tests applied in both machine and cross directions, higher kinetic friction coefficient values were measured, especially in 17 g/m² mass per unit area nonwoven fabric sample, compared to other samples. This is interpreted to have been caused by irregular distribution of fiber orientation in samples with low weight [42].

As a result of friction tests realized under fabric wooden friction environment, kinetic friction coefficient values were higher for polyester-based samples (especially 100 g/m²) as weight of surface structure in both machine and cross directions increased and gained a softer structure. As for polypropylene-based samples, on the other hand, as mass per unit area increased, surface structure became smoother and therefore friction coefficient tended to decrease [42].

In fabric-metal friction environment, as mass per unit area increased, friction coefficient values for both samples tended to increase as well, which is interpreted to have been caused by the softening of surface [42].

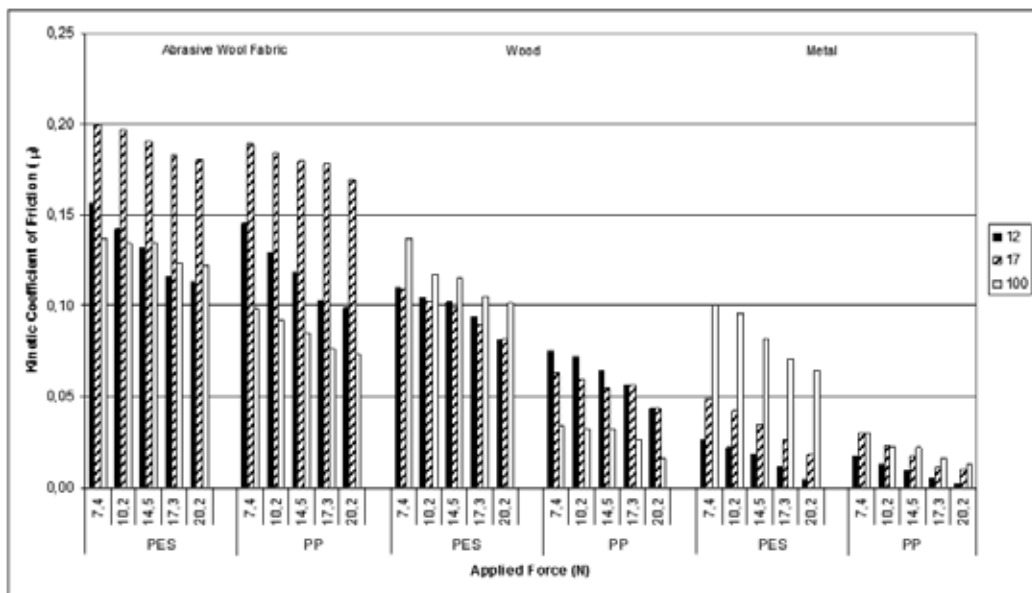


Figure 13. MD Kinetic Friction Coefficient

The statistical analyses show that the best fitting model is the quadratic model for spunbond nonwoven fabrics (Tables 7 and 8).

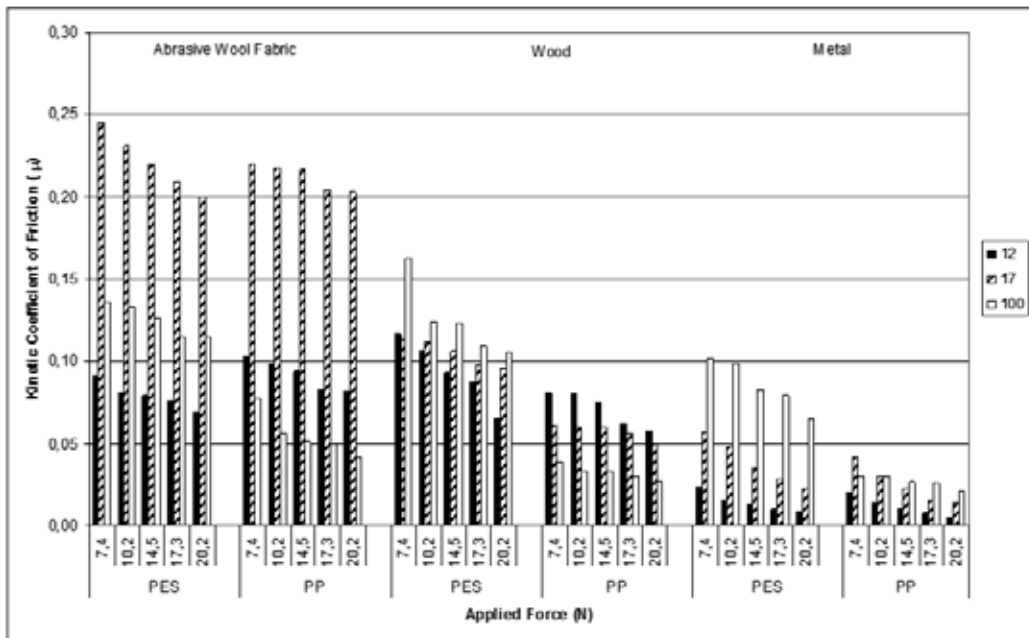


Figure 14. CD Kinetic Friction Coefficient

Source	P Value	Adjusted R ²	Predicted R ²
Linear	<0.0001	0.6361	0.6214
2FI	<0.0001	0.7905	0.7680
Quadratic	≤ 0.0001	0.8586	0.8485
Cubics	<0.0001	0.7719	0.7605

Table 7. Model summary statistics (static)

ANOVA results for friction coefficient of nonwoven fabric samples are given in Table 9. When ANOVA table is examined, it can be seen that weight, fiber type, applied force, and contact surface of nonwoven fabrics have significant impact on friction coefficient values, whereas fabric direction showed no significant impact. In addition, according to the table, the R² value of the model turned out to be some 0.86. In this case, terms in the model can explain the model at 86% ratio. This case shows that the model created for friction coefficient can express with rather high accuracy the relation between independent variables and dependent variable and that experimental work results were acceptable as accurate [42].

Source	P Value	Adjusted R ²	Predicted R ²
Linear	<0.0001	0.6451	0.6290
2FI	<0.0001	0.7765	0.7536
Quadratic	≤ 0.0001	0.8554	0.8456
Cubics	<0.0001	0.7726	0.7611

Table 8. Model summary statistics (kinetic)

Factor	Static		Kinetic	
	F Value	Prob>F	F Value	Prob>F
Model	91.58	<0.0001	89.28	<0.0001
Mass Per Unit Area	5.40	0.0213	4.22	0.0415
Fiber Type	138.62	<0.0001	111.04	<0.0001
Applied Force	38.32	<0.0001	31.58	<0.0001
Contact Surface	318.75	<0.0001	333.38	<0.0001
Fabric Direction	3.32	0.0701	7.395E-004	0.9783
Weight ²	72.95	<0.0001	83.57	<0.0001
Weight × Applied Force	86.79	<0.0001	57.47	<0.0001
Weight × Contact Surface	50.17	<0.0001	48.94	<0.0001
Fiber Type × Contact Surface	7.83	0.0006	9.40	0.0001
R ²	0.8681		0.8651	
Adjusted R ² _d	0.8586		0.8554	
Predicted R ² _{pre}	0.8485		0.8456	

Table 9. ANOVA table

The regression equation of the quadratic model for spunbond nonwoven sample is as follows;

$$\text{Static Friction Coefficient} = 0.24 + 0.00364 \times A - 0.019 \times B - 0.015 \times C + 0.045 \times D + 0.003 \times E - 0.001931 \times AC - 0.023 \times AD + 0.005 \times BD - 0.16 \times A^2$$

$$\text{Kinetic Friction Coefficient} = 0.24 + 0.004678 \times A - 0.017 \times B - 0.013 \times C + 0.047 \times D - 0.004 \times E + 0.00012 \times AC - 0.022 \times AD + 0.0060 \times BD - 0.17 \times A^2$$

According to model performance values, the correlation coefficient between predicted and observed air permeability values is 0.85, indicating a strong predictive capacity of the regression model for spunbond nonwoven samples.

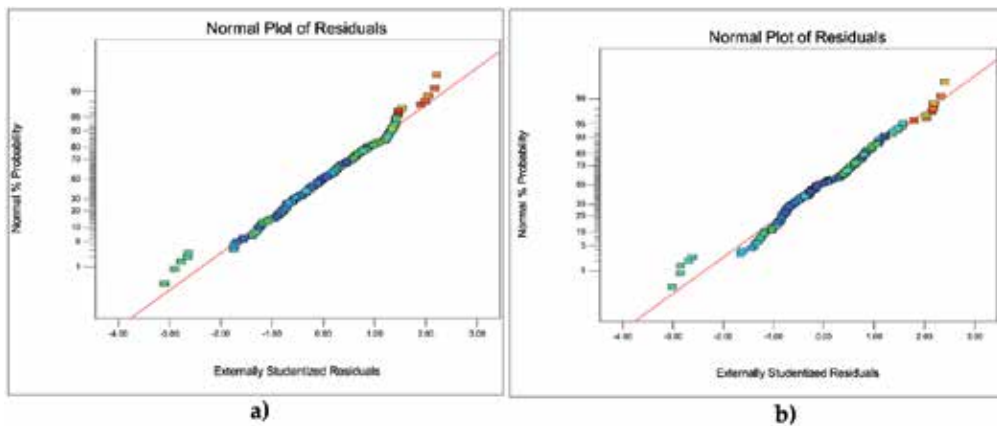


Figure 15. Normal Plot of Residual Coefficient of Friction Values: (a) Static and (b) Kinetic

Figure 15 gives normal distribution graph of residuals for quadratic model. As can be seen from the figure, no problems are observed in normal distribution in the chosen model. This analysis also supports the conformity of chosen model.

4. Conclusion

Nonwoven industry brings a wealth of advantages to people throughout the world by providing the superior products. For example, modern disposable baby diapers have made an important contribution to the quality of life of millions of people. Since their introduction, modern single-use diaper products have improved steadily through scientific advances in design and basic raw materials, becoming lighter, more compact, more absorbent, and easier to use. For this reason, selection of raw material is very important for nonwoven manufacturers. Raw materials have not only delivered significant product improvements but also benefited people using these products by providing hygiene and comfort.

Author details

Nazan Avcioglu Kalebek^{1*} and Osman Babaarslan²

*Address all correspondence to: nkalebek@gantep.edu.tr

1 Gaziantep University, Fine Art Faculty, Textile and Fashion Design Department, Gaziantep, Turkey

2 Cukurova University, Engineering and Architecture Faculty, Textile Engineering Department, Adana, Turkey

References

- [1] Turbak A.F. *Nonwovens: Theory, Process, Performance, and Testing*. Tappi Press; 1993. 255p. ISBN: 089852265
- [2] Corbman B.P. *Textiles Fiber to Fabric*, 6th ed. McGraw Hill Inc.; 1983. 594p. ISBN: 0070131376
- [3] Elsasser V.H. *Textiles*, 2nd ed. Fairchild Publication Inc.; 2007. 252p. ISBN: 1563673002
- [4] Wynne A. *Textiles*, Macmillan Education Ltd.; 1997. 309p. ISBN: 0333616588
- [5] Tortora P.G. and Collier B.J. *Understanding Textiles*, 5thed. Prentice Hall; 1997. 530p. ISBN: 0134392256
- [6] Albrecht W. *Nonwoven Fabrics*. Wiley; 2003. 748p. ISBN: 3527304061
- [7] Pakistan Textile Journal [Internet]. 2015. Available from <http://ptj.com.pk/> (accessed 2015.09.02)
- [8] Association of the Nonwoven Fabric Industry; *Advanced Nonwoven Worldwide* [Internet]. 2013. Available from <http://www.inda.org> (accessed 2014.05.01)
- [9] Russell S. *Handbook of Nonwovens*. Woodhead Publishing; 2006. 544p. ISBN: 9781885736030
- [10] Purdy A.T. *Development of Nonwovens*. The Textile Institute; 1983. 90p.
- [11] Wulfhorst B., Gries T. and Veit D. *Textile Technology*. Hanser Publishers; 2006. 320p. ISBN: 9783446229631
- [12] Gupta V.B., and Kothari V.K. *Manufactured Fibre Technology*. Chapman & Hall; 1997. 661p. ISBN: 0412540304
- [13] Morton W.E. and Hearle J.W.S. *Physical Properties of Textile Fibres*. Woodhead Publishing; 2008. 776p. ISBN: 9781845692209
- [14] University of Tennessee [Internet]. 2015. Available from <http://utnrl.engr.utk.edu/TEXTILES/> (accessed 2015.06.26)
- [15] Hongu T., Phillips G.O. and Takigami M. *New Millennium Fibers*. Woodhead Publishing Limited; 2000. 299p. ISBN: 9781855736016
- [16] Yan L., Chouw N and Jayaraman K. *Flax Fibre and Its Composites-A Review*. *Composites: Part B*, 2014; 56: 296-317.
- [17] Information Portal for Textile [Internet]. 2015. Available from <http://textileschool.com> (accessed 2015.08.30)
- [18] Simpson W.S. and Crawshaw G.H. *Wool Science and Technology*. Woodhead Publishing Limited; 2002. 368p. ISBN:1855735741

- [19] Johnson N.A.G., Wood E.J., Ingham P.E., McNeil S.J. and Macfarlane I.D. Wool as a Technical Fibre. *The Journal of the Textile Institute*: 2009; 94: 26-41. DOI: 0.1080/00405000308630626
- [20] Grawshaw G.H. and Russell S.J. Chapter 10: Carpets, Felts and Nonwoven Fabrics. In Simpson W.S. and Crawshaw G.H., editors. *Wool: Science and Technology*. Woodhead Publishing Limited; 2002. p. 290-313
- [21] McIntyre J.E. *Synthetic Fibres*. Woodhead Publishing Limited; 2005. 300p. ISBN: 1855735881
- [22] Fourné F. *Synthetic Fibers*. Hanser Publishers; 1999. 885p. ISBN: 156990250
- [23] E-learning Courses from the IITS & IISC [Internet]. 2015. Available from <http://nptel.ac.in/courses/11610202006/18> (accessed 2015.06.07)
- [24] Textile Learner: One Stop Solution for Textiles [Internet]. 2015. Available from <http://textilelearner.blogspot.com> (accessed 2015.09.01)
- [25] Hollingsworth & Vose Company [Internet]. 2015. Available from <http://www.hollingsworth-voose.com> (accessed 2015.05.02)
- [26] Reemay Filtration [Internet]. 2015. Available from http://www.reemay.com/filtration/fp_synergex.html (accessed 2015.07.01)
- [27] DuPont Company [Internet]. 2015. Available from <http://www.dupont.com> (accessed 2015.06.20)
- [28] Dharmadhikary R.K., Gilmore T.F., Davis H.A. and Batra S.K. Thermal Bonding of Nonwoven Fabrics. *The Textile Institute*; 1995. 39p. ISBN: 1870812786
- [29] Goswami B.C. Chapter 19. Spunbonding and Melt-Blowing Process. In Gupta V.B. and Kothari V.K. editors. *Manufactured Fibre Technology*. Chapman & Hall; 1997. p. 560-594
- [30] Deopura B.L. and Mukherjee A.K. Chapter 13. Nylon 6 and Nylon 66 Fibers. In Gupta V.B. and Kothari V.K. editors. *Manufactured Fibre Technology*. Chapman & Hall; 1997. p. 318-359
- [31] Sengupta A.K. Chapter 17. Rayon Fibres. In Gupta V.B. and Kothari V.K., editors. *Manufactured Fibre Technology*. Chapman & Hall; 1997. p. 480-513
- [32] Usenko V. *Processing Man-Made Fibers*. Mir Publishers; 1979. 429p.
- [33] Atwater M.A., Mousavi A.K., Leseman Z.C. and Phillips J. Direct Synthesis and Characterization of a Nonwoven Structure Comprised of Carbon Nanofibers, *Carbon*, 2013; 57: 363-370
- [34] World of Garment-Textile-Fashion [Internet]. 2015. Available from <http://fibre2fashion.com> (accessed 2015.09.01)

- [35] Hongu T., Phillips G.O. and Takigami M. Chapter 9. Fibres in Medical Healthcare. In Hongu T., Phillips G.O., and Takigami M., editors. *New Millennium Fibers*. Woodhead Publishing Limited; 2005. p.269-288
- [36] Feng C. Recent Progress in the Preparation, Characterization, and Applications of Nanofibers and Nanofiber Membranes via Electrospinning/Interfacial Polymerization. *Journal of Applied Polymer Science*, 2010; 115: 756-776, DOI:10.1002/app.31059
- [37] Bhat G. and Lee Y. Recent Advancements in Electrospun Nanofiber, Proceedings of the Twelfth International Symposium of Processing and Fabrication of Advanced Materials, 2003, Pittsburgh, PA (USA)
- [38] Ziabicki A. *Fundamentals of Fiber Formation*. John Wiley & Sons Ltd.; 1976. 488p. ISBN: 0471982202
- [39] Indorama Ventures: Closer than You Think [Internet]. 2015. Available from <http://www.indoramaventures.com/EN/Home/> (accessed 2015.09.14)
- [40] Pourmohammadi A. Chapter 6. Thermal Bonding. In Russell S.J. editors. *Handbook of Nonwovens*. Woodhead Publishing Limited; 2007. p. 298-329
- [41] Edana Nonwoven [Internet]. 2015. Available from <http://www.edana.org/docs/default-source/default-document-library/sustainability-report-2007-2008-absorbent-hygiene-products> (accessed 2015.02.28)
- [42] Babaarslan O. and Kalebek N.A. A Study on the Friction Behaviour of Spunbond Nonwovens Used with Different Weights. *Tekstil and Konfeksiyon*, 2011; 3: 210-216
- [43] Babaarslan O. and Kalebek N.A. Horizontal Platform Experimental Device for Determination of Friction Coefficient on Fibrous Textile Surfaces. Turkish Patent Institute (TPE); 2008/01016

Electrospinning Technology in Non-Woven Fabric Manufacturing

Haoyi Li and Weimin Yang

Additional information is available at the end of the chapter

<http://dx.doi.org/10.5772/62200>

Abstract

In the past two decades, research on electrospinning has boomed due to its simple process, small fiber diameter, and special physical and chemical properties. The electrospun fiber is spontaneously collected in a non-woven status in most cases. Therefore, the electrospinning method is becoming an ideal candidate for non-woven fabric manufacturing on a nano scale. More than 50,000 research papers have been published linked to the concept of "electrospinning", and the number is still increasing rapidly. At the early stage of electrospinning research, most of the published papers mainly focused on the research of spinning theories, material systems, and spinning processing. Since then research has turned to functional electrospun fiber preparation and characterization. In recent years, more and more researchers have started to develop a scaling-up method related to the applied products of electrospinning. Interestingly, most electrospinning products are in a non-woven state; that is why we dedicate one chapter to exhibit ongoing, on-woven fabric manufacturing and the basic research progress made using the electrospinning method.

Keywords: Electrospinning, non-woven fabrics, process, applications

1. Introduction

1.1. Electrospinning principle for manufacturing non-woven fabrics

The electrospinning method, as a versatile nanofiber preparation process, has drawn great attention in the past decades, due to its simple setup, easy process, extensive material options, and capability to form non-woven fabrics without any post processes.

The origin of electrospinning as a viable fiber-spinning technique can be traced back hundreds of years [1]. The process of electrospinning, also termed electrostatic spinning, was first

conceived by Lord Rayleigh [2] in the late 19th century. In 1902, Morton [3] and Cooley [4] disclosed a patent using the electrospinning process via a composite solution. This patent was issued for the production of fibers from a solution jet using an electric field. From 1934 to 1944, Formhals published a series of patents [5-9], describing an experimental setup for the production of polymer filaments using an electrostatic force. Since then, electrospinning truly emerged as a feasible technique for spinning fibers with small diameters.

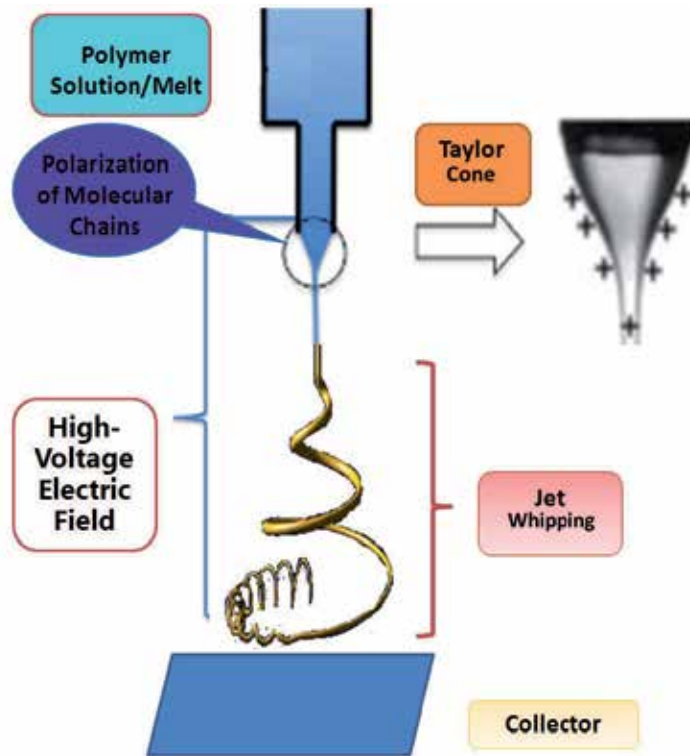


Figure 1. Diagram showing the principle of the electrospinning process.

A formal electrospinning process can be defined as below [10]: a polymer solution or melt is held at the end of a capillary tube and is subjected to a high static electric field (commonly $1-6 \times 10^6$ V/m); the charges are then induced on the liquid surface; the mutual charge repulsion causes a force directly opposite to the surface tension; as the intensity of the electric field increases, the hemispherical surface of the solution or melt elongates to form a conical shape known as a Taylor cone; when the static electric field surpasses a critical value, the repulsive electrical forces overcome surface tension forces, resulting in a charged jet ejected from the tip of the Taylor cone. The route and thinning of this jet can be controlled by the electric field. At the same time, the solvent either evaporates or the polymer melt solidifies, leaving behind a charged polymer fiber. Continuous fibers are finally collected in the form of a non-woven fabric.

Electrospinning technology uses a totally different method for non-woven fabrics than the manufacturing in any other methods used in industry. The excellent characteristics of electrospinning technology include the following.

1.1. Low power consumption

In the electrospinning process, the driving force during jet thinning is the electrostatic force. Usually, in electrospinning the current carried by a typical jet is around 0.1-1 μ A [11]. This means that one jet in the electrospinning process consumes less than 0.1 W/h (power per hour). In other words, a mobile phone battery can drive more than 5-10 electrospinning jets for more than ten hours. Consequently, it is easy to develop handheld electrospinning equipment [12].

1.2. Nanoscale fibers

Although only a few fibers smaller than 1 μ m can be detected in traditional non-woven processes as for so-called "sea-island melt spinning"[13] and the recently developed flash-spinning process [14], small continuous fibers with nanoscale diameters can be easily attained via the electrospinning process. Before the 1990s, researches had produced ultrafine fiber around 1 μ m and found this method had the potential for nanometer fiber preparation. Until 1996, works by Darrell H Reneker and Iksoo Chun [11] demonstrated that many polymer solutions and melts can be produced into nanofiber in the range 40-2000nm. After that, great attention was given to this technique for nanofiber production. Nowadays more than 3,000 papers and patents per year (Figure 2) are published on electrospun nanofiber preparation and its applications based on more than 200 kinds of polymers.

Non-woven fabrics using nanoscale fibers always exhibit a high specific surface area and smaller pores and channels though the fabric, which means more functional molecules become exposed on the surface of the fiber or channels. This advantage can be applied into several high-end fields like high sensitive flexible sensor, efficient filter element, immobilized catalyst, and high energy storage element.

1.3. Long and continuous fiber [15]

The electrospinning process usually produced long nanofibers as any other traditional non-woven processes did; so scholars claimed electrospinning as a continuous nanofiber manufacturing method. In Beachley V's results [15], an electrospun polycaprolactone (PCL) fiber had a length ranging from 30 to 50cm, which is close to that of melt-blown nanofiber lengths obtained by Christopher J. Ellison [16]. This high draft ratio is attributed to the principle of electrospinning: electromicro stretch. Traditional industrial spinning fiber is stretched from one end. All the molecular chains between the spinning pool and the jet end are stretched by the force transferring from its end, as shown in Figure 3a. However, the driving force of polymer chains in electrospinning is different; not from the end, but between the adjacent charges which endure a repulsion or attracting force in the electric field, shown in Figure 3b. In this way, an electrospinning jet represents an equilibrium state in a tug of war between

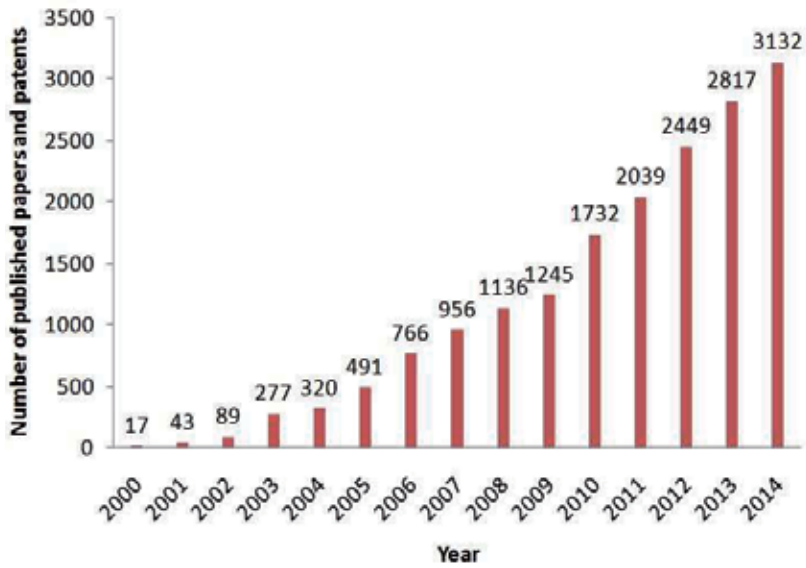


Figure 2. Number of published papers and patents containing the concept of the “electrospinning” process searched for on web “SciFinder”.

electrostatic force and surface tension force. Liu et al. [17] demonstrated this tug of war process by a simulation method of dissipative particle dynamics.

Non-woven fabrics produced by nanofibers may have eliminated the falling out of short fibers and hence avoid some potential pollution of nanomaterials.

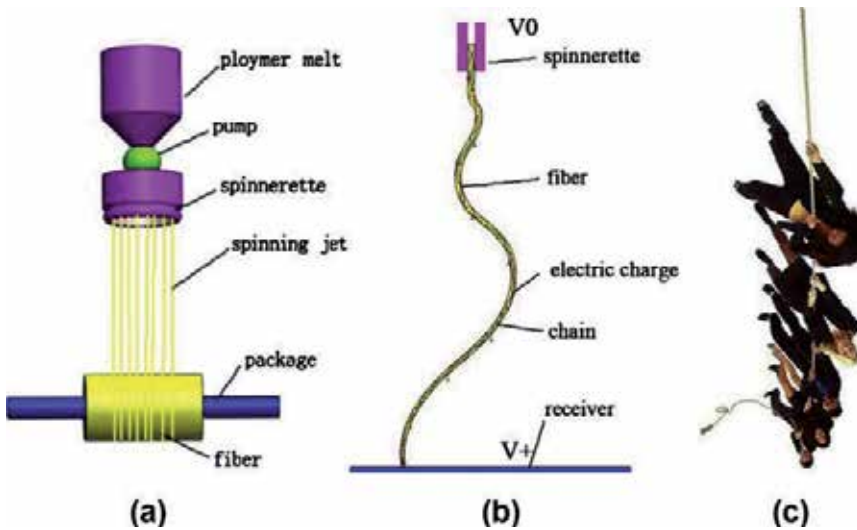


Figure 3. Schematic process of (a) industrial melt spinning, (b) melt electrospinning, and (c) tug of war [17].

2. Electrospinning parameters and fiber properties

Electrospinning can be divided into two methods based on material properties: melt electrospinning and solution electrospinning. The former is less investigated because of its thick resultant fiber and high applied voltage [18], while the latter is widely researched and applied in several areas such as non-woven fabrics. However, melt electrospinning is attracting more and more attention since it can process Polypropylene(PP), polyethylene(PE), and otherthermoplastic polymers without using any toxic solvents. Processing parameters always play important roles in judging spinnability and controlling fiber properties in both electrospinning processes.

2.1. Viscosity

Viscosity of the polymer melt or solution has a great effect on spinnability. Over a certain range, decreasing viscosity contributes to better spinnability, and smaller fiber diameter. The viscosity of the electrospun materials must be within a certain range (for solution electrospinning, it is commonly 5–20 Pa.s, while for melt electrospinning, it is commonly 20–200 Pa.s [18]). If the solution viscosity is lower than a certain value, some microspheres may be electrically ejected onto the fabrics because of insufficient chain entanglement [19]. They would then melt with a low viscosity due to a very low molecular weight and would also be unable to produce fiber. Commonly, polymer melt or solutions with high viscosity produce thick fiber, while a modified material with a viscosity reducer [20] or surfactant [21] can produce a relatively small fiber. For example, in order to prepare fiber smaller than 1 μm by melt electrospinning, researchers have tried a variety of methods to reduce the melt viscosity – including using plasticizer and conductive additives [22-23].

2.2. Applied voltage

The electrospinning process generates fiber when the applied voltage surpassed a given value required to balance the surface tension of the solution or melt. The electrical field intensity is estimated as the applied voltage divided by the distance between the tip and collector in most research. A higher electric field intensity value is obtained either through decreasing the distance between the tip and collector or by applying higher voltages. In 1969, Taylor deduced the threshold voltage of electrospinning [24], which defined the relationship between threshold voltage and the processed material. That is to say when the applied voltage exceeds this value, it breaks the balance between the electric force and the surface tension of the droplet, so a jet is ejected.

For solution electrospinning, it is commonly found that fiber diameter decreases with an increase in the applied voltage. However, for some polymer solutions like polyvinyl alcohol (PVA) and polyethylene oxide (PEO), they do not follow this rule [25]. The applied voltage has an important effect on non-woven morphology as well. Too weak or too strong an electrical field intensity, may cause beads of fiber in solution electrospun, non-woven fabrics and result in a rough surface [25]. For different materials, there is a suitable applied voltage range when other parameters are fixed.

For melt electrospinning, because of the dielectric properties and high viscosity of the polymer melt, the applied voltage is more than 2 times that used in solution electrospinning. Therefore, 20–100 kV is needed to polarize the polymer melt, and induce the generation of polymer jets [26], while usually 5–20 kV is loaded on the end of the syringe needle in solution electrospinning. Increasing the voltage is a common measure used to obtain finer fiber in melt electrospinning, but it can cause corona or breakdown if the voltage is too high. Rattapol [27] proposed a vacuum melt electrospinning method, improving the threshold voltage, in which the loading voltage can reach 1–30 kV/cm without breakdown, however, this method may prove costly if used in large-scale production.

2.3. Conductivity

High conductivity of processed material means a greater number of net charges on the jet when high voltage is loaded, therefore, a smaller fiber diameter can be attained by elevating the conductivity. Higher conductivity also may cause a drastic whipping of the electrospun jet, especially for polymer solutions, however, this may lead to a wide diameter distribution of the electrospun, non-woven fabrics. A widely used method to improve conductivity is by adding salts [28–29], pyridine [30], or carbon nano tube(CNT) [31] in polymer solution or polymer melts. However, this may change the original fiber properties. Some researchers have investigated additives that evaporate when jetting [32].

2.4. Spinning distance

Spinning distance was defined as the distance between the spinning tip and the collector. This distance is exactly the route that the electrospun jet experiences. Changing the spinning distance may cause a change in solvent evaporating velocity, the electrical field intensity, and the solidifying state, and thus affect the fiber properties indirectly. When the spinning distance is too short, the fiber will not be thinned enough because of a lack of the whipping process and inadequate solvent evaporation, as a result, the beads may accrue and even prepared fabrics may dissolve back into concentrated solution at this stage [33]. On the contrary, if there is an increase in the spinning distance, and a fixed electric field intensity, smaller fiber can be produced, and naturally, a larger area of deposited non-woven fabrics is prepared [34]. The spinning distance in most cases was set at 7–15 cm.

It should be noticed that near-field electrospinning has been developed for a patterned deposition of nanofiber, in which the spinning distance was set smaller than 1 mm and jet whipping was almost eliminated [35].

2.5. Solvent properties

Solvent properties including the surface tension [36] and conductivity [37], determine the final solution properties, and effect fiber properties indirectly. Solvent with low surface tension is a good candidate for better electrospinning solution preparation, thus the electrospinning process can be easily carried out by loading a relatively low voltage [36]. Volatility should be another concern when choosing the right solvent. If the volatility is too high, a blockage at the

spinneret may occur from time to time [38]; if the solvent evaporates as slowly as water, then an adhesive and thick fiber may be obtained [39]. In addition, inadequate evaporation of the solvent in the spinning solution may cause a toxic solvent residual in fabrics, which is not wanted in medicinal and sensor applications [40]. Solution conductivity in electrospinning has been discussed. In a solution system, the selected solvent's conductivity is the first factor defining solution conductivity, and using additives to improve conductivity is the second factor considered to adjust the solution's conductivity [37].

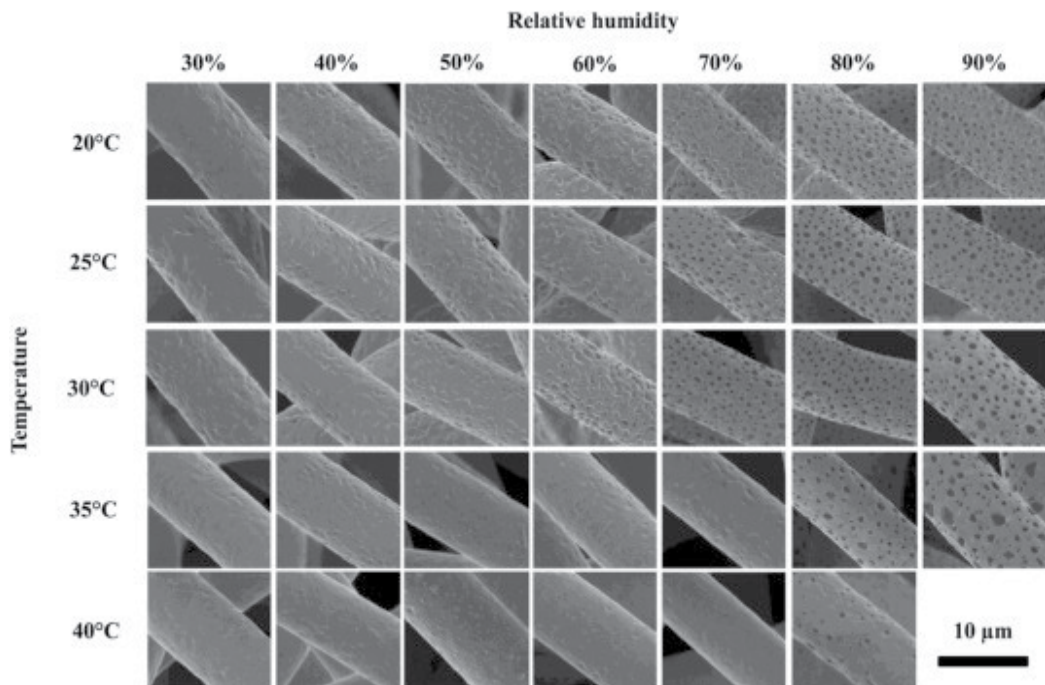


Figure 4. SEM pictures of solution electrospun fibers at different temperatures and relative humidities [45].

2.6. Collector

Non-woven fabrics are usually defined as random deposited fibers. However, sometimes controlled deposition of fibers, at least partially oriented fibers or patterned fabrics are needed in areas like cell scaffolds, sensors, and tailored filters. Therefore, different collectors or collectors with certain movement were utilized to realize specially controlled fabrics in electrospinning. Li, Wang, and Xia [41] have demonstrated that the nanofibers can be uniaxially aligned by introducing an insulating gap into the conductive collector. Other interesting methods including the use of collector-like knife-edged blades [42], rotating wire drums [43], rings placed in parallel [44], etc., have also been proposed and tested.

2.7. Ambient temperature and humidity

High temperature and low humidity in the spinning area benefit the evaporation of solvent, and this is helpful to obtain smaller fiber diameters [45]. When the temperature is too high in solution electrospinning, the spinneret may easily be blocked because of fast evaporation. In melt electrospinning, the high ambient temperature can keep the spinning jet in melt state for a long time, which increases the thinning time of the jet and is beneficial to smaller fiber production [46]. The electrospinning process can rarely be carried out when the humidity surpasses some value since a corona or breakdown may happen [47]. Obvious changes on the surface of the solution electrospun fiber have been observed when spinning temperatures and humidities change [45].

3. Scaling-up the technology of electrospinning

A basic electrospinning setup includes a chamber of polymer melt or solution, a spinning head, a high-voltage supplier, and a collector. Most electrospinning setups have their spinning heads connected to a positive high-voltage output end while the collectors are earthed or connected to a relatively low negative voltage. The electrospinning process requires a very small flow rate supply, so a microfluidic pump or fluid distributor is usually used to control the flow.

However, output of most solution-based, single-jet electrospinning setups is only 0.01-0.1g per hour, which is much smaller than that of traditional melt-blowing processes [48]. A lot of researchers have made great effort to improve the efficiency of the electrospinning process in different ways. The methods used can be grouped into two types. One method works by multiplying the output by establishing matrices of commonly used orifices (Figure 5a) [49]. The other uses a fluid-free surface or creates some protuberances on a fluid-free surface to motivate multiple jets by loading extremely high voltages (Figure 5b) [50].

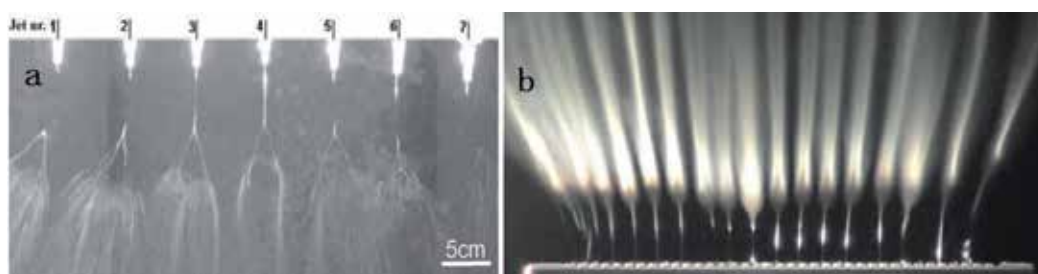


Figure 5. Pictures of (a) multineedle electrospinning and (b) needleless electrospinning setups [49, 50].

The spinneret matrices for scaling-up electrospinning as figure 5(a) shows is an on-brain method by simply copying single spinnerets. Its most impressive advantage is that there is no risk in carrying out any scaling-up processes of materials that are realized in a single needle setup. However, if the neighboring spinning heads are too close, the jets' distribution on the

deposited fabrics will not be even because of the electrical field interference between the needles [49]. In order to deal with this problem, it has been suggested that the array parameters, of the spinning heads, be improved [49]. It has also been demonstrated that the interference of the electrical field can be minimized by adding a hat to the spinning head [51].

The latter method, needleless electrospinning [50] or so-called free-surface electrospinning [52] or the nozzleless electrospinning method [53], is much simpler than the method mentioned above. This was first published by A.L. Yarin and E. Zussman [54] in 2003. They used magnetic f1003 prepared by mixing magnetic powder in kerosene with oleic acid as a stabilizer to initiate multiple jetting from the free surface under the action of the normal magnetic and electric field, which yields about 26 jets/cm², while the former method with nine orifices yields only 2.25 jets/cm² [49]. Subsequently, many kinds of varieties of method emerged by improving the spinning heads (as shown in Table 1). Outputs have been listed below, from which we can find that most of them have yield close to 10g/h.

Character of spinning head	Fiber diameter (nm)	Spinning voltage (kV)	Output (g/h)
Single orifice	3–500	<30	0.01–0.1
Laser heated linear sheet	<1000	16–41	0.36–1.28
Circling linear head	282–552	25–55	4.2
Edge of a disc	595–1235	20–50	6.85
Magnetic fluid surface	200–800	>32	0.12–1.2
Cylinder surface	100–800	40–70	1.25–12.5
Spraying from cylinder surface	150–400	40–50	0.44–6
Bubbles	50–200	10–35	0.06–0.6
Layered pyramid	87–289	55–70	2.3–5.7
Conical coil	100–700	45–70	0.86–2.75
Spiral coil	164–424	40–70	2.94–9.42

Table 1. Comparison of different nozzles [55].

It is hard to evaluate and compare which method is the best when considering jet number per unit area. However, the most popularly used systems in industry may reflect such an evaluation. Table 2 lists some pioneering companies which have used electrospinning machines for scaling-up production, among which, Elmarco is the most popular company supplying complete equipment [56]. Their technology has evolved from drum type to wire type, which can produce 80,000,000m²/year using an NS 8S1600U machine. For melt electrospinning, thick fiber and high voltage security have always represented an obstacle until Yang's team developed a new method called melt differential electrospinning [57]. In this method more than 60 simultaneous electrified jets are attained using umbellate systems with a flow rate of about 12 g/h [57–58]. The authors also indicated that a scaling-up machine has been established for non-woven fabric production with a 1-m width [58].

Company name	Country	Product/Service	Website
Elmarco	Czech Republic	Supplier of industrial level and lab-scale electrospinning machines	http://www.elmarco.cz/
MECC Co. Ltd	Japan	Supplier of lab-scale and semi-industrial level electrospinning machines	http://www.mecc.co.jp/en/html/nanon/list.html
Fuence	Japan	Lab-scale electrospinning setup and semi-industrial level electrospinning machines Contract manufacturing of nanofibers	http://www.fuence.co.jp/en
ANSTCO (Asian Nanostructures Technology Company)	Iran	Supplier of industrial level and lab-scale electrospinning machines	http://anstco.com/english/indexen.html
Fnm Co. (Fanavaran Nano-Meghyas)	Iran	Supplier of industrial level and lab-scale electrospinning machines and accessories	http://en.fnm.ir/
Inovenso	Turkey	Supplier of industrial level and lab-scale electrospinning machines	http://www.inovenso.com
Yflow	Spain	Supplier of lab-scale and industrial level electrospinning machines	http://www.yflow.com/
SPUR	Czech Republic	Supplier of industrial level setups	http://www.spur-nanotechnologies.cz/
Bioinicia	Spain	Custom manufacturer of electrospinning machines and accessories, both basic and industry setups	http://bioinicia.com/Fuidnatek@ http://fluidnatek.com/
Yinglan Lab	China	Scaling-up melt electrospinning machines	http://www.p-processing.com/

Table 2. Companies supplying mass production machines

4. Prospects of electrospinning technology for non-woven fabric production

4.1. Productivity improvement

Different measures have been adopted to improve the productivity of electrospinning for non-woven fabric production [56], however, limited output still exists compared with traditional processes. Needleless electrospinning has shown great potential having advantages over needle-based lines, but a lot of problems remain to be solved. The electrospinning conditions

required restrict control of temperature, humidity, and dust around the spinning pool; the processed polymer should be well dissolved into the solvent and kept for hours or days; and the evaporated solvent should be completely collected and recycled during electrospinning. These requirements change when the material changes. Presently, only a few polymers like PAN, PA6, and PVA can be processed well on a needleless electrospinning line. More polymers and their composites need to be tested to find suitable processing parameters. It should be noticed that it would be difficult to carry out electrospinning without needle-based setups for some materials and morphologies, especially for two component nanofiber and core-shell nanofiber [59]. Therefore, fundamental research should be carried out to optimize on-going production lines to cater for different requirements.

4.2. Eco-friendly material and processes

The use of toxic solvents in solution electrospinning has brought about 3 main problems. First, most of the solvents used in solution electrospinning are toxic [23], such as dimethyl formamide (DMF), isopropyl alcohol, acetone, hexafluoroisopropanol (HFIP), and trifluoroacetic acid (TFA)[60], which means the whole manufacturing process from mix processing of solvents to post-processing of fibers needs a closed environment to ensure worker safety or to measure up to the required standards [61]. Extra processes increase costs and more importantly, fibers with residual toxicity for applications in biomedicine can bring about significant damage to cells [62]. Second, during the mass production process, solvent evaporation may cause a change in ambient temperature and humidity, which means an extra temperature–humidity control system is needed. More specifically, the solvent ratio in most solution systems exceeds 90% in solution electrospinning, and air humidity needs to remain below 30% [63], this means there will be an increase in the cost of mass production [62]. Third, solvent evaporation will cause tiny holes on the fiber surface – ranging from a few to dozens of nanometers in size, which weakens the strength of single fibers. In addition, it is difficult to find solvents for some special polymers at ambient temperature [64].

On the contrary, solvent-free melt electrospinning has some advantages in nature. Melt electrospinning has no complicated process route like solution mixing and recycling. The surface of the resultant fiber is smooth and the fiber has high intensity. Polymer melt is completely transformed into the target product [62]. This method can process almost all thermoplastic polymers such as polypropylene (PP)[65], polyethylene (PE)[66], polyamide (PA), polylactic acid (PLA), polycaprolactone (PCL)[67], polyethylene glycol terephthalate (PET)[68], polyphenylene sulfide (PPS), and thermoplastic polyurethane (TPU)[69]. So a stable melt electrospinning route for nanofiber mass production would be an important choice in pursuing eco-friendly manufacturing methods [63]. More attention should also be given to some water soluble polymers or modified water soluble polymers that can be solution electrospun.

4.3. Fundamental research of as-pun, non-woven fabrics

Although mountains of research work has been done on the process and fiber morphology of electrospinning non-woven fabrics, little information about the as-spun, non-woven fabrics

has been revealed. Specifically, we know little about its mechanical properties including tensile strength, tearing strength, and bursting strength. The combination of electrospun non-woven fabrics with traditional non-woven fabrics or textiles should also be tested since the bonding of nanofiber to thick fiber-based substrate seems difficult.

5. Applications of electrospun non-woven fabrics

Electrospun non-woven fabrics have been used in several fields including high-efficiency filtration, battery separation, biological medicine, sensors, and functional nanofiber textiles, because of their high specific surface area, small pores, and special physical and chemical properties like high conductivity, heat insulating ability, electromagnetic shielding, and biocompatibility [70].

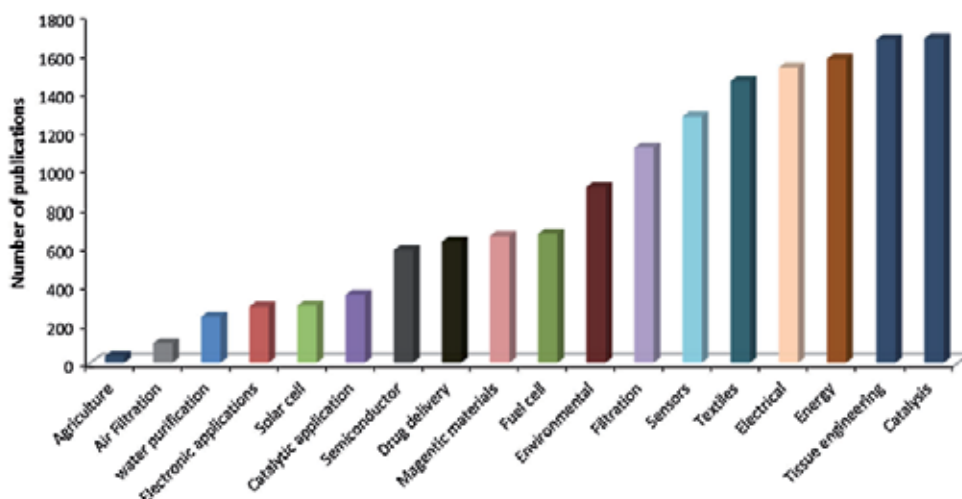


Figure 6. Overview of the number of publications featuring nanofibers used in various applications [70].

5.1. Filtration

In the air filtration field, electrospun non-woven fabrics are taking the place of traditional filter media like activated carbon and fiberglass, because of their excellent performance in filter efficiency and pressure loss. It has been demonstrated by various authors [71] that electrospun nanofibers can remove the volatile organic compounds (VOC) in the air, with some samples filtering faster than conventional activated carbon. Scientists have found that the slip flow mechanism becomes dominant due to the ability of the smaller fiber to disturb the air flow instead of non-slip flow in traditional filters [72]. Surface loading of dust particles takes place on non-woven fabrics coating conventional filters. In one work, Heikkila et al. [73] optimized the coating thickness of polyamide nanofibers required to improve filtration efficiency and

obtain an efficiency of over 95% (0.16 μm Particles) for a 0.5 g/m^2 coating; in another work, Hung et al. [74] studied the effect of fiber diameter on capture efficiency and pressure drop and they observed that when fiber diameter was reduced from 185 to 94 nm, the filtration of 50–500 nm nanoaerosol can be achieved only with a significant increase in the pressure drop.

In the water filtration field, typically used membranes for ultra-filtration (UF) or nano-filtration (NF) filters are made using the phase immersion method. The torturous porosity in these membranes usually has a low flux rate. Therefore, some researchers turned to electrospun non-woven fabrics to make use of their high flux rates. The electrospun non-woven fabrics usually appear as a functional layer in a composite membrane. Yoon et al. [75] studied a composite membrane containing an electrospun PAN scaffold with an average diameter from 124 to 720 nm and a porosity of about 70%, together with a chitosan top layer, and found this membrane exhibited a flux rate that was an order magnitude higher than commercial NF membranes over 24 hours of operation, while maintaining the same rejection efficiency (>99.9%) for oily wastewater filtration. Many other materials having composite membranes with electrospun non-woven layers also have proved this characteristic [76-78]. Some other research has also demonstrated electrospun non-woven fabrics' notable performance in selective filtration of cells or bacteria and adsorption for viruses from fluid [79-80].

5.2. Medical applications

Biopolymers including polysaccharides (cellulose, chitin, chitosan, and dextrose), proteins (collagen, gelatin, silk, etc.), and DNA [81], as well as some biopolymer derivatives and composites, have been successfully electrospun into non-woven fabrics [82]. Applications of these as-spun fabrics have been carried out in many medical fields like tissue engineering, drug delivery, and wound dressing.

Using electrospun non-woven fabrics or partially aligned fabrics as cell scaffold in tissue engineering is one promising application. Scientists found that alignment of fiber in scaffold would be beneficial. Cell elongation and proliferation have been demonstrated to occur along the direction of these nanofibers, which could improve tissue engineering applications [83]. In some other examples, it was found that the number of anchoring points for cells, wetting-properties, and degradation rates can all be varied by adjusting the porosity of as-spun fabrics [84]. However, in most cases, the pores in solution electrospun fabrics were too small for cells to pass through and influenced both cellular and enzymatic behavior [85]. Thus, a lot of measures were adopted to enlarge the diameter of the pores between as-spun fibers including multilayering and mixing electrospinning techniques [86] and combination of electrospun fiber and traditional microscale fiber [81, 87]. A more effective solution was to use the melt electrospinning method and its meshed fabrics as scaffolds, which, had large spaces for cell penetration and tailored aliment for effective cell proliferation [88].

Drug delivery alleviating medical conditions is another application of electrospun fabrics because nanofiber can be controlled to deliver drugs efficiently to a specific area at a controlled release rate via a dissoluble starting material [89]. Most cases focused on drug delivery materials specially applied in tissue engineering scaffold such as bioactive growth factors or

factors to prevent infection while repair and regeneration occur [90], other samples used these non-woven fabrics as a targeted drug carrier for oral medicine [91].

However, electrospinning is still an emerging technology, which requires further theoretical and experimental study. Consideration should be given to the design of a patient-compliant dosage form, material choice, and process controlling. Scaling-up and commercial production are other challenges which need to be overcome for biopolymer composites.

5.3. Functional nanofiber textiles

A lot of functions have been realized or enhanced by the use of nanotechnology in traditional textile materials. Electrospun non-woven fabrics, are widely investigated as a functional layer on some traditional substrates because of its high specific surface area, high gas permeability, and softness. The most promising application is that of protective cloth [92]. In some cases, TiO_2 [93], ZnO [94], or MOF [95] was added in the electrospun fiber or spun into core-shell nanofiber as a photocatalyst [93] or adsorbent to prevent the penetration of organic toxic gas or fluid and UV light. Some research used PP [96], PA66 [97], or PAN [98] to directly produce a non-woven layer on a substrate layer as a protective textile. Yan, Jian, and Zachariah [99] prepared non-woven, fabric-based thermite textiles and tested their reactive properties. He found that this material can yield up to a 1000 times increase in propagation rate compared to its micro-sized counterparts. Other applications of electrospun non-woven materials as a functional layer in textiles include full-color, light-emitting electrospun nanofiber [100] and energy harvesting and self-powered textiles [101].

These applications illustrate the bright future of electrospun non-woven fabrics in functional textiles, however, few industrial products have been pushed to market. More fundamental research work is still required to find out how to adhere non-woven fabrics to traditional textiles without influencing their properties [97]. Although mass production has been carried out by some companies, fewer examples have been revealed using functional materials.

5.4. Sensors

Many kinds of materials such as polymers [102], semiconductors [103], and organic/inorganic composites [104] have been used as sensing materials to detect targeted toxic gases, toxic solid, or toxic fluid materials based on various sensing techniques and principles. Electrospun non-woven fabrics have a specific surface approximately 1–2 orders of magnitude larger than flat films, making them excellent candidates for applications in ultrasensitive sensors. Different electrospun non-woven materials have been applied as ultrasensitive sensors to detect the signal changes of acoustic waves [105], resistivity [106], photoelectricity [107], optical waves [108], and amperometric parameters [109]. It was found that parameters including specific surface area, fiber diameter, and membrane thickness have great influence on the detecting properties of sensors. Higher surface-to-volume ratios of electrospun non-woven fabrics represents the key to guarantee fast and sensitive mass transport, electric charge transport, and signal-to-noise current ratios. Therefore, regulating the parameters of the electrospinning process or solution properties has been adopted to produce more porous fiber and even hollow

fiber structures [110]. A thick membrane was found to own a larger sensing area and vacant volume into which more analytes could be absorbed and diffused [111]. However, more experimental studies and theoretical work is required in order to achieve a better control over the size and secondary structure of electrospun non-woven fabrics.

Author details

Haoyi Li^{1,2} and Weimin Yang^{1,2*}

*Address all correspondence to: lihaoyi-hoy@163.com

1 College of Mechanical and Electrical Engineering, Beijing University of Chemical Technology, Beijing, China

2 State Key Laboratory of Organic-Inorganic Composites, Beijing University of Chemical Technology, Beijing, China

References

- [1] Gilbert W, Thompson S P. On the Magnet, Magnetic Bodies Also, and on the Great Magnet the Earth: A New Physiology, Demonstrated by Many Arguments & Experiments [M]. Chiswick Press, 1900.
- [2] Ayres C E, Jha B S, Sell S A, et al. Nanotechnology in the design of soft tissue scaffolds: innovations in structure and function[J]. *Wiley Interdisciplinary Reviews: Nanomedicine and Nanobiotechnology*, 2010, 2(1): 20–34.
- [3] Morton W J. Method of dispersing fluids: U.S. Patent 705,691[P]. 1902-7-29.
- [4] Cooley J F. Apparatus for electrically dispersing fluids: U.S. Patent 692,631[P]. 1902-2-4.
- [5] Anton F. Process and apparatus for preparing artificial threads: U.S. Patent 1,975,504[P]. 1934-10-2.
- [6] Anton F. Method and apparatus for spinning: U.S. Patent 2,160,962[P]. 1939-6-6.
- [7] Anton F. Artificial thread and method of producing same: U.S. Patent 2,187,306[P]. 1940-1-16..
- [8] Anton F. Production of artificial fibers from fiber forming liquids: U.S. Patent 2,323,025[P]. 1943-6-29.
- [9] Anton F. Method and apparatus for spinning: U.S. Patent 2,349,950[P]. 1944-5-30.

- [10] Doshi J, Reneker D H. Electrospinning process and applications of electrospun fibers. Industry Applications Society Annual Meeting, 1993., Conference Record of the 1993 IEEE. IEEE, 1993: 1698–1703.
- [11] Reneker D H, Chun I. Nanometre diameter fibres of polymer, produced by electrospinning. *Nanotechnology*, 1996, 7(3): 216.
- [12] Xu S C, Qin C C, Yu M, et al. A battery-operated portable handheld electrospinning apparatus. *Nanoscale*, 2015, 7(29): 12351–12355.
- [13] Pourdeyhimi B, Fedorova N V, Sharp S R. High strength, durable micro and nano-fiber fabrics produced by fibrillating bicomponent islands in the sea fibers: U.S. Patent 8,420,556[P]. 2013-4-16.
- [14] Weinberg M, Dee G, Harding T. Flash spun web containing sub-micron filaments and process for forming same: U.S. Patent Application 11/015,527[P]. 2004-12-17.
- [15] Beachley V, Wen X. Effect of electrospinning parameters on the nanofiber diameter and length. *Materials Science and Engineering: C*, 2009, 29(3): 663–668.
- [16] Ellison C J, Phatak A, Giles D W, et al. Melt blown nanofibers: Fiber diameter distributions and onset of fiber breakup. *Polymer*, 2007, 48(11): 3306–3316.
- [17] Liu Z, Liu Y, Ding Y, et al. Tug of war effect in melt electrospinning. *Journal of Non-Newtonian Fluid Mechanics*, 2013, 202: 131–136.
- [18] Hutmacher D W, Dalton P D. Melt electrospinning. *Chemistry, an Asian journal*, 2011, 6(1): 44–56.
- [19] Fong H, Chun I, Reneker D H. Beaded nanofibers formed during electrospinning. *Polymer*, 1999, 40(16): 4585–4592.
- [20] Wang X. Melt-electrospinning of PMMA. *Chinese Journal of Polymer Science*, 2010, 28(1): 45–53.
- [21] Jia L, Qin X. The effect of different surfactants on the electrospinning poly (vinyl alcohol)(PVA) nanofibers. *Journal of thermal analysis and calorimetry*, 2013, 112(2): 595–605.
- [22] Ogata N, Yamaguchi S, Shimada N, et al. Poly (lactide) nanofibers produced by a melt-electrospinning system with a laser melting device. *Journal of applied polymer science*, 2007, 104(3): 1640–1645.
- [23] Dalton P D, Grafahrend D, Klinkhammer K, et al. Electrospinning of polymer melts: Phenomenological observations. *Polymer*, 2007, 48(23): 6823–6833.
- [24] Taylor G I. Electrically Driven Jets. *London Ser A*, 1969, 313(1515): 453–457.
- [25] Demir M M, Yilgor I, Yilgor E E A, et al. Electrospinning of polyurethane fibers. *Polymer*, 2002, 43(11): 3303–3309.

- [26] Hao Mingfeng, Liu Yong, Deng Rongjian, et al. Research on typical materials by melt electrospinning. *Engineering Plastics Application*, 2010, 38(3): 24–27 (in Chinese).
- [27] Ratthapol R, Darrell H R. Electrospinning Process of Molten Polypropylene in Vacuum. *Journal of Metals, Materials and Minerals*, 2003, 12(2): 81–87.
- [28] Lee C K, Kim S I, Kim S J. The influence of added ionic salt on nanofiber uniformity for electrospinning of electrolyte polymer. *Synthetic metals*, 2005, 154(1–3): 209–212.
- [29] Nayak R, Kyratzis I L, Truong Y B, et al. Melt-electrospinning of polypropylene with conductive additives. *Journal of Materials Science*, 2012, 47(17): 6387–6396.
- [30] Tan S H, Inai R, Kotaki M, et al. Systematic parameter study for ultra-fine fiber fabrication via electrospinning process. *Polymer*, 2005, 46(16): 6128–6134.
- [31] Mazinani S, Aiji A, Dubois C. Morphology, structure and properties of conductive PS/CNT nanocomposite electrospun mat. *Polymer*, 2009, 50(14): 3329–3342.
- [32] Moghe A K, Hufenus R, Hudson S M, et al. Effect of the addition of a fugitive salt on electrospinnability of poly (ϵ -caprolactone). *Polymer*, 2009, 50(14): 3311–3318.
- [33] Ki C S, Baek D H, Gang K D, et al. Characterization of gelatin nanofiber prepared from gelatin–formic acid solution. *Polymer*, 2005, 46(14): 5094–5102.
- [34] Zhang Y, He X, Li J, et al. Fabrication and ethanol-sensing properties of micro gas sensor based on electrospun SnO₂ nanofibers. *Sensors and Actuators B: Chemical*, 2008, 132(1): 67–73.
- [35] Chang C, Limkrailassiri K, Lin L. Continuous near-field electrospinning for large area deposition of orderly nanofiber patterns. *Applied Physics Letters*, 2008, 93(12): 123111(1-3).
- [36] Lee K H, Kim H Y, Bang H J, et al. The change of bead morphology formed on electrospun polystyrene fibers. *Polymer*, 2003, 44(14): 4029–4034.
- [37] Uyar T, Besenbacher F. Electrospinning of uniform polystyrene fibers: The effect of solvent conductivity. *Polymer*, 2008, 49(24): 5336–5343.
- [38] Sun G E, Teng H, Zhang C L, et al. Preparation of Ultrafine Water-soluble Polymers Nanofiber Mats via Electrospinning. *Chemical Research in Chinese Universities*, 2010, 26(2): 318–322.
- [39] Subbiah T, Bhat G S, Tock R W, et al. Electrospinning of nanofibers. *Journal of Applied Polymer Science*, 2005, 96(2): 557–569.
- [40] Wei A, Wang J, Wang X, et al. Preparation and characterization of the electrospun nanofibers loaded with clarithromycin. *Journal of Applied Polymer Science*, 2010, 118(1): 346–352.
- [41] Li D, Wang Y, Xia Y. Electrospinning nanofibers as uniaxially aligned arrays and layer-by-layer stacked films. *Advanced Materials*, 2004, 16(4): 361–366.

- [42] Teo W E, Ramakrishna S. Electrospun fibre bundle made of aligned nanofibres over two fixed points. *Nanotechnology*, 2005, 16(9): 1878-1884
- [43] Katta P, Alessandro M, Ramsier R D, et al. Continuous electrospinning of aligned polymer nanofibers onto a wire drum collector. *Nano Letters*, 2004, 4(11): 2215-2218.
- [44] Dalton P D, Klee D, Möller M. Electrospinning with dual collection rings. *Polymer*, 2005, 46(3): 611-614.
- [45] Putti M, Simonet M, Solberg R, et al. Electrospinning poly (ϵ -caprolactone) under controlled environmental conditions: Influence on fiber morphology and orientation. *Polymer*, 2015, 63: 189-195.
- [46] Zhou H, Green T B, Joo Y L. The thermal effects on electrospinning of polylactic acid melts. *Polymer*, 2006, 47(21): 7497-7505.
- [47] Kalayci V E, Patra P K, Kim Y K, et al. Charge consequences in electrospun polyacrylonitrile (PAN) nanofibers. *Polymer*, 2005, 46(18): 7191-7200.
- [48] Pinchuk L S, Goldade V A, Makarevich A V, et al. Melt blowing: Equipment, Technology, and Polymer Fibrous Materials. Springer Science & Business Media, 2012.
- [49] Theron S A, Yarin A L, Zussman E, et al. Multiple jets in electrospinning: experiment and modeling. *Polymer*, 2005, 46(9): 2889-2899.
- [50] Niu H, Lin T. Fiber generators in needleless electrospinning. *Journal of Nanomaterials*, 2012, 2012: 1-12.
- [51] Kim G H, Cho Y S, Kim W D. Stability analysis for multi-jets electrospinning process modified with a cylindrical electrode. *European Polymer Journal*, 2006, 42(9): 2031-2038.
- [52] Lukas D, Sarkar A, Pokorny P. Self-organization of jets in electrospinning from free liquid surface: a generalized approach. *Journal of Applied Physics*, 2008, 103(8): 084309(1-7).
- [53] Petrik S, Maly M. Production nozzle-less electrospinning nanofiber technology. MRS Proceedings. Cambridge University Press, 2009, 1240: 1240-WW03-07.
- [54] Yarin A L, Zussman E. Upward needleless electrospinning of multiple nanofibers. *Polymer*, 2004, 45(9): 2977-2980.
- [55] Xiao G, Li H, Li X, et al. Research progress of fluid differential electrostatic spinning nozzle design. *Journal of Textile Research*, 2014, 35(12): 153-158 (in Chinese).
- [56] Persano L, Camposeo A, Tekmen C, et al. Industrial upscaling of electrospinning and applications of polymer nanofibers: a review. *Macromolecular Materials and Engineering*, 2013, 298(5): 504-520.

- [57] Li H, Chen H, Zhong X, et al. Interjet distance in needleless melt differential electrospinning with umbellate nozzles. *Journal of Applied Polymer Science*, 2014, 131(15): 40515(1-8)
- [58] Li H Y, Bubakir M M, Xia T, et al. Mass production of ultra-fine fibre by melt electrospinning method using umbellate spinneret. *Materials Research Innovations*, 2014, 18(S4): 921-925.
- [59] Forward K M, Flores A, Rutledge G C. Production of core/shell fibers by electrospinning from a free surface. *Chemical Engineering Science*, 2013, 104: 250–259.
- [60] Jiang Q, Reddy N, Yang Y. Cytocompatible cross-linking of electrospun zein fibers for the development of water-stable tissue engineering scaffolds. *Acta Biomaterialia*, 2010, 6(10): 4042–4051.
- [61] Wei A, Wang J, Wang X, et al. Preparation and characterization of the electrospun nanofibers loaded with clarithromycin. *Journal of Applied Polymer Science*, 2010, 118(1): 346–352.
- [62] Nagy Z K, Balogh A, Drávavölgyi G, et al. Solvent-free melt electrospinning for preparation of fast dissolving drug delivery system and comparison with solvent-based electrospun and melt extruded systems. *Journal of Pharmaceutical Sciences*, 2013, 102(2): 508–517.
- [63] Wang C, Lu X F. High Voltage Electrospinning and Nanofibers. Science Press, 2011: 21. 31–48 (in Chinese)
- [64] Sarkar K, Gomez C, Zambrano S, et al. Electrospinning to forcespinning™. *Materials Today*, 2010, 13(11): 12–14.
- [65] Fang J, Zhang L, Sutton D, et al. Needleless melt-electrospinning of polypropylene nanofibres. *Journal of Nanomaterials*, 2012, 2012: 1-9.
- [66] Deng R, Liu Y, Ding Y, et al. Melt electrospinning of low-density polyethylene having a low-melt flow index. *Journal of Applied Polymer Science*, 2009, 114(1): 166–175.
- [67] Hao. M. F, Liu. Y, Deng. J. R, et, al. Researches on melt electrospinning of typical materials. *Engineering Plastics Application*, 2010, 38(3): 24–27 (in Chinese).
- [68] Ogata N, Shimada N, Yamaguchi S, et al. Melt-electrospinning of poly (ethylene terephthalate) and polyalirate. *Journal of Applied Polymer Science*, 2007, 105(3): 1127–1132.
- [69] Dasdemir M, Topalbekiroglu M, Demir A. Electrospinning of thermoplastic polyurethane microfibers and nanofibers from polymer solution and melt. *Journal of Applied Polymer Science*, 2013, 127(3): 1901–1908.
- [70] Kaur S, Sundarrajan S, Rana D, et al. Review: the characterization of electrospun nanofibrous liquid filtration membranes. *Journal of Materials Science*, 2014, 49(18): 6143–6159.

- [71] Scholten E, Bromberg L, Rutledge G C, et al. Electrospun polyurethane fibers for absorption of volatile organic compounds from air. *ACS Applied Materials & Interfaces*, 2011, 3(10): 3902–3909.
- [72] Graham K, Ouyang M, Raether T, et al. Polymeric nanofibers in air filtration applications. Fifteenth Annual Technical Conference & Expo of the American Filtration & Separations Society, Galveston, Texas. 2002: 9–12.
- [73] Heikkilä P, Taipale A, Lehtimäki M, et al. Electrospinning of polyamides with different chain compositions for filtration application. *Polymer Engineering & Science*, 2008, 48(6): 1168–1176.
- [74] Hung C H, Leung W W F. Filtration of nano-aerosol using nanofiber filter under low Peclet number and transitional flow regime. *Separation and Purification Technology*, 2011, 79(1): 34–42.
- [75] Yoon K, Kim K, Wang X, et al. High flux ultrafiltration membranes based on electrospun nanofibrous PAN scaffolds and chitosan coating. *Polymer*, 2006, 47(7): 2434–2441.
- [76] Aussawasathien D, Teerawattananon C, Vongachariya A. Separation of micron to sub-micron particles from water: electrospun nylon-6 nanofibrous membranes as pre-filters. *Journal of Membrane Science*, 2008, 315(1): 11–19.
- [77] Yoon K, Hsiao B S, Chu B. Formation of functional polyethersulfone electrospun membrane for water purification by mixed solvent and oxidation processes. *Polymer*, 2009, 50(13): 2893–2899.
- [78] Gopal R, Kaur S, Feng C Y, et al. Electrospun nanofibrous polysulfone membranes as pre-filters: Particulate removal. *Journal of Membrane Science*, 2007, 289(1): 210–219.
- [79] Lemma S M, Esposito A, Mason M, et al. Removal of bacteria and yeast in water and beer by nylon nanofibrous membranes. *Journal of Food Engineering*, 2015, 157: 1–6.
- [80] Sato A, Wang R, Ma H, et al. Novel nanofibrous scaffolds for water filtration with bacteria and virus removal capability. *Journal of Electron Microscopy*, 2011,60(3:201-209)
- [81] Luu Y K, Kim K, Hsiao B S, et al. Development of a nanostructured DNA delivery scaffold via electrospinning of PLGA and PLA-PEG block copolymers. *Journal of Controlled Release*, 2003, 89(2): 341–353.
- [82] Schiffman J D, Schauer C L. A review: electrospinning of biopolymer nanofibers and their applications. *Polymer Reviews*, 2008, 48(2): 317–352.
- [83] Teo W E, Ramakrishna S. A review on electrospinning design and nanofibre assemblies. *Nanotechnology*, 2006, 17(14): R89.

- [84] Casper C L, Stephens J S, Tassi N G, et al. Controlling surface morphology of electrospun polystyrene fibers: effect of humidity and molecular weight in the electrospinning process. *Macromolecules*, 2004, 37(2): 573–578.
- [85] Shin S H, Purevdorj O, Castano O, et al. A short review: recent advances in electrospinning for bone tissue regeneration. *Journal of Tissue Engineering*, 2012, 3(1): 2041731412443530(1-11).
- [86] Kidoaki S, Kwon I K, Matsuda T. Mesoscopic spatial designs of nano-and microfiber meshes for tissue-engineering matrix and scaffold based on newly devised multi-layering and mixing electrospinning techniques. *Biomaterials*, 2005, 26(1): 37–46.
- [87] Thorvaldsson A, Stenhamre H, Gatenholm P, et al. Electrospinning of highly porous scaffolds for cartilage regeneration. *Biomacromolecules*, 2008, 9(3): 1044–1049.
- [88] Lourdes M C M, Hutmacher Dietmar W, Dalton Paul D. Melt electrospinning and its technologization in tissue engineering. *Tissue Engineering Part B: Reviews*, 2015, 21(2): 187-202
- [89] Kenawy E R, Abdel-Hay F I, El-Newehy M H, et al. Processing of polymer nanofibers through electrospinning as drug delivery systems. *Materials Chemistry and Physics*, 2009, 113(1): 296–302.
- [90] Pham Q P, Sharma U, Mikos A G. Electrospinning of polymeric nanofibers for tissue engineering applications: a review. *Tissue Engineering*, 2006, 12(5): 1197–1211.
- [91] Ignatious F, Sun L, Lee C P, et al. Electrospun nanofibers in oral drug delivery. *Pharmaceutical Research*, 2010, 27(4): 576–588.
- [92] Schreuder-Gibson H, Gibson P, Senecal K, et al. Protective textile materials based on electrospun nanofibers. *Journal of Advanced Materials*, 2002, 34(3): 44–55.
- [93] Pant H R, Bajgai M P, Nam K T, et al. Electrospun nylon-6 spider-net like nanofiber mat containing TiO₂ nanoparticles: a multifunctional nanocomposite textile material. *Journal of Hazardous Materials*, 2011, 185(1): 124–130.
- [94] Lee S. Developing UV-protective textiles based on electrospun zinc oxide nanocomposite fibers. *Fibers and Polymers*, 2009, 10(3): 295–301.
- [95] Rose M, Boehringer B, Jolly M, et al. MOF processing by electrospinning for functional textiles. *Advanced Engineering Materials*, 2011, 13(4): 356–360.
- [96] Lee S, Kay Obendorf S. Developing protective textile materials as barriers to liquid penetration using melt-electrospinning. *Journal of Applied Polymer Science*, 2006, 102(4): 3430–3437.
- [97] Heikkilä P, Sipilä A, Peltola M, et al. Electrospun PA-66 coating on textile surfaces. *Textile Research Journal*, 2007, 77(11): 864–870.

- [98] Bagherzadeh R, Latifi M, Najar S S, et al. Transport properties of multi-layer fabric based on electrospun nanofiber mats as a breathable barrier textile material. *Textile Research Journal*, 2012, 82(1): 70–76.
- [99] Yan S, Jian G, Zachariah M R. Electrospun nanofiber-based thermite textiles and their reactive properties. *ACS Applied Materials & Interfaces*, 2012, 4(12): 6432–6435.
- [100] Moran-Mirabal J M, Slinker J D, DeFranco J A, et al. Electrospun light-emitting nanofibers. *Nano Letters*, 2007, 7(2): 458–463.
- [101] Gheibi A, Latifi M, Merati A A, et al. Piezoelectric electrospun nanofibrous materials for self-powering wearable electronic textiles applications. *Journal of Polymer Research*, 2014, 21(7): 1–7.
- [102] Slater J M, Paynter J, Watt E J. Multi-layer conducting polymer gas sensor arrays for olfactory sensing. *Analyst*, 1993, 118(4): 379–384.
- [103] Savage N, Chwieroth B, Ginwalla A, et al. Composite n–p semiconducting titanium oxides as gas sensors. *Sensors and Actuators B: Chemical*, 2001, 79(1): 17–27.
- [104] Unde S, Ganu J, Radhakrishnan S. Conducting polymer-based chemical sensor: Characteristics and evaluation of polyaniline composite films. *Advanced Materials for Optics and Electronics*, 1996, 6(3): 151–157.
- [105] Sheng L, Dajing C, Yuquan C. A surface acoustic wave humidity sensor with high sensitivity based on electrospun MWCNT/Nafion nanofiber films. *Nanotechnology*, 2011, 22(26) : 265504-265504.
- [106] Modafferi V, Panzera G, Donato A, et al. Highly sensitive ammonia resistive sensor based on electrospun V₂O₅ fibers. *Sensors and Actuators B: Chemical*, 2012, 163(1): 61–68.
- [107] Yang M, Xie T, Peng L, et al. Fabrication and photoelectric oxygen sensing characteristics of electrospun Co doped ZnO nanofibres. *Applied Physics A*, 2007, 89(2): 427–430.
- [108] Wang X, Drew C, Lee S H, et al. Electrospun nanofibrous membranes for highly sensitive optical sensors. *Nano Letters*, 2002, 2(11): 1273–1275.
- [109] Hu G, Zhou Z, Guo Y, et al. Electrospun rhodium nanoparticle-loaded carbon nanofibers for highly selective amperometric sensing of hydrazine. *Electrochemistry Communications*, 2010, 12(3): 422–426.
- [110] Li D, McCann J T, Xia Y. Use of electrospinning to directly fabricate hollow nanofibers with functionalized inner and outer surfaces. *Small*, 2005, 1(1): 83–86.
- [111] Ding B, Wang M, Wang X, et al. Electrospun nanomaterials for ultrasensitive sensors. *Materials Today*, 2010, 13(11): 16–27.

Variance Analysis and Autocorrelation Function for 2D Fiber Lap Statistical Analysis

Jean-Yves Drean and Omar Harzallah

Additional information is available at the end of the chapter

<http://dx.doi.org/10.5772/61795>

Abstract

This chapter reports on the statistical analysis of 2D fiber lap using variance analysis and autocorrelation function. It begins with a short overview of the nonwoven processes showing the importance of lap and web formation. It then proceeds to describe the theory of the ideal fiber web. The real defects are taken into account based on random irregularity, periodic irregularity, and compound irregularity. To conclude, the chapter highlights the efficiency of this theoretical approach and its application on 2D fibrous material.

Keywords: Fiber lap, fiber web, textile processes, statistical analysis, variance analysis, autocorrelation

1. Introduction

Textile and nonwoven industries are fiber-based industries. They use both continuous fibers as filament yarns and/or short fibers as staple fibers. During the manufacturing processes, these fibers, very thin 1D elements, are transformed in oriented or random 2D laps or webs. Then, these products are converted in 1D end product as staple yarns or 2D end products as woven or knitted fabrics or nonwoven fabrics. The physical and mechanical properties of these end products strongly depend on the regularity of laps or webs. Therefore, an accurate knowledge of the web and lap formation as well as the associated theoretical approach are absolutely necessary.

2. Textile processes

The classical textile spinning process is based on Figure 1. First of all, staple fibers highly compacted in form of bales are opened with the help of a bale opening line. Moving through a coarse and a fine opener, the size of fiber tufts is reduced to be able to feed the carding machine chute. The chute delivers a lap of fibers to the carding machine feed rolls.

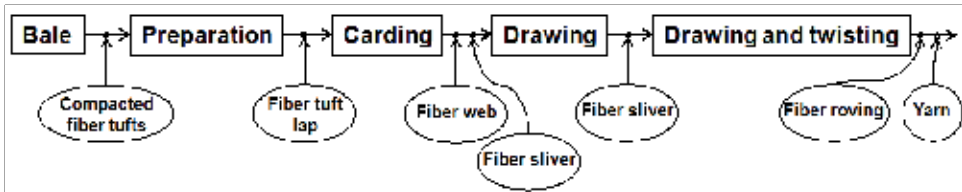


Figure 1. Scheme of classical textile process

In a second time, the carding machine, as shown in Figure 2, individualizes the fibers tufts and delivers the fibers in the form of a web. The web is then condensed in a form of sliver.

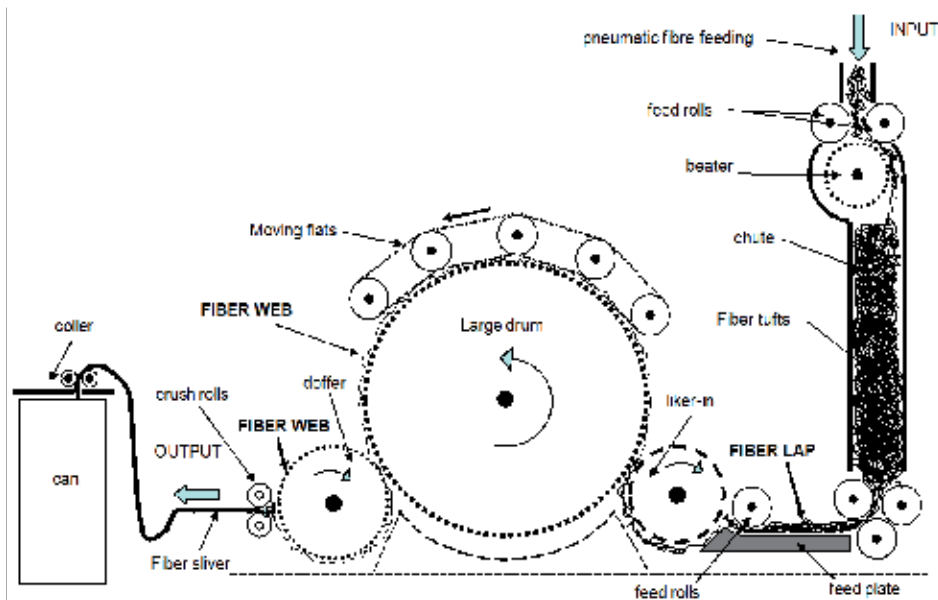


Figure 2. Carding machine

The sliver goes through a drawing frame and a roving frame which produces slivers which are drawn and twisted on a spinning machine, that is, ring spinning frame. The quality of the final product strongly depends on the efficiency of the carding operation. It can be noticed that this efficiency is strongly correlated to the quality and the evenness of both the fed lap and

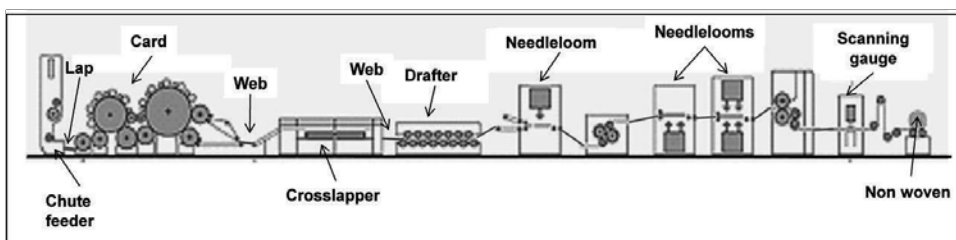


Figure 3. Drylaid needle-punched nonwoven line (Doc. ANDRITZ)

delivered web. An exact knowledge of the quality of these 2D textiles is absolutely necessary [1,16,17].

3. Nonwoven processes

Nonwoven materials can be considered as “**sheet or web** structures bonded together by entangling fibers or filaments, by various mechanical, thermal and/or chemical processes. These are made directly from separate fibers or from molten plastic or plastic film [1]” or as “a manufactured sheet, **web or mat** of directionally or randomly orientated fibers, bonded by friction, and/or cohesion and/or adhesion, excluding paper and products which are woven, knitted, tufted, stitch-bonded incorporating binding yarns of filaments, or felted by wet-milling, whether or not additionally needled [2]”. As above defined, the web formation is a very important part of the nonwoven processes.

Nonwoven production systems are normally based on deposition or laying the fiber material or extruded thermoplastic polymers on a forming or conveying surface. The physical environment at this phase can be dry, quenched in air, wet, or molten – drylaid, wetlaid, or spun [3].

3.1. Nonwoven formation

In a general point of view, there are three main methods for nonwoven forming:

- The drylaid system with carding or airlaying
- The wetlaid system
- The polymer-based system, which includes spunlaying (spunbonding) or specialized technologies like meltblown, or flashspun fabrics [4]

The following chapter presents a non-exhaustive overview of a nonwoven manufacturing process.

3.2. Drylaid nonwoven

The drylaid nonwoven process consists in fiber preparation, web formation, web bonding, and stabilization (Figure 4).

The fiber preparation is close to classical textile industry staple fiber preparation including bale opening, blending, coarse, and fine opening. Then the web forming machine is fed with the help of a chute in case of short staple fibers or with the help of a hopper in case of long staple fibers. The fibers fed by a chute or hopper condensed into the form of a lap are introduced into a carding machine. The carding machine separates fibers, starts the process of individualization, and delivers the fibers in the form of a web [24,25].

The web is then formed into the desired web structure by layering the webs extracted from the carding machine. Based on the final chosen weight and web structure, the layering can be completed by using longitudinal layering, cross layering, or perpendicular layering.

Web strengthening can be done mechanically with the help of needle punching which consists in bonding nonwoven web by mechanically interlocking the fibers through the web using barbed needles (Figure 4), with the help of stitch bonding which consists in consolidating fiber webs using knitting elements or with the help of hydro-entanglement which consists in locking the fibers together using fine high pressure water jets directed across the web.

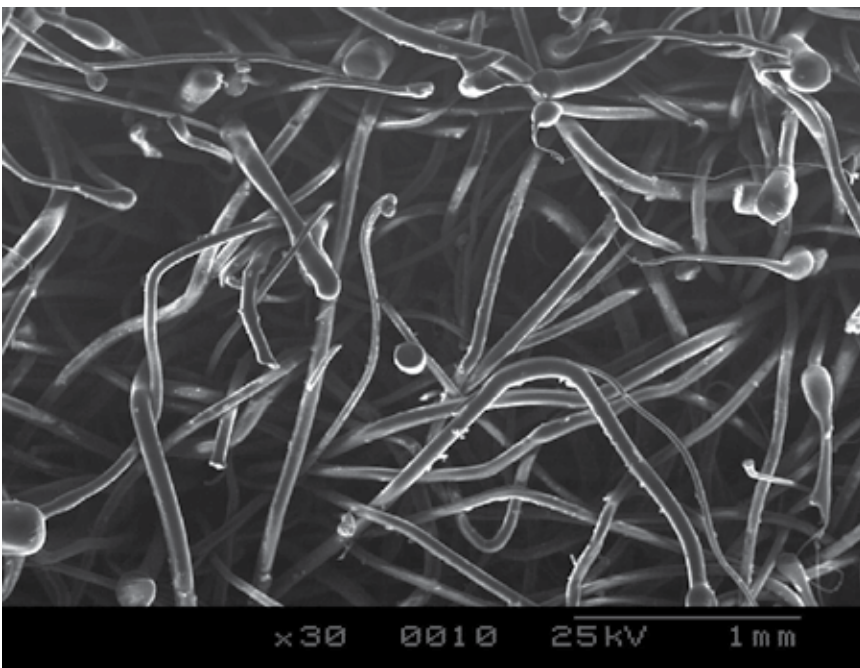


Figure 4. SEM photomicrograph of needle-punched nonwoven (natural and synthetic fibers)

Mechanical bonding can be replaced with web chemical bonding which consists in applying the chemical binder to the web and curing it.

In case of thermoplastic and thermostable fiber blend web, the strengthening can be achieved by thermal bonding.

3.3. Wetlaid nonwovens

This method relates to paper-based nonwoven fabrics which are manufactured by suspending short length fibers in water and pumping the suspension over a moving mesh in order to form a fibrous **web** [3].

Figure 5 is a schematic illustration of wetlaid technique. The blades of a very strong mixer transform fibers, wood pulp, and water to a perfect slurry suspension. Webformer deposits the suspension over the screen, and depending on the application of nonwoven, it will pass through a suitable bonding stage. Finally, nonwoven will be dried and wound up.

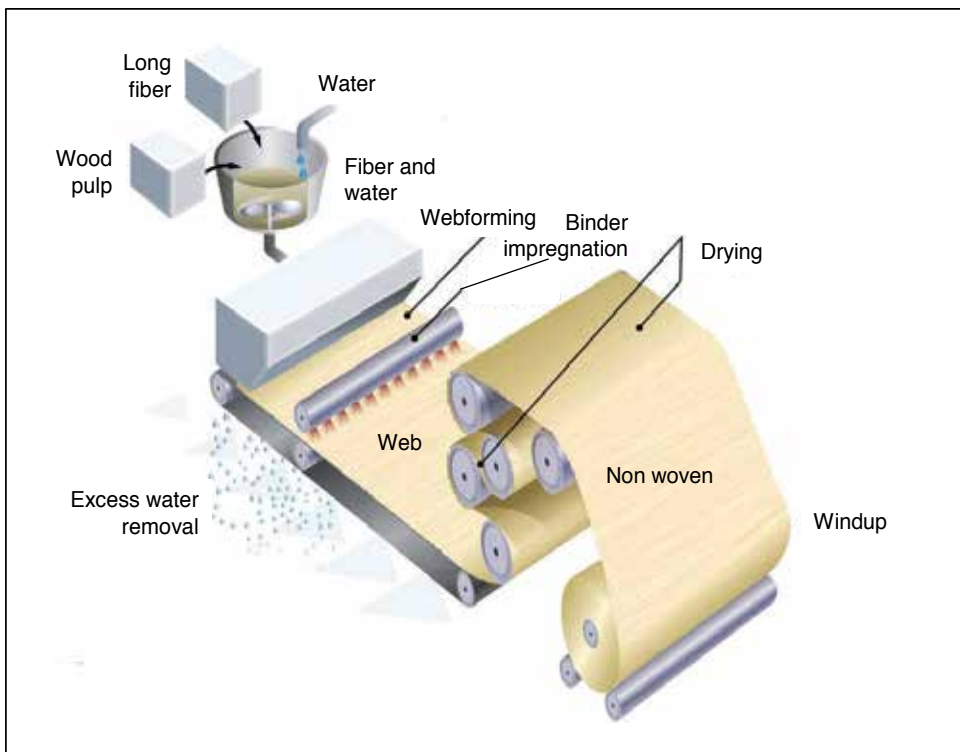


Figure 5. Wetlaid web formation [www.edana.org]

All fibers which are dispersible in fluids and do not dissolve can be transformed into a **web** form by using the wetlaid method. One of the main advantages of the wetlaid method is a very good product homogeneity due to the very good homogeneity of the **web**.

3.4. Meltblown nonwoven

As mentioned before, the meltblown process belongs to the general category of polymer-laid nonwoven material. It has been defined as below:

“Meltblowing is a process in which, usually, a thermoplastic fiber forming polymer is extruded through a linear die containing several hundred small orifices. Convergent streams of hot air (exiting from the top and bottom sides of the die nosepiece) rapidly attenuate the extruded polymer streams to form extremely fine diameter fibers (1–5 μm). The attenuated fibers are subsequently blown by high-velocity air onto a collector conveyor, forming a fine fibered self-bonded nonwoven meltblown **web** [1,4].” Figure 6 shows the schematic illustration of meltblown process.

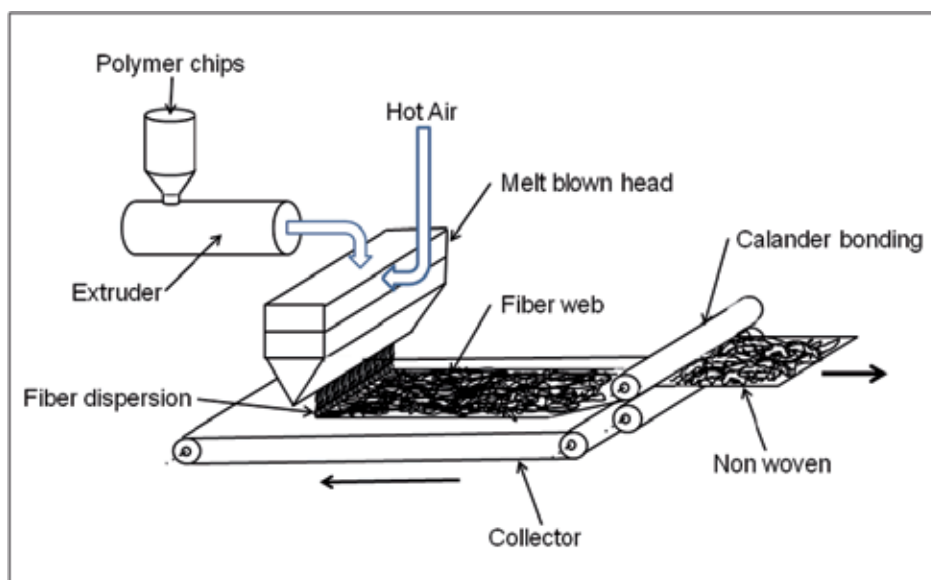


Figure 6. Meltblowing process; primary and secondary air flow and web formation

The main force that holds meltblown fibers together in a nonwoven structure is a combination of entanglement and cohesive sticking. Nonwoven produced by meltblown method have low to moderate strength. During the process, the fibers are drawn to their final diameters while still in the semi-molten state; there is no downstream method of drawing the fibers before they are deposited onto the collector, and this is the reason of moderate mechanical properties of meltblown nonwovens (Figure 7).

All the above-described processes are based on fibers and fibrous laps or webs. The characteristics of the web are determined by the mode of web formation which is related to web geometry. This web geometry takes into account fiber orientation (oriented or random), type of bonding, crimp, mass per unit area, and weight evenness and distribution.

The knowledge of the web geometry is very important because physical and mechanical properties are directly related to it. For instance, as far as geotextile properties are concerned, separation, reinforcement, stabilization, filtration, and drainage are related to the mass per unit area and the distribution of mass per unit area [5,23].

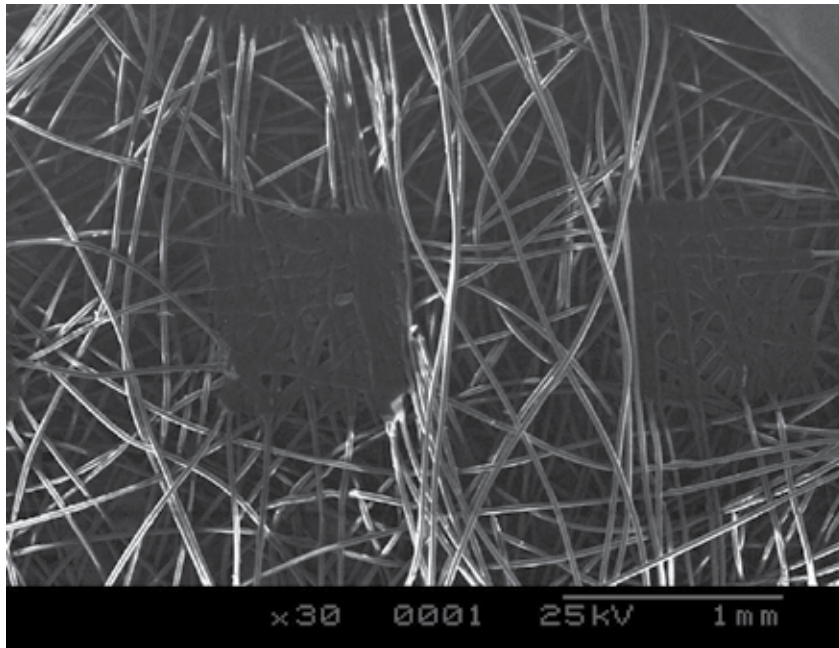


Figure 7. SEM photomicrograph of heat bonded meltblown nonwoven

The following paragraphs will present a theoretical approach of an ideal fiber web. This theoretical approach will simulate the real faults of the fiber-web forming-step during the industrial process, random irregularity, periodic irregularity, and compound irregularity.

4. Theoretical approach

4.1. The ideal fibrous web

In this chapter, the fiber web is split into several macro sample-elements; these elements have the same area A (Figure 8). The fiber web element area A is defined as the sum of fiber micro-strand da with $A = n \cdot da$, where n is the number of micro-elements in the macro-fiber-sample.

The width L of the macro-web-element is considered constant. Its length is $l = \frac{A}{L}$ called cut length. Then, we suppose that $da = L \cdot dt$, where dt is the length of the fibrous micro-element located at the distance t from the strand origin. The abscissa origin 0 is located in the middle of the fiber web [6,7,8,9,26].

We assume that $\mu = \left(\frac{m}{da}\right)$ as the fiber strand area density of the fiber web (web manufactured by the textile machines); m is defined as the micro-elementary fiber-strand-mass. In this theory, the two random variables related to the cutting length l are μ and a , where μ can be described with the help of the usual statistical parameters as the mean and the variance [10,11].

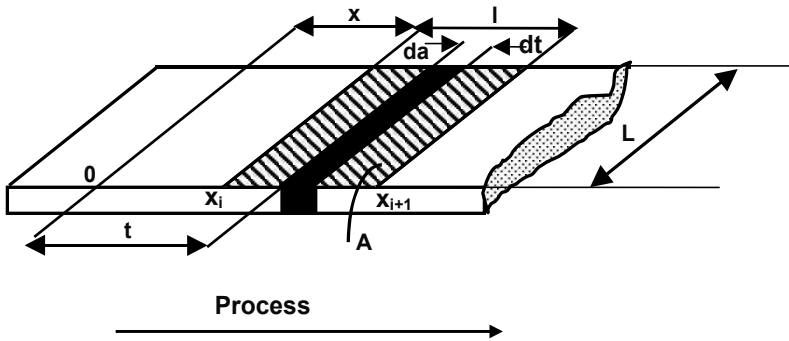


Figure 8. Scheme of an ideal fiber web

The unevenness of the area density of the fiber web can be characterized by the above-mentioned dispersion parameters which give an approach of the overall irregularity. The overall variance is denoted by the following limit conditions:

$$A \rightarrow \infty \quad \text{and} \quad da \rightarrow 0$$

$$n \rightarrow \infty$$

When the limits are taken, the variation coefficient of the fiber web and the overall variance can be written, respectively, as follows:

$$CV(0, \infty) = CV(\infty)$$

$$V(0, \infty) = V(\infty)$$

Taking into account that these values are not directly measurable, an estimation of the values can be calculated by extrapolation. Based on previous studies, [12,13,14,15,27], the mean and overall variance can be estimated as follows:

$$\bar{\mu}_i = \frac{\sum \mu_i}{n} = \frac{M}{A} \tag{1}$$

where M is the web-element-mass

and

$$\sigma_{\mu_i}^2 = \frac{\sum (\mu_i - \bar{\mu}_i)^2}{n} \tag{2}$$

4.2. $B(A)$ and $CB(A)$ functions

Let $B(A)$ be the variance between areas density of the i^{th} macro-fibrous-element. Also, we define the macro-fiber-area density $\mu(x, A)$, where A is the mean value of the surface element and x is the abscissa (location of the element) [14,15,28,29].

$$\int_{y_0}^{y_0+L} \int_{x_0}^{x_0+A/L} \mu(x, y) dx dy = m(l, L) \tag{3}$$

We designate $E(\mu)$ as the average of the random variable $\mu(x, y)$; where E is the symbol of the mathematical expectation. $E(\mu) = E(\mu(x, y))$ can also be written as follows:

$$E(\mu(x, y)) = E \left[\int_{x_0}^{x_0+A/L} \int_{y_0}^{y_0+L} \mu(x, y) dx dy \right] \tag{4}$$

and based on the properties of the E operator:

$$E[m(l, L)] = \int_{x_0}^{x_0+A/L} \int_{y_0}^{y_0+L} E[\mu(x, y)] dx dy = l \cdot L \cdot E[\mu(x, y)] = A \cdot E[\mu(x, y)] \tag{5}$$

In the framework of this theory, the $B(A)$ variance between areas density is described by the second order moment as follows:

$$B[m(l, L)] = E[m(l, L) - E(\mu(l, L))]^2 \tag{6}$$

When Equation (5) is substituted into Equation (6), we obtain the following relationship:

$$B[m(l, L)] = E \left[\int_{x_0}^{x_0+A/L} \int_{y_0}^{y_0+L} (\mu(x, y) - E(\mu(x, y))) dx dy \right]^2 = E \left[\int_{x_0}^{x_0+A/L} \int_{y_0}^{y_0+L} \mu_c(x, y) dx dy \right]^2 \tag{7}$$

where $\mu_c(x, y) = \mu(x, y) - E(\mu(x, y))$

Then we set $u = \xi - x$ and $v = \eta - y$. The $B(A)$ function can be converted into a double integral assuming independence of position variables u and v . So, the $B(A)$ function can be written as follows:

$$B(A) = E \left[\int_{x_0}^{x_0+A/L} \int_{y_0}^{y_0+L} \int_{x_0}^{x_0+A/L} \int_{y_0}^{y_0+L} \mu_c(x, y) \mu_c(\xi, \eta) dx dy d\xi d\eta \right] \tag{8}$$

If we consider the two random functions $[\mu(x, y) - E(\mu(x, y))]$ and $[\mu(\xi, \eta) - E(\mu(\xi, \eta))]$, the Γ covariance function can be defined as follows:

$$\Gamma(u, v) = E\left[\left(\mu(x, y) - E(\mu(x, y))\right) \cdot \left(\mu_c(x + u, y + v) - E(\mu_c(x + u, y + v))\right)\right] \quad (9)$$

Hence $\Gamma(0, 0) = E[\mu(x, y) - E(\mu(x, y))]^2 = V[\mu(x, y)]$.

This allows showing that the covariance of the random variable $\mu(x, y)$ is a stationary random variable of second order [18,26]. In this case, the covariance is only depending on the difference of positions $(v + x)$ and on $(w + x)$:

$$(v + x) - (w + x) = v - w \quad (10)$$

Moreover, this covariance is an even function having the following property:

$$\Gamma(v - w) = \Gamma(w - v) \quad (11)$$

So, the new $B(A)$ equation can be defined as follows:

$$B[m(l, L)] = \int_{x=0}^{L/2} \int_{y=0}^L \int_0^{L/2} \int_0^L \Gamma(u, v) dv dw \quad (12)$$

The covariance is only a function of u where $u = v - w$; thus $B(A)$ can be reduced to a simple integral [27]. Thereby, the covariance function $B(A)$ can be rewritten in the following form:

$$B(A) = 2 \cdot \frac{L^2}{A^2} \int_0^{A/2} \int_0^L \Gamma(u, v) \cdot \left(\frac{A}{L} - u\right) du dv \quad (13)$$

Let us now introduce the autocorrelation function [21]:

$$\rho(u, v) = \frac{\Gamma(u, v)}{\Gamma(0, 0)} \quad (14)$$

Hence, a new form of the variance between areas density $B(A)$ can be expressed as follows:

$$B(A) = 2\Gamma(0) \cdot \frac{L^2}{A^2} \int_0^{A/2} \rho(u) \cdot \left(\frac{A}{L} - u\right) du \quad (15)$$

Then, let us use the initial function $B(A) = E[\mu(x, A) - E(\mu(x, A))]^2$ to estimate $B(0)$.

In the interval $[x_i, x_{i+1}]$ shown in Figure 1, if $\frac{A}{L} \rightarrow 0$, then $\mu(x, A) \rightarrow \mu(t)$. This means that the punctual area density is given by the following equation:

$$B(0) = E[\mu(t) - E(\mu(t))]^2 = V[\mu(t)] = \sigma_{\mu_i}^2 \tag{16}$$

$\sigma_{\mu_i}^2$ representing the overall variance of the fiber-web-element.

Finally, $B(A)$ can be written as follows:

$$B(A) = 2B(0) \cdot \frac{L^2}{S^2} \int_0^{S/L} \left(\frac{S}{L} - u\right) \rho(u) du \tag{17}$$

We designate $CB(A)$ as the variation coefficient associated to the between-area-density variance $B(A)$. Therefore:

$$CB^2(A) = \frac{B(A)}{E(\mu)^2} = \frac{2 \cdot CV_{\mu_i}^2}{\frac{A}{L}} \int_0^{A/L} \left(\frac{A}{L} - u\right) \rho(u) du \tag{18}$$

and $CV_{\mu}^2 = \frac{\sigma_{\mu_i}^2}{E(\mu)^2}$ called the overall variation coefficient of the fiber web.

5. Discussion

5.1. Random irregularity

The fiber flocks length distribution is always considered of a great importance for textile laps and web processing. Nowadays, it is still a source of statistical interpretations more or less empirical, such as cumulative frequency diagram.

In the following part, the cumulative frequency function $q(\ell)$ of the fiber length ℓ is calculated by taking into account the shape of the most common distributions as isoprobable, equiprobable, and uniform distributions.

Based on textile sciences, these diagrams are usually represented by permuting the coordinated axes, that is, by plotting the value of the fiber length ℓ in the ordinate and $q(\ell)$ in abscissa, as shown in Table 1.

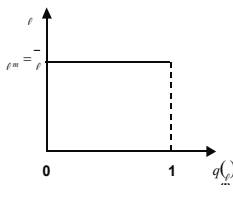
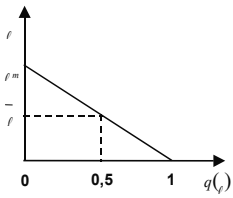
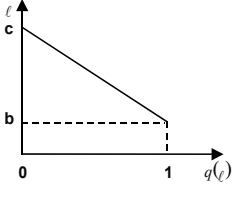
	Isoprobable distribution	Equiprobable distribution	Uniform distribution
Cumulative frequency diagram of the fiber length			
Mean length of fiber web flock	$\bar{\ell} = \ell_m = \ell$	$\bar{\ell} = \frac{\ell_m}{2}$	$\bar{\ell} = \frac{c+b}{2}$
Autocorrelation function: $\rho(u) = \frac{1}{\bar{\ell}} \cdot \int_u^{\ell_m} q(\ell) \ell d\ell$			
$\frac{S}{L} = I \leq \ell_m$	$\rho(u) = 1 - \frac{u}{\bar{\ell}}$	$\rho(u) = \left(1 - \frac{u}{2\bar{\ell}}\right)^2$	$\frac{A}{L} = I \leq b$; $\rho(u) = 1 - \frac{u}{\bar{\ell}}$ $b < \frac{A}{L} = I \leq c$; $\rho_2(u) = \frac{(c-u)^2}{c^2 - b^2}$
$\frac{A}{L} = I \geq \ell_m$	0	0	0

Table 1. Diagrams of distribution

The usual empirical criterion for the quality estimation of the fiber web is based on the shape of the diagram. If all fiber flocks have the same length $\ell = \ell_m = \bar{\ell}$ and same m mass, the diagram of cumulative frequency would obviously be a rectangle (Table 1); $\bar{\ell}$ and ℓ_m being, respectively, the mean and the maximum flock fiber length. This type of distribution is designated as “isoprobable”. In case of a cumulative frequency of length distribution triangular shape, the distribution is considered an equiprobable distribution. Such a shape shows the presence of a linear unevenness of length. The combination the two previous distributions leads to define a new third distribution called “uniform”. In this distribution, the fiber length decreases linearly between two values b and c as shown in Table 1. Considering the three above-described distributions, the calculated mean lengths are given in Table 1 and are, respectively, mathematically expressed as follows:

$$\begin{aligned} \bar{\ell} &= \ell_m \\ \bar{\ell} &= \frac{\ell_m}{2} \text{ and} \\ \bar{\ell} &= \frac{c+b}{2}. \end{aligned}$$

Based on the shape of the diagram of cumulative frequency, the function $q(\ell)$ can be defined. On the other hand, the autocorrelation function $\rho(\ell=u)$ of the fiber flocks is given by the following equation:

$$\rho(u) = \frac{1}{\ell} \cdot \int_{\ell=u}^{\ell_m} q(\ell) d\ell \tag{19}$$

where ℓ_m is the length of the longest fiber flocks.

It can be highlighted that the autocorrelation function is a double integration of the histogram (frequency distribution function) of a fiber web numerical sample.

The cumulative frequency function $q(\ell)$ and the autocorrelation function exist only if the cut length of a fibrous web $l = \frac{A}{L}$ is small, that is, $l \leq \ell_m$ as clearly shown in Table 1. Otherwise if $\frac{A}{L} = l$ is large, $l \geq \ell_m$, we can demonstrate easily that $\rho(u) = 0$. Considering these parameters, the between-area-density variance $B(A)$ can be calculated using the following equation, if $l \leq \ell_m$:

$$B(A) = \frac{2B(0)}{l^2} \int_0^l (l-u) \cdot \rho(u) du \tag{20}$$

While, if $\frac{A}{L} = l$ is large, $l \geq \ell_m$, we have $\rho(u) = 0$. The function $B(A)$ takes the following expression:

$$B(A) = B(0) \left[1 - \frac{2}{l^2} \int_0^{\ell_m} (l-u) \cdot (1-\rho(u)) du - \frac{2}{l^2} \int_{\ell_m}^l (l-u) du \right] \tag{21}$$

Then $B(A)$ and $CB^2(A)$ can be normalized:

$$\beta(A) = \frac{B(A)}{B(0)} = \frac{CB^2(A)}{CB^2(0)} \tag{22}$$

with $CB^2(A) = \frac{B(A)}{E(\mu)^2}$

For a fiber web having the **isoprobable distribution** of the fiber flocks, the normalized between-area-density variance $\beta(A)$ takes the following expressions:

$$\text{if } l \leq \ell_m \quad \beta(A) = \frac{B(A)}{B(0)} = \frac{CB^2(A)}{CB^2(0)} = \left[1 - \frac{l}{3\ell} \right] \tag{23}$$

$$\text{if } l \geq \ell_m \quad \beta(A) = \frac{B(A)}{B(0)} = \frac{CB^2(A)}{CB^2(0)} = \left[\frac{\bar{\ell}}{l} - \frac{\bar{\ell}^2}{3l^2} \right] \tag{24}$$

The difference between a “short” and a “long” fiber web element is shown by the diagrams of $\beta(A)$ in Figures 9 and 10. In case of $l \leq \ell_m$, the functions $B(A)$ and $CB^2(A)$ present straight segments in the interval $[0, \ell_m]$ as mentioned in Figures 9 and 10. The slope $\beta(A)$ curve at the origin is $-\frac{1}{3\ell}$. It can be noticed that the two branches of the $\beta(A)$ graph are connected to point B coordinates $(\ell, \frac{2}{3})$.

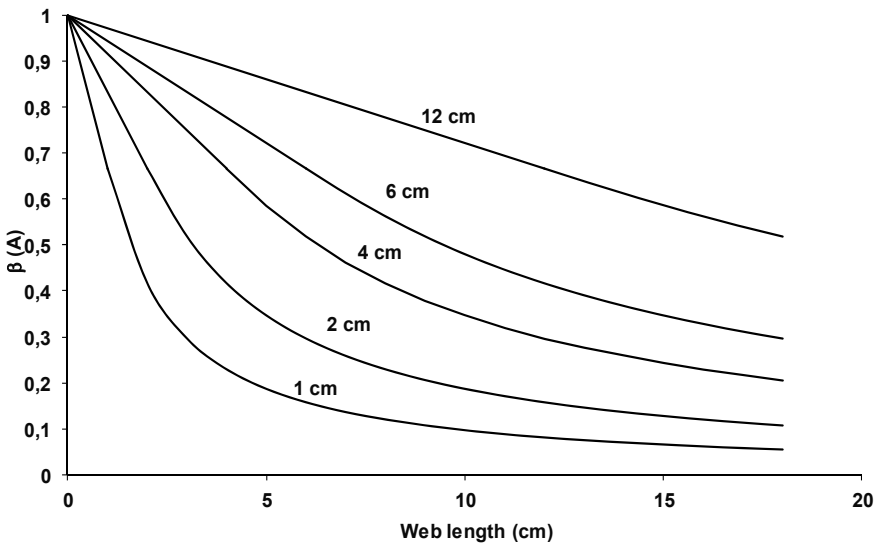


Figure 9. Short-term irregularity – between-area-density variance vs. fiber web length: Case of length isoprobable distribution

Otherwise, for the **equiprobable distribution**, the corresponding diagram has a triangular shape (see Table 1). By a similar calculation to the previous we obtain two expressions for $\beta(A)$:

$$\text{if } 0 \leq l \leq \ell_m \quad \beta(A) = \frac{B(A)}{B(0)} = \frac{CB^2(A)}{CB^2(0)} = \left[1 - \frac{l}{3\ell} + \frac{l^2}{24\ell^2} \right] \tag{25}$$

$$\text{if } l > \ell_m \quad \beta(A) = \frac{B(A)}{B(0)} = \frac{CB^2(A)}{CB^2(0)} = \left[\frac{4\bar{\ell}}{3l} - \frac{2\bar{\ell}^2}{3l^2} \right] \tag{26}$$

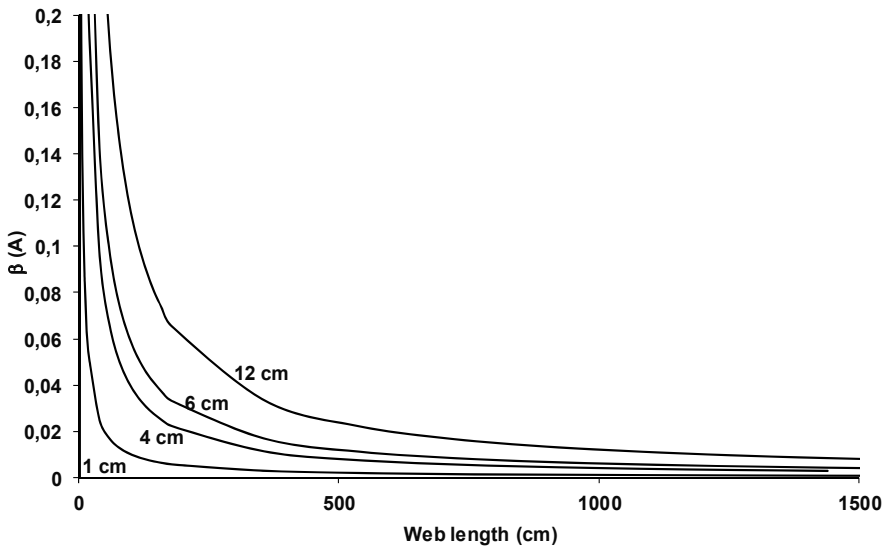


Figure 10. Long-term irregularity – between-area-density variance vs. fiber web length: Case of length isoprobable distribution

It can be noticed that the graph of $\beta(A)$ related to the equiprobable distribution is always above the one corresponding to the associated isoprobable distribution for the same ℓ (Figure. 11).

Finally, the $q(\ell)$ **uniform distribution** that has a trapezoidal shape (Table 1) has the mean and the variation coefficient respectively expressed [22] as follows:

$$\bar{\ell} = \frac{c+b}{2} \text{ and } CV\% = \frac{100}{\sqrt{3}} \cdot \left(\frac{c-b}{c+b} \right) \quad (27)$$

It can be noticed that if $b=c=\ell$ the distribution is isoprobable, then if $b=0$ and $c=2\ell$ the distribution is equiprobable.

In this case of uniform distribution, the cumulative frequency function and the autocorrelation function have, respectively, the following expressions:

$$\begin{aligned} &\text{if } 0 \leq \frac{A}{L} = l \leq b, q_1(\ell) = 1 \text{ hence:} \\ \rho_1(u) &= \frac{1}{\ell} \int_l^{\ell_m=c} q(u) du = \frac{1}{\ell} \int_l^b q_1(u) du + \frac{1}{\ell} \int_b^c q_2(u) du \end{aligned} \quad (28)$$

After integration $\rho_1(u)$ becomes:

$$\rho_1(u) = 1 - \frac{l}{\ell} \quad (29)$$

$$\text{if } b < A/L = l \leq c, q_2(u) = \left(\frac{c-l}{c-b}\right) \text{ hence:} \tag{30}$$

$$\rho_2(u) = \frac{1}{\ell} \int_l^{m=c} q(u) du = \frac{(c-l)^2}{c^2 - b^2}$$

$$\text{if } A/L > c, q_3(\ell) = 0, \text{ hence :} \tag{31}$$

$$\rho_3(u) = \frac{1}{\ell} \int_a^\infty q(u) du = 0$$

According to the values of A/L , $\beta(A)$ takes the following expressions [28,29]:

$$\text{if } 0 \leq A/L = l \leq b \quad \beta(A) = \left[1 - \frac{l}{3\ell} \right] \tag{32}$$

$$\text{if } b < A/L = l \leq c \quad \beta(A) = \frac{2}{l^2} \cdot \left[\frac{lcb}{2\ell} - \frac{b^2(3c-b)}{12\ell} + \frac{(c-b)^3}{24\ell} \left(\left(\frac{c-l}{c-b}\right)^4 - 4\left(\frac{c-l}{c-b}\right) + 3 \right) \right] \tag{33}$$

$$\text{if } A/L > c \quad \beta(A) = \frac{2}{l^2} \cdot \left[l \frac{(c^2 + b^2 + cb)}{6\ell} - \frac{(c+b)(c^2 + b^2)}{24\ell} \right] \tag{34}$$

As shown in Figure 12, if $0 \leq A/L = l \leq b$, the functions $B(A)$ and $C B^2(A)$ present straight segments in the interval $[0, b]$. The slope of $\beta(A)$ curve at the origin is $-\frac{1}{3\ell}$. Based on this figure, we can note that if b/c is low while the flocks length variation coefficient is high, the slope of $\beta(A)$ decreases more slowly.

Considering the three above-described distributions, the random unevenness varies with the variation of the fibrous web length and as shown is Figures 9 and 10, if l increases, $\beta(A)$ decreases.

This can be explained by a greater possibility of compensating local irregularities in case of longer surfaces of fiber web. Normally, the $\beta(A)$ fiber web curve has a decreasing course, tending toward zero for $l \rightarrow \infty$.

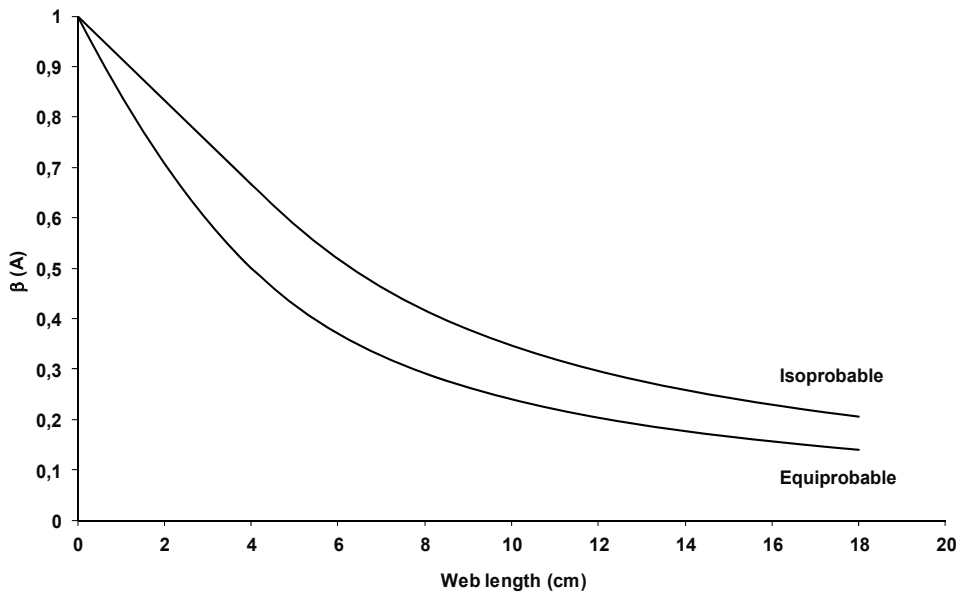


Figure 11. Comparison between the $\beta(A)$ curves of the isoprobable and equiprobable distributions for the same length l

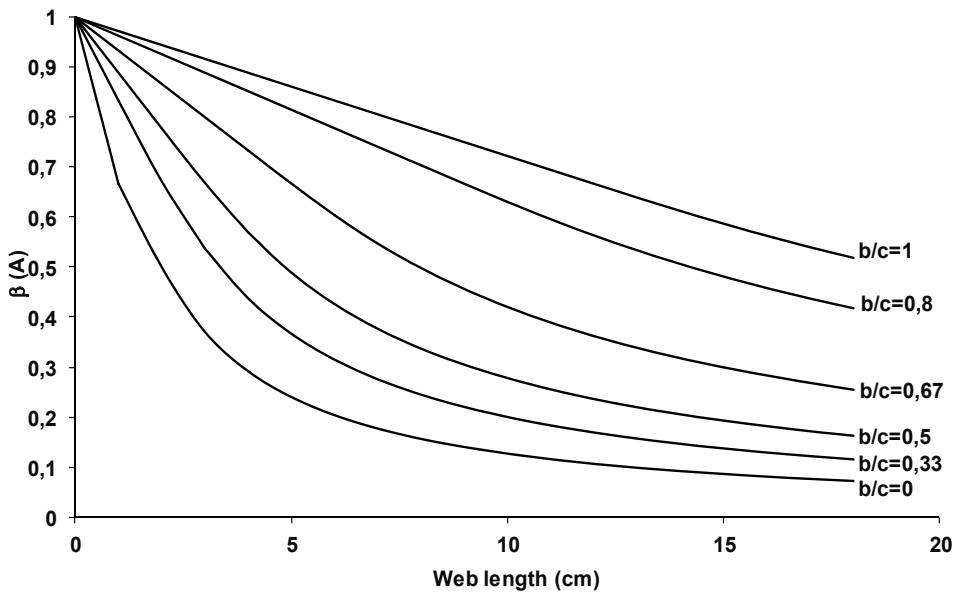


Figure 12. Short-term irregularity - between-area-density variance vs. fiber web length: Case of length uniform distribution

5.2. Periodic unevenness

We suppose that the area density of the fibrous web is defined as follows:

$$\mu(t) = \mu + a \cos(\omega t) \quad (35)$$

where μ : average area density, assumed constant

a : amplitude of the sinusoidal component irregularity

ω : pulsation of the sinusoidal component irregularity

We have seen that $B(A)$ can be written as follows:

$$B(A) = E \left[\frac{L}{A} \int_x^{x+A/L} (\mu(t) - E(\mu)) dt \right]^2 \quad (36)$$

with $E(\mu(t)) = \mu$.

Hence by replacing $\mu(t)$ by its value:

$$B(A) = E \left[\frac{L}{A} \int_x^{x+A/L} a \cos(\omega t) dt \right]^2 \quad (37)$$

and finally after integration:

$$B(A) = \frac{a^2}{2} \cdot \frac{\sin^2\left(\frac{\omega \cdot A/L}{2}\right)}{\left(\frac{\omega \cdot A/L}{2}\right)^2} \text{ and } B(0) = \frac{a^2}{2} \quad (38)$$

$$B(A) = B(0) \cdot \frac{\sin^2\left(\frac{\omega \cdot A/L}{2}\right)}{\left(\frac{\omega \cdot A/L}{2}\right)^2} \text{ and the normalized for } \beta(A) = \frac{B(A)}{B(0)} = \frac{\sin^2\left(\frac{\omega \cdot A/L}{2}\right)}{\left(\frac{\omega \cdot A/L}{2}\right)^2}.$$

Hence we deduce the corresponding variation coefficient:

$$CB(A) = CB(0) \cdot \frac{\sin\left|\frac{\omega \cdot A/L}{2}\right|}{\left(\frac{\omega \cdot A/L}{2}\right)} \text{ and} \tag{39}$$

$$\gamma(A) = \frac{CB(A)}{CB(0)} = \frac{\sin\left|\frac{\omega \cdot A/L}{2}\right|}{\left(\frac{\omega \cdot A/L}{2}\right)} \text{ (normalized form)}$$

where $\omega = \frac{2\pi v}{\lambda}$ is the pulsation of the irregularity sinusoidal component

v represents the fiber flow velocity through the sensor

λ is the wavelength irregularity

The $\beta(A)$ and $\gamma(A)$ curves show a periodic-arches succession with a decreasing amplitude and a $\frac{\pi\lambda}{v}$ (Figures 13 and 14). The shape of these curves is totally different from those corresponding to the random distribution. This result is very significant for the production manager in order to detect the defects origin.

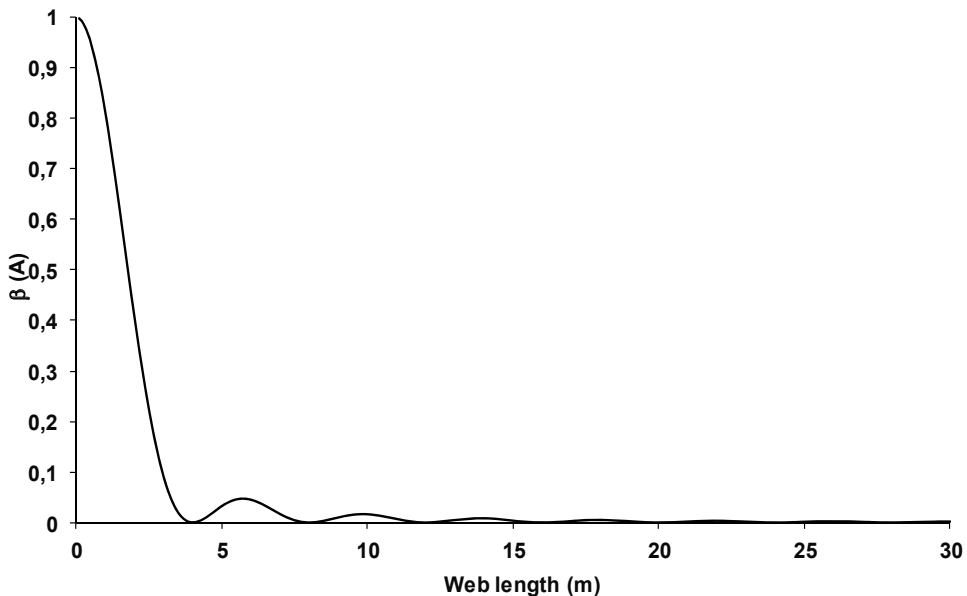


Figure 13. Normalized between-area-density variance curve – periodic irregularity $\lambda = 4 \text{ m}$

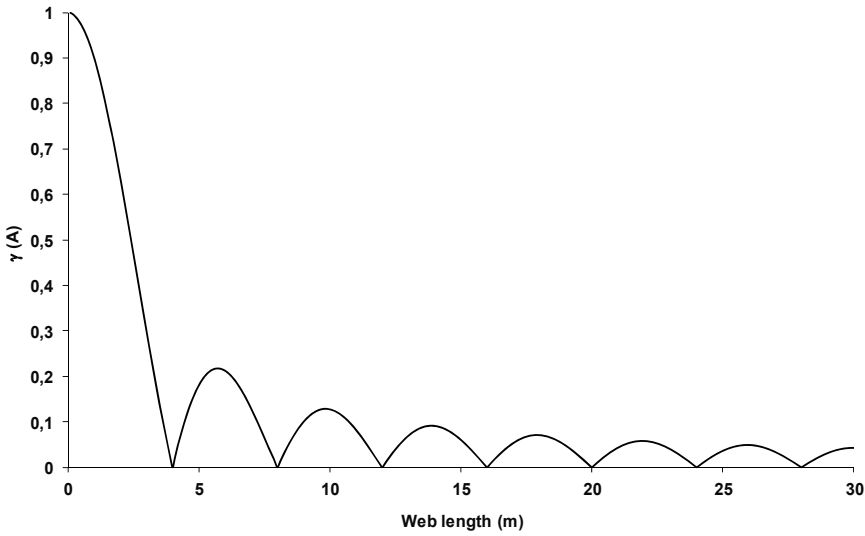


Figure 14. Normalized between-area-density variance coefficient curve – periodic irregularity $\lambda = 4 \text{ m}$

5.3. Compound unevenness

In the above-mentioned development, we have intentionally unheeded the random component and assumed the presence of only one type of periodic sinusoidal irregularity. In fact, the random component is always present in the 2D textile fibrous structures and is existing; the additional components are of several sinusoidal types generated by the manufacturing process. That way, the periodic irregularity has to be split according to Fourier series [17] and the composition of the $B(A)$ variance concerning the various components (random and periodic) of the area density irregularity have to be calculated. The calculation is based on the additivity property of variances of independent variables.

Firstly, only one type of sinusoidal periodic irregularity is taken in account as follows:

$$M(x) = \mu(x) + a \cos(\omega x) \tag{40}$$

where $\mu(x)$ = random component of the area density of the fibrous web

$a \cos(\omega x)$ = sinusoidal component of amplitude a and pulsation ω

Based on the law of additive covariances composition [26], we deduce the expression of the autocorrelation function $\rho(u)$:

$$\rho(u) = \left(\frac{\sigma_a^2}{\sigma_\mu^2} \right) \cdot \rho_a(u) + \left(\frac{\sigma_p^2}{\sigma_\mu^2} \right) \cdot \rho_p(u) \tag{41}$$

Let $\eta = \left(\frac{\sigma_p^2}{\sigma_\mu^2} \right)$. With η being the weighting factor ($0 \leq \eta \leq 1$).

$$\rho(u) = (1 - \eta) \cdot \rho_a(u) + (\eta) \cdot \rho_p(u) \tag{42}$$

with σ_μ^2 = overall variance of the area density irregularity

σ_a^2 = variance due to the random component

σ_p^2 = variance due to the periodic component

ρ_a = autocorrelation function of the random component

ρ_p = autocorrelation function of the periodic component

The figure [28] shows that the standardized form of the variance composition can be written as follows:

$$\beta(A) = \eta \cdot \beta_p(A) + (1 - \eta) \cdot \beta_a(A) \tag{43}$$

The extension of the above results to the more general case of the superposition of n sinusoidal type irregularities can be written as follows:

$$M(x) = \mu_a(x) + \sum_1^n a_i \cos(\omega_i x + \phi_i) \tag{44}$$

where $\mu_a(x)$ is the random component and the following term $\left(\sum_1^n a_i \cos(\omega_i x + \phi_i) \right)$ is the element due to Fourier series developments of the periodic components. Hence

$$\beta(A) = \sum_1^n \left[\eta_i \cdot \beta_{p_i}(A) \right] + \left(1 - \sum_1^n \eta_i \right) \cdot \beta_a(A) \tag{45}$$

η_i being the weighting factor for the periodic component of rank i.

Figures 15 and 16 show some simulation examples of compositions of one or two sinusoidal irregularities with a random irregularity (isoprobable distribution). The interpretation of the curves $\beta(A)$ respectively $\gamma(A)$ becomes much more difficult. Of course the presence of "arches" or "sinuosities" indicates the presence of periodic irregularity.

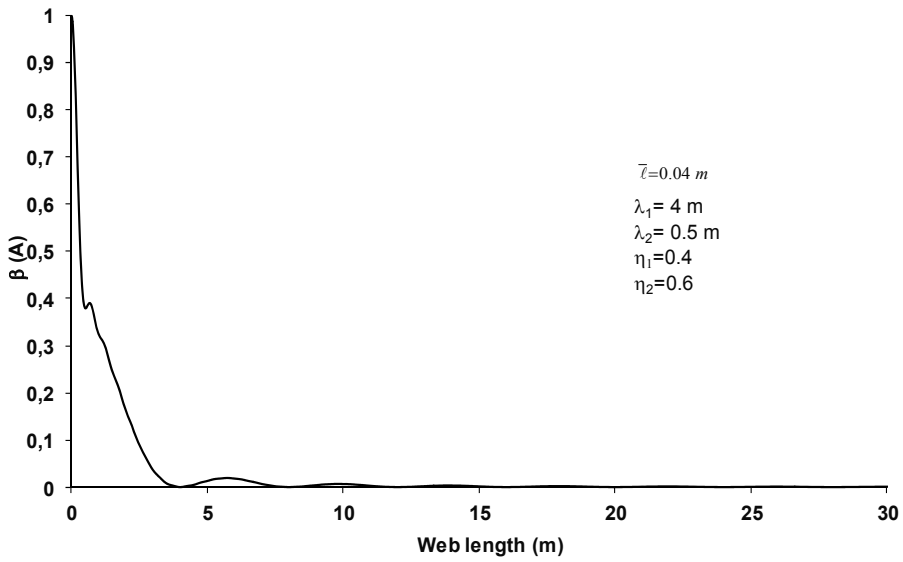


Figure 15. Normalized between-area-density variance curve – compound irregularity

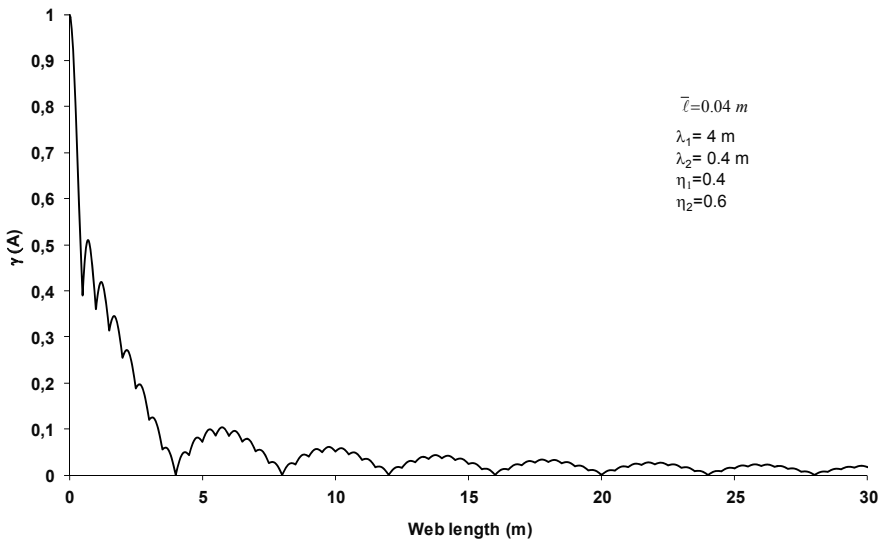


Figure 16. Normalized between-area-density variance coefficient curve – compound irregularity.

6. Conclusion

Nonwoven industries are fiber-based industries. Based on their physical and mechanical properties, the nonwoven applications are increasing inducing a strong growth of the non-

woven production. The physical and mechanical properties of these products strongly depend on the evenness of laps or webs. Thus, the nonwoven manufacturers absolutely need tools to evaluate these properties. Hence, an accurate knowledge of the web and lap formation as well as the associated theoretical approach is absolutely necessary. In this paper we propose a theoretical approach simulating the real faults of the fiber-web forming-step during the industrial process. Thanks to this theory, we were able to calculate from measurements both the random and periodic components of the real defects for all textile types as fibrous webs and nonwovens. The periodic component depends on the production machine and the random component depends mainly on the characteristics of the fibers. In this study, we are not interested in uniformity of the visual appearance (2-D uniformity) of the fiber web but we assess the 3-D uniformity from the area density. This uniformity is determined from small surface-elements and not from image analysis [16,24]. We did not analyze the correlation between the irregularity of the yarns and the woven fabric [20] but measured directly surface and mass irregularities thereof. This involves the use of specific sensors (such as capacitive, ultrasonic, and radioactive sensors). To highlight these irregularities (random or periodic), the fiber web is divided into several elements that have the same surface. Then the between-area-density variance function is defined with the help of the autocorrelation function. The common distribution functions of the fiber flocks are used to carry out the random component of the equation. Finally, according to the law of additive covariances composition, periodic defects have been added to the random component in order to determine the theoretical equation. This information is fundamental to the production manager in order to detect the earliest possible manufacturing breakdown and to optimize the machine settings and textile production quality.

Author details

Jean-Yves Drean and Omar Harzallah*

*Address all correspondence to: o.harzallah@uha.fr

Université de Haute Alsace – Laboratoire de Physique et Mécanique Textiles, Mulhouse, France

References

- [1] S. J. Russell, *Handbook of nonwovens*, The Textile Institute, Woodhead Publishing Limited, Cambridge, England, 2007.
- [2] G. Tanchis, *Reference book of textile technologies: the nonwovens*, Fondazione ACIMIT, Italy, 2008.

- [3] R. A. Chapman, *Applications of nonwovens in technical textiles*, Woodhead Publishing Limited, Cambridge, England, 2010.
- [4] W. Albrecht, H. Fuchs and W. Kittelmann, *Nonwoven fabrics*, WILEY-VCH Verlag GmbH & Co. KGaA, Weinheim, 2003.
- [5] R. M. Koerner, *Designing with geosynthetics*, Second Edition, Prentice-Hall, Englewood Cliffs, 1990.
- [6] J. L. Spencer-Smith and H. A. C. Todd, A time series met with in textile research. Supplement to the *Journal of the Royal Statistical Society*, 7(2), 131-145, 1941.
- [7] J. G. Martindale, A new method of measuring the irregularity of yarns with some observations on the origin of irregularities in worsted slivers and yarns. *Journal of the Textile Institute*, 36, T35-47, March 1945.
- [8] M. W. H. Townsend and D. R. Cox, The analysis of yarn irregularity. *Journal of the Textile Institute*, 42, P107-113, 1951.
- [9] M. W. H. Townsend and D. R. Cox, The use of correlograms for measuring yarn irregularities. *Journal of the Textile Institute*, 42, P145-151, 1951.
- [10] H. Breny, The calculation of the variance-length curve from the length distribution of fibers. *The Journal of the Textile Institute*, Part I, 44, P1-P9, January 1953.
- [11] H. Breny, The calculation of the variance-length curve from the length distribution of fibers. *Journal of the Textile Institute*, Part II, 44, P10-P14, January 1953.
- [12] P. Grosberg and R. C. Palmer, On the determination of the B-L curve by cutting and weighing. *Journal of the Textile Institute*, 4(45), April 1954.
- [13] P. Grosberg, The medium and long-term variations of yarn. *Journal of the Textile Institute*, 46, T301-T309, May 1955.
- [14] A. Kirschner, R. Petiteau and R. A. Schutz, Contribution à l'Analyse Spectrale des Structures Textiles Linéaires. *Bulletin Scientifique ITF*, 19(5), Août 1976.
- [15] W. Wegener, The irregularity of woven and knitted fabrics. *Journal of the Textile Institute*, 77(2), 69-75, March-April 1986.
- [16] Y. Wu, B. Pourdeyhimi and M. S. Spivak, Textural evaluation of carpets using image analysis. *Textile Research Journal*, 61, 407-419, 1991.
- [17] E. J. Wood, Applying Fourier and associated transforms to pattern characterization in textiles. *Textile Research Journal*, 60, 212-220, 1990.
- [18] D. Han, *Development of fabric image models and invariance property of variance-area curve within fabric*. Master's thesis, NCSU, College of Textiles, Raleigh, 2002.

- [19] M. W. Suh, M. Günay and W. J. Jasper, Prediction of surface uniformity in woven fabrics through 2-D anisotropy measures, Part I: Definitions and theoretical Model. *Journal of the Textile Institute*, 98(2), 109-116, 2007.
- [20] M. Günay, M. W. Suh and W. J. Jasper, Prediction of surface uniformity in woven fabrics through 2-D anisotropy measures, Part II: Simulation and verification of the prediction model. *Journal of the Textile Institute*, 98(2), 117-126, 2007.
- [21] P. Andrianarisoa, M. Averous, J. Y. Drean and R. A. Schutz, Evaluation de la Distribution de la Masse Surfaccique des Fibres dans les Textiles Surfacciques. *Bulletin Scientifique ITF*, 51(13), 3-19, 1984.
- [22] A. Cherkassky, A two-dimensional mathematical model of the carding process. *Textile Research Journal*, 64(3), 169-175, 1994.
- [23] R. K. Aggarwal, W. R. Kennon and I. Porat, Scanned-laser technique for monitoring fibrous webs and nonwoven fabrics. *Journal of the Textile Institute*, 83(3), 386-398, 1992.
- [24] A. Cherkassky, Analysis and simulation of nonwoven irregularity and nonhomogeneity. *Textile Research Journal*, 68(4), 242-253, 1998.
- [25] A. Cherkassky, Analysis of the smoothing effect of the card cylinder using simulation. *Textile Research Journal*, 65(12), 723-730, 1995.
- [26] Papoulis, *Probability, random variables and stochastic processes*, McGraw-Hill, New-York, 1968.
- [27] A. Kirschner, Contribution à l'Etude des Variables et Processus Aléatoires Associés aux Structures Textiles Linéaires. D.Sc., Université de Haute Alsace, 87MULH47, 1987.
- [28] J. Y. Drean, et M. Renner, Contribution à l'Etude Théorique et Expérimentale du Processus d'Obtention des Textiles Linéaires. D.Sc., Université de Haute Alsace, 86MULH19, 1986.
- [29] J. Y. Drean, O. Harzzallah and M. Renner, Textile surfaces analysis and modelling based on statistical methods: Variance analysis and autocorrelation functions. *Textile Research Journal*, 80(17), 1833-1845, 2010

3D Fabrics for Technical Textile Applications

Kadir Bilisik, Nesrin Sahbaz Karaduman and Nedim Erman Bilisik

Additional information is available at the end of the chapter

<http://dx.doi.org/10.5772/61224>

Abstract

Two dimensional (2D) woven, braided, knitted and nonwoven fabrics have been used for the fabrication of soft and rigid structural composite parts in various industrial areas. However, composite structure from biaxial layered fabrics is subject to delamination between layers due to the lack of through-the-thickness fibers. It also suffers from crimp which reduces the mechanical properties. Triaxial fabrics have an open structure and low fiber volume fraction. However, in-plane properties of triaxial fabrics are more homogeneous due to bias yarns. A 3D woven fabric has multiple layers and is free of delamination due to the z-fibers. However, 3D woven fabric has low in-plane properties. Three dimensional braided fabrics have multiple layers and they are without delamination due to intertwine type out-of-plane interlacement. However, they have low transverse properties. A 3D knitted fabric has low fiber volume fraction due to its looped structure. A 3D nonwoven fabric is composed of short fibers and is reinforced by stitching. However, it shows low mechanical properties due to lack of fiber continuity. Various unit cell based models on 3D woven, braided, knitted and nonwoven structures were developed to define the geometrical and mechanical properties of these structures. Most of the unit cell based models include micromechanics and numerical techniques.

Keywords: Fabric architecture, woven fabric, braided fabric, knitted fabric, 3D nonwoven fabric

1. Introduction

The objective of this chapter is to provide up-to-date information on the development of 2D and 3D fabric formation and formation techniques particularly on 2D and 3D nonwoven fabrics, methods, and properties of nonwoven web, including possible emerging application areas. Three-dimensional (3D) fiber structures produced by textile processes are used in various industrial applications since they have distinct properties when compared to conven-

tional materials. The most important application area of 3D textiles, by far, is composite industry, where they are used as reinforcement materials in combination with several matrices to make textile structural composites. These composites are used extensively in various fields such as civil engineering and military industry [1, 2], thanks to their exceptional mechanical properties and lower density in comparison with common engineering materials like metals and ceramics [3, 4]. Textile structural composites are also superior to conventional unidirectional composites when the delamination resistance and damage tolerance are taken into account [5]. Textile preforms are readily available, low-cost, and not labor intensive [1]. They can be manufactured by weaving, braiding, knitting, stitching, and by using nonwoven techniques. Each manufacturing technique has its own advantages and disadvantages in terms of specific composite properties and the selection can be made based on the end-use. The simplest form of 3D woven preforms is made up of two dimensional (2D) woven fabrics that are stacked one on top of another and stitched together in the thickness direction to impart through-the-thickness reinforcement. Three-dimensional weaving is another preform production technique that can be employed to manufacture 3D woven preforms by using specially designed automated looms. Near-net shape parts can be produced with this technique which substantially reduces the amount of scrap [6, 7]. In-plane properties of 3D woven composites are generally low due to through-the-thickness fiber reinforcement, despite of its positive effect on out-of-plane properties [8]. Simple 3D braided preform consists of 2D biaxial fabrics that are stitched together in the thickness direction depending on a chosen stacking sequence. Three-dimensional braiding is a preform technique used in the multidirectional near-net shape manufacturing of high damage tolerant structural composites [9, 10]. Three-dimensional braiding is highly automated and readily available. Three-dimensional braided preforms are fabricated by various techniques such as traditional maypole braiding (slotted horn gear matrix), novel 4-step and 2-step braiding (track and column) or more recently 3D rotary braiding and multi-step braiding [11, 12]. The fabrication of small sectional 3D braided preforms is low-cost, and not labor intensive [1]. However, the fabrication of large 3D braided preforms may not be feasible due to position displacement of the yarn carriers. Three-dimensional knitted preforms are fabricated by the 3D spatial formation of 2D warp or weft knitted fabrics in order to make near-net shape structures like spheres, cones, ellipsoids and T-pipe junctions. Three-dimensional knitted composites generally have low mechanical properties as a result of their characteristic looped architecture and low fiber volume fraction. A 3D nonwoven preform is a web or felt structure consisting of randomly positioned short fibers. There is no particular textile-type interlacing or intertwining between the fibers other than random entanglements. Through-the-thickness stitching of layered nonwoven webs is also possible. The most common methods for nonwoven production are needle-punching, stitch-bonding, high-frequency welding, chemical bonding, ultrasound and laminating. Recently, electrospinning method is utilized to make nonwoven nano web structure [13]. The entanglement type defines the fabric properties such as strength and modulus, flexibility, porosity and density [14]. Nonwoven fabrics and their composites display low mechanical properties due to fiber discontinuity. Multiaxis knitted preform comprises four fiber sets such as +bias, -bias, warp (0°) and weft (90°) along with stitching fibers which enhance in-plane properties [15]. Multiaxis knitted preform suffer from limitation in fiber architecture, through-

thickness reinforcement due to the thermoplastic stitching thread and three dimensional shaping during molding [3]. Multiaxis 3D woven preforms and their composites exhibit improved in-plane properties due to off-axis fiber positioning [16, 17].

In this chapter, 3D fabrics including 3D nonwoven for technical textile applications are reviewed in the light of the existing literature. First, the classification of textile fabric structures was introduced based on various classification schemes suggested by experts in the field. Types of textile fabric structures were explained under two main groups such as 2D and 3D fabrics. Various formation techniques including 2D and 3D nonwoven techniques were reviewed with regard to manufacturing processes and resulting fabric and composite properties. Applications of technical textiles in various industrial areas were covered with an emphasis on the future trends and technologies.

2. Classification of fabrics

Three-dimensional woven preforms are classified based on various parameters such as fiber type and formation, fiber orientation and interlacements and micro- and macro-unit cells. One of the general classification schemes has been proposed by Ko and Chou [3]. Another classification scheme regarding yarn interlacement and process type was proposed (Table 1) [18]. In this scheme, 3D woven preforms are subdivided into orthogonal and multiaxis fabrics, and their processes have been categorized as traditional or new weaving, and specially designed looms. Chen [19] categorized 3D woven preforms made by traditional weaving techniques based on their macro-geometry. According to this classification, 3D woven preforms are grouped as solid, hollow, shell, and nodal structures with varying architectures and shapes (Table 2). Bilisik [20] suggested a more precise classification of 3D woven preforms according to their interlacement types (fully interlaced woven/non-interlaced orthogonal), macro geometry (cartesian/polar) and reinforcement direction (2-15) (Table 3).

Non-interlacing Orthogonally Orientating and Binding	Type Uniaxial	Direct	Modified 2D Weaving Machine	Thick Panel [21]	
		Binding	Specially Designed Machine	Profiled Bar/Beam [22]	
		Indirect	Modified 2D Weaving Machine	Profiled Bar/Beam [23]	
		Binding	Specially Designed Machines	Profiled Bar/Beam [24-26]	
	Type Multiaxial	Direct	Binding	Specially Designed Machine	Thick Tubular [27]
					Thin Panel [29]
		Indirect	Binding	Specially Designed Machines	Thick Panel [30, 31]
					Thin Panel [32]

Table 1. Three-dimensional woven fabric classification based on non-interlace structuring [18].

Structure	Architecture	Shape
Solid	Multilayer; Orthogonal; Angle interlock	Compound structure with regular or tapered geometry
Hollow	Multilayer	Uneven surfaces, even surfaces, and tunnels on different levels in multi-directions
Shell	Single layer; Multilayer	Spherical shells and open box shells
Nodal	Multilayer; Orthogonal; Angle interlock	Tubular nodes and solid nodes

Table 2. Three-dimensional woven fabric classification based on macro-structure [19].

Direction	Three dimensional weaving			
	Woven		Orthogonal nonwoven	
	Cartesian	Polar	Cartesian	Polar
2 or 3	Angle interlock; Layer-to-layer; Through the thickness Core structure	Tubular	Weft-insertion	Weft-winding and sewing
3	Plain and Plain laid-in Twill and Twill laid-in Satin and Satin laid-in	Plain and Plain laid-in Twill and Twill laid-in Satin and Satin laid-in	Open-lattice Solid	Tubular
4	Plain and Plain laid-in Twill and Twill laid-in Satin and Satin laid-in	Plain and Plain laid-in Twill and Twill laid-in Satin and Satin laid-in	Corner across Face across	Tubular
5	Plain and Plain laid-in Twill and Twill laid-in Satin and Satin laid-in	Plain and Plain laid-in Twill and Twill laid-in Satin and Satin laid-in	Solid	Tubular
6 to 15	Rectangular array Hexagonal array	Rectangular array Hexagonal array	Rectangular array Hexagonal array	Rectangular array Hexagonal array

Table 3. The classification of three-dimensional weaving based on interlacement and fiber axis [20].

Three-dimensional braided preforms are classified based on various parameters, including manufacturing technique, fiber type and orientation, interlacement patterns, micro-meso unit

cells and macro-geometry [10, 33]. Kamiya et al. [2] considered manufacturing techniques i.e., solid, 2-step, 4-step and multistep to classify 3D braided preforms. Grishanovi et al. [34] used a topological approach based on knot theory to describe and group braided structures whereby the braided fabric is considered as a multiknot structure. Bilisik [35] classified 3D braided structures as 3D braid, 3D axial braid, and multiaxis 3D braid, as shown in Table 4. These three categories were further divided according to their fiber directions (2-6) and geometry (cartesian/polar).

Number of Yarn Sets	Three Dimensional Braiding					
	3D Braid		3D Axial Braid		Multiaxis 3D Braid	
	Cartesian	Polar	Cartesian	Polar	Cartesian	Polar
1 or 2	Square	Tubular			Rectangular (Out-of-plane at an angle)	Tubular (Out-of-plane at an angle)
	Rectangular (Out-of-plane at an angle) 1×1 pattern 3×1 pattern	(Out-of-plane at an angle) 1×1 pattern 3×1 pattern				
3			Triaxial fabric (In-plane)	Triaxial fabric (In-plane)	Rectangular	Tubular
			Rectangular (Out-of-plane at an angle) 1×1 pattern 3×1 pattern	Tubular (Out-of-plane at an angle) 1×1 pattern 3×1 pattern	(Out-of-plane at an angle)	(Out-of-plane at an angle)
4					Rectangular (Out-of-plane at an angle)	Tubular (Out-of-plane at an angle)
5 or 6					Rectangular (Out-of-plane at an angle)	Tubular (Out-of-plane at an angle)

Table 4. The classification of 3D braiding based on interlacement and fiber axis [35].

Hamada et al. [36] classified 3D knitted structures based on engineering applications, as shown in Table 5. Type I fabrics are simple 2-D flat knitted fabrics. These fabrics can be cut to the required dimensions and laminated just as woven fabric composites. Two dimensional knitted fabrics with 3D shapes are categorized as Type II fabrics. Type III fabrics are multiaxial warp knitted fabrics. Type IV fabrics are called sandwich fabrics or 3D hollow fabrics. Type IV fabrics are sometimes called “2.5 D fabrics” and are very effective for the production of high damage-tolerant composites [37].

Type	Fabric classification	Weft knitted fabric	Warp knitted fabric
I	2D fabric	Plain, Milano rib, inlaid fabrics	Dembigh, Atlas
II	2D fabric base 3D shape	Plain, rib	Dembigh, Atlas
III	3D solid fabric	Plain and rib fabrics with inlay fiber yarns	Multiaxial warp knitted fabrics
IV	3D hollow fabric/sandwiched fabric	Single jersey face structure	Single Dembigh face structure

Table 5. Classification of typical warp and weft knitted fabrics [36].

Two- and three-dimensional nonwoven preforms are classified depending upon web bonding techniques, web structure, and fiber orientation (Table 6). The nonwoven structure is composed of short fibers that are held together by employing various techniques. The extent of fiber-fiber bonding is dependent upon fiber geometry, fiber tenacity and flexural rigidity, fiber location within the web, the areal mass of the web, etc. Mechanical, chemical or thermal methods can be utilized to achieve fiber-fiber bonding and thus create a continuous nonwoven web. Mechanical methods aim to commingle the fibers by an applied force (i.e., needling or water-jet) so that fiber-fiber entanglements occur in the web holding the structure together. In the chemical method, fiber surfaces are bonded together by using suitable binding agents, or the bonding is achieved by dissolving the fiber surfaces with a solvent followed by merging and solidification. Thermal bonding is generally used for thermoplastic fibers and powders. Fibers are melted by heat exposure, merged together, and solidified again by cooling [38]. Two- and three-dimensional nonwoven nano-web fabricated via electrospinning is a new development to make nanofiber-based nonwoven fabrics [39].

Nonwoven fabric	Web formation	Formation techniques	Web structure	Fiber orientation in web
2D fabric 3D fabric	Mechanical	Needling	Plugs	In plane and out-of-plane fiber orientation
		Looping	Loops	Short fiber in plane and continuous fiber in the out-of-plane orientation
	Thermal Chemical	Entangling	Balls	In plane fiber placement and entanglement
		Hot air; Calendaring; Welding	-	-
		Impregnation; Spraying; Printing; Foaming	-	-

Nonwoven fabric	Web formation	Formation techniques	Web structure	Fiber orientation in web
	Electric field	Nanofiber entanglement under electric energy	nanofiber	In plane continuous nano fiber placement and entanglement

Table 6. Classification of nonwoven fabrics [38].

3. Types of fabrics

3.1. Two-dimensional fabrics

3.1.1. Woven fabric

The 2D woven fabric is the most widely used material in the composite industry. It contains two yarn sets i.e., warp (0°) and weft (90°), that lie perpendicular to each other in the fabric plane. Warp and weft yarns make a series of interlacements with one another according to a weave type and pattern to make the woven fabric. Basic weave types produced by traditional weaving are plain, twill and satin. Different fabric structures can be constructed from a weave type by changing the weave pattern. There are also derivative weave types that are created to obtain desired combinations of fabric properties. Some of the weave types are shown in Figure 1 [40]. In plain weave, each warp yarn passes alternately under and over each weft yarn. Hence, it is symmetrical and has a good dimensional stability. However, plain woven fabric has high crimp and is difficult to form during molding due to high number of interlacements for a given area. In twill weave, a warp yarn passes over and under two or more weft yarns based on a diagonal pattern. The twill woven fabric has a smoother surface in comparison with plain weave, simply because of multiple jumps between interlacements. It has also lower crimp. In addition, it has a good wettability and drapability. However, it shows less dimensional stability compared to the plain weave. In satin weave, warp yarns alternately weave over and under two or more weft yarns to make fewer intersections. Therefore, it has a smooth surface, good wettability and a high degree of drapability. It has also low crimp. However, it has low stability and an asymmetrical structure. Another 2D woven architecture is leno weave in which adjacent warp yarn is twisted around consecutive weft yarn. One of the derivatives of the leno weave is mock leno in which occasional warp deviate from the alternate under-over interlacing and interlaces every two or more weft. This results in a thick and rough surface with high porosity [41-43].

Two dimensional woven fabric composites show poor impact resistance as a consequence of fabric crimp. They also have low in-plane shear properties due to absence of off-axis fiber orientation other than material principle directions [4]. Another major problem of these composites is that they experience delamination under load due to lack of through-the-thickness binder yarns (z-yarns). Through-the-thickness reinforcement eliminates the delamination problem, but it reduces the in-plane properties [1, 2]. Biaxial noncrimped fabric was

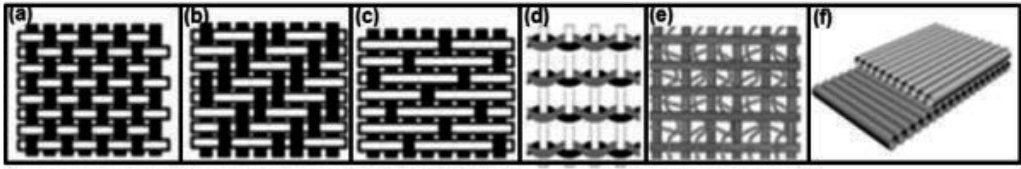


Figure 1. Two dimensional various woven fabrics (a) uniform plain (b) twill (2/2) (c) satin (4/1) (d) leno (1/1), and (e) non-interlace woven fabric with stitching (f) non-interlace woven fabric without stitching yarn [41-43].

developed to replace the unidirectional cross-ply laminate [42]. This fabric has warp (0° direction) and filling yarns (90° direction) as separate layers so that there is no interlacement between them, unlike traditional woven fabrics. Warp and weft layers are linked at intersection points by two sets of stitching yarns, one in 0° direction and another in 90° direction, as shown in Figure 1. Biaxial noncrimped fabrics largely eliminate the crimp and delamination problems of 2D woven composites.

3.1.2. *Triaxial woven fabric*

Triaxial weave structure consists of three yarn sets such as +bias (+warp), -bias (-warp), and filling [44]. These yarn sets make interlacements as in traditional biaxial fabric (Figure 2). The fabric generally has large hexagonal openings between interlacements. Open-reed process used in the fabrication of this type of fabric does not allow making fabrics as dense as a traditional woven fabric. Triaxial fabrics have two variants, namely, loose-weave and tight-weave. It was shown that loose-weave fabric has certain stability and higher shear stiffness in $\pm 45^\circ$ directions when compared to the biaxial fabrics as well as having a more isotropic structure. Quart-axial fabric has four sets of yarns such as +bias, -bias, warp and filling as shown in Figure 2. All yarns are interlaced to each other to form the fabric structure [45]. Warp yarns are inserted to the fabric at selected places to increase directional strength and stiffness properties. Therefore the fabric structure can be tailored to fulfill various end-use requirements.

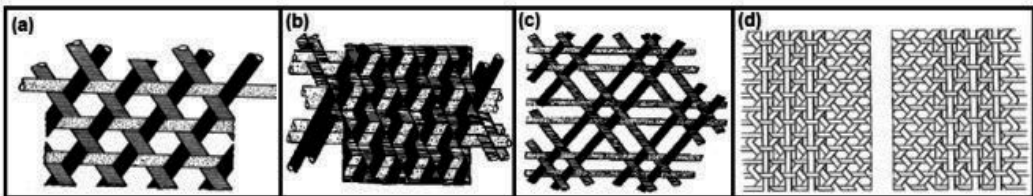


Figure 2. Triaxial woven fabrics (a) loose fabric (b) tight fabric (c) one variant of triaxial woven fabric, and (d) quart-axial woven fabric [44, 45].

3.1.3. *Braided fabric*

Two-dimensional braided fabrics are extensively used in industrial textiles and composites. It has one yarn set, braiders oriented in $+\theta$ and $-\theta$ directions. In order to produce the fabric

surface shown in Figure 3, braiders are intertwined with each other. Basic braid patterns that can be produced by traditional methods are diamond, regular and hercules braid [46]. The 2D braided fabric reinforced composite fabrication is similar to that of 2D woven composites. Multiple braided fabrics can be stacked one on top of another to produce reinforced composites. These composites suffer from yarn crimp and lack through-the-thickness reinforcement (z-yarns) and thus experience delamination leading to a poor impact behavior [4]. In order to overcome the delamination and related problems, 2D fabric layers can be stitched together in the thickness direction to impart out of plane fiber reinforcement. Stitching was shown to substantially decrease delamination but it can lead to a reduction in in-plane properties due to the holes created by stitching needle which act as stress concentration points.

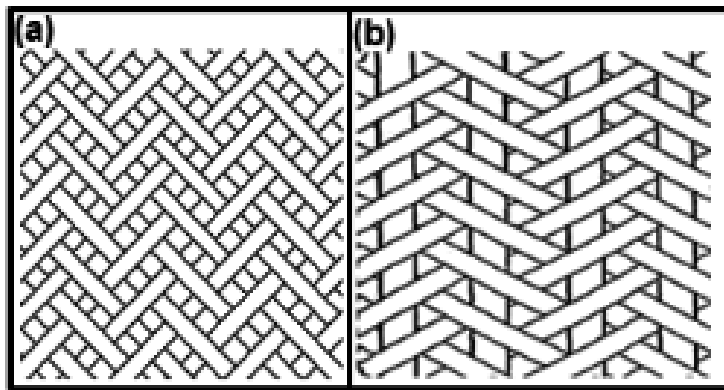


Figure 3. (a) Two-dimensional traditional biaxial braided fabric, and (b) triaxial braided fabric [47].

3.1.4. Triaxial braided fabric

Triaxial braided fabric has basically three sets of yarns: +braid (+bias), -braid (-bias), and warp (axial). Axial yarns lie across the fabric whereas braided yarns intertwine with each other around the axial yarns making about 45° angle (Figure 3). The intertwining is similar to that of a traditional braided fabric. -Braided yarns cross under and over the +braided yarns according to a pattern and this process is repeated throughout the fabric structure. Triaxial braided fabric generally has large openings between the axial yarns, intertwining regions. Although dense fabrics can be produced, the process is not suitable for the fabrication of fabrics as dense as a traditional biaxial braided fabric. It was shown that the mechanical properties of triaxial fabric are significantly higher than biaxial braided fabrics, especially in the direction of axial yarns [47]. This shows that the incorporation of axial yarns strongly enhances the directional properties of the fabric.

3.1.5. Knitted fabric

Knitted fabric is composed of yarn loops connected to each other and to the neighboring rows and columns by various techniques. This process is also called “interloping.” The basic knitting

types are weft knitting and warp knitting. In weft knitting, a continuous yarn forms one horizontal row of loops called a “course” connecting it to the previously formed courses in the process (Figure 4). The vertical columns of loops are called “wale.” In warp knitting, yarn loops are connected vertically to form the fabric structure. Knitted fabrics are characterized by their ‘wale density’ and ‘course density.’ The wale density is defined as the number of wales per unit length in the course direction. The course density is defined as the number of courses per unit length in the wale direction. Stitch density is the product of course density and wale density [36, 48].

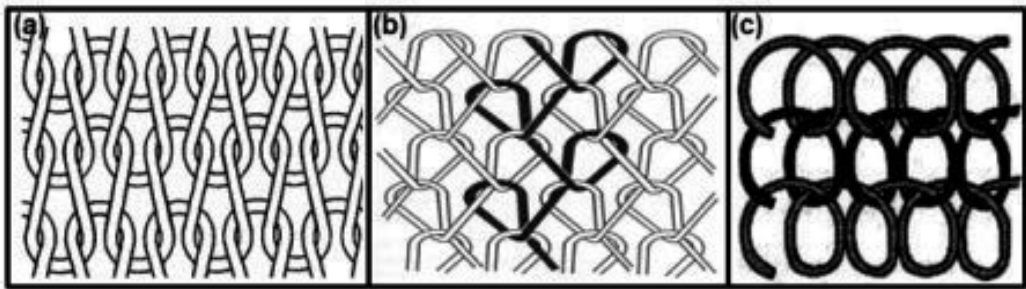


Figure 4. (a) Two-dimensional weft knitted fabric (b) warp knitted fabric, and (c) spiral knitted fabric [36].

3.1.6. Uniaxial knitted fabric

The special looped structure of knitted fabrics results in large gaps in the fabric structure. This reduces the overall fiber volume fraction of the composite leading to low mechanical properties. Furthermore, the fabric is loosely formed unlike a woven fabric, which leads to high elongation and low stiffness. These problems have led to structural modifications of knitted fabrics by using inlay yarns either in fabric length or width direction to increase the mechanical properties of the resulting composites. Figure 5 presents the schematic views of these modifications. The inlay yarns are trapped inside the knitted loops during the fabric formation. It was shown that the tensile strength of uniaxial knitted fabric composites can be improved significantly in the inlaid directions [49].

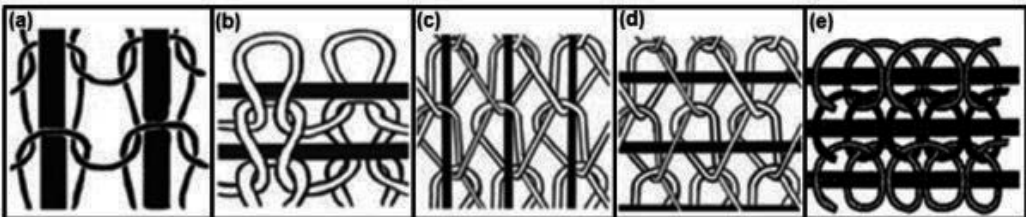


Figure 5. (a) Two-dimensional warp in-laid weft knitted fabric (b) 2D weft in-laid weft knitted fabric (c) 2D warp in-laid warp knitted fabric (d) 2D weft in-laid warp knitted fabric, and (e) 2D weft in-laid spiral knitted fabric [49].

3.1.7. Biaxial knitted fabric

Biaxial knitted structures were developed by the insertion of warp (0°), weft (90°) or diagonal ($\pm 45^\circ$) yarns to the weft or warp knitted fabrics, as shown in Figure 6. The in-laid yarns improve the directional mechanical properties of the resulting composites.

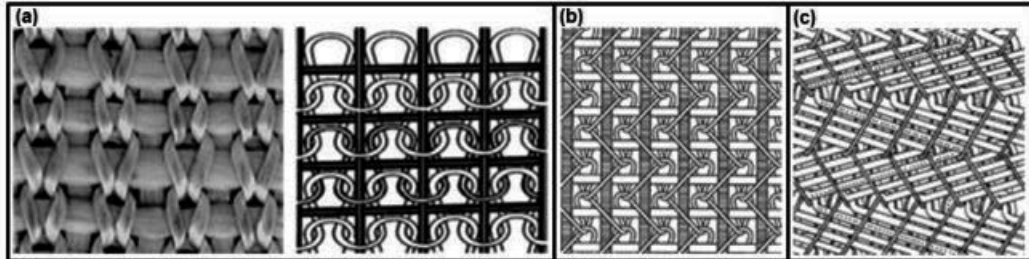


Figure 6. (a) Two-dimensional weft in-laid $0^\circ/90^\circ$ knitted fabric and schematic view (b) warp in-laid $0^\circ/90^\circ$ knitted fabric, and (c) warp in-laid $\pm 45^\circ$ knitted fabric [50-52].

3.1.8. Nonwoven fabric

Nonwoven fabric is a web structure made up of short fibers that are held together by various techniques. These techniques include needling, knitting, stitching, thermal bonding, chemical bonding, and electrospinning. Needling is a method where vertically positioned barbed needles or water jets strike into the fiber web so as to entangle the fibers and create a mechanical locking between them. Knitting aims to entrap the fibers and fix them in position with the aid of knitting loops. In stitching technique, the fiber web is stitched in through-the-thickness direction. Thermal bonding is generally applied to thermoplastic fibers and powders. Fiber web is subjected to heat treatment which softens and unifies the neighboring fiber surfaces. This process is followed by cooling that solidifies the fibers and gives the web its final form. In the chemical process, polymer dispersions are used as binders to consolidate the nonwoven fabric. In electrospinning method, polymer solution is drawn under high electric energy field by using needles. Various fibers can be used to make nonwoven nano fibers such as polyurethane, polyvinyl alcohol and carbon. The nonwoven produced from these fibers can provide interesting physical and electrical properties with their high surface area. Nanofibers with diameters in the range of 40-2000 nm ($0.04\text{-}2\ \mu\text{m}$) can be made. Fiber diameters can be varied and controlled [53-55]. Figure 7 shows the schematic and real views of 2D nonwoven fabrics manufactured by various methods [56, 57].

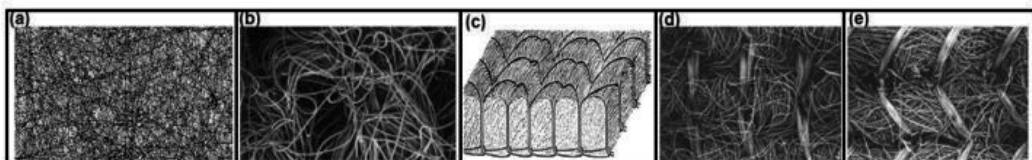


Figure 7. Schematic view of 2D nonwoven fabric by (a) mechanical needling (b) hydroentanglement (c) schematic view of stitched nonwoven structure (d) knitting loop surface, and (e) knitting loop reverse surface [58].

3.2. Three-dimensional fabrics

3.2.1. Non-interlaced fabric structures

Non-interlaced fabrics consist of multiple fiber layers that are stacked one on top of another. There is no interlacement between these layers so the fibers lie across the structure without crimping. This is an obvious advantage for in-plane properties since the fibers are well oriented in in-plane directions. Out-of-plane properties, however, are poor due to lack of through-the-thickness fibers (z-fibers). If the fabric has one set of yarn oriented in 0° direction it is referred to as uniaxial non-interlaced fabric preform. Biaxial non-interlaced fabric preform consists of two fiber sets oriented at $0/90^\circ$. A multiaxis non-interlaced fabric preform has four fiber sets oriented in $0/90/\pm 45^\circ$ directions (Figure 8) [43].



Figure 8. (a) Unidirectional non-interlaced fabric schematic and fabric (b) biaxial non-interlaced fabric schematic and fabric, and (c) multiaxis non-interlaced fabric schematic and fabric [43].

3.2.2. Multistitched fabric structures

A multistitched fabric preform is produced by stitching 2D fabric layers in thickness direction. Stitching can be applied (i) only in 0° direction, (ii) 0° and 90° directions, and (iii) 0° , 90° and \pm bias directions as shown in Figure 9. Lockstitch is commonly used for preform production. Stitching can be done manually or with the aid of a stitching machine. Stitching can be applied to all fabric types such as woven fabrics, braided fabrics, knitted fabrics, or nonwoven fabrics [59].

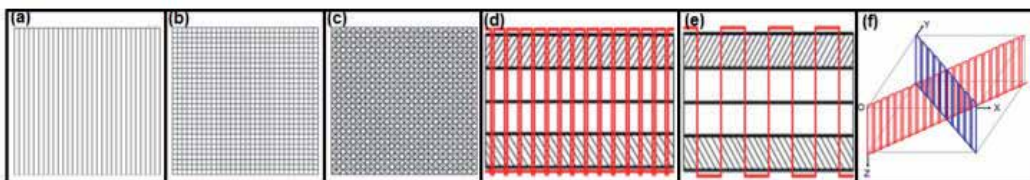


Figure 9. Schematic views of multistitched 2D woven fabric. Stitching directions (a) one direction (b) two direction (c) four direction; cross-sectional view of four directionally machine and hand stitched structures on (d) 0° , (e) 90° , (f) $+45^\circ$, and -45° [59].

3.2.3. Fully interlaced woven fabric structure

The 3D flat fully interlaced woven fabric structure consists of three yarn sets such as warp, weft and z-yarn. The weaving process takes place in in-plane and out-of-plane directions according to respective weave patterns. Warp yarns are interlaced with weft yarns at each

layer according to the weave pattern in in-plane principal directions, whereas z-yarns are interlaced with warp yarns at each layer according to the weave pattern in out-of-plane principal directions. Three dimensional fully plain, 3D fully twill and 3D fully satin preform structures are shown in Figure 10. If the warp and weft yarn sets are interlaced based on any weave pattern but the z-yarns are not interlaced and only laid-in orthogonally between each warp layers, these 3D woven structures are called semi-interlaced woven structures.

The 3D circular fully interlaced woven fabric structure is composed of three yarn sets such as axial (warp), circumferential (weft) and radial (z-yarn) yarns. Here, radial yarns are similar to z-yarns in flat woven fabrics. Circumferential yarns are interlaced with axial yarns at each circular layer according to the weave pattern in circumferential direction, whereas radial yarns are interlaced with axial yarns at each layer according to the weave pattern in radial directions. Figure 11 shows the 3D fully plain, 3D fully twill and 3D fully satin circular woven preform structures [60, 61].

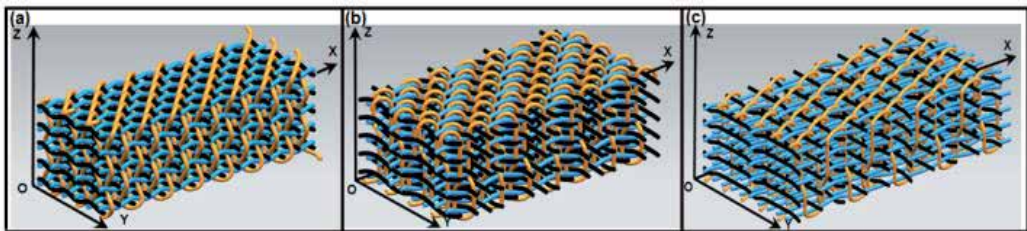


Figure 10. Three-dimensional fully-interlaced woven preform structures. General view of the five-layer computer-aided drawing of (a) 3D plain (b) 3D twill, and (c) 3D satin woven preform structures [60].

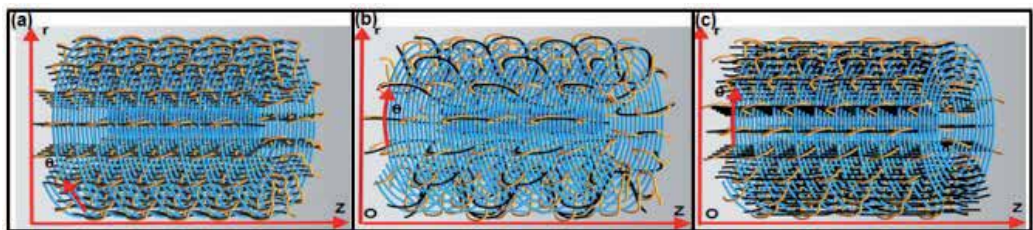


Figure 11. Three-dimensional fully-interlaced circular woven preform structures. General view of the five-layer computer-aided drawing of (a) 3D plain (b) 3D twill, and (c) 3D satin circular woven preform structures [61].

3.2.4. Orthogonal woven fabric

In orthogonal woven fabric, warp, filling, and z-yarn sets constitute the fabric. They are interlaced to one another and oriented in three orthogonal directions to form the fabric [60]. The schematic and real views of fabric unit cell are shown in Figure 12 [60, 62]. Warp yarns are placed in the fabric length direction whereas filling yarns are inserted between the warp

layers to form double picks. Z-yarns lock the other two yarn sets and provide structural integrity.

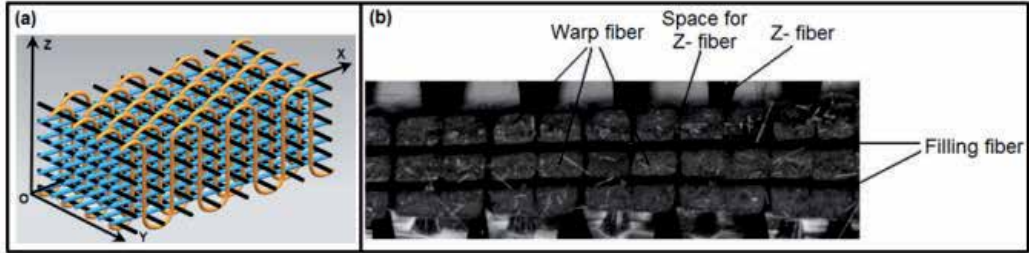


Figure 12. (a) Schematic view of 3D orthogonal woven unit cell (b) 3D woven carbon fabric preform [60, 62].

The 3D angle interlock is another type of 3D woven fabric that is produced by 3D weaving loom [63]. The fabric has a total of four yarn sets namely filling yarns, +bias yarns, -bias yarn, and stuffer (warp) yarns. Bias yarns are oriented in the thickness direction. There are two types of this fabric structure such as layer-to-layer and through-the-thickness as shown in Figure 13. In layer-to-layer fabric, bias yarns travel between two successive fabric layers making interlacements with several filling yarns according to the weave pattern. In through-the-thickness fabric, on the other hand, bias yarns take a straight path along the fabric thickness until reaching to the top or bottom surface and then reverse its movement to make the same travel until reaching the other surface (Figure 13). This zig-zag movement continues across the fabric length. Bias yarns are locked by several filling yarns in the process depending upon the number of layers [60].

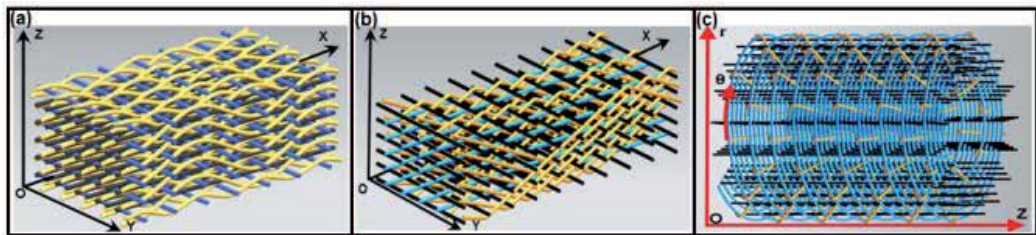


Figure 13. General view of the five-layer computer aided drawing of traditional (a) 3D angle interlock (b) 3D through-the-thickness, and (c) 3D circular orthogonal woven preform structures [60, 61].

Three-dimensional circular weaving (i.e., 3D polar weaving) and fabric was developed [64]. The preform has mainly three sets of yarns such as axial, radial and circumferential as shown in Figure 13. In addition, central yarns are inserted to form the rod. Circumferential yarns are laid between adjacent axial yarn layers, whereas radial yarns are inserted between adjacent axial yarn layers in radial direction.

3.2.5. Multiaxis woven fabric

Multiaxis 3D woven fabric, method and machine based on lappet weaving principals were developed by Ruzand and Guenot [65]. The fabric is composed of four yarn sets i.e., +bias, -bias, warp, and filling. Bias yarns are oriented across the fabric width. They are placed on the top and bottom surfaces of the fabric and are kept in place by selected weft yarns that are interlaced with warp yarns. Other warp and weft yarns are interlaced together forming the middle layers of the structure.

Uchida et al. [66] developed a five-axis 3D woven fabric. This fabric is composed of five yarn sets such as +bias, -bias, filling, warp, and z-yarn. The fabric is made up of four layers and sequences i.e., +bias, -bias, warp and filling from top to bottom. All the layers are fixed by z-yarns. Mohamed and Bilisik [30] developed a multiaxis 3D woven fabric, method and machine. The fabric is made up of five yarn sets such as +bias, -bias, warp, filling, and z-yarn. \pm Bias yarns are placed on the front and back face of the structure. These yarns are locked to the other yarn sets by the z-yarns (Figure 14). Many of the warp yarns, on the other hand, lay at the center of the preform. This structure can enhance the in-plane properties of the resulting composites.

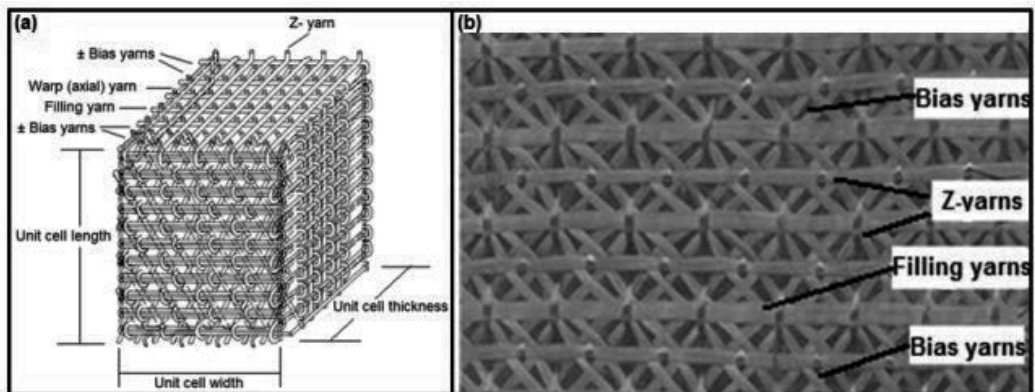


Figure 14. (a) The unit cell of multiaxis fabric (b) Top surface of multiaxis small tow size carbon fabric [30, 67].

Bilisik [28] developed a multiaxis 3D circular woven fabric, method and machine. The schematic view of the preform is shown in Figure 15 together with a real aramid preform structure. The 3D circular woven fabric consists of axial and radial yarns along with circumferential and \pm bias layers. The axial yarns (warp) are arranged in radial rows and circumferential layers within the required cross-sectional shape. \pm Bias yarns are placed at the outside and the inside ring of the cylinder surface. Filling (circumferential) yarns lay between each helical corridor of warp yarns. Radial yarns (z-fiber) were locked to the all yarn sets to form the cylindrical 3D preform. Cylindrical preform can be made with thin and thick wall sections depending upon end-use requirements.

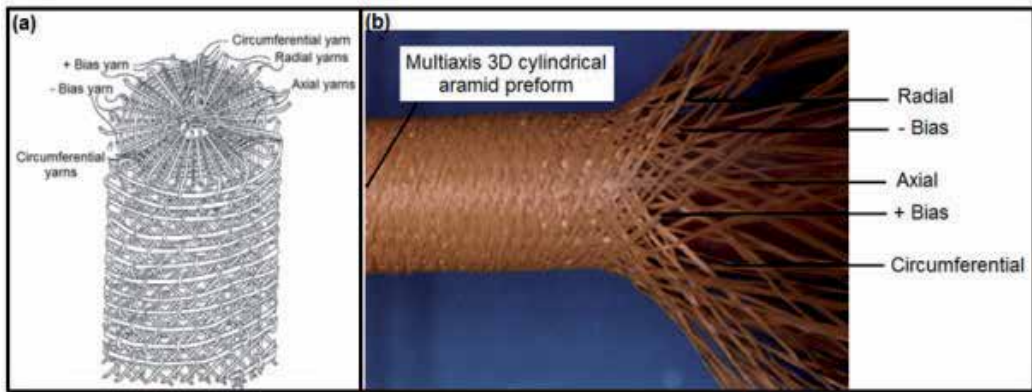


Figure 15. (a) The unit cell of multiaxis 3D circular woven fabric (b) Multiaxis 3D aramid circular woven fabric [28, 68].

3.2.6. Three-dimensional fully braided fabric

Florentine developed a 3D braided preform and a method [69]. The preform is layered and yarns are intertwined with each other according to a predetermined path. Yarn travels through the thickness of the fabric and is biased such that the width of the fabric is at an angle between 10° and 70°. The representative and the schematic views of the 3D braided preform with yarn paths are shown in Figure 16.

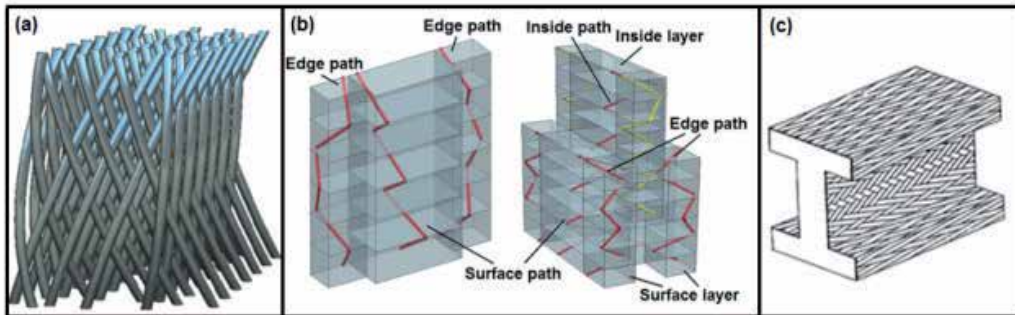


Figure 16. (a) Unit cell of 3D braided preform (b) braider yarn path on the edge and inside of the 3D representative braided preform with 4 layers (left) and 6 layers (right) [70], and (c) schematic views of 3D braided I-beam preform [71].

Tsuzuki [71] developed various 3D sectional braided preform in which four yarn carriers can surround a rotor and move in four diagonal directions. The addition and subtraction of braider yarns allow the making of various fabric geometries such as I-beam, H-beam, TT-beam etc.

3.2.7. Three-dimensional axial braided fabric

The 3D circular axial braided preform can be manufactured by maypole technique which requires two yarn sets such as warp (axial) and braider yarns. The axial yarns are fixed and

the braiders intertwine with axial yarns by making radial movements along circumferential paths. This allows more flexibility in the preform size, shape and microstructure. This type of braided structure is also called “solid braided fabric,” as shown in Figure 17 [72].

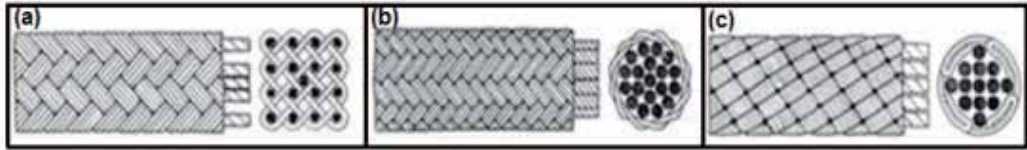


Figure 17. Solid braid fabrics (a) 4×4 axial braided fabric (b) axial round core braided fabric, and (c) axial spiral core braided fabric [72].

A tubular fabric with a helical structure was developed by Brookstein et al. [73]. This fabric is made up of warp (axial) yarns and braiders (\pm bias yarns) (Figure 18). Each axial yarn is held in place by braiders through an intertwine-type pattern. It is well suited to produce thick tubular structures and also has a potential for other geometries with a mandrel. Another 3D braided preform in a 1×1 braid pattern was developed. The braider carrier and the axial yarns are arranged in a matrix of rows and columns. The braider yarns are intertwined around each axial yarn row and column to the through-the-thickness direction as shown in Figure 18. McConnell and Popper developed a 3D axial braided fabric with a layered structure [74]. The fabric consists of axial and braider yarns. Axial yarns are positioned with regard to a pre-determined cross-section whereas braider yarns travel through the gaps between axial yarns in the row and column directions. In this way, the braided yarns are intertwined to make a bias orientation through the thickness and on the surface of the structure.

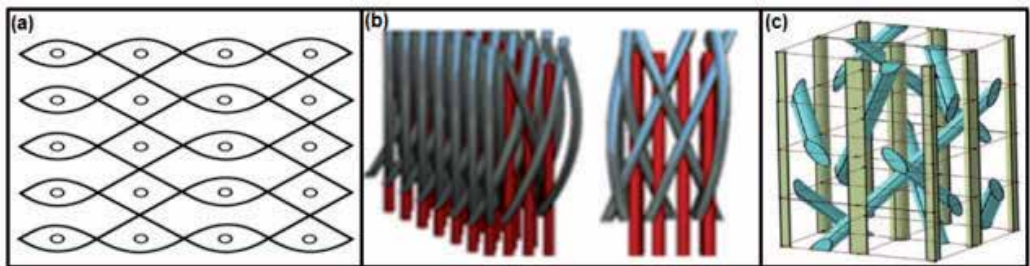


Figure 18. (a) Unit cell of the 3D braided preform [73], (b) 3D axial braided preform and unit cell [75], (c) schematic view of 3D axial braided preform [76].

3.2.8. Multiaxis 3D braided fabric

Multiaxial 3D braided structure is shown schematically in Figure 19. This fabric is constituted from \pm braider yarns, warp (axial), filling, and z-yarns. The braider yarns are intertwined with the orthogonal yarn sets to form the multiaxis 3D braided preform. This preform structure has enhanced properties especially in transverse direction. Moreover, it has identical directional

Poisson’s ratios throughout its structure [77]. Another multiaxial 3D braided structure has \pm bias yarns placed in-plane, and warp (axial), radial (z-yarns), and \pm braider yarns placed out-of-plane [78]. The braider yarns are intertwined with the axial yarns whereas \pm bias yarns are oriented at the surface of the structure and locked by the radial yarns to the other yarn sets. Figure 19 shows the multiaxial cylindrical and conical para-aramid 3D braided structures. The properties of the multiaxial 3D braided structure in the transverse direction can be enhanced and the non-uniformity in the directional Poisson’s ratios can be decreased [78].

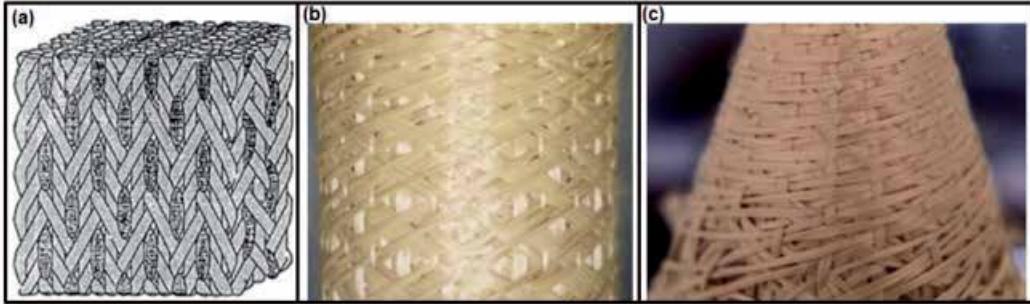


Figure 19. (a) The unit cell of multiaxis 3D braided preform [77]; multiaxis 3D braided para-aramid preforms (b) cylindrical Kevlar® preform and (c) conic Kevlar® preform [78].

3.2.9. *Three-dimensional knitted fabric*

Wunner [32] developed a multiaxis warp knit machine for Liba GmbH. The machine uses a total of four yarn sets such as \pm bias, warp and filling. These yarn sets are placed as separate layers and these layers are locked by stitching yarn by using tricot pattern, as shown in Figure 20.

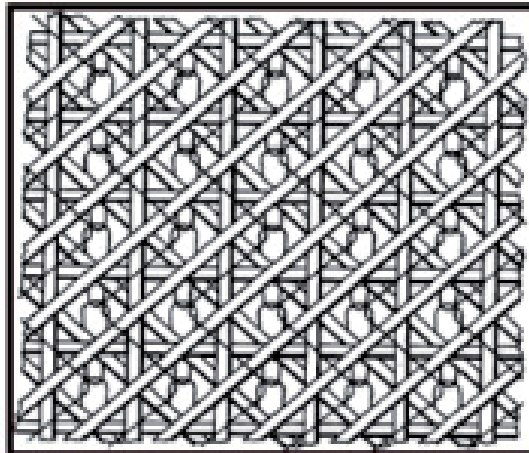


Figure 20. Multiaxis warp knit structure [32].

3.2.10. Three-dimensional knitted spacer or sandwiched structure

The 3D knitted spacer fabric consists of two separate fabric layers (top and bottom surfaces) that are connected by intermediary yarns or knitted layers [79]. The top and bottom fabrics can be weft or warp knitted fabrics with or without inlays. Three-dimensional spacer fabrics are renowned for their excellent resilience and air permeability properties. Figure 21 shows schematic and real views of various 3D knitted sandwich fabrics.

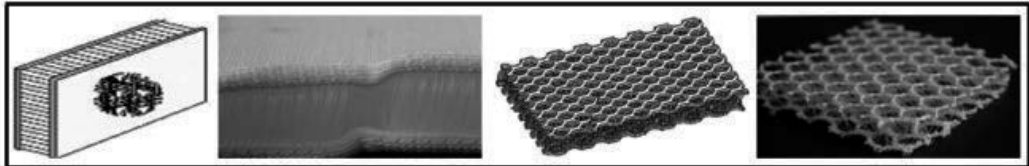


Figure 21. Various developed actual and schematic 3D knitted sandwich or spacer fabrics [79].

3.2.11. Three-dimensional nonwoven fabric

Multiple layers of 2D nonwoven webs are stacked and stitched together in thickness direction to obtain 3D nonwoven fabric. Stitching yarn provides through-the-thickness reinforcement in an effort to impart out-of-plane structural integrity and reduce delamination failures. Olry developed a method called “Noveltex” for 3D nonwoven preform fabrication [80]. This method uses needle punching as a means of fiber entanglement. A 3D nonwoven preform was developed using hydroentanglement method to create through-thickness fiber insertion. Biaxially reinforced nonwoven fabric is another type of 3D nonwoven preforms that is manufactured by employing warp knitting technology. The preform consists of warp and weft yarns along with a fiber web. Warp and weft yarns can be thought of as inlays such that they are laid in fabric structure as separate layers without any interlacements. Warp yarns, weft yarns and fiber web are all connected by stitching yarns to form an integrated structure as shown in Figure 22 [81]. Geogrid structures can be considered as a special type of nonwoven fabric. They can be classified based on their shape such as uniaxial, biaxial and triaxial geogrid structures used in wall, slope and road applications; and manufacturing methods such as punched and drawn geogrids, coated yarn geogrid and laser welded geogrids. The basic functions of geogrid structures are to interlock the aggregates, to redistribute the load over wider area to reduce the vertical stress, and to provide lateral restraint, improved bearing capacity, and tension membrane effect [82].

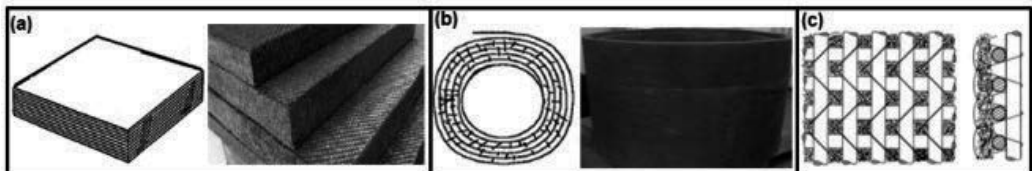


Figure 22. Three-dimensional nonwoven fabric; (a) schematic view of flat 3D nonwoven preform (left) and 3D PAN-based graphite felt composite (right); (b) schematic view of circular 3D nonwoven preform (left) and 3D PAN-based graphite felt composite (right); (c) top and side views of 3D biaxially reinforced nonwoven preform [80, 81, 83].

4. Fabrication of fabrics

4.1. Weaving

4.1.1. Two-dimensional weaving

The 2D woven fabric is the most widely used material in the composite industry with a share of about 70%. Traditional weaving machine (Figure 23) is used to manufacture the fabric [4, 84]. This machine is constituted of several units such as warp let-off, fabric take-up, shedding, weft insertion and beat-up. Recently, traditional weaving machine was modified to weave high modulus fibers such as carbon, E-glass, S-glass, and para-aramid. The machine is capable of weaving a range of fabric types and patterns including plain, twill, satin, and leno. It is also possible to fabricate hybrid fabrics by incorporating different fiber types in warp or weft yarns. Another approach is to use warp and weft yarns consisting of different types of fibers [4].

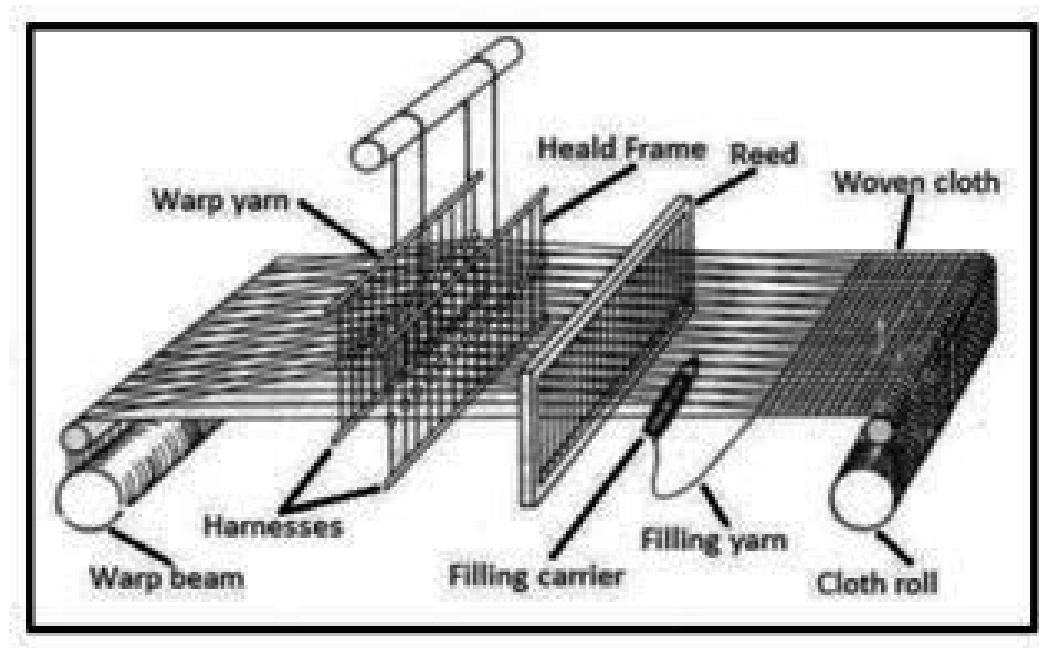


Figure 23. Schematic view of 2D weaving and shedding unit [4, 84].

4.1.2. Triaxial weaving

Triaxial weaving machine consists of multiple \pm warp beams, filling insertion, open beat-up, rotating heddle and take-up unit, as shown in Figure 24. Warp beams are located above the machine. \pm Warp yarns unwind from these beams and head to a separation unit where the warp yarns from each beam are separated into two layers. Then these layers are fed vertically into

the interlacing zone. The front layer is directed to the right, whereas the rear layer heads to the left. The directions are reversed after the outmost warp end reaches the edge of the fabric. As a result, the warp makes the bias intersecting in the fabric. Special hook heddles govern the shedding action by shifting after each pick. Two opposite reeds that are positioned in the front and back sides of the warp layers beat up the pick [45]. In order to make quart-axial fabric, warp yarns are inserted to the triaxial woven fabric at selected places depending upon the end-use. After that, \pm bias yarns rotate just one bobbin distance and heddles are shifted one heddle distance. Then warp is fed to the weaving zone and the shedding action is carried out by the heddles. Filling yarn is inserted and is beaten against the fell to complete the fabric formation. Finally, the fabric is removed from the weaving zone with the aid of a take-up unit [45].

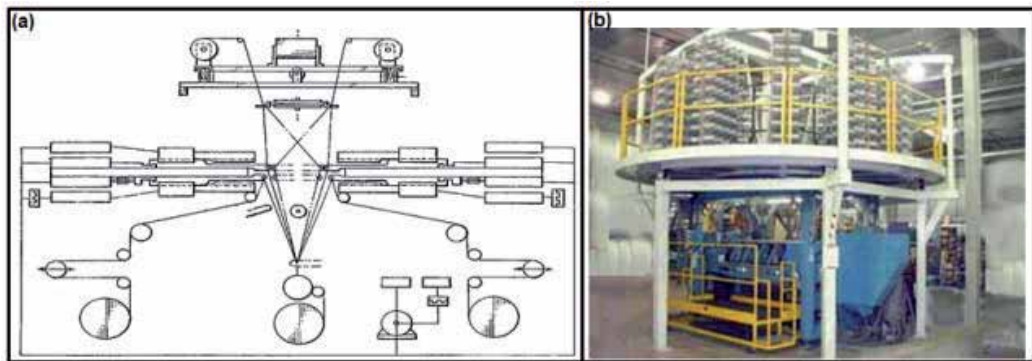


Figure 24. (a) Schematic view of (b) actual triaxial weaving loom [45, 85].

4.1.3. Three-dimensional weaving

In order to make the representative 3D plain woven preform, the warp must be arranged in a matrix of rows and columns, as shown in Figure 25. The first step is the one-step sequential movement of an even number of warp layers in the column direction (a2). This was accomplished with the aid of a 2D shedding unit (not shown). The second step is to insert filling yarn between each warp layer in the row direction (a3). The third step is the one-step sequential movement of an even number of warp layers in the row direction (a4). This was also accomplished via the 2D shedding unit. The fourth step is z-yarn insertion between each warp layer in the column direction (a5). After fulfilling the cycle of steps (a2-a5), 3D woven fabric is formed (a6). The length of the preform determines the number of cycles to be performed. Figure 25 shows the pattern of 3D plain-z yarn orthogonal preform. Steps (a1-a6) are followed to form the fabric structure. Z-yarn is inserted with no interlacement (a4-a6). Again, the preform dimensions determine how many warp layers to be used in the row and column directions [60].

Figure 26 shows the steps necessary to form a 3D circular plain woven fabric. In such an arrangement, axial yarns are positioned in a matrix of circular rows and radial columns according to desired cross section. The first step in the process is the one-step sequential movement of an even and odd number of axial layers in the radial column direction (a2). This

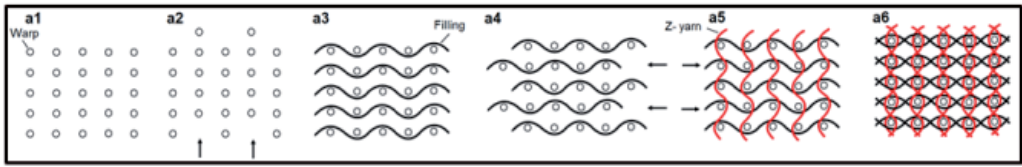


Figure 25. Three-dimensional weaving method to make representative fully-interlaced woven preforms; 3D plain woven preform (a1-a6) [60].

can be accomplished via a 2D circular shedding unit (not shown). The second step is to insert circumferential yarn between each axial layer in the circular row direction (a3). The third step is the one-step sequential movement of an even and odd number of axial layers in the circular row direction (a4) which is also accomplished with the aid of the 2D circular shedding unit. The fourth step is radial yarn insertion between each axial layer in the radial column direction (a4). The 3D circular plain woven preform is formed (a5) after repeating the steps (a2-a4). The length of the preform determines the number of repeats. The unit cell of 3D orthogonal circular woven preform consists of three yarn sets such as axial, circumferential and radial yarns. Axial yarns are arranged in a matrix of circular rows and radial columns. Circumferential yarns are single-end and are laid down between each adjacent axial yarn row. Radial ends are positioned between each axial row through the preform thickness and they locked all other yarn sets. Hence the structural integrity of the preform is achieved. An individual shuttle for circumferential yarn that is mounted on each individually rotated ring was used for the preform fabrication. In addition, the radial carriers reciprocated linearly to the radial corridor of the 2D shedding plane on the rig thus crossing the radial yarns in the preform structure (crossing shedding) [61].

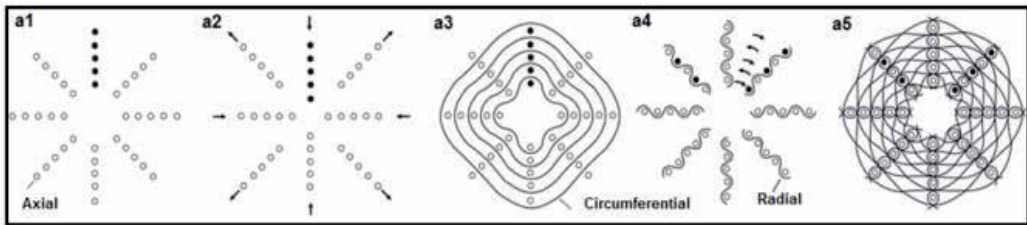


Figure 26. Three-dimensional weaving method to make representative fully-interlaced circular woven preform; 3D circular plain woven preform (a1-a5) [61].

The state-of-the-art weaving loom was modified to make 3D orthogonal woven fabric [86]. For instance, one of the looms which has three rigid rapier insertions with dobby type shed control systems was converted to make 3D woven preform. The new weaving loom was also designed to make various sectional 3D woven preform fabrics [23]. The 3D circular weaving method and fabric (or 3D polar weaving) were developed [63]. The device consists of a table that can rotate and a pair of carriers. The table holds the axial yarns. Each carrier contains radial yarn bobbins together with a guide frame to regulate the weaving position. The main task of the

carriers is to move vertically up and down in order to insert the radial yarns. A circumferential yarn bobbin is placed radial to axial yarns. After the circumferential yarn is wound over the vertically positioned radial yarn, the radial yarn is placed radially to outer ring of the preform.

Multiaxis 3D woven fabric, method and machine based on lappet weaving principals were introduced by Ruzand and Guenet [65]. The basis of the technique is an extension of lappet weaving in which pairs of lappet bars are reused on one or both sides of the fabric. Uchida et al. [66] developed a fabric called five-axis 3D woven which has five yarn sets such as \pm bias, filling, warp and z-fiber. The process includes a bias rotating unit; filling and z-yarn insertion units; warp, \pm bias and z-fiber feeding units; and a take-up unit. The yarns are oriented by the rotation of horizontal bias chain while the filling is inserted to the fixed shed. All yarns are locked together by z-yarns. This is followed by beat-up and fabric take up procedures. Mohamed and Bilisik [30] developed a multiaxis 3D woven fabric, method and machine. This fabric is constituted from five yarn sets, such as \pm bias, warp, filling and z-yarns. \pm Bias yarns are placed on the front and back face of the structure. These yarns are locked to the other yarn sets by the z-yarns. Warp yarns, on the other hand, generally lay at the center of the preform (Figure 27). This formation generally improves the composite in-plane properties.

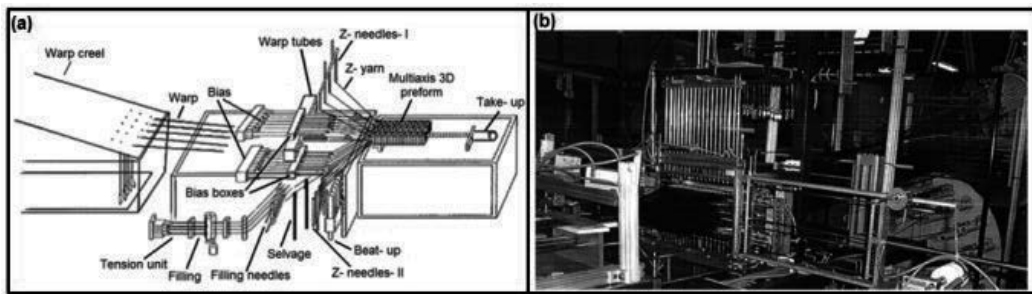


Figure 27. (a) Schematic view of multiaxis weaving machine (b) Side view of multiaxis weaving machine [30, 67].

The warp yarns are arranged in a matrix of rows and columns within the desired cross-section. First, a pair of tube rapiers positions the front and back bias yarns relative to each other. This is followed by the incorporation of filling yarns via needles between warp rows. Then selvage and latch needles lock the filling yarns by using selvage yarns before returning to their starting position. Z-yarns are inserted across the filling yarns by z-yarn needles. Then filling needles insert the filling yarns and these yarns are locked by selvage needles located at the opposite side of the preform. After that, the filling needles return to their initial position. Then bias yarns and filling yarns are secured in place by z-yarns which return to their initial position by traveling between the warp yarns. This is followed by beat up and fabric take-up procedures. Bilisik [28] developed a multiaxis 3D circular woven fabric, method and machine. The preform consists of axial and radial yarns together with circumferential and \pm bias layers (Figure 28). The axial yarns (warp) are arranged in radial rows and circumferential layers within the desired cross section. \pm Bias yarns are placed outside and inside ring of the cylinder surface. Filling (circumferential) yarns lay between each warp yarn helical corridors. In order to achieve

the cylindrical form, radial yarns (z-yarns) are linked with other yarns. The thickness of the preform section can be adjusted regarding the end-use. The process requires a machine bed, \pm bias and filling ring carriers, a radial braider, a warp creel and a take-up unit. First, shedding mechanism orients the bias yarns at an angle of $\pm 45^\circ$ to each other. Then the carriers wind the circumferential layers by rotating about the adjacent axial yarns. Special carrier units insert the radial yarns and link the circumferential yarn layers with \pm bias and axial layers. Then the fabric is removed from the weaving zone by take-up unit. This process results in enhanced torsional properties for both preform and composite owing to bias yarns.

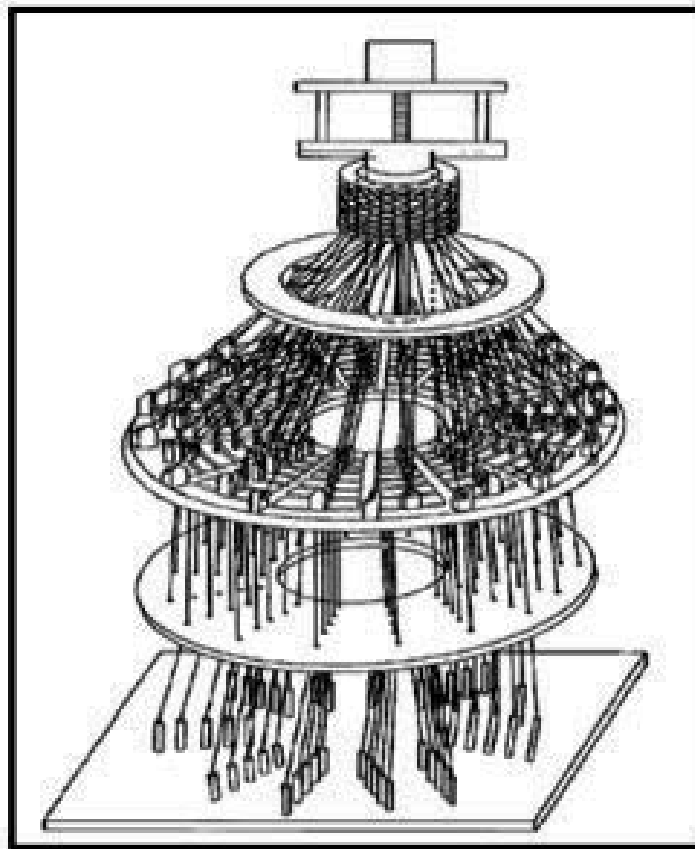


Figure 28. Schematic view of multi-axis 3D circular weaving loom [28, 68].

4.2. Braiding

4.2.1. Three-dimensional braiding

Two-dimensional braiding is a simple traditional textile based process to make bias fabric. A typical braiding machine consists of a track plate, a spool carrier, a former, and a take-up. The

track plate supports the carriers, which travel along the path of the tracks. The movement of the carriers can be provided by horn gears, which propel the carriers around in a maypole arrangement. The carriers are devices that carry the yarn packages around the tracks and control the tension of the braiding yarns. At the point of braiding, a former is often used to control the dimension and shape of the braid. The braid is then delivered through the take-up roll at a predetermined rate. If the number of carriers and the take-up speed are properly selected, the orientation of the yarn (braiding angle) and the diameter of the braid can be controlled. Braiding can take place in horizontal or vertical direction [87].

4.2.2. Triaxial braiding

A large scale 2D circular triaxial machine was developed by the Boeing Company (Figure 29). The fabric consists of warp (axial) and \pm bias fibers. It is possible to cast variously shaped structural elements by using a mandrel [88].

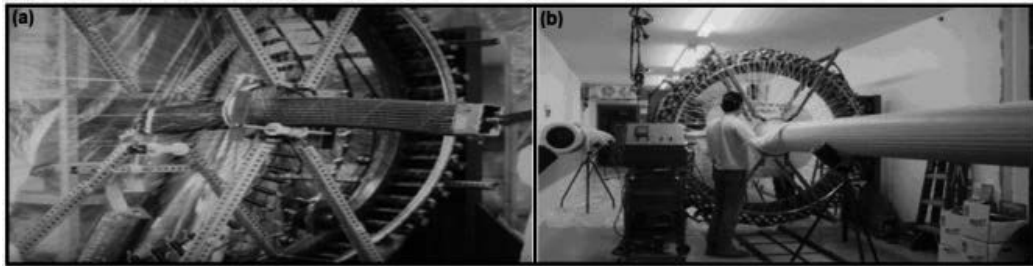


Figure 29. Two-dimensional triaxial braiding machine (a) by Boeing Inc. [88] and (b) by Fiber innovation Inc. [89].

Fiber Innovation Inc. developed a large circular 2D triaxial braider machine (Figure 29). The machine consists of a circular bed, an axial guiding tube, a large braider carrier together with formation, mandrel, and take-up units. The braider carrier moves around the axial fiber tubes according to a predetermined path to make \pm bias orientation around the axial yarn. Thick structures can be produced by over-braiding on the mandrel. Complex structural parts can be made by cutting/stitching the fabrics [89].

4.2.3. Three-dimensional fully braided fabric

4.2.3.1. By 4-step braiding method

In the 4-step braiding method, each machine cycle involves four different motions in order to intertwine the longitudinal yarns that are positioned in row and column directions along the cross-section. Braider yarns, on the other hand, are intertwined by braider carriers that move in predetermined paths within the matrix so as to form the fabric. Florentine developed a 3D braided preform that has a layered structure [69]. Yarns are intertwined with each other according to a certain path and are biased such that the width of the fabric is at an angle between 10° and 70° . The process involves rectangular layout of individual row/column arrangements

in the machine bed. Each individual row has a braider carrier in order to carry out four different cartesian motions (Figure 30).

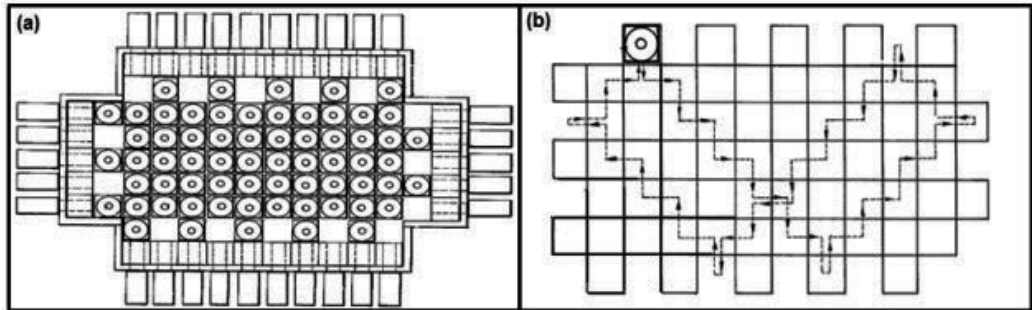


Figure 30. Schematic views of (a) 3D braiding machine and (b) yarn carrier path [69].

Brown developed a 3D circular braided fabric having one set of fiber sets [90]. In order to form the fabric structure, these fiber sets are intertwined with each other. The machine has concentric rings that are attached to a joint axis. Braid carriers are circumferentially mounted to the inside diameter of the ring. The ring is adjusted depending upon the thickness of the fabric. The rings rotate one braid carrier distance depending on a pre-determined path. Then, the braid carriers move in the axial direction. After that, the cycles are repeated in the above sequence. The fabric has \pm bias yarn orientation through the thickness of the cylinder wall and cylinder surface at the helical path, as shown in Figure 31.

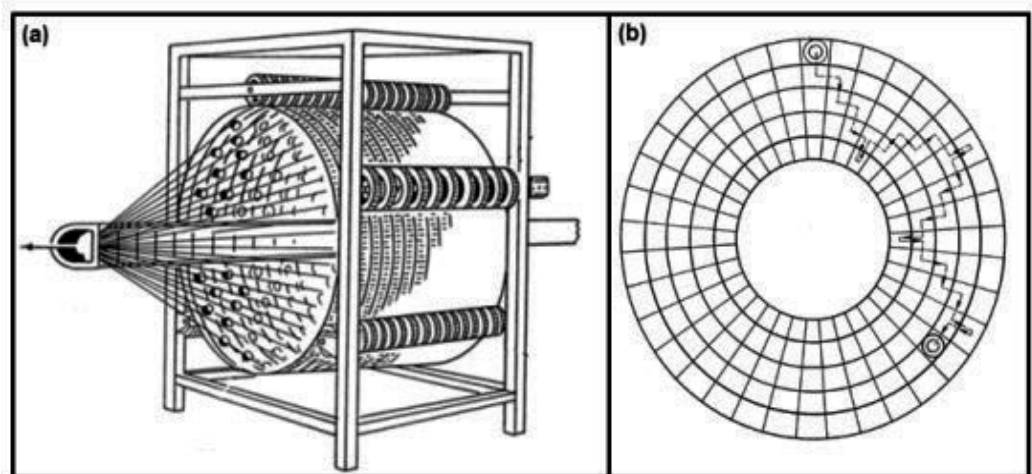


Figure 31. (a) Schematic views of 3D circular braiding machine [90] (b) yarn carrier path [69].

4.2.3.2. By rotary braiding

This method is essentially a derivative of the maypole braiding. In 3D rotary braiding braider carrier can move freely and arbitrarily over a base plate. Hence, each braider yarn can be interlaced into the fabric [9, 91]. Tsuzuki developed a 3D braider that contains star-shaped rotors arranged in a matrix of multiple rows and columns [92]. Each rotor is surrounded by four carriers that are able to move in four diagonal directions. The directions in which the carriers move are governed by the rotation of the rotors (Figure 32).

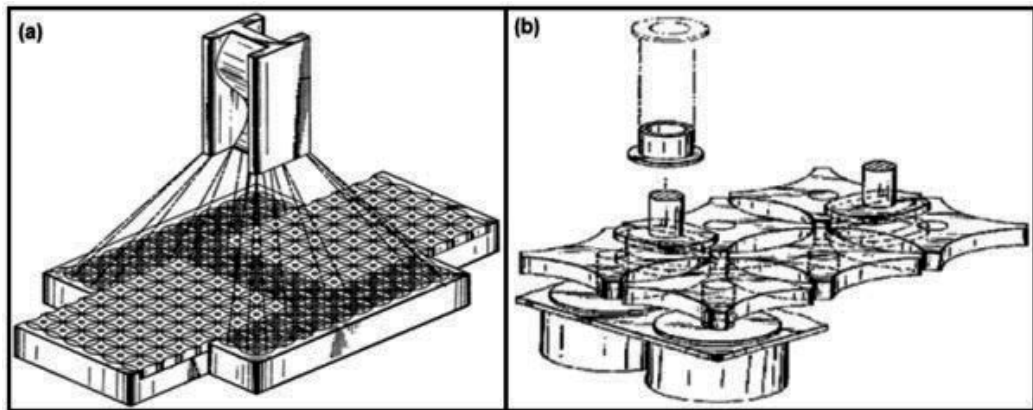


Figure 32. Schematic views of (a) 3D rotary braiding machine and (b) yarn carrier actuation unit [92].

4.2.4. Three-dimensional axial braided fabric

4.2.4.1. By maypole braiding method

Maypole braiding method requires two yarns sets such as warp (axial) and braider yarns. Axial yarns are fixed and the braiders intertwine with the axial yarns by moving back and forth radially about circumferential paths. Uozumi [93] produced a 3D circular braided fabric by using multi-reciprocal braiding process. This process relies on the 2D circular triaxial braiding essentials and requires two sets of yarns such as \pm bias (braider) and warp (axial) yarns. Thick fabrics with different cross sections including structural joint, end-fitting and flange tube were made by over-braiding [9]. Multi-reciprocal braiding process is shown in Figure 33.

Brookstein et al. [94] developed a tubular fabric that consists of braiders (\pm bias yarns) and warp (axial) yarns. Braiders intertwined around each axial yarn so that they lock each individual axial yarn in its place. This intertwining forms a helix structure. In the process, a horn-gear type machine bed is arranged cylindrically so that the axial and braider carrier are positioned inside the diameter of the cylinder. In this way, adding layers and ensuring the structure compactness becomes easy. A horn gear mechanism governs the movement of the braider yarns. They travel in a pre-defined path about the axial yarns to form the fabric (Figure 34). A take-up unit removes the preform from the weaving zone. This process is well suited to

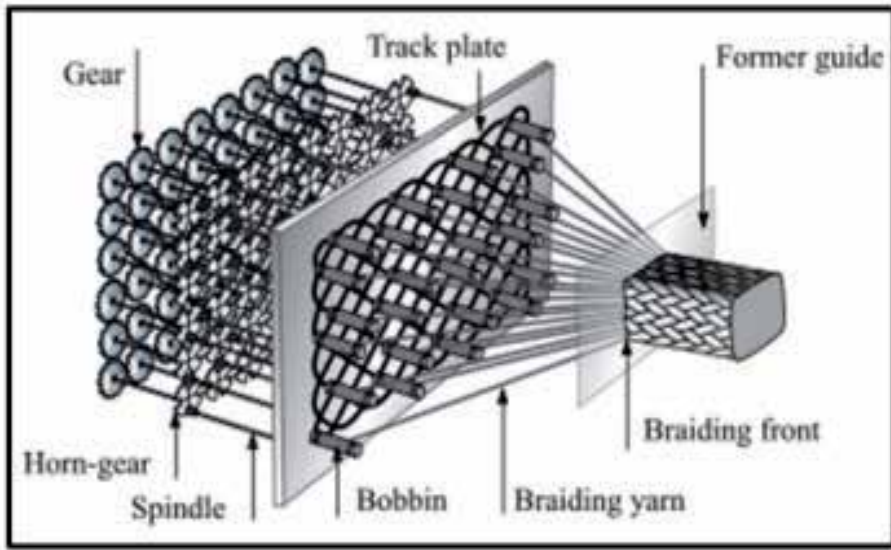


Figure 33. Schematic view of 3D circular axial braiding based on maypole method [9].

produce thick tubular structures and also has the potential for other geometries with a mandrel. Similar 3D axial braiding machine based on maypole method was also developed by Japan as shown in Figure 34 [95].

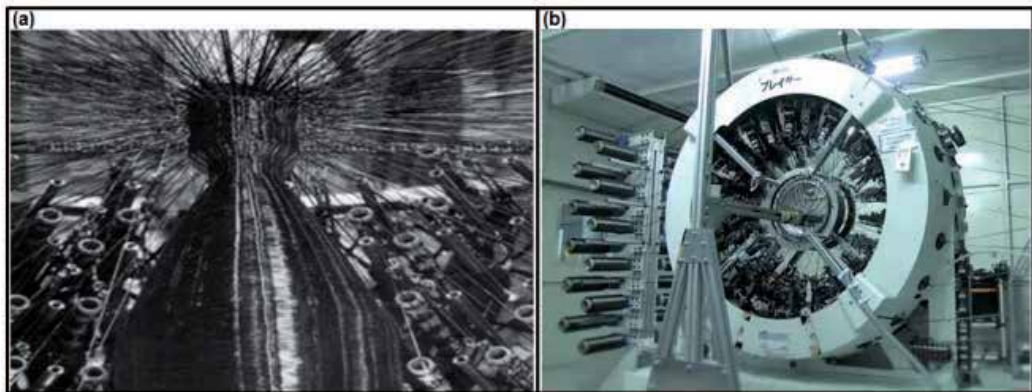


Figure 34. (a) 3D circular braiding by maypole method [94] (b) another type 3D axial braiding machine from Japan [95].

4.2.4.2. By 4-step braiding method

Figure 35 shows the required matrix setting for braider carriers and axial yarns so as to form a 3D fabric having 1×1 pattern. The steps involved are the following: The first step is sequential

and the reversal movement of the braider carriers in the column direction (b). The second step is sequential and the reversal movement of the braider carriers placed on the rapier in the row direction (c). The third step is again sequential and the reversal movement of the braider carriers in the column direction (d). The fourth step is again sequential and the reversal movement of the braider carriers placed the rapier in the row direction (e). The number of these steps can be adjusted regarding the desired fabric length. More braider carriers and axial yarn may be used if the preform dimensions are to be increased [75].

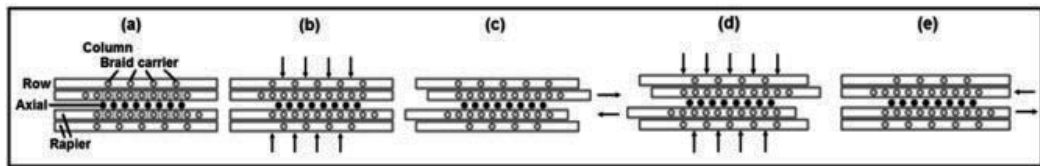


Figure 35. Three-dimensional axial braided preform fabrication principles (steps a-e) [75].

4.2.4.3. By 2-step braiding method

In this method, the cross sectional geometry of the fabric determines the matrix setting of axial yarns. Braider yarns travel diagonally along the matrix arrangement and lock the axial yarns so as to form the required shape. Each braider carrier makes two distinct motions [12, 96]. The process demands relatively fewer braider yarns to impart directional reinforcement. Since the number of braider carriers is reduced, the process can easily be automated. It is possible to produce various shapes such as T, H, TT and bifurcated fabrics [12]. Mc Connell and Popper developed a 3D axial braided fabric [74]. The machine comprises a machine bed, an axial unit, a braider carrier, and a compaction unit. The preform consists of layered and axial yarns. The shape of the cross section determines the positioning of axial yarns. Braider yarns are intertwined and oriented in bias directions along the thickness and the surface of the preform. They travel between the axial layers across the row and column direction. The braid carrier travels about the axial unit depending on a pre-defined path to make two distinct cartesian motions for creating braider type interlacements. The axial unit feeds the axial (0°) yarns in the machine direction. The final preform is formed by the compaction unit (Figure 36).

4.2.4.4. By rotary braiding method

Schneider et al. [91] developed a method and machine to make a 3D braided fabric which has multiple axial yarn networks and braider yarns. The method is called 3D rotary braiding which is similar to Tsuzuki's rotor braiding. Figure 37 shows the flat and circular 3D axial braiding machine. The machine is equipped with horn gears that can be activated individually by a servo motor. A clutch-brake mechanism controls the step and rotation of individual horn gears, axial yarn guide and braider carrier. If desired, a computer-aided design (CAD) tool can be added to produce different shapes and cross sections. In addition, this method employs

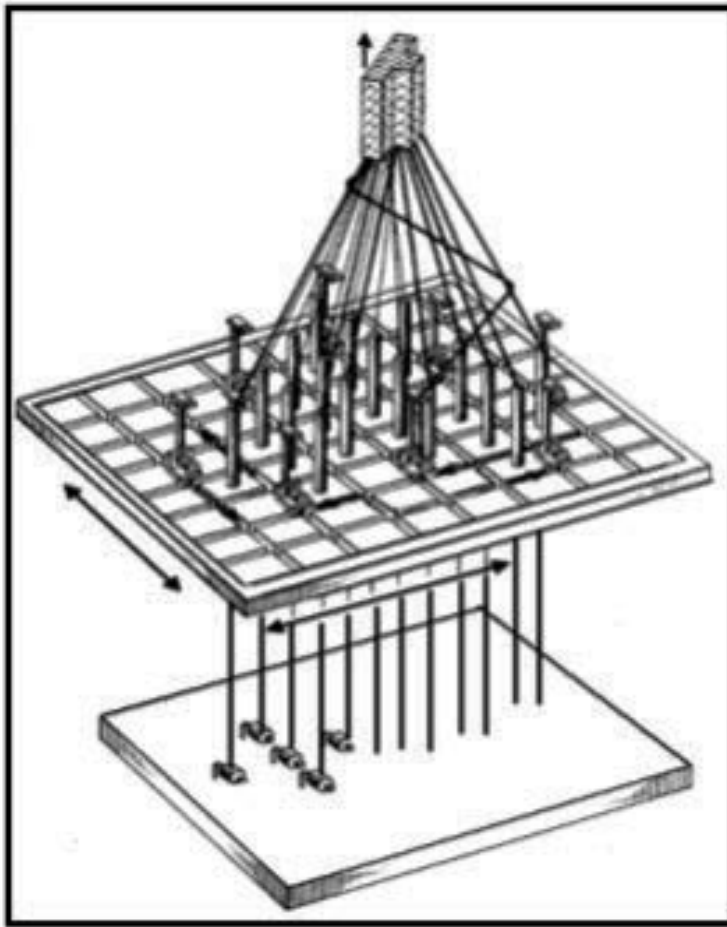


Figure 36. Schematic view of the 3D axial braiding by 2-step braiding [74].

individually controlled gripping forks, which can quickly move yarn carriers between the horn gears according to a pre-determined pattern [97].

4.2.5. Multiaxis 3D braided fabric

4.2.5.1. By 6-step braiding method

This method employs \pm braider yarns, warp (axial), filling, and z-yarns. In order to form the fabric, the braider yarns are intertwined with the orthogonal yarn sets. The properties of the multiaxial 3D braided structure in the transverse direction are enhanced and the directional Poisson's ratios of the structure are identical. In this process, there are six distinct steps in each cycle. Steps 1 and 2 are identical to the 4-step method. Step 3 inserts yarn in the transverse direction. Steps 4 and 5 are identical to the steps 1 and 2, and step 6 inserts yarn in the thickness

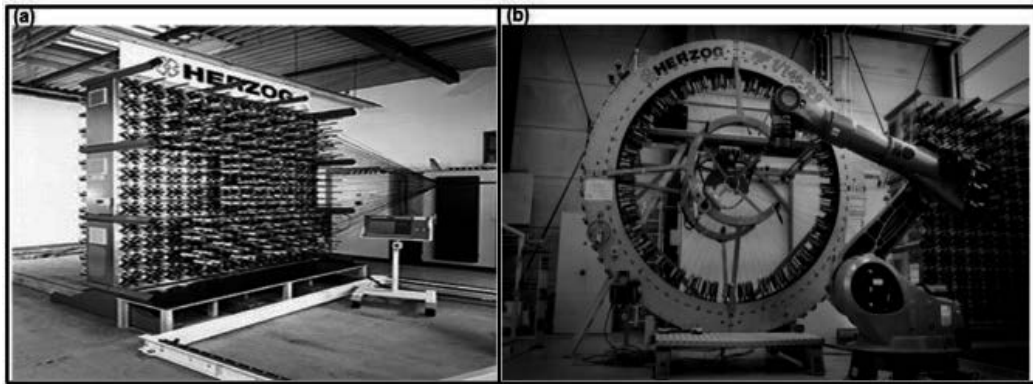


Figure 37. (a) 3D flat and (b) 3D circular axial braiding machines [91].

direction [77]. Another multiaxial 3D braided fabric produced by the 6-step method consists of \pm bias, warp (axial), radial (z-yarns) and \pm braider yarns. \pm Bias yarns are oriented in-plane whereas the others are positioned out-of-plane [78]. The axial and braider yarns are intertwined with each other while \pm bias yarns are positioned at the surface of the preform and secured by the radial yarns to the other yarn sets. The process takes place over six steps in each cycle. In steps 1 and 2, \pm braider yarns are intertwined around the axial yarns as in the 4-step method. In step 3, \pm bias yarns are laid down on the surface of the structure. In step 4, the radial yarns move in the thickness direction of the structure and lock the \pm bias yarns to the \pm braider and axial yarns. In steps 5 and 6, the \pm braider yarns are intertwined around the axial yarns as in the 4-step method.

4.3. Nonwoven

4.3.1. Two-dimensional nonwoven fabric

The first step in the fabrication of a 2D nonwoven fabric is to prepare a short fiber web using various methods such as dry-laying, wet-laying and spun-laying. This web structure is loosely formed without any strong binding or connection between individual fibers other than weak cohesive forces. In order to obtain a continuous fabric structure with adequate strength, this fiber web must be consolidated by entangling or binding the individual fibers together. In order to achieve this, various techniques are used including mechanical ones such as needling, stitching and water-jet entangling; chemical methods such as impregnating, coating and spraying; or cohesion-based techniques like calendering, air blowing and ultrasonic impact [57].

4.3.1.1. By needling method

Needling method uses barbed needles located vertical to the fabric plane in order to achieve entanglement between the short fibers. These needles are fixed on a reciprocating needle board located above the fiber web. The needles strike in the web catching the fibers with their barbs

and orienting them in random in-plane and out-of-plane directions (Figure 38) [57, 98]. The most important goal of needling process is to reorient the fibers in fabric out-of-plane (i.e., thickness) direction as much as possible so that these fibers can act like a lock restraining any fiber movement and keeping the web together. It is essential to apply a certain pressure during the process in order to increase the so called “friction-lock” among fibers and to improve the degree of bonding in the felt. Important processing parameters during needling are needle design, needle density per fabric width, the stroke frequency, the delivery speeds and the working width [99-101].

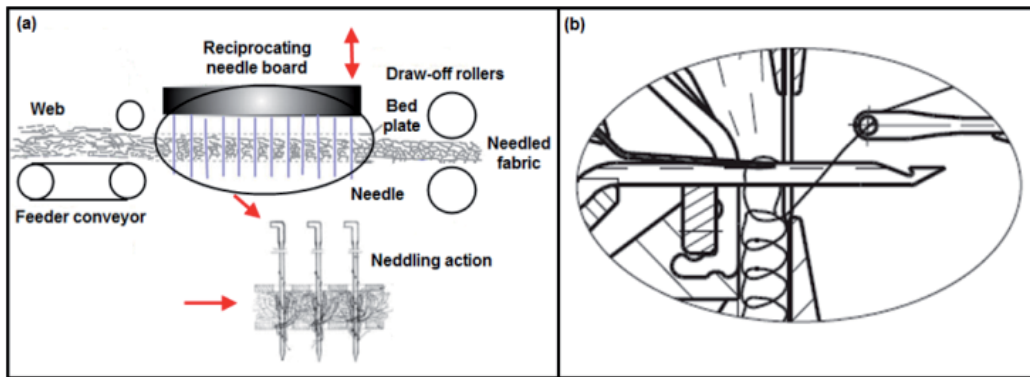


Figure 38. (a) Principle of needling a fiber web [57, 98] (b) Schematic views of stitching method in which loop formation cycle of a stitch bonding machine is shown [57].

The fiber movement caused by needling process leads to changes in fabric dimensions and local areal mass of the fabric. Needling can also result in fiber breakages due to fiber-fiber and needle-fiber frictions. The later can be minimized by treating the fibers with a suitable finishing agent prior to needling [57]. Web feeding and take-up speeds are important process parameters. The stitch density which is the number of penetrations per square area of the felt is calculated by using Eq. (1).

$$Ed = \frac{n_h \cdot N_D}{V_v \cdot 10^4} \tag{1}$$

where, E_d is the stitches per area (stroke per cm^2), n_h is the number of lifts (per min.), N_D is the number of needles by nonwoven fabric width (per m), and V_v is the web take-up speed (m/min).

4.3.1.2. By stitching method

Stitching method involves through-the-thickness stitching of the fiber web in order to consolidate the nonwoven fabric. Nonwoven production process consists of a carding machine, a

cross lapper and a stitch bonding machine. The stitching loop formation technique is shown in Figure 38 [56, 57]. The main elements for stitching process are the compound needle, closing wire, compound needle hook and guide. Compound needle and closing wire bar are connected to the driving cams and the knocking over sinker. Stitch bonding machines are equipped with one or two guide bars. Lapping is accomplished by the swinging and shogging movements. The swinging action is carried out by means of a rotary cam and a crank drive. Shogging allows the use of a cam disc. Working with two guide bars allows to use one guide for pillar stitch and the other for tricot-stitch. The degree of bonding is determined by the number of stitching loops per unit area which is a function of wale density (number of wales per unit length) and course density (number of courses per unit length). The density of stitching loops is determined by machine gauge and the stitch length. Twisted yarns, textured filaments and film yarns can be used for stitching.

4.3.1.3. *By hydroentanglement method*

In hydroentanglement method, water jets are used to entangle the fibers and obtain a continuous nonwoven surface. The main principle is the same as that of the needling method. Water jets strike onto the nonwoven web and reorient a portion of fibers in out-of-plane directions. These reoriented fibers wrap and lock the others in their vicinity ensuring a continuous surface. The web is soaked from the bottom side only after they have passed the jets which neutralize the part of the web densification [57, 102]. The effect of striking jets on fibers varies depending upon the position of the fiber in the web. Fibers located on the surface facing the water jets are influenced more in comparison with fibers at the bottom. The main process parameter that determines the bonding efficiency is the jet speed. The following relation can be used to find the jet speed.

$$v_w = a \cdot \sqrt{\frac{2 \cdot \Delta p}{\rho}} \quad (2)$$

where, v_w is the speed of the jet at the exit point, Δp is the pressure differential between the nozzle element and the surroundings, ρ is the density of the medium, and a accounts for the friction.

4.3.1.4. *By thermal and chemical methods*

Thermal bonding process starts with a hot-air treatment to soften the thermoplastic fibers. Then calendaring and welding processes are carried out to consolidate nonwovens. Chemical bonding involves the application of binder dispersions then curing and drying of the impregnated webs [57].

4.3.1.5. *By electrospinning method*

Electrospinning method uses an electric energy field to spin a polymer solution from the tip of single or multiple needles to a flat or cylindrical collector. A voltage is applied to the polymer

which causes a jet of the solution to be drawn towards a grounded collector. The fine jet stretches and elongates as it travels under energy field and is collected as a nonwoven nano-web structure [103]. Various publications indicate that the voltage required to produce fibers range from 5 kV to 30 kV [104]. This range of voltage is good enough to overcome the surface tension of the polymeric solution and to produce very fine charged jets of liquid towards a grounded target. This charged jet before hitting the target undergoes splitting and drawing and forming fibers with different sizes and shapes before evaporating to form a nonwoven nano-web structure. The electrospinning system consists of two separate entities, a sprayer and a collecting device. The sprayer essentially consists of a glass spinneret, which holds the polymer solution. One of the metal electrodes from the high voltage supply is given to the solution, which serves as the positive terminal. A collector, which collects the fibers is given the other end of the electrode, which serves as the negative terminal [105].

4.3.2. Three-dimensional nonwoven fabric

4.3.2.1. By needling method

Olry [80] developed a 3D nonwoven process based on the needling method. The method is essentially the same as 2D nonwoven process except for the usage of multiple nonwoven webs for fabric production. These webs are stacked one on top of another and needled in thickness direction to form a thick 3D structure. Figure 39 shows 3D flat and circular nonwoven machines schematically. Fukuta developed a hydroentanglement process where fluid jets are used to produce 3D nonwoven fabric [81].

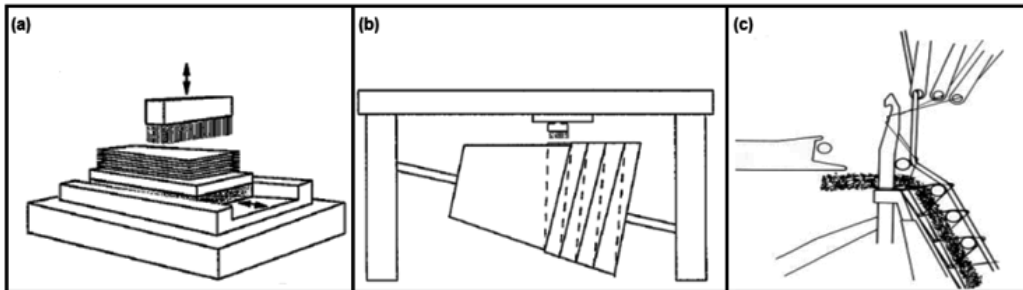


Figure 39. (a) 3D flat non-woven machine (b) 3D circular non-woven machine [80, 81] (c) Schematic view of 3D biaxially reinforced nonwoven structure made by warp knitting machine [57].

4.3.2.2. By stitching method

The 3D nonwoven structure is formed by using a warp knitting machine. Warp yarns are fed by one or more guide bars. Weft yarns are inserted between the warp yarns and the nonwoven web, whereas bias yarns are laid over the warp layers. Multiple compound needles insert the stitching yarns to lock the nonwoven web with warp, weft and bias yarns (Figure 39) [56, 57].

4.4. Knitting

4.4.1. Two-dimensional knitted fabric

The 2D knitted fabric is produced by mainly two methods, namely, weft knitting and warp knitting. In weft knitting, latch needles are arranged circumferentially in the axial and radial direction of the machine bed. Yarn guiding bars feed the yarns to the axial latch needles mounted on the cylinder. Both axial and radial latch needles interloop the yarns to make 2D circular weft knitted fabric for various composite applications. Figure 40 shows the interlooping action, 2D glass weft knitted fabric and cylinder section of a 2D circular weft knitting machine [49].

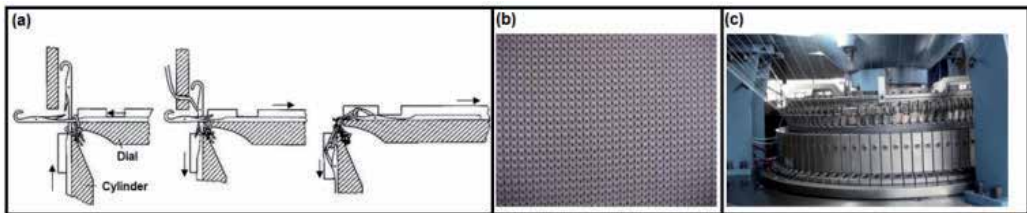


Figure 40. (a) Schematic views of 2D weft knitted fabric during formation (b) 2D weft knitted glass fabric (c) 2D weft knitting machine [49, 79].

Warp knitting consists of a yarn feeding unit, multiple yarn guiding bars, multiple axial latch needles, a sinker and a fabric take-up unit. The guide bars are located at the front of the machine. The sinker bar holds the fabric by moving forward while the needle bar starts to rise from knocks-over (holding down action). As the needle bar rises to its full height, the old overlaps open the latches and slip down onto the stems. Then, the sinker bar withdraws in order to enable the overlapping of guide bars (clearing action). The guide bars move to the back of the machine and then make a shogging for the overlap (overlap action). Then the guide bars swing to the front and the yarns wrap into the needle hooks (return swing action). The needle bar moves down in order that the old overlaps contact and close the latches, trapping the new overlaps inside. The sinker bar now starts to move forward (latch closing action). As the needle bar continues to descend, its head passes below the surface of the trick-plate, drawing the new overlap through the old overlap, and as the sinkers advance over the trick-plate, the underlap shogging of the guide bar is commenced (knocking-over and underlap action). These knitting actions and the machine are shown in Figure 41 [49, 106].

4.4.2. Three-dimensional knitted fabric

4.4.2.1. By weft knitting method

The 3D weft knitting method was developed by Offermann et al. [108]. The weft knitting machine consists of warp and weft feeding, warp yarn guide track, weft yarn carrier, stitch yarn carrier, yarn feeding unit and fabric take-up unit as shown in Figure 42. Two layers of

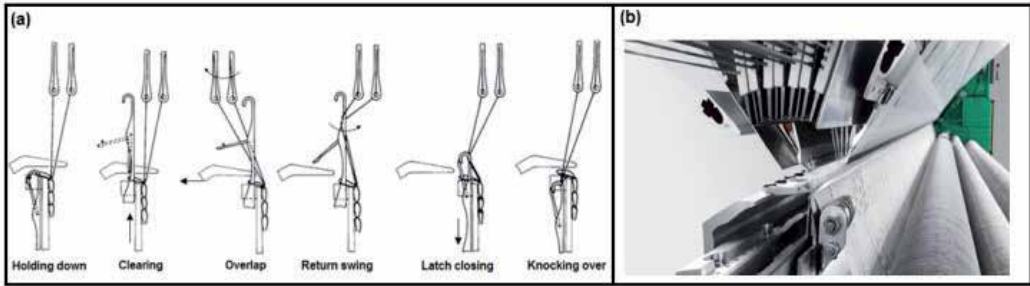


Figure 41. (a) Schematic views of the warp knitting action to form the 2D warp knitted fabric structure using the latch (b) Actual 2D warp knitting machine [36, 49, 107].

warp yarns are laid by warp yarn guide track. Two layers of weft yarns are laid over the warp layers by weft yarn carriers. The stitching yarn locks the warp and weft yarn sets using multiple latch needles in which stitched yarns were structured as weft loops. Simple as well as complex sectional knitted preforms were fabricated by the special take-up device. The critical process parameters are warp and weft densities, stitching density, yarn feeding, and fabric take-up ratios [51, 109].

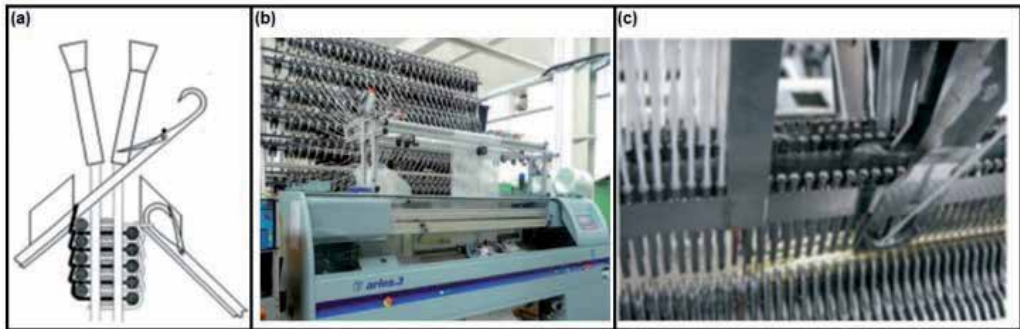


Figure 42. (a) Schematic views of 3D weft knitting methods (b) 3D knitting machine; and (c) weft yarn carrier during knitting [108, 109].

4.4.3. Multiaxis 3D knitted fabric

4.4.3.1. By warp knitting method

Wunner [32] designed a multiaxis warp knit machine for Liba GmbH. The machine is equipped with a pinned conveyor bed, a fiber carrier for each yarn set, a stitching unit, yarn creels and a take-up unit. It employs \pm bias, warp and filling (90° yarn) yarn sets together with stitching yarn. Stitching yarn unites all the layers and provides structural integrity (Figure 43). Tricot pattern is generally used for this process.

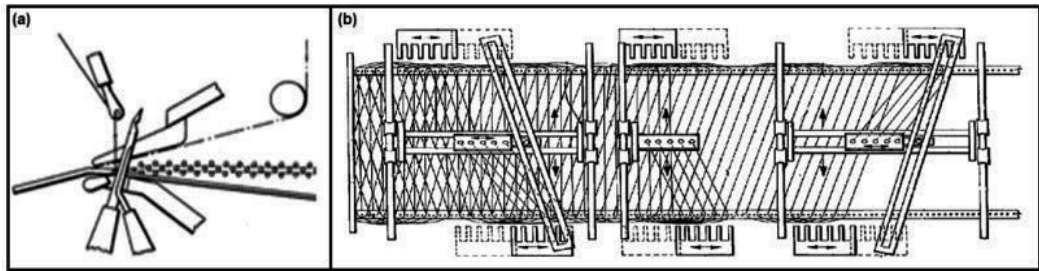


Figure 43. (a) Stitching unit and (b) warp knitting machine [32].

5. Properties of fabrics and composites

5.1. Two-dimensional fabric

5.1.1. Woven fabric structure

The 2D biaxial woven fabric is produced with a simple and highly automated process. It is by far the most economical structure in the composite industry in terms of fabric and composite production costs. The fabric is very stable and easy to handle during processing as well as has good drapability, which facilitates the fabrication of various countered parts. The fabric, however, contains numerous warp/weft interlacement points throughout its structure which impair fiber alignment and thus the load distribution capability of the reinforcing fibers. For this reason, the in-plane properties of 2D woven composite are somewhat lower than those of an equivalent UD composite. However, 2D woven composite still provides acceptably high in-plane properties especially in 0° and 90° direction due to fiber orientation in these directions. On the other hand, the in-plane properties of 3D woven composites are significantly lower than 2D woven composites for a number of reasons. Firstly, the 3D woven structure has z-yarns inserted in through-the-thickness direction in order to improve weak out-of-plane properties of 2D layered woven composites such as delamination resistance and impact strength. However, the incorporation of z-yarns reduces the in-plane directional volume fraction of the composite and leads to lower in-plane properties. One of the problematic issues with the biaxial fabric composites is their low mechanical properties in bias directions such as $\pm 45^\circ$ and $\pm 60^\circ$. Triaxial fabrics bring a solution with their multidirectional fiber architecture. Scardino and Ko [110] reported that triaxial fabric has better properties in the bias directions when compared to biaxial fabric. The study revealed a 4-fold tearing strength and 5-fold abrasion resistance compared with a biaxial fabric with the same setting. Elongation and strength properties were found to be roughly the same. Schwartz [111] compared triaxial fabrics with leno and biaxial fabrics. He defined the triaxial unit cell and proposed the fabric moduli at crimp removal stage. He concluded that it is crucial to strictly define the fabric equivalency before comparing various kinds of fabrics. It was shown that triaxial fabric shows better isotropy compared to leno and plain fabric. This brings a clear advantage since isotropy

plays an important role in fabric bursting and tearing strength as well as shearing and bending properties. Skelton [112] proposed a relation between the bending rigidity and the angle of orientation. It was found that the bending behavior of highly isotropic structures like triaxial fabrics is not dependent upon the orientation angle. Triaxial fabric is more stable in comparison with an orthogonal fabric with the same percentage of open area. Triaxial fabric also shows a greater isotropy in flexure and has greater shear resistance when compared to an equivalent orthogonal fabric.

5.1.2. Braided fabric structure

Nishimoto et al. [113] investigated 2D circular biaxial braided fabrics. They used a step response model to examine the temporal change in braiding angle under unsteady-state conditions. An examination of the flow pattern during the consolidation revealed that the permeability of the fabric is determined by spaces between the fibers especially in the case of low braid angle. Permeability and porosity may result in a non-uniform flow pattern during liquid molding [114]. The effect of braiding angle on the mechanical properties of 2D biaxial braided composite was analyzed. It was shown that when the braiding angle is increased, the bending modulus and strength decreased [115]. Smallest braiding angle (approximately 15°) resulted in the highest bending properties [116]. The mechanical properties of 2D biaxial 2×2 pattern braided fabric composites were studied by a 3D finite element micromechanics model and compared with equivalent 2×2 twill fabrics to analyze their fracture modes under various loading requirements [117]. The biaxial compressive strength properties of 2D triaxial braided cylinders were investigated. It was reported that the fiber waviness affects the axial compression strength. The composites exhibited considerably higher compression and tension strength in the axial direction when compared to those in the braid direction [118]. Smith and Swanson [119] studied the response of 2D triaxial braided composites under compressive loading. It was shown that the laminated plate theory provided good stiffness predictions for low braid angle, whereas a fiber inclination model yielded close estimations for various braid angles. Tsai et al. [120] investigated the burst strengths of 2D biaxial and triaxial braided cylindrical composites. It was reported that the crack formation in biaxial braided composite starts in tow direction. In a triaxial fabric composite, on the other hand, the cracks first appear in the longitudinal direction.

Byun [121] developed an analytical approach to predict the geometric characteristics and mechanical properties of 2D triaxial braided textile composites. The model is based on the unit cell geometry of the braided structure. It was reported that the geometrical model can accurately predict some important properties such as the braid angle and fiber volume fraction. An averaging technique based on the engineering constants was used to calculate the stiffness properties of the composites. It was shown that the averaging technique yields more precise results when worked with small braid angles. It was also reported that the model gives more accurate results when the bundle size of the axial yarns is much larger in comparison with that of the braider yarns. Yan and Hoa [122] used an energy approach for predicting the mechanical behavior of 2D triaxially braided composites.

5.1.3. Nonwoven fabric structure

Properties of 2D nonwoven fabric structure depend on fiber type and size, packing density (fiber volume fraction), pore size and distribution in the web volume, and fiber orientation in the web [56]. The packing density (α) of a web is defined as the ratio of the volume occupied by the fibers to the whole volume of the web as defined by Eqs. (3) and (4):

$$\alpha = \text{total fiber volume} / \text{total web volume} = \frac{V_f}{V_{web}} = \frac{W_f / \rho_f}{t A} = \frac{\text{Basis weight}}{t \rho_f} \quad (3)$$

where, V_f is the volume of fibers; V_{web} is the volume of the web; W_f is the weight of fibers = weight of the web; ρ_f is the fiber or polymer density; t is the thickness of the web and A is the area of the web.

Porosity (ϵ) can be obtained by following relation:

$$\epsilon = 1 - \alpha \quad (4)$$

Nonwovens are composed of short fibers that are entangled or bonded together to form a continuous fabric structure. Therefore the mechanical properties of the fabric and its composite strictly depend upon fiber strength/stiffness and the bonding strength between the fibers. Unlike many other forms of reinforcement, nonwoven fabrics with randomly oriented fibers can be regarded as isotropic structures bearing similar properties in all possible in-plane directions. The main parameters that determine the mechanical properties of a nonwoven composite are fiber modulus/tenacity, packing density/fiber volume fraction, fiber orientation distribution and fiber length distribution [123].

It is demonstrated that various polymer solutions can be used in electrospinning process to make various sectional nanofibers including cylinder, rod, ellipse, flat ribbons and branched fibers. The arrangement of fibers in the nano-web is generally random, with a slight bias to the machine direction due to movement of the collector and the air drag/suction [124-126]. The process parameters in electrospinning are electric voltage, the distance between the spinneret and the collector, the polymer concentration, the diameter of the spinneret, and the web structural design parameters [127]. It is noted that the critical part of the electrospinning is the fluid instability. At high electric fields, the jet becomes unstable and has an appearance of inverted cone, which is a single, rapidly whipping jet [128, 129]. The dominant instability strongly depends on the fluid parameters of the jet, namely, the viscosity, the dielectric constant, the conductivity and the static charge density on the jet [130].

5.1.4. Knitted fabric structure

The 2D knitted fabric is thicker than an equivalent woven structure due to its special loop elements which are buckled toward an additional (third) fabric dimension. The fabric is highly extensible with a low flexural rigidity [131]. It was reported that the knit preform properties

are greatly influenced by the fiber strength and modulus, knitted structure, stitch density, pre-stretch parameters and incorporation of inlays [36]. The deformation behavior of knitted preforms can be predicted by initial load-elongation properties of knitted fabrics. The knitting process parameters influence the knitted preform during fabrication. Loop formation during the knitting process imposes dramatic bends and twists on fibers that cause fiber/machine element failures when working with high modulus/brittle fibers. It was shown that the knittability of these fibers depends on frictional properties, bending strength, stiffness, and fiber/yarn strength [49]. The knittability of a given yarn can be improved by certain machine parameter adjustments including low tension application during yarn input, fabric take down tension setting, and loop length control which is adjusted by stitch cam settings [109]. Also, the knittability of high performance yarns mainly depends on yarn-to-metal friction characteristics. Positive yarn feeding control and tension compensator improve the dimensional stability of the knitted preform. It was demonstrated that yarn bending rigidity and inter-yarn coefficient of friction are very important determinants for loop shape while the loop length of high performance yarns, glass yarns in particular, was found to vary with needle diameter, stitching cam setting and machine setting [49, 79, 109].

5.2. Three-dimensional fabric

5.2.1. Non-interlaced fabric structures

Bilisik and Yolacan [132] investigated the mechanical properties of non-interlaced/non-z single layer and multilayered uniaxial, biaxial and multiaxial E-glass/polyester composites. They reported that the number of layers as well as yarn orientation greatly affects the mechanical properties. An increment in packing density led to higher tensile and flexural strength which was attributed to increase in fiber volume fraction. All samples experienced mode-I delamination and subsequent failure under tensile loading due to layer/layer separation. This was attributed to the lack of z-yarns and the resulting weakness in out-of-plane direction. Bilisik [133] carried out the experimental determination of ballistic performance of novel composite structures with soft backing aramid fabric. It was reported that specific energy absorption of non-interlaced/non-z E-glass/polyester composite plate with para-aramid soft layered dense woven fabric structure is higher than that of the 3D woven carbon/epoxy and non-interlaced/non-z E-glass/polyester composite plates with para-aramid soft layered loose woven fabric structure. Damage propagation in the 3D woven structure is smaller than that of the non-interlaced/non-z multiaxial structure, and impact damage was restricted by the z-fiber. Carbon fiber shows brittle behavior during energy absorption, but E-glass fiber shows high extension and distributes the energy around the impacted zone.

5.2.2. Multistitched fabric structures

Warp and weft directional specific tensile strength and modulus of unstitched structure were higher than those of the four- and two-directional light and dense multistitched structures. Stitching causes minor filament breakages as well as creating stitching holes throughout the structure which reduces the in-plane properties of the stitched composite. Accordingly, when

the number of stitching directions, and stitching density increased, their warp and weft directional tensile strength and modulus decreased. These results indicated that stitching yarn type, stitching directions and stitching density generally influenced the warp and weft directional tensile properties of multistitched E-glass/polyester woven composites. On the other hand, the damage tolerance performance of the multistitched structures was enhanced due to stitching (in particular, four-directional stitching) [134]. In addition, stitching yarn type, stitching directions, stitching density, and amount of nano materials generally influenced the bending properties of multistitched E-glass/polyester woven composites [135].

5.2.3. Fully interlaced woven fabric structure

Geometrical properties of the representative 3D fully interlaced woven preforms were analyzed and the results are shown in Figure 53. Crimps in the 3D fully-interlaced and semi-interlaced representative woven preform structure were calculated based on the structure dimensions and the uncrimped representative yarn lengths [60]. The following relations can be used:

$$cw (\%) = (lw - Sl) \times 100 / Sl \quad (5)$$

$$cf (\%) = (lf - Sw) \times 100 / Sw \quad (6)$$

$$cz (\%) = (lzt - St \times 100) / St \quad (7)$$

where, cw is the warp crimp (%), lw is the uncrimped warp length (cm), Sl is the structure length (cm), cf is the filling crimp (%), lf is the uncrimped filling length (cm), Sw is the structure width (cm), cz is the z-yarn crimp (%), lzt is the uncrimped total z-yarn length (cm) and St is the structure thickness. In addition, crimps in the 3D fully-interlaced representative circular woven preform structure were calculated based on the structure dimensions and the uncrimped representative yarn lengths [61]. The following relations can be used:

$$Ca (\%) = (la - Sl) \times 100 / Sl \quad (8)$$

$$Cc (\%) = (lc - Ssl) \times 100 / Ssl \quad (9)$$

$$Cr (\%) = (lrt - St \times 100) / St \quad (10)$$

where, Ca is the axial crimp (%), la is the uncrimped axial length (cm), Sl is the structures length (cm), Cc is the circumferential crimp (%), lc is the uncrimped circumferential length (cm), Ssl

is the structures outside surface length (cm), Cr is the radial crimp (%), l_{rt} is the uncrimped total radial length (cm) and St is the structures wall thickness.

5.2.4. Orthogonal woven fabric structure

Gowayed and Pastore [136] reviewed computational methods for 3D woven fabric. The developed analytical methods were stiffness averaging, fabric geometry and inclination models. They were based on classical lamination theory, and a micromechanical approach was considered. Gu [137] reported that the directional/total fiber volume fraction in 3D woven preforms is influenced by the take-up rate during weaving process. It is possible to obtain higher packing densities by applying double beat-up. Cox et al. [5] stated that 3D woven preform with a low volume fraction may perform well under the impact load compared to 3D woven preform with a high volume fraction. Dickinson [138] studied 3D carbon/epoxy composites. It is realized that the amount and placement of z-yarn in 3D woven preform influence the in-plane properties of the 3D woven structure. When the volume ratio of z-yarns was increased, in-plane properties of the 3D woven fabric decreased. On the other hand, local delamination was monitored when the ratio of z-yarns was decreased. Bobcock and Rose [139] found that when 3D woven or 2D woven/stitched composites were subjected to an impact loading, the impact energy was confined to a limited area owing to the z-yarns.

5.2.5. Multiaxis woven fabric structure

Uchida et al. [17] examined five-axis 3D woven fabric composites. They reported that multiaxis woven fabric and stitched 2D laminate composites showed similar results in terms of tensile and compression properties whereas multiaxis fabric composite yielded better open hole tensile and compression values. Impact tests revealed that the damaged area is smaller in 3D woven composites when compared to that of the stitched laminate. Furthermore, 5-axis 3D woven composite gave better results in Compression After Impact (CAI) tests in comparison with stitched fabric composite. Bilisik [67] stated that the most important process parameters for multiaxis 3D flat woven preform production are bias angle, width ratio, packing, tension and fiber waviness. The bias angle can be manipulated by tube-block movement.

Bilisik and Mohamed [140] investigated the mechanical properties of 3D carbon/epoxy composites by applying the stiffness averaging method. The directional tensile and shear constants obtained are shown in Table 7. The shear properties were influenced by the orientation of yarns within the preform.

The process parameters for multiaxis 3D circular weaving are the following: bias orientation, radial and circumferential yarn insertion, beat-up and take-up. Bias yarns on the outer and inner surfaces of the structure create helical paths and there is a slight angle difference between them particularly in the case of thick-walled fabrics. It was shown that there is a correlation between preform density (fiber volume fraction), bias yarn orientation and take-up rate. The excessive yarn length during circumferential yarn insertion is because diameter ratio (preform outer diameter/outermost ring diameter) is not equal to 1. The diameter ratio depends on the number of the rings. When the excessive circumferential yarn is not retracted, it causes

waviness in the structure. However, there must be an adequate tension on the circumferential yarns to get proper packing during beat-up [68].

		Carbon Fiber	Epoxy Matrix	
		Thornel™ T-300 PAN	(Tactix™ 123)	
Material Properties	Tensile Strength (MPa)	3450	76.50	
	Tensile Modulus (GPa)	230	3.45	
	Modulus of Rigidity (GPa)	88.50	1.30	
	Elongation (%)	1.62	5.70	
	Poisson's ratio (ν)	0.27	0.31	
	Density (g/cm^3)	1.76	1.16	
		Preform 1	Preform 2	
Bias angle (°) (measured)		30°	40°	
	+ Bias	9.43	11.7	
	- Bias	9.43	11.7	
Fractional volume (%) (measured at preform)	Warp	10.5	13.7	
	Filling	5.42	4.77	
	z-yarn	3.67	5.61	
	Total Volume (%)	38.4	47.5	
Elastic constants (calculated)	Modulus of elasticity (GPa)	E_{11}	48.33	48.00
		E_{22}	19.87	23.85
		E_{33}	9.86	14.24
	Modulus of rigidity (GPa)	G_{12}	10.42	15.65
		G_{23}	2.78	3.47
		G_{31}	2.80	3.47
	Poisson's ratio	ν_{12}	0.446	0.530

Table 7. Multiaxis 3D woven preform elastic constants from multiaxis 3D weaving [140].

5.2.6. Three-dimensional fully braided fabric structure

Geometric relations on the representative 3D fully braided and 3D axial braided structures were investigated in terms of unit cell angle, unit cell yarn length and unit cell yarn path. The results show that the unit cell from 4-step method is influenced by braid patterns for both preform types. Fully interconnected unit cell structures are obtained when patterns on odd numbered rows were used. Patterns on even numbered rows, on the other hand, mostly led to layer-to-layer connection on the unit cell edge forming an empty pocket between each

braided layer. The unit cell structure has a fine intertwine in the 1×1 pattern, whereas it has a coarse intertwine for other braid patterns. When the influence of number of layers is considered, it was found that, for all braid patterns, the unit cell thickness increases when the number of layers is increased in 3D braided and 3D axial braided structures. Furthermore, for the same number of layers, the unit cell thickness in the 1×1 pattern is less when compared to other patterns. This showed that all braid patterns except 1×1 resulted in a coarse form of unit cell structure [70].

Byun and Chou [141] examined the process-microstructure relationships of 2-step and 4-step braided composites by geometrical modeling of unit cells. The effect of process parameters such as braid pattern and take-up rate on the microstructural properties like braid yarn angle and fiber volume fraction was investigated. They also studied the fabric jamming phenomenon. Three-dimensional braided composites were characterized by using the fabric geometry model (FGM). This model uses the processing parameters as well as the properties of the fibers and the matrix. It basically relies on two parameters such as the fabric geometry and the fiber volume fraction. Fabric geometry is a function of the take-up rate, whereas row and column motions determine the yarn displacement values, which are expressed as number of yarns. The yarn orientation in a 3D preform is dependent upon fabric shape and construction as well as the dimensions of the braiding loom [142].

5.2.7. Three-dimensional axial braided fabric structure

Kuo [143] investigated topology of 3D braided fabrics by using pultruded rods as axial reinforcements. The effect of yarns size and spacing as well as the pitch length on the final preform geometry was examined. Structural analysis of 3D axial braided preforms revealed that braider yarn orientation and yarn volume fraction can be predicted from the measured values of yarn sizes, preform contour sizes, pitch length and number of axial and braider yarns [144]. Li [145] studied the structural mechanics of 3D braided preforms. It was observed that the load in the axial direction was mostly carried by axial yarns whereas the braider yarns carry the transverse loads. Therefore, it was desirable for the orientation angle of the braiders to be large.

5.2.8. Three-dimensional nonwoven fabric structure

The 3D nonwovens are anisotropic materials in which the fiber strength and modulus, fiber length and thickness, fiber volume fraction and fiber angle in the in-plane and out-of-plane directions are important preform properties [56]. The general stress–strain relationship is given by:

$$\sigma = C : \varepsilon \quad (11)$$

where σ is the stress, a second order tensor, ε is the strain, also a second-order tensor, and C is the stiffness constant, a fourth-order tensor [56]. For two-dimensional nonwovens, the in-plane directional stiffness of the nonwoven is given in Eqs. (12) and (13) based on fiber web theory [56].

$$C_{11} = E_f \int_0^{\pi} \cos^4 f(\theta) d\theta \quad (12)$$

$$C_{12} = E_f \int_0^{\pi} \cos^2 \theta \sin^2 \theta f(\theta) d\theta \quad (13)$$

where C_{11} is the stiffness constant in the x-direction on the plane perpendicular to the x-axis, C_{12} is the stiffness constant in the y-direction on the plane perpendicular to the x-axis, E_f is the fiber modulus and $f(\theta)$ is the distribution of fiber orientation.

Directional stiffness constants of a web can be obtained, given the fiber modulus and the fiber orientation distribution in the web. The fiber web theory can be applied to the 3D nonwoven preform in which some amount of z-fiber is oriented in the thickness direction of the web [102, 146]. It was claimed that there is a good agreement between the fiber web theory and the experimental measurement of needle punched web where the fibers between two bonded points are straight and that fibers are rigidly bonded. It is tedious and time consuming to determine the fiber orientation distribution in a web. However, several practical methods have been developed to measure the fiber orientation as X-ray diffraction, laser light diffraction, light reflection and refraction intensity [147].

5.2.9. Three-dimensional knitted fabric structure

The properties of 3D knitted structures including multilayered weft or warp knitted fabrics and 3D multiaxis warp knitted preforms were studied by various researchers. The fiber volume fraction of the 3D multilayered weft knitted structure was proposed by Eq. (14):

$$V_f = \frac{n_k D_y L_s C W}{9 \rho_f A t} \times 10^{-5} \quad (14)$$

where n_k is the number of plies of the fabric in the composite, D_y is the yarn linear density, L_s is the length of yarn in one loop of the unit cell, C is the course density, W is the wale density, ρ_f is the density of fiber and A is the planar area over which W and C are measured, and t is the structure thickness.

It was concluded that the fiber content of weft knitted fabric composites can be increased by increasing D_y using the coarser yarns [36]. In general, the coarser yarns are difficult to knit and the coarsest yarn knittable is dependent on the yarn type and knitting needle size. In addition, the maximum V_f is limited by the knitting needles used in the knitting machine based on the relation $N = C/W$, where N is the stitching density. Hence, V_f is proportional to the structure parameters of L_s and N . The maximum V_f can be achieved by increasing the stitch density or the tightness of the knitted fabric. It was claimed that the attainable volume fraction of knitted fabric composite can be 40% [36, 79]. It was stated that the failure

mechanisms for weft knitted structures were dependent on both the wale and the course directional crack propagations, and demonstrated better interlaminar fracture toughness properties due to the 3D loop structure [49]. It was found that the failure process of weft knitted structures under tensile load includes crack branching, loop to loop friction, yarn bridging and fiber breakages. It was also shown that an increase in loop length or stitch density has opposite effects on the tensile strength and impact performance of the weft-knitted composites. The plain weft knitted structure exhibited good energy absorption capacity. Matrix cracking, matrix/fiber debonding, and fiber breakage were the major damage mechanisms [36, 49, 109]. The 3D loop structure was studied, and it was proposed that the loop structure was constituted by sets of arcs. Adoption of the arc shape loop geometry into micromechanical technique considers the influence of knitting parameters and the estimation of elastic properties of knitted composites [148].

6. Application of fabrics in technical textiles

6.1. Structural components

Two- and three-dimensional woven, braided, knitted and nonwoven composites as structural components for various industrial applications fulfilled the general requirements such as low cost, manufacturability, good mechanical performance and energy absorption, corrosion resistance, repairability and recyclability, fuel economy and low noise level [149]. Typical structural components in various industrial applications are knot elements for space frame-like structures, beams, shells, exhaust, seats and chassis. For instance, the use of woven and braided composites in structural applications allows a significant reduction in component number and provides a substantial weight reduction compared with metal [87]. In addition, 2D and 3D woven, braided and knitted composites as T-joints and T-shape connectors, cones, pipes, and I-beams are attractive applications in general engineering fields. Two- and three-dimensional nonwoven composites can be used in construction industry as a roofing and tile underlay, thermal and noise insulation, and house wrap. Some geotextile applications of 2D or multilayered 3D nonwoven composites are asphalt overlay, soil stabilization, drainage, sedimentation and erosion control. Industrial applications of the 2D or 3D nonwoven structures are cable insulation, battery separators, satellite dishes and coating [149]. The 2D nonwoven nano web structures are increasingly finding applications in filtration industry, electromagnetic interference (EMI) shielding, electrical conductors, thermal and lightning protection, energy field in batteries, photovoltaic cells, polymer electrolytes and membrane fuel cells and advanced structural composites.

6.2. Ballistic applications

Two- and three-dimensional woven fabric and rigid ballistic plate are used extensively to protect the human and goods from various threats such as projectile, blast, fragment and high energy explosives. In addition, 2D and 3D braided, knitted and nonwoven fabrics and rigid composites can be utilized as protective products for vehicular crash guards, composite

helmet, interlinings, insulation and protective industrial workwear and firefighter suits [49, 149]. Two- and three-dimensional woven, braided, knitted and nonwoven structures for soft and rigid ballistic applications are made by using high modulus and high strength fibers like para-aramid and polyethylene. Ballistic structures are manufactured as multilayer to obtain required structural thickness by using the above mentioned 2D fabrics. In some cases, to enhance the out-of-plane properties, those 2D fabrics are formed by stitching or quilting. In particular, 2D woven fabric for soft ballistic applications is very effective due to the in-plane crimp between yarn sets since the crimps act as a secondary energy absorbing mechanism due to local intra-yarn frictional forces generated during impact loads. In addition, 2D nanofiber-based nonwovens are being applied as sound absorption materials and in protective clothing to combat chemical and biological warfare agents.

6.3. Space and aerospace applications

Two- and three-dimensional woven and braided fabrics are used in aerospace applications as soft space suits for astronauts, space shuttle components and aircraft seat cushions. Two- and three-dimensional woven, braided and multiaxis warp knitted composites are currently employed in critical structures of both civil and military aircrafts such as the fuselage, wings, and skin of the aircraft. Other areas of use are top and side tail units, fuselage panelling, leading edges on side rudders, and engine panelling. It was reported that multiaxis 3D warp knitted composites are also being evaluated for rotor blades, outer skin and ballistic protection for helicopters. Three-dimensional weft or warp knitted ceramic composite was also developed for use as a structural parts for jet engine vanes, radomes and rudder tip fairing [49].

6.4. Automotive applications

Fiber based dry and soft textile fabrics or structures are the main interior materials for automobiles as well as trains, aircrafts and ships. This provides the users well-being and comfort. They also withstand daylight and ultraviolet radiation. The maintenance cost is low and easy to care. Two- and three-dimensional woven and knitted fabrics are used as airbag, and car seat parts which has better air permeability and moisture removal properties and car seat cover for the aesthetic and durability requirements. Two- and three-dimensional textile preform composite structures are widely used as parts of the suspension, gears, drive belts, tires, heater hoses, battery separators, brake and clutch linings, air filters, gaskets and crash helmets. Two- and three-dimensional warp knitted fabrics and nonwovens are widely used as preassembled interior components such as boot liners, seatbacks, door panels, oil and cabin air filters, molded bonnet liners, heat shields, wheelhouse covers, parcel shelves and shelf trim. Two- and three-dimensional braided preform and composites have been used in racing car bodies, structural members such as beams which are made up of foam cores over braided with a carbon preform structure, aprons and spoilers, connecting rods, drive shafting and flexible couplings. Also, car noses, monocoques and bumpers are made from braided carbon structures. They reduce weight and improve the crash behavior [49, 149].

6.5. Medical applications

Two- and three-dimensional fiber based structures are used in protective medical apparel such as baby diapers, feminine hygiene products, adult incontinence items, dry and wet pads, nursing pads or nasal strips, operation drapes, gowns and packs, face masks, surgical dressings. Two- and three-dimensional woven, braid, warp knitted and nonwoven structures find also more functional applications as in vascular prosthesis due to good mechanical properties and better ingrowth of tissue to seal the prosthesis walls, grafts for inborn vessel anomaly or arteriosclerotic damage, soft tissue such as skin and cartilage, artificial tendons and ligaments, wound dressing, absorbable and non-absorbable sutures, stents, tissue engineering scaffolds as to repair or regenerate tissues through combinations of implanted cells-biomaterial scaffolds-biologically active molecules, blood filters, plasters, compression bandages, surgical hosiery, and hospital bedding. It was also demonstrated that 2D and 3D fabrics are dimensionally stable, have similar mechanical properties with human organs and are biocompatible [57, 87, 149]. Recently, 2D nanofiber-based nonwoven fabrics are considered to be used in wound healing, artificial organ components and tissue engineering and implant materials.

6.6. Sports applications

Two- and three-dimensional woven and braided composite structures are employed in various sports especially golf, baseball and tennis. The specific applications are roller blades, bike frames, golf stick, tennis rackets, baseball stick, ski and surf equipment and footwear. Three-dimensional warp knitted spacer fabrics are also extensively used in both sports shoes and garments due to its lightweight, springiness, washability and air permeability properties [149].

7. Future trend and technology nonwoven fabrics

Two- and three-dimensional textile fabrics are increasingly utilized technical textile areas from garments to structural load-bearing materials for various industries such as aerospace, defense, civil engineering, and transportation industries [150]. Novel fabric formation techniques are also being developed from the fundamental methods like weaving, braiding, knitting and nonwoven technology.

The 2D nonwoven fabric is the basic planar sheet material that can be produced by various methods including needling, stitching, hydroentanglement, spunbonding, meltblown and electrospinning techniques. In addition, 3D nonwoven fabric serves as a thick fabric structure with various uses and is fabricated by needling, stitching and electrospinning techniques. More development on nonwoven technology is expected with the evolution of electrospinning process to make nano-fiber-based nonwoven planar sheet or 3D entangled fabrics. This will open up new opportunities especially in medical and hygiene applications. Furthermore, the use of bioactive and alloy fibers in nonwoven materials produced by needlepunching or hydroentanglement improves the performance of hygiene nonwoven materials from many aspects such as absorbency, thermo-physical and comfort properties, prevention of cross-infection of diseases and suppression of the generation of unpleasant odors. The reliability and

durability of surgical implants such as hip and knee replacements could be improved by electrospun nanofiber coatings [151]. The filtration materials could be reusable, and durable, as well as biodegradable, and recyclable [152]. The natural fiber based nonwoven fabric will be extensively used for the future transportation industries due to the fuel efficiency, environment protection, recycling and economic performance [153]. Nonwoven nanomaterials are expected to be the subject of future research and will find extensive usage in medical, energy, electronics, automotive and other industrial applications.

8. Conclusions

Two and three-dimensional fabric architectures and fabrication techniques have been reviewed. Two dimensional woven, braided, knitted and nonwoven fabrics have been widely used as various structural composite parts in civilian and defense related areas. However, composite structure from biaxial layered fabrics is prone to delamination between layers due to the lack of z-fibers and has crimp that lowers the properties. Biaxial fabric method and techniques are well developed. Triaxial fabrics have an open structure and low fabric volume fractions. However, in-plane properties of triaxial fabric are more homogeneous in comparison with biaxial fabric due to bias yarns. On the other hand, biaxial and triaxial braided fabrics have size and thickness limitations. Triaxial fabric method and techniques are also well developed.

The woven fabric consists of multiple layers and is not subject to delamination due to the z-fibers. However, 3D woven fabric has low in-plane properties because of low fiber volume fraction. Three-dimensional braided fabrics are constituted from multiple layers. The characteristic intertwine type interlacement of these fabrics provides out-of-plane reinforcement preventing any delamination. Nevertheless, 3D braided fabrics suffer from low transverse properties due to lack of filling yarns like those in a 3D woven fabric. They also have limitations in terms of size and thickness. Various 3D woven and braided fabrication method and techniques are commercially available.

Various unit cell-base models on 3D woven, braided and knitted structures were developed to define the geometrical and mechanical properties of these structures. Most of the unit cell based models include micromechanics and numerical techniques.

Multiaxis 3D knitted fabric has four layers integrated with stitching. The production process has been perfected. The fabric is not subject to delamination owing to the out-of-plane reinforcement provided by the stitching yarn. It has also superior in-plane properties due to \pm bias yarns. However, it has some limitations related to layering. Multiaxis 3D woven fabric consists of multiple layers. Out-of-plane reinforcement is provided by z-fibers which prevent delamination. In-plane properties are improved by \pm bias yarn layers. Multiaxis 3D braided fabrics have also multiple layers and no delamination, and their in-plane properties are enhanced due to the \pm bias yarn layers. However, multiaxis 3D technique has its early development stages. This will be the future technological challenge in multiaxis 3D preform formation subject.

Acknowledgements

The authors would like to thank Dr. Yekta Karaduman and Dr. Ilhan Ozen for their help in the preparation of this manuscript especially for their critical editing and suggestions.

Author details

Kadir Bilisik^{1*}, Nesrin Sahbaz Karaduman² and Nedim Erman Bilisik³

*Address all correspondence to: kadirbilisik@gmail.com

1 Faculty of Engineering, Erciyes University, Talas-Kayseri, Turkey

2 Akdagmadeni Vocational High School, Bozok University, Akdagmadeni-Yozgat, Turkey

3 Ege University, Bornova-Izmir, Turkey

References

- [1] Dow MB, Dexter HB. Development of stitched, braided and woven composite structures in the ACT Program and at Langley Research Center (1985 to 1997). NASA/TP-97-206234;1997.
- [2] Kamiya R, Cheeseman BA, Popper P, Chou TW. Some recent advances in the fabrication and design of three dimensional textile preforms: A review. *Composites Science and Technology*. 2000;60:33-47. DOI:10.1016/S0266-3538(99)00093-7.
- [3] Ko FK, Chou TW, editors. *Textile Structural Composites*. New York: Elsevier; 1989. 480 p. DOI: 10.1002/adma.19890011016.
- [4] Chou TW. *Microstructural Design of Fiber Composites*. Cambridge: Cambridge University Press; 1992. 569 p. DOI: 10.1002/adma.19920041025.
- [5] Cox BN, Dadkhah MS, Morris WL, Flintoff JG. Failure mechanisms of 3D woven composites in tension, compression and bending. *Acta Metallurgica et Materialia*. 1993;42:3967-3984. DOI:10.1016/0956-7151(94)90174-0.
- [6] Brandt J, Drechsler K, Filsinger J. Advanced textile technologies for the cost effective manufacturing of high performance composites. RTO AVT Specialist Meeting on Low Cost Composite Structures; 7-11 May 2001; Loen, Norway.
- [7] Mohamed MH. Three dimensional textiles. *American Scientist*. 1990;78:530-541.

- [8] Bilisik A, Mohamed MH. Multiaxis 3D weaving machine and properties of multiaxial 3D woven carbon/epoxy composites. 39th International SAMPE Symposium; 11-14 April 1994; Anaheim, USA.
- [9] Uozumi T, Iwahori Y, Iwasawa S et al. Braiding technologies for airplane applications using RTM process. 7th Japan International SAMPE Symposium; 2001; Tokyo, Japan.
- [10] Ko FK. Braiding. In: Reinhart TJ, editor. *Engineered Materials Handbook*, Ohio: ASM International; 1987. p. 519-528.
- [11] Florentine RA. Magnaweave process-from fundamentals to applications. *Textile Research Journal*. 1983;53:620-623. DOI: 10.1177/004051758305301008.
- [12] Popper P, McConnell R. A new 3D braid for integrated parts manufacture and improved delamination resistance-the 2-step process. In: *Proceedings of 32nd International SAMPE Symposium and Exhibition*; 1987; Anaheim, CA, USA.
- [13] Nanofibres: From finer filters to advances in electronics, energy and medical applications, *Technical Textile Markets*; 3rd quarter 2008.
- [14] INDA, Airlaid pulp nonwoven primer. Association for the Nonwovens Fabrics Industry; January 2003.
- [15] Dexter HB, Hasko GH. Mechanical properties and damage tolerance of multiaxial warp-knit composites. *Composites Science and Technology*. 1996;51:367-380. DOI: 10.1016/0266-3538(95)00107-7.
- [16] Mohamed MH, Bilisik AK. Multilayered 3D fabric and method for producing. US Patent 5465760, 14 Nov 1995.
- [17] Uchida H, Yamamoto T, Takashima H. Development of Low Cost Damage Resistant Composites [Internet]. 2000. Available from: <http://www.muratec.net/jp> [Accessed: 2008-05-14].
- [18] Khokar N. Noobing: a nonwoven 3D fabric-forming process explained, *Journal of the Textile Institute*. 2002;93:52-74. DOI: 10.1080/00405000208630552.
- [19] Chen X. Technical aspect: 3D woven architectures. NWTexNet 2007 Conference; 2007; Blackburn, UK.
- [20] Bilisik K. Multiaxis three dimensional weaving for composites: A review. *Textile Research Journal*. 2012;82:725-743. DOI: 10.1177/0040517511435013.
- [21] Greenwood K. Loom. US Patent 3818951, 1974.
- [22] Khokar N, Domeij T. Device for producing integrated nonwoven three dimensional fabric. Sweden Patent SE 509 944, 29 Jan 1998.
- [23] Mohamed MH, Zhang ZH. Method of forming variable cross-sectional shaped three dimensional fabrics. US Patent 5085252, 4 Feb 1992.

- [24] Fukuta K, Nagatsuka Y, Tsuburaya S, et al. Three dimensional fabric, and method and loom construction for the production thereof. US Patent 3834424, 10 Sept 1974.
- [25] King RW. Three dimensional fabric material. US Patent 4038440, 26 July 1977.
- [26] Weinberg A. Method of shed opening of planar warp for high density three dimensional weaving. US Patent 5449025, 12 Sept 1995.
- [27] Banos J, Cantagrel JC, Cahvzac Q, Durrieux JL. Method and machine for 3D weaving for obtaining woven hollow reinforcements of revolution. US Patent 4183232, 15 Jan 1980.
- [28] Bilisik AK. Multiaxial three dimensional (3D) circular woven fabric. US Patent 6129122, 10 Dec 2000.
- [29] Wilkens C. Warp knitted ware with reinforcing thread. US Patent 4518640, 1985.
- [30] Mohamed MH, Bilisik K. Multilayered 3D fabric and method for producing. US Patent 5465760, 14 Nov 1995.
- [31] Anahara M, Yasui Y, Sadon M, Nishitani, M. Three dimensional fabric with symmetrically arranged warp and bias yarn layers. US Patent 5270094, 14 Dec 1993.
- [32] Wunner R. Apparatus for laying transverse weft threads for a warp knitting machine. US Patent 4872323, 7 July 1987.
- [33] Lee SM. International Encyclopedia of Composites. New York: VHC Publisher Inc.; 1990. 548 p.
- [34] Grishanovi S, Meshkov V, Omelchenko A. A topological study of textile structures, Part I: An introduction to topological methods. *Textile Research Journal*. 2009;79: 702-713. DOI: 10.1177/0040517508095600.
- [35] Bilisik K. Three dimensional braiding for composites: A review. *Textile Research Journal*. 2013;83:1414-1436. DOI: 10.1177/0040517512450766.
- [36] Hamada H, Ramakrishna S, Huang ZM. Knitted fabric composites, 3-D textile reinforcements in composite materials. In: Miravete A, editor. *3-D Textile Reinforcements in Composite Materials*. Cambridge: Woodhead Publishing Ltd; 1999. p. 180-216.
- [37] Ramakrishna S, Hamada H, Kanamaru R, Maekawa Z. Mechanical properties of 2.5 dimensional warp knitted fabric reinforced composites. In: Hoa SV, editor. *Design and Manufacture of Composites*. Montreal: Concordia University; 1994; p. 254–263.
- [38] Albrecht W, Fuchs H, Kittelmann W, editors. *Nonwoven Fabrics: Raw Materials, Manufacture, Applications, Characteristics, Testing Processes*. Weinheim: Wiley; 2003. 772 p. DOI: 10.1002/3527603344.
- [39] Lackowski M, Krupa A, Jaworek A. Nonwoven filtration mat production by electrospinning method, *Journal of Physics: Conference Series*. 2011; 301:1-4. DOI: 10.1088/1742-6596/301/1/012013.

- [40] Bilisik K. Multiaxis three dimensional (3D) woven fabric. In: Vassiliadis SG, editor. *Advances in Modern Woven Fabrics Technology*. Rijeka: InTech-Open Access; 2011. p. 79-106. DOI: 10.5772/678.
- [41] Kevra Advanced Composite Technology. Reinforcements [Internet]. 2015. Available from: <http://www.kevra.fi/en/Products/Reinforcements/> [Accessed: 2015-03-20].
- [42] Bhatnagar A, Parrish ES. Bidirectional and multiaxial fabric and fabric composites. US Patent 7073538, 11 July 2006.
- [43] Bilisik K, Yilmaz B. Multiaxis multilayered non-interlaced/non-Z e-glass/polyester preform and analysis of tensile properties of composite structures by statistical model. *Textile Research Journal*. 2012;82:336-351. DOI: 10.1177/0040517511420762.
- [44] Dow NF. Triaxial fabric. US Patent 3446251, 27 May 1969.
- [45] Lida S, Ohmori C, Ito T. Multiaxial fabric with triaxial and quartaxial portions. US Patent 5472020, 5 Dec 1995.
- [46] Brunnschweiler D. Braids and braiding. *Journal of the Textile Institute*. 1953;44: 666-686. DOI: 10.1080/19447015308687874.
- [47] Rogers CW, Crist SR. Braided preform for composite bodies. US Patent 5619903, 15 Apr 1997.
- [48] Ramakrishna S, Hamada H, Kotaki M et al. Future of knitted fabric reinforced polymer composites. In: *Proceedings of 3rd Japan international SAMPE symposium*; 7-10 December 1993; Chiba.
- [49] Padaki NV, Alagirusamy R, Sugun BS. Knitted preforms for composite applications. *Journal of Industrial Textiles*. 2006;35:295-321. DOI: 10.1177/1528083706060784.
- [50] Technische Universitat Dresden [Internet]. 2015. Available from: http://tu-dresden.de / die_tu_dresden/fakultaeten/fakultaet_maschinenwesen/itm/forschung/forschungsthemen/gl_gestrick [Accessed: 2015-03-20].
- [51] Cebulla H, Diestel O, Offermann P. Fully fashioned biaxial weft knitted fabrics. *AUTEX Research Journal*. 2002;2:8-13.
- [52] Gehring GG, Reisfeld A Jr. Pointed thrust weapons protective fabric system, US Patent 6233978B1, 22 May 2001.
- [53] Grafe T, Graham K. Polymeric nanofibers and nanofiber webs: A new class of non-wovens. *International Nonwovens Journal*. 2003;12:51-55.
- [54] Doshi J, Reneker DH. Electrospinning process and applications of electrospun fibers. *Journal of Electrostatics*. 1995;35:151-160. DOI:10.1016/0304-3886(95)00041-8.
- [55] Li D, Xia Y. Electrospinning of nanofibers: Reinventing the wheel? *Advanced Materials*. 2004; 16:1151-1170. DOI: 10.1002/fadma.200400719.

- [56] Chapman RA, editor. Applications of Nonwovens in Technical Textiles. Oxford: Woodhead Publishing Limited; 2010. 224 p.
- [57] Albrecht W, Fuchs H, Kittelmann W, editors. Nonwoven Fabrics: Raw Materials, Manufacture, Applications, Characteristics, Testing Processes. Weinheim: Wiley; 2003. 772 p. DOI: 10.1002/3527603344.
- [58] Stanford University. Homogenization Techniques [Internet]. 2015. Available from: <https://micromechanics.stanford.edu/advanced-homogenization-techniques-soft-matter-materials> [Accessed: 2015-03-20].
- [59] Bilisik K, Yolacan G. Experimental characterization of multistitched two dimensional (2D) woven E-glass/polyester composites under low velocity impact load. *Journal of Composite Materials*. 2014;48:2145-2162. DOI: 10.1177/0021998313494918.
- [60] Bilisik K, Karaduman NS, Bilisik NE, Bilisik HE. Three dimensional (3D) fully interlaced woven preforms for composites. *Textile Research Journal*. 2013;83: 2060-2084. DOI: 10.1177/0040517513487791.
- [61] Bilisik K, Karaduman NS, Bilisik NE, Bilisik HE. Three-dimensional circular various weave patterns in woven preform structures. *Textile Research Journal*. 2014;84: 638-654. DOI: 10.1177/0040517513499437.
- [62] Bilisik K. Multiaxis 3D woven preform and properties of multiaxis 3D woven and 3D orthogonal woven carbon/epoxy composites. *Journal of Reinforced Plastics and Composites*. 2010;29:1173-1186. DOI: 10.1177/0731684409103153.
- [63] Crawford JA. Recent developments in multidirectional weaving. NASA Publication No. 2420. 1985.
- [64] Yasui Y, Anahara M, Omori H. Three dimensional fabric and method for making the same. US Patent 5091246, 25 Feb 1992.
- [65] Ruzand JM, Guenot G. Multiaxial three-dimensional fabric and process for its manufacture. International Patent WO 94/20658, 15 Sept 1994.
- [66] Uchida H, Yamamoto T, Takashima H et al. Three dimensional weaving machine. US Patent 6003563, 21 Dec 1999.
- [67] Bilisik K. Dimensional stability of multiaxis 3D woven carbon preform. *Journal of the Textile Institute*. 2010;101:380-388. DOI: 10.1080/00405000802440066.
- [68] Bilisik K. Multiaxis three dimensional (3D) circular woven preforms-“Radial crossing weaving” and “Radial in-out weaving”: Preliminary investigation of feasibility of weaving and methods. *Journal of the Textile Institute*. 2010;101:967-987. DOI: 10.1080/00405000903080985.
- [69] Florentine RA. Apparatus for weaving a three dimensional article. US Patent 4312261, 26 Jan 1982.

- [70] Bilisik K, Sahbaz N. Structure-unit cell base approach on three dimensional (3D) representative braided preforms from 4-step braiding: Experimental determination of effect of structure-process parameters on predetermined yarn path. *Textile Research Journal*. 2012;82:220-241. DOI: 10.1177/00405175111404597.
- [71] Tsuzuki M. Three dimensional woven fabric with varied thread orientations. US Patent 5348056, 20 Sept 1994.
- [72] Kostar TD, Chou T-W. Braided structures, 3D textile reinforcements in composite materials. In: Miravete A, editor. *3-D Textile Reinforcements in Composite Materials*, Cambridge: Woodhead Publishing Ltd; 1999. p. 217-240.
- [73] Brookstein DS, Rose D, Dent R et al. Apparatus for making a braid structure. US Patent 5501133, 26 March 1996.
- [74] McConnell RF, Popper P. Complex shaped braided structures. US Patent 4719837, 19 Jan 1988.
- [75] Bilisik K. Three dimensional (3D) axial braided preforms: Experimental determination of effects of structure-process parameters on unit cell. *Textile Research Journal*. 2011;81:2095-2116. DOI: 10.1177/00405175111414978.
- [76] Li D, Lu Z, Chen L, Li JI. Microstructure and mechanical properties of three-dimensional five-directional braided composites. *International Journal of Solids and Structures*. 2009;46:3422-3432. DOI:10.1016/j.ijsolstr.2009.05.013.
- [77] Chen JL, El-Shiekh A. Construction and geometry of 6 step braided preforms for composites. 39th international SAMPE symposium; 11-14 April 1994; Anaheim, CA.
- [78] Bilisik AK. Multiaxial and multilayered 8-step circular braided preform for composite application. 8. International Machine Design and Production Conference; 9-11 September 1998; Middle East Technical University, Ankara, Turkey.
- [79] Ciobanu L. Development of 3D knitted fabrics for advanced composite materials. In: Attaf B, editor. *Advances in Composite Materials-Ecodesign and Analysis*. Rijeka: In-Tech Open Access; 2011. p. 161-192. DOI: 10.5772/580.
- [80] Olry P. Process for manufacturing homogeneously needled a three-dimensional structures of fibrous material. US Patent 4,790,052, 13 Dec 1988.
- [81] Ko FK. 3-D textile reinforcements in composite materials. In: Miravete A, editor. *3-D Textile Reinforcements in Composite Materials*. Cambridge: Woodhead Publishing Ltd; 1999. p. 9-41.
- [82] Yoo H, Jeon H-Y, Chang Y-C. Evaluation of engineering properties of geogrids for soil retaining walls. *Textile Research Journal*. 2010; 80:184-192. DOI: 10.1177/0040517508093442.
- [83] CFC Carbon Ltd. Graphite felt [Internet]. 2015. Available from: <http://www.cfccarbon.com/graphite-felt/pan-rigid-graphite-felt.html> [Accessed: 2015-03-20].

- [84] Textile Learner Blog. Weaving Mechanism [Internet]. 2015. Available from: http://textilelearner.blogspot.com.tr/2011/06/weaving-weaving-mechanism_643.html [Accessed: 2015-03-20].
- [85] Triaxial. Triaxial Fabric History [Internet]. 2015. Available from: <http://www.triaxial.us/Triaxial%20Fabric%20History%204.php> [Accessed: 2015-03-20].
- [86] Deemey S. The new generation of carpet weaving machines combines flexibility and productivity. Technical notes, Van de Wiele Incorporations; 2002.
- [87] Bilisik K, Karaduman NS, Bilisik NE. Applications of braided structures in transportation. In: Fanguero R, Rana S, editors. Braided Structures and Composites: Production, Properties, Mechanics and Technical Applications. Boca Raton: Taylor and Francis; 2015.
- [88] Wilden KS, Harris CG, Flynn BW, et al. Advanced technology composite fuselage-manufacturing, The Boeing Company, NASA Contractor Report 4735; 1997.
- [89] Fiber innovations Inc. Technical documents, 8 Jan 2002.
- [90] Brown RT. Braiding apparatus. UK Patent 2205861 A, 31 May 1988.
- [91] Schneider M, Pickett AK, Wulforth B. A new rotary braiding machine and CAE procedures to produce efficient 3D braided textiles for composites. 45th International SAMPE Symposium; 21-25 May 2000; Long Beach, CA.
- [92] Tsuzuki M, Kimbara M, Fukuta K et al. Three dimensional fabric woven by interlacing threads with rotor driven carriers. US Patent 5067525, 26 Nov 1991.
- [93] Uozumi T. Braid structure body. US Patent 5438904, 8 August 1995.
- [94] Brookstein DS, Rose D, Dent R, et al. Apparatus for making a braid structure. US Patent 5501133, 26 March 1996.
- [95] Core77. 360 degree carbon fiber loom [Internet]. 2015. Available from: http://www.core77.com/blog/materials/video_of_lexus_360-degree_carbon_fiber_loom_19146.asp [Accessed: 2015-03-20].
- [96] Spain RG. Method for making 3D fiber reinforced metal/glass matrix composite article. US Patent 4916997, 17 April 1990.
- [97] Mungalov D, Duke P, Bogdanovich A. High performance 3-D braided fiber preforms: Design and manufacturing advancements for complex composite structures. SAMPE Journal. 2007;43:53-60.
- [98] National Programme on Technology Enhanced Learning. [Internet]. 2015. Available from: <http://nptel.ac.in/courses/116102005/3> [Accessed: 2015-03-20].
- [99] Kittelmann W, Dilo JP, Gupta VP, et al. Web bonding. In: Albrecht W, Fuchs H, Kittelmann W, editors. Nonwoven Fabrics: Raw Materials, Manufacture, Applications,

- Characteristics, Testing Processes. Weinheim: Wiley; 2003. p. 772. DOI: 10.1002/3527603344.
- [100] Kuo C-F, Su, TL, Tsai C-P. Optimization of the needle punching process for the non-woven fabrics with multiple quality characteristics by grey-based Taguchi method. *Fibers and Polymers*. 2007;8:654-664. DOI: 10.1007/BF02876005.
- [101] Hong G-B, Su T-L. Study on an optimal design of mechanical properties for PP/PET nonwovens. *Fibres and Textiles in Eastern Europe*. 2012;94:75-79.
- [102] Tausif M, Russell SJ. Characterisation of the z-directional tensile strength of composite hydroentangled nonwovens. *Polymer Testing*. 2012;31:944-952. DOI:10.1016/j.polymertesting.2012.06.011.
- [103] Mohan A. Formation and characterization of electrospun nonwoven webs [thesis]. Raleigh: NCSU; 2002.
- [104] Gibson HLS, Gibson P. Transport properties of electrospun nonwoven membranes. *International Nonwovens Journal*. 2002;11:21-26.
- [105] Doshi J. The electrospinning process and applications of electrospun fibers [thesis]. Akron: The University of Akron; 1994.
- [106] Dewalt PL, Reichard RP. Just how good are knitted fabrics? *Journal of Reinforced Plastics and Composites*. 1994;13:908-917. DOI: 10.1177/073168449401301005.
- [107] Textile Learner Blog. Knitting action of single needle bar [Internet]. 2015. Available from: http://textilelearner.blogspot.com/2011/06/knitting-action-of-single-needle-bar_204.html#ixzz3OXswDfAO [Accessed: 2015-03-20].
- [108] Offermann P, Hoffmann G, Engelmann U. Mehrlagengestricke und verfahren zu seiner herstellung. DE Patent 4419985C2, 4 April 1996.
- [109] Cherif C, Krzywinski S, Diestel O, et al. Development of a process chain for the realization of multilayer weft knitted fabrics showing complex 2D/3D geometries for composite applications. *Textile Research Journal*. 2012;82:1195-1210. DOI: 10.1177/0040517511429602.
- [110] Scardino FL, Ko FK. Triaxial woven fabrics: Part I: Behavior under tensile, shear and burst deformations. *Textile Research Journal*. 1981;51:80-89. DOI: 10.1177/004051758105100205.
- [111] Schwartz P. The mechanical behavior of fabrics having three, non-orthogonal thread directions (triaxial) and the equivalence of conventional fabrics [thesis]. Raleigh: North Carolina State University; 1981.
- [112] Skelton J. Triaxially woven fabrics: Their structure and properties. *Textile Research Journal*. 1971;41:637-647. DOI: 10.1177/004051757104100801.

- [113] Nishimoto H, Ohtani A, Nakai A, Hamada H. Prediction method for temporal change in fiber orientation on cylindrical braided performs. *Textile Research Journal*. 2010;80:814-821. DOI: 10.1177/0040517509352523.
- [114] Long AC. Process modelling for liquid moulding of braided performs. *Composites Part A: Applied Science and Manufacturing*. 2001;32:941-953. DOI:10.1016/S1359-835X(00)00153-6.
- [115] Nasu S, Ohtani A, Nakai A, Hamada H. Deformation behavior and mechanical properties of braided rectangular pipes. *Composite Structures*. 2010;92:752-756. DOI: 10.1016/j.compstruct.2009.09.004.
- [116] Fujihara K, Yoshida E, Nakai A, Ramakrishna S, Hamada H. Influence of microstructures on bending properties of braided laminated composites. *Composites Science and Technology*. 2007;67:2191-2198. DOI:10.1016/j.compscitech.2005.08.003.
- [117] Goyal D, Tang XD, Whitcomb JD, Kelkar AD. Effect of various parameters on effective engineering properties of 2×2 braided composites. *Mechanics of Advanced Materials and Structures*. 2005;12:113-128. DOI: 10.1080/15376490490493998.
- [118] Smith LV, Swanson SR. Effect of architecture on the strength of braided tubes under biaxial tension and compression. *Journal of Engineering Materials and Technology*. 1996;118:478-484. DOI: 10.1115/1.2805945.
- [119] Smith LV, Swanson SR. Response of braided composites under compressive loading. *Composites Engineering*. 1993;3:1165-1184. DOI:10.1016/0961-9526(93)90072-R
- [120] Tsai JS, Li SJ, Lee LJ. Microstructural analysis of composite tubes made from braided preform and resin transfer molding. *Journal of Composite Materials*. 1998;32:829-850. DOI: 10.1177/002199839803200902.
- [121] Byun JH. The analytical characterization of 2-D braided textile composites. *Composites Science and Technology*. 2000;60:705-716. DOI:10.1016/S0266-3538(99)00173-6.
- [122] Yan Y, Hoa SV. Energy approach for prediction of mechanical behavior of 2-D triaxially braided composites Part II: Parameter analysis. *Journal of Composite Materials*. 2002;36:1233-1253. DOI: 10.1177/0021998302036010460.
- [123] Backer S, Petterson DR. Some principles of nonwoven fabrics. *Textile Research Journal*. 1960; 30:704-711. DOI: 10.1177/004051756003000912.
- [124] Koombhongse S, Liu W, Reneker DH. Flat polymer ribbons and other shapes by electrospinning. *Journal of Polymer Science: Part B: Polymer Physics*. 2001; 39: 2598-2606. DOI: 10.1002/polb.10015.
- [125] Bergshoef MM, Vancso GJ. Transparent nanocomposites with ultrathin electrospun nylon-4, 6 fiber reinforcement. *Advanced Materials*. 1999;11:1362-1365. DOI: 10.1002/(SICI)1521-4095(199911)11:16<1362::AID-ADMA1362>3.0.CO;2-X.

- [126] Kim J-S, Reneker DH. Polybenzimidazole nanofiber produced by electrospinning. *Polymer Engineering and Science*. 1999; 39:849-854.
- [127] Malkan SR, Wadsworth LC. Process-structure-property relationships in melt blowing of different molecular weight polypropylene resins: Part I: Physical properties. *INDA Journal* 1991;3:21-34.
- [128] Reneker DH, Yarin AL, Fong H, Koombhongse S. Bending instability of electrically charged liquid jets of polymer solutions in electrospinning. *Journal of Applied Physics*. 2000; 87:4531-4547.
- [129] Shin YM, Hohman MM, Brenner MP, Rutledge GC. Electrospinning: A whipping fluid jet generates submicron polymer fibers. *Applied Physics Letters*. 2001; 78: 1149-1151.
- [130] Hohman MM, Shin M, Rutledge G, Brenner MP. Electrospinning and electrically forced jets. II. Applications. *Physics of Fluids*. 2001; 13:2221-2236. DOI: 10.1063/1.1384013.
- [131] Ramakrishna S, Hamada H, Rydin R, Chou TW. Impact damage resistance of knitted glass fiber fabric reinforced polypropylene composites. *Science and Engineering of Composite Materials*. 1995;4:61-72. DOI: 10.1515/SECM.1995.4.2.61.
- [132] Bilisik K, Yolacan G. Multiaxis multilayered non-interlaced/non-Z e-glass/polyester preform composites and determination of flexural properties by statistical model. *Journal of Reinforced Plastics and Composites*. 2011;30:1065-1083. DOI: 10.1177/0731684411414753.
- [133] Bilisik K. Experimental determination of ballistic performance of newly developed multiaxis non-interlaced/non-Z E-glass/polyester and 3D woven carbon/epoxy composites with soft backing aramid fabric structures. *Textile Research Journal*. 2011;81:520-537. DOI: 10.1177/0040517510383613.
- [134] Bilisik K, Yolacan G. Warp and weft directional tensile properties of multistitched biaxial woven E-glass/polyester composites. *Journal of the Textile Institute*. 2014;105:1014-1028. DOI: 10.1080/00405000.2013.869433.
- [135] Bilisik K, Yolacan G. Warp-weft directional bending properties of multistitched biaxial woven E-glass/polyester nano composites. *Journal of Industrial Textiles*. 2015; 45: 66-100. DOI:10.1177/1528083714523163.
- [136] Gawayed YA, Pastore CM. FIBER-TEX-92, The Sixth Conference on Advanced Engineering Fibers and Textile Structures for Composites; 1992; North Carolina State University, Raleigh.
- [137] Gu P. Analysis of 3D woven preforms and their composite properties [thesis]. Raleigh: North Carolina State University; 1994.

- [138] Dickinson LC. Evaluation of 3D woven carbon/epoxy composites [thesis]. Raleigh: North Carolina State University; 1990.
- [139] Babcock W, Rose D. Composite preforms. *The AMPTIAC Newsletter* 2001;5:7-11.
- [140] Bilisik K, Mohamed MH. Multiaxis three dimensional (3D) flat woven preform-tube carrier weaving. *Textile Research Journal*. 2010e; 80: 696-711. DOI: 10.1177/0040517509340602.
- [141] Byun JH, Chou TW. Process-microstructure relationships of 2-step and 4-step braided composites. *Composites Science and Technology*. 1996;56:235-251. DOI: 10.1016/0266-3538(95)00112-3.
- [142] Ko F. Development of high damage tolerant, net shape composites through textile structural design. In: *Proceedings of 5th International Conference on Composite Materials ICCM-V*; 1985; San Diego, CA.
- [143] Kuo WS. Topology of three-dimensionally braided fabrics using pultruded rods as axial reinforcements. *Textile Research Journal*. 1997;67:623-634. DOI: 10.1177/004051759706700901.
- [144] Li W, Hammad M, El-Shiekh A. Structural analysis of 3D braided preforms for composites Part II: The two step preforms. *Journal of Textile Institute*. 1990;81: 515-537. DOI: 10.1080/00405009008658726.
- [145] Li W. On the structural mechanics of 3D braided preforms for composites [thesis]. Raleigh: North Carolina State University; 1990.
- [146] Cox HL. The elasticity and strength of paper and other fibrous materials. *British Journal of Applied Physics*. 1952;3:72-74. DOI:10.1088/0508-3443/3/3/302.
- [147] Tsai, PP, Bresee, R. Fiber orientation distribution from electrical measurements. Part I: Theory. *INDA Journal*. 1991;3:36-40.
- [148] Ramakrishna S, Fujita A, Cuong NK, et al. Tensile failure mechanisms of knitted glass fiber fabric reinforced epoxy composites. In: *Proceedings of 4th Japan international SAMPE symposium and exhibition*; 24-28 Sep 1995; Tokyo.
- [149] Jinlian HU. 3-D Fibrous Assemblies: Properties, Applications and Modelling of Three Dimensional Textile Structures. Cambridge: Woodhead Publishing Ltd; 2008. 280 p.
- [150] Banerjee, PK. Principles of Fabric Formation. Mumbai: CRC Press; 2014. p. 9-19.
- [151] Ajmeri JR, Ajmeri CJ. Nonwoven personal hygiene materials and products. In: Chapman RA, editor. *Applications of Nonwovens in Technical Textiles*. Oxford: Woodhead Publishing Limited; 2010. p. 85-102.
- [152] Zobel S, Gries T. The use of nonwovens as filtration materials. In: Chapman RA, editor. *Applications of Nonwovens in Technical Textiles*. Oxford: Woodhead Publishing Limited; 2010. p. 160-183.

- [153] Chen JY, Nonwoven textiles in automotive interiors. In: Chapman RA, editor. Applications of Nonwovens in Technical Textiles. Oxford: Woodhead Publishing Limited; 2010. p. 184-201.

Geometrical Draping of Nonwoven Fabrics

Abel Cherouat and Houman Borouchaki

Additional information is available at the end of the chapter

<http://dx.doi.org/10.5772/61667>

Abstract

This paper presents an optimization-based kinematic method for simulation of forming processes of nonwoven-fabric-reinforced composites using geometrical approach. The geometrical approach allows the defining of the 3D ply shapes, 2D flat pattern, and fiber distortions. Some numerical simulations of draping are proposed and compared with the experimental results.

Keywords: Woven and nonwoven, Carbon fabric, Draping, Geometrical approach, Fiber distortions

1. Introduction

Composite reinforced by woven or UD fabric is known to have high specific stiffness and, in combination with automatic manufacturing processes, makes it possible to fabricate complex components in various industry sectors (aircraft, boat, automotive, and military). Over the last years, the demand for high stiffness and strength and low-weight materials, such as fiber-reinforced plastics, has grown in the transport industry. Especially in the aeronautical industry, the use of woven-fabric-reinforced plastics has increased significantly. The main objective of aerospace industries is to reduce to half the amount of fuel by 2020 and at least 70% less by 2025. Composite manufacturing processes have undergone substantial evolution in recent years [1, 2]. Although the traditional layup process will remain the process of choice for some applications, new developments in Resin Transfer Molding (RTM), Liquid Composite Molding (LCM), or Sheet Molding Compound (SMC), low-temperature curing pre-pregs and low-pressure molding compounds have matured significantly, and are now being exploited in high-technology areas such as aerospace and automotive industries [3-7].

The manufacturing of reinforced composites needs different forming step in which the preform fabric (woven or nonwoven) takes the desired product's shape. The main deformation

mechanism during forming of woven or nonwoven-reinforced composites is shear, which causes a change in fiber orientations. Fiber reorientation is one of the major factors causing fabric distortions, shrinking, and warpage defect. The fiber reorientation is an important factor that should be taken into account when designing composite products, since it will influence the overall thermomechanical properties and performance.

In this context, numerical simulation methods are needed to anticipate the performance of the final product, but also to predict the reinforcement preforming and the resin injection. Several modeling approaches have been developed in the literature to account for the evolution of the fiber orientation [8-11]. The earliest technique is based on discrete mapping approaches. In contrast to these mapping schemes, the constitutive behavior is required for continuum mechanical approaches [9, 12, 13].

The mapping approach, the so-called kinematic method, is used to determine the deformed shape of draped fabrics. The main assumptions are that the warp and weft fibers are inextensible, intersection points between warp and weft yarns are fixed during preforming, and the angle between warp and weft yarns are free. This method, where the fabric is placed progressively from an initial line, provides a close enough resemblance to hand-made draping [14-17].

The alternative to the kinematic approach consists of the use of Finite Element (FE) methods to simulate the fabric deformation under the boundary conditions prescribed by the forming process by considering the fabric as a homogeneous material using computationally efficient constitutive laws and continuum FEs. The limitation of the FE method is that the fabric is not really a continuum but can be more closely likened to a structure comprising discrete rods, possibly intertwined (for woven fabric), or loosely held together with stitching (for nonwoven fabric). The draping of composite fabric using a mechanical approach requires the resolution of equilibrium PDE's problems by the FE method. In general, in the case of complex surfaces, the boundary conditions are not well-defined and the contact between the surface and the fabric is difficult to manage [18, 19, 20]. Furthermore, the resolution of such a problem can be too long in CPU time and is detrimental to the optimization stage of draping regarding the initial fiber directions. All of these facts lead us to consider rather a kinematic approach, which is very fast and more robust, allowing simultaneously to define the stratification sequences and the flat pattern for different plies and to predict difficult impregnated areas that involve manual operation like dart insertion or, on the contrary, the shortage of fabric [21-38].

This paper presents an optimization-based method for simulation of forming processes of woven and nonwoven fabric reinforced composites using geometrical approach. Two draping simulation examples are given. These simulations are performed using the geometrical analysis computer code. For each example, we assume that a mesh of the mold to drape is given. The first example is the draping of woven fabric on double dome mold geometry. The second example shows the influence of the woven fabric and nonwoven on the draping process. The effects of the initial conditions (fiber orientation and start point) on the draped preform are discussed.

2. Kinematic approach

Several methods are used for predicting the fiber reorientation of the fabric. The geometrical model, also referred to as the kinematics or fishnet model is a widely used model to predict the resulting fiber reorientation for doubly curved fabric reinforced products [39, 40]. Based on a pinned-joint description of the weave, the model assumes inextensible fibers pinned together at their crossings, allowing free rotation at these joints. They analytically solved the fiber redistribution of a fabric orientated in the bias direction on the circumference of simple surfaces of revolution, such as cones, spheres, and spheroids. The resulting fiber orientations were solved as a function of the constant height coordinate of the circumference.

In the last 20 years, many authors have presented numerically based drape solutions, based on the same assumptions. The author refers to [6, 15, 41]. Typically, geometrical or kinematic fabric draping starts from a start point and two initial warp–weft fiber directions. Further points are then generated on the mold surface at a fixed equal distance from the previous points, creating a fabric mesh of quadrilateral element.

As the surface drape is generally complex and that the layup depends on the starting point and two ply directions, so there is no unique solution for the iterative geometrical simulation. This problem is generally solved by defining two fiber paths on the drape surface. Based on draping criteria such as maximum mold surface covering, minimum fabric drape covering, and minimum shear angle between warp and weft fibers, the geometrical approach can constitute the predimensioning or the preoptimization stage of the manufacturing in the product development process. The local change in composite properties must be taken into account to predict the properties of a composite product.

In this study, we propose a new discrete geometrical algorithm that takes into account the true geometry of the nonwoven fabric mesh element plotted onto the surface. The proposed approach is based on the fishnet method for which a fabric mesh element is subjected only to shear deformation. The difficulty of such a method is the mapping of the nonwoven fabric mesh element onto any surface [42].

Such a fabric mesh element is then defined by a curved quadrilateral, whose edges are geodesic lines with the same length plotted onto the surface to drape. Given three vertices of the fabric mesh element on the surface, we propose an optimization algorithm to define the fourth vertex of the fabric mesh element. The nonwoven fabric is a fabric-like material made from long fibers and expandable filaments bonded together by mechanical weaving, in order to obtain suitable shear deformation. If the shear angles of fibres are significant, then is allowed step-by-step elongations of filaments and this through an optimized iterative procedure.

Let Σ denote the surface of the part to drape and we assume that a geometrical mesh \mathbf{T}_{Σ} of surface is known. Let \mathcal{F} be the woven composite fabric modeled by two families (warp and weft) of mutually orthogonal and inextensible fiber described by the local coordinates $x=(\xi, \eta)$. These families constitute regular quadrilateral fabric mesh $\mathbf{T}_{\mathcal{F}}$ of the fabric \mathcal{F} (Fig. 1 gives example of draping steps of complex surface). The problem of geometrical draping of \mathcal{F} onto the surface Σ consists of calculating each node displacement of fabric mesh $\mathbf{T}_{\mathcal{F}}$ with a point of the surface mesh \mathbf{T}_{Σ} such that the lengths of the edge of the corresponding mesh $\mathbf{T}_{\mathcal{F}}^{\Sigma}$ on the

surface are preserved (no extensible). This problem presents infinity of solutions depending on:

1. Starting point P associated with a node of fabric \mathbf{T}_F^Σ
2. Initial warp-and-weft orientation θ

Thus, to ensure a unique solution, we suppose that the points of impact on the part surface as well as the fabric orientation are given. The draping scheme is given by the following step [31]:

1. Choose a starting point A (corresponding to the point of impact of the machine: to drape) on the surface on geometrical part mesh $\mathbf{x}_0^\Sigma = (\xi_0, \eta_0)$.
2. Compute iteratively the warp nodes of \mathbf{T}_F^Σ , classified as α -**nodes**, from the starting point, associated with nodes (ξ, η_0) of \mathbf{T}_F .
3. Compute iteratively step-by-step the weft nodes of \mathbf{T}_F^Σ , classified also as α -**nodes**, from the starting point, associated with nodes (ξ_0, η) of \mathbf{T}_F .
4. Compute iteratively cell-by-cell all the other nodes of \mathbf{T}_F^Σ , classified as β -**nodes**, from x_0 and the nodes associated with nodes (ξ, η_0) and (ξ_0, η) of \mathbf{T}_F .

The nodes of \mathbf{T}_F^Σ associated with nodes (ξ, η_0) and (ξ_0, η) of \mathbf{T}_F and the α -**nodes** are located on the surface along the geodesic lines emanating from the point of impact. Regarding the β -**nodes**, various algorithms are proposed. Most of them use an analytical expression of the surface and formulate the draping problem in terms of nonlinear partial differential equations. Other algorithms are also proposed to simplify these equations by using a finite element discretization of the surface by flat triangular face (i.e., a mesh of the surface). Based on this latter approach, we propose a new algorithm. β -**nodes** are computed by solving an optimization problem corresponding to determine a vertex of an equilateral quadrilateral plotted on the surface from the data of the three other vertices. This optimization problem concerns the following:

1. **Problem 1:** Determine the geodesic curve with a given length from a point of surface according to a given woven or nonwoven fabric direction. This problem is solved by isometrically unfolding the mesh elements along a given direction. The geodesic curve is then a strait segment. The latter is then mapped back to the surface using the unfolded elements to obtain the desired geodesic line.
2. **Problem 2:** Determine the directions of two geodesic curves with a given length from two different points of surface reaching to the same point. To solve the second problem, an iterative approach is applied to find the searched directions. Let us consider a starting point P; its successor P_1 along a warp direction and its successor P_2 along a weft direction (see Fig. 1).

The problem is to find point Q such that curve P_1Q and curve P_2Q are the geodesic lines with a given length. Thus, we have to determine the directions \vec{u}_1 and \vec{u}_2 of these geodesic lines from

P_1 and P_2 . Initially, these directions are set to $\vec{u}_1 = \vec{P}P_2$ and $\vec{u}_2 = \vec{P}P_1$ and geodesic curves P_1Q_1 and P_2Q_2 are obtained. Then iteratively these directions are set to $\vec{u}_1 = \vec{P}_1\vec{Q}_{12}$ and $\vec{u}_2 = \vec{P}_2\vec{Q}_{12}$, where $Q_{12} = (P_1 + P_2)/2$; while Q_1 is different than Q_2 .

The proposed algorithm can easily extended to the case of nonwoven intended, if the shear angle at the point Q is greater than a threshold value depending on nonwoven properties. In order to obtain suitable deformation of nonwoven during the draping operation, the algorithm to find the optimized position of the point Q is based on the shear angle criterion. If the shear angles are lower than the locking angle, the algorithm is identical to the case of woven fabric, and if the shear angles are significant, then the algorithm allows step-by-step elongations of filaments and this through an optimized iterative procedure.

The kinematic approach is well-adapted to preliminary design level. It is based on a modified MOSAIC algorithm, which is suitable to generate a regular quad mesh representing the layout of the curved surfaces. The method is implemented in the GeomDrap software, which is now integrated in the ESI-Pam QUICK software. Pam QUICK software allows to estimate a fiber quality charter (showing distortion of fiber, drop rate, and drape surface ratio) to predict local bending due to overlapping of the fibers in the shear exceeds the limit value depending on the properties of the fabric. It can be used to optimize the draping process by improving the layout directions or the marker data location [43].

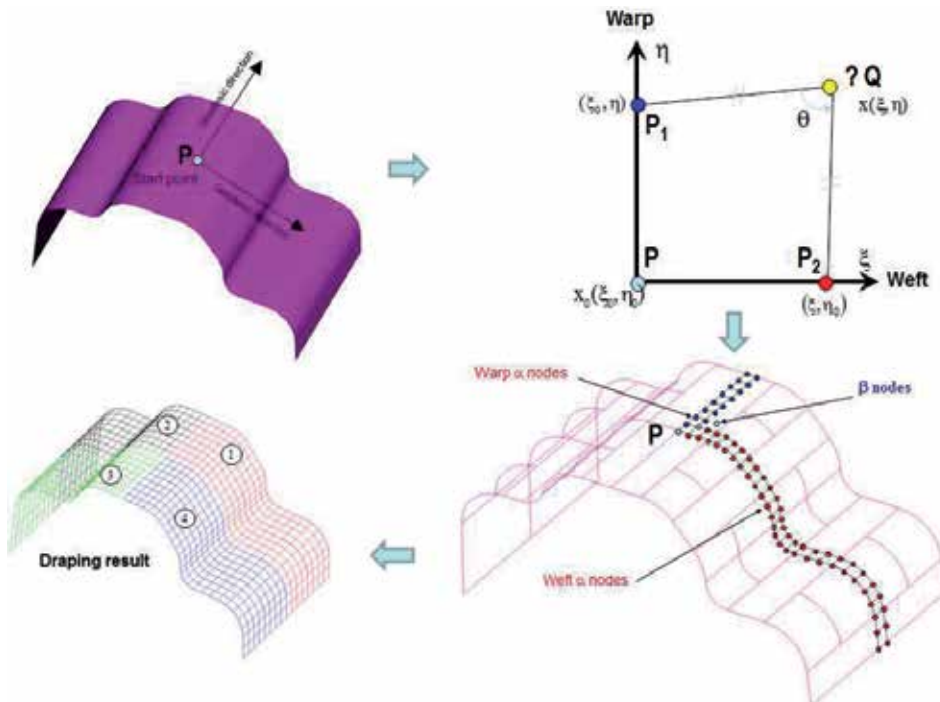


Figure 1. Geometrical draping steps of woven composite fabric

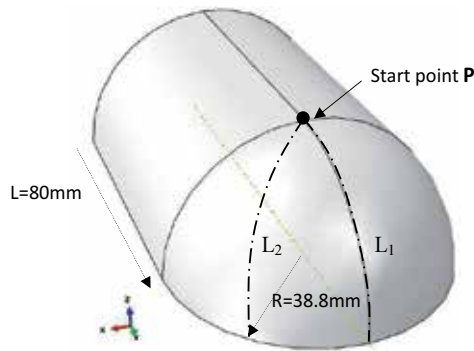


Figure 2. Schematic view of the half hemisphere connected by a half cylinder

3. Applications

The simulated results for the complex geometry are presented here. Draping is simulated with a geometrical draping method described in section 2. For each example, we assume that a mesh of the mold to drape is given. The material properties of the composite product can be predicted from the local fiber volume fraction and the shear angle, which represents the angle between the local warps/weft fiber directions. In the first example, we present the draping of woven or nonwoven composite mold on non-developable geometry in order to validate the proposed model. In this case, we compare the fiber distribution and distribution of the shear angle between the fibers in the deformed fabric. In this example, we study the effect of the excessive fiber distortion and the cutting chisel on the draping process of half hemisphere connected by a half cylinder. Comparison with experimental results is illustrated in order to validate the proposed approach. The second example compares the draping of woven and nonwoven carbon fabric on complex mold. The third and the last example show the influence of the initial start point and fiber orientation on the flat pattern of the nonwoven fabric.

3.1. Validation of the geometrical algorithm

The highest procedure presented above is used to simulate the draping of composite woven dry fabric on complex mold. In this case, we consider the draping of woven carbon fabric on two half hemispheres with a radius of $R = 38.8$ mm connected by a half cylinder with a length of $L = 80$ mm (see Fig. 2). Drape experiments results have been performed by [43]. Boundary conditions consist of an initial start point and warp/weft directions in this point. The mold surface is modeled using triangular and quadrilateral shells elements. In order to assess the influence of the initial constraints, two fabric orientations are considered. The initial contact point P of the drape is the center point of the hemisphere part of the mold and two fiber directions, 0° and 45° fabric orientations are presented.

In order to compare the experimental warp/weft angles with the predicted results, two cross sections along the symmetrical line noted L_1 (for 45° ply orientation) and the diagonal line noted L_2 (for 0° ply orientation) where most shearing occurs are examined (see Fig. 2).

In order to evaluate qualitatively the drape simulation, the enclosed fiber angle was measured in the area between the half hemisphere and cylinder at the longitudinal and diagonal axis of the mold. Figure 3 shows the resulting 3D surface draping for $[0^\circ/90^\circ]$ and $[-45^\circ/+45^\circ]$ fiber orientations. One can notice that in both cases, the mold is completely draped but the shear angles between warp and weft fibers are very excessive (greater than 80°) which is impossible and can induce defects in the composite properties after resin injection or polymerization. Figure 4 presents shaded contours interpolated from the map of the shear angles for $[0^\circ/90^\circ]$ ply orientation and Fig. 5 presents shear angles for $[-45^\circ/+45^\circ]$ ply orientation. The shear angle for both $[0^\circ/90^\circ]$ and $[-45^\circ/+45^\circ]$ draping is large (70°) but the maximum shear angle localization is different. The evolution of a draping simulation shows that the red areas indicate that with this fabric, a single sheet will not be able to cover the hemisphere without creasing. Splits can be added to the fabric, or fiber stretching can be allowed in order to minimize the shear angle.

In order to optimize the draping operation and drape completely the mold without excessive fiber distortion (fiber locking $<50^\circ$) depending on fabric properties, it is necessary to either:

- Make cuts chisel along the line C_2 for $[0^\circ/90^\circ]$ fiber orientation (Fig. 4a) and along the line C_1 for $[-45^\circ/+45^\circ]$ fiber orientation (Fig. 4b). With the cutting chisel operation, the shear limit reached 38° in the case of $[0^\circ/90^\circ]$ and 68° in the case of $[-45^\circ/+45^\circ]$.
- Allow warp and weft fiber stretching of 20%. Without the cutting chisel operation, the mold is completely draped and the shear limit reached 52° in the case of $[0^\circ/90^\circ]$ fiber orientation (Fig. 5a) and 89° in the case of $[-45^\circ/+45^\circ]$ (Fig. 5b).

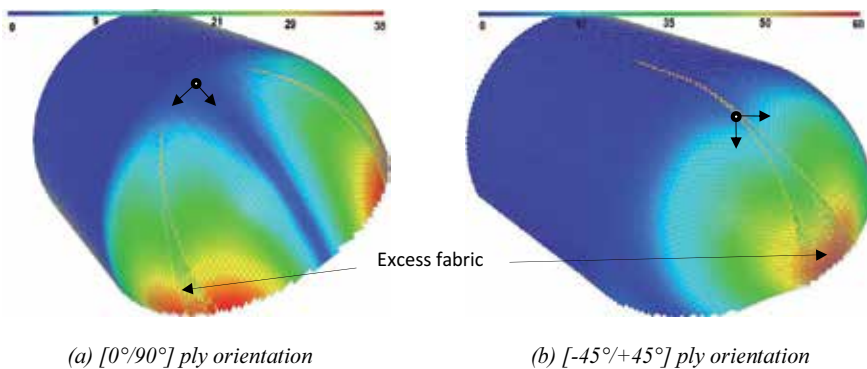


Figure 3. Drape results on shear angles of 0° and 45° ply orientations

To compare the predicted shear angles with the experimental result given by [44], measurements of angles along the lines where the highest shear angles occur were performed. From Fig. 6 it can be concluded that for the $[0^\circ/90^\circ]$ ply orientation along the diagonal line L2, the agreement between the experimental shear angles and the predicted draping results is good. On the other side, for $[-45^\circ/+45^\circ]$ ply orientation along the symmetrical line L1, the predicted results do not agree at all with the experimental values. The oversimplification of the fabric deformation in the geometrical model gives shear angles up to 89° in case of the 45° ply orientation, which is impossible for woven fabric. The geometrical model is used with a cutoff

shear angle based either on an experimentally determined locking angle, or the maximum orientation that the designer is prepared to tolerate. When defining cutoff angle of 38° , which equals the experimentally determined locking angle, one can, in this case, drape the mould, which has high shear angles, with nonwoven fabric.

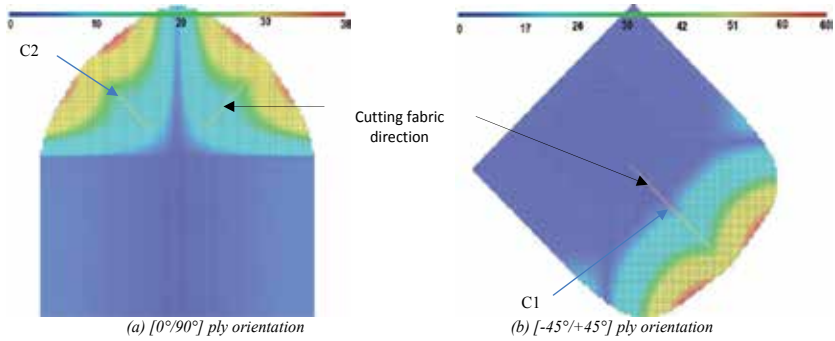


Figure 4. flat pattern results of 0° and 45° ply orientations

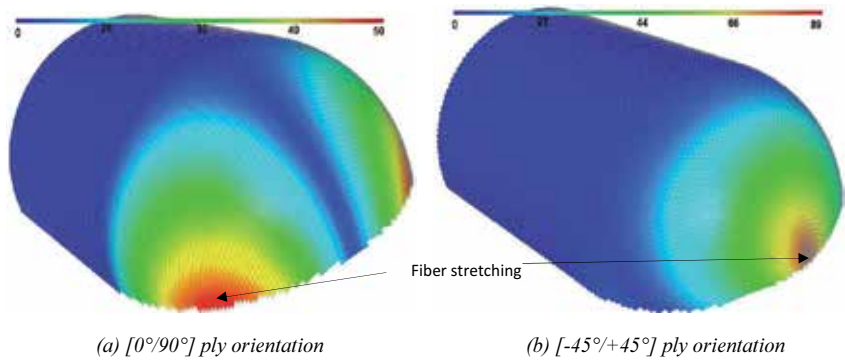


Figure 5. Optimized drape results on shear angles of 0° and 45° ply orientations

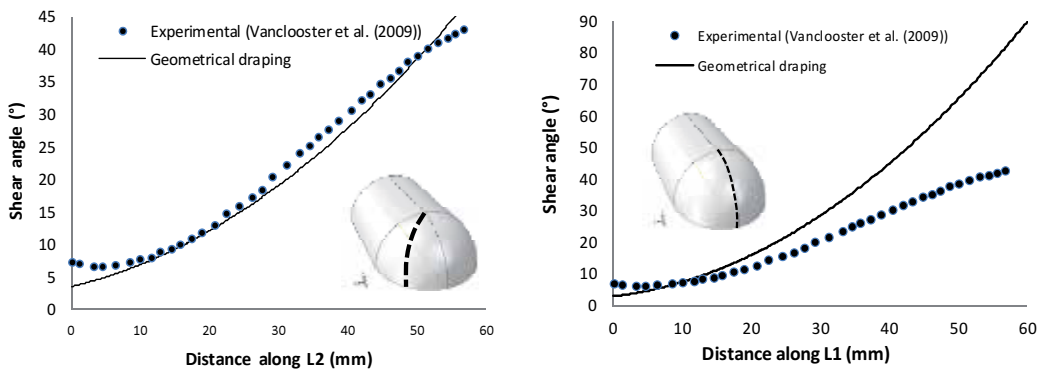


Figure 6. Shear angles along (a) the line L1 of 45° orientation and (b) along L2 of 0° orientation

3.2. Comparison of woven and nonwoven fabric draping

The second example concerns the draping of woven and nonwoven carbon fabric on complex plastic mold. The initial rectangular taffeta fabric dimensions are: length = 700 mm and width = 350 mm (Fig. 7). The start point P in the simulation was the center of mass and the initial fiber direction is 45° with the geodesic mold directions (see Fig. 8). Figure 9 shows the resulting 3D draping for the woven and nonwoven fabric. We can note that all part surfaces are completely draped with woven and nonwoven fabric but with defect, the outline shapes of flat pattern are different, and the location of the maximum shear angles is the same as in the draped surface. Figure 10 presents shaded contours interpolated from the map of the fiber shear angles. For the draping of the surface with nonwoven fabric, we note that also all part of surface is completely draped with large shear angle ($\theta > 85^\circ$) with fiber disentanglement and junction unraveling. For drape orientation, the results from geometrical model agree with the experimental results. One can conclude, in the considered cases, the draped surface of the product with 45° fiber orientation with woven or nonwoven fabric is impossible without cutting chisel operation. The very excessive shear angles induce defects and superposition of the cross-ply in the composite part after resin injection or polymerization.

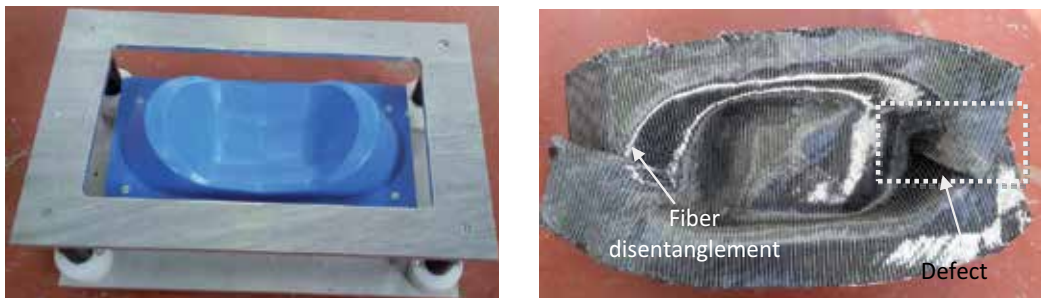


Figure 7. Mold design and experimental nonwoven draping result

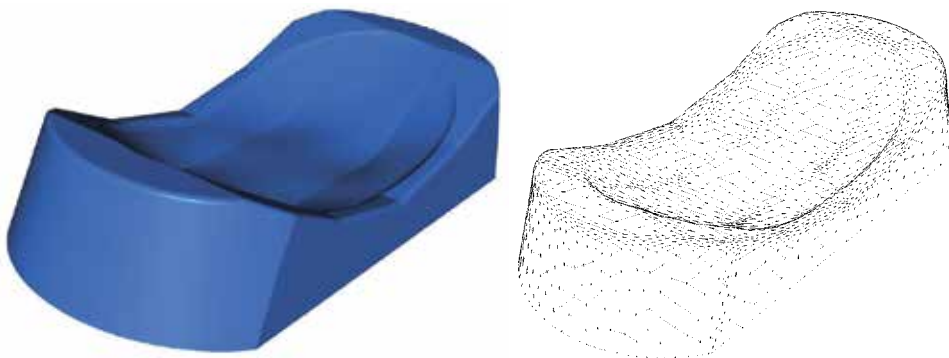


Figure 8. CAD and mesh of the mold

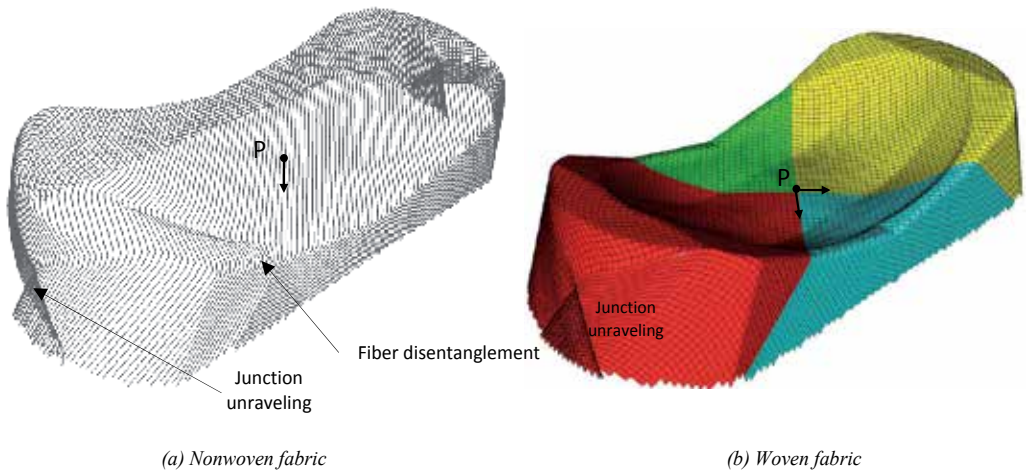


Figure 9. 3D geometrical draping using UD fabric and woven carbon fabric

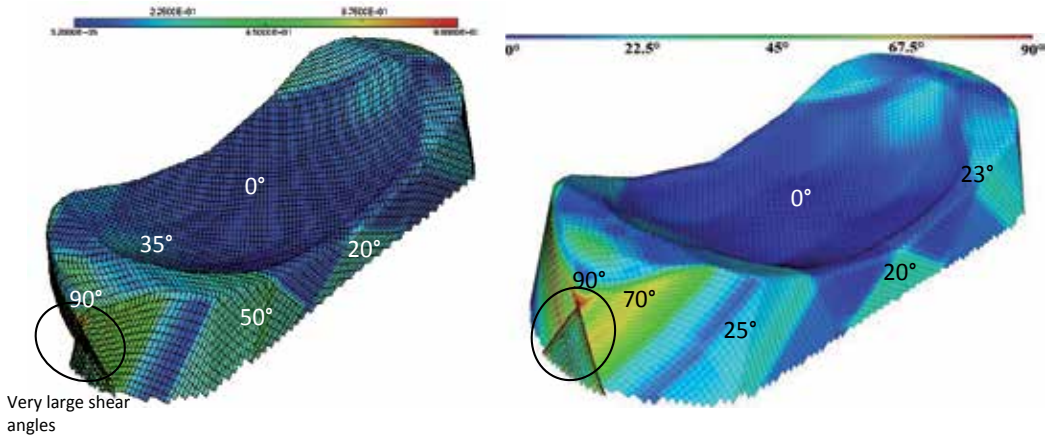


Figure 10. Shear angle of draped UD fabric and woven carbon fabric

3.3. Effect of nonwoven fabric orientation

The mechanical response of nonwoven fabrics exhibits an anisotropic response biased toward the direction of preferential alignment of constituent fibers. The deformation mechanisms governing the fabric response under bias-loads include textural evolution by means of reorientation of constituent fibers, fiber stretch, relative fiber slip, as well as fiber disentanglement and junction unraveling.

The proposed mold shape is now draped geometrically using three fiber orientations. Here, only the predicted fiber orientations on the mold shape are compared. Figures 11, 12, and 13

show the resulting 3D nonwoven fabric draping for the 0°, 90°, and 45° drape orientations, respectively, and the corresponding shaded contours interpolated from the map of the fiber orientation. From these figures it can be concluded that for the same initial contact point, the shear angle ($\theta > 80^\circ$) localization is different and level is highly dependent on the mold geometry and the boundary conditions. Various defects such as unraveling of weaving and disentanglement of the fibers produced during the layup and may have effects on the quality of the final composite part after the injection of resin or polymerization.

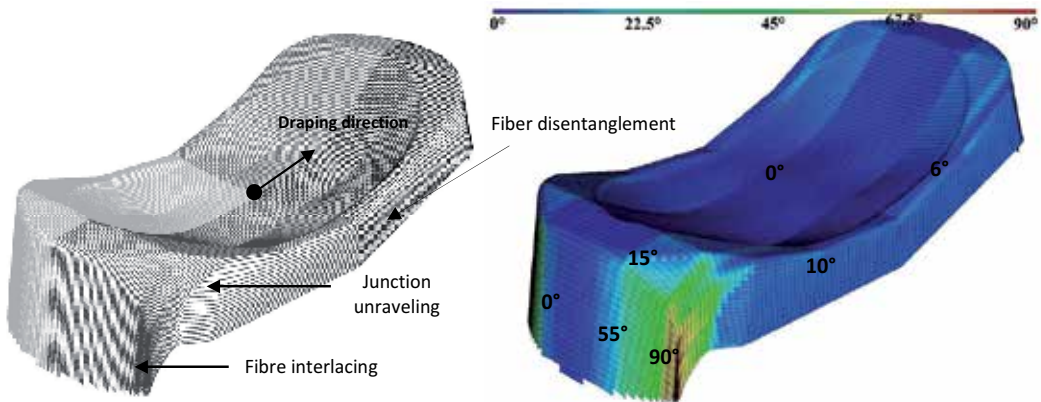


Figure 11. 3D draping and iso-values of fiber angles of the 0° nonwoven draping

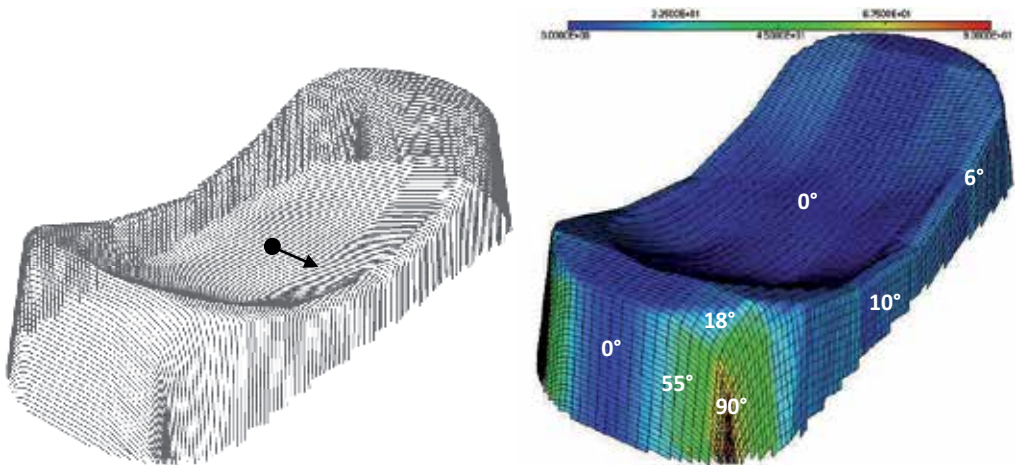


Figure 12. 3D draping and iso-values of fiber angles of the 90° nonwoven draping

3.4. Effect of the draping start point

To study the effect of the initial start point on the draping results, a surface double dome is draped by non-woven fabric (Fig. 14). The mold shape consists of two coinciding hemispheres with different radii (small sphere radius $R = 75$ mm and large sphere radius $R = 100$ mm). The

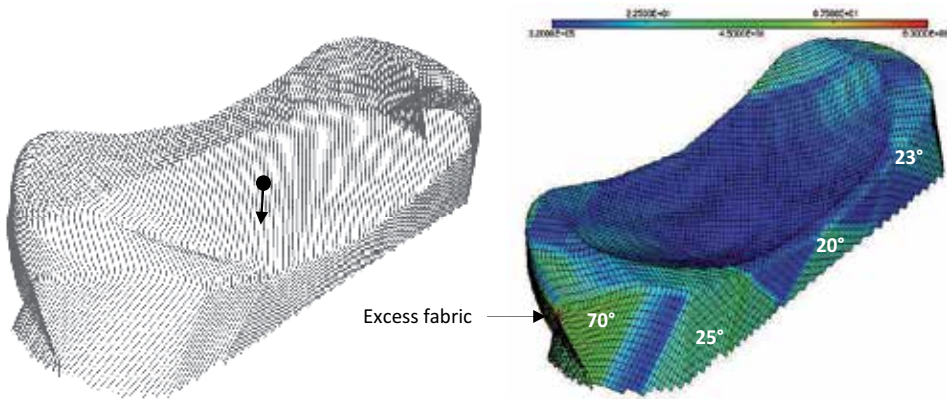


Figure 13. 3D draping and iso-values of fiber angles of the 45° nonwoven draping

initial start point P in the simulation was chosen as the top of the small (D1) or the large hemisphere part (D2). The initial ply orientation was perpendicular to the main axis of the mold (Fig. 15). Here, the predicted 3D draping, shear fiber orientations on the double dome shape, and the 2D flat pattern are compared [45].

1. At first glance, the results look very similar for the draping on the smaller sphere start point and on the large sphere start point (see Figs. 16 and 17). Both cases predict the same fiber directions along the main mold perpendicular axis and the same 2D fabric flat pattern (Fig. 19).
2. With the geometrical simulation, large fabric deformations occur (up to 80°) for the D1 draping; however, smaller fabric deformations occur (up to 60°) for the D2 draping (Fig. 18).
3. For the inner areas on the two domes, the geometrical draping method predicts smaller nonwoven fabric shear angles for the two case draping D1 and D2 (marked with E, F, G, and H) (see Fig. 18).
4. For the outer areas, both cases predict different fiber orientations in regions A, B, and C (see Fig. 18). The main differences occur in the concave area between the two hemispheres (region B) and outer areas of the large hemisphere (region A) and small hemisphere (region C). With the geometrical simulation, on both, the larger and the smaller hemispheres, large fabric deformations occur (up to 70°).

This difference can be explained from the D1 draping, which starts from the top of the small hemisphere and extends outward from the highest point at the edge, resulting in gradually downward moving fibers and fiber disentanglement. When the fiber reaches the edge of the intersection fillet (position C), it will extend from that position onward (marked A), up and over the top of the larger hemisphere, resulting in a large fabric deformation at the outer area of the hemispheres and fiber interlacing.

The D2 draping starts from the top of the large hemisphere and extends outward from the lower point at the edge, resulting in gradually downward moving fiber and fiber disentan-

gement. When the fiber reaches the edge of the intersection fillet, it will extend from that position onward (marked B), up and over the top of the larger hemisphere, resulting in a large fabric deformation at the outer area of the hemispheres and fiber interlacing.

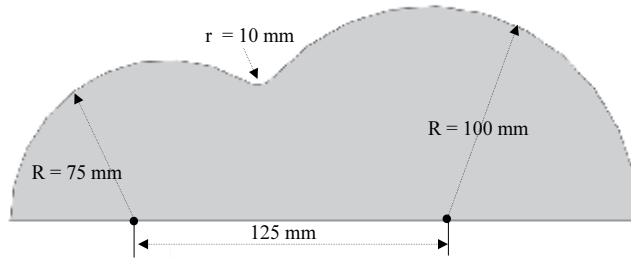


Figure 14. Schematic view of the double dome

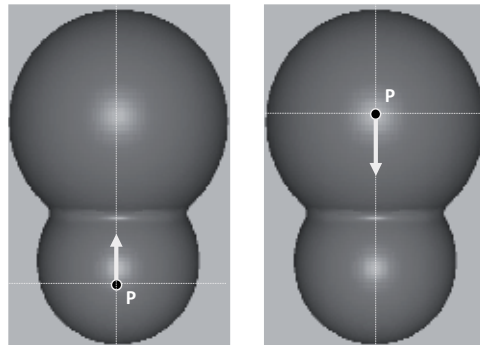


Figure 15. Initial start point on the top of the small sphere (draping D1) and on the large sphere (draping D2)

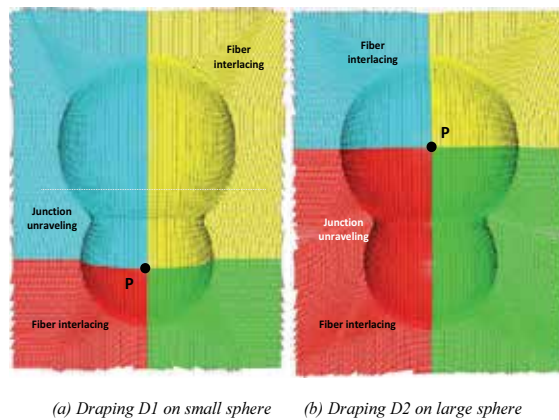


Figure 16. 3D draping results of nonwoven fabric on double dome

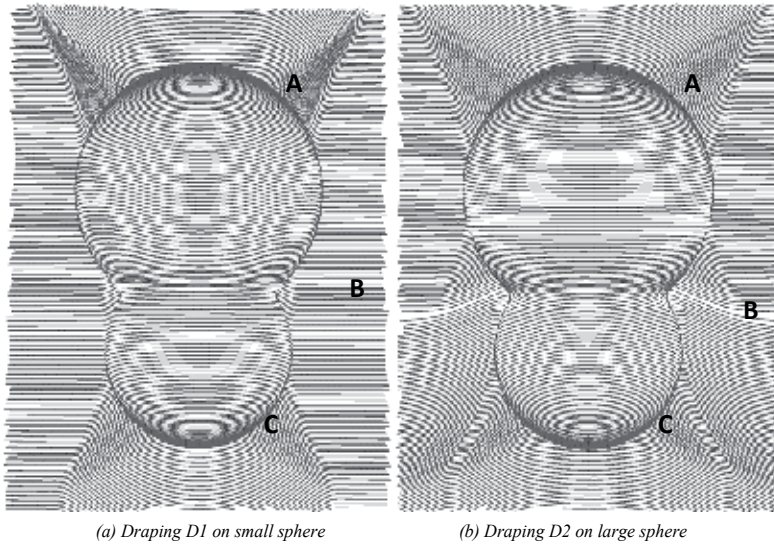


Figure 17. Predicted fiber orientation of the nonwoven fabric on double dome

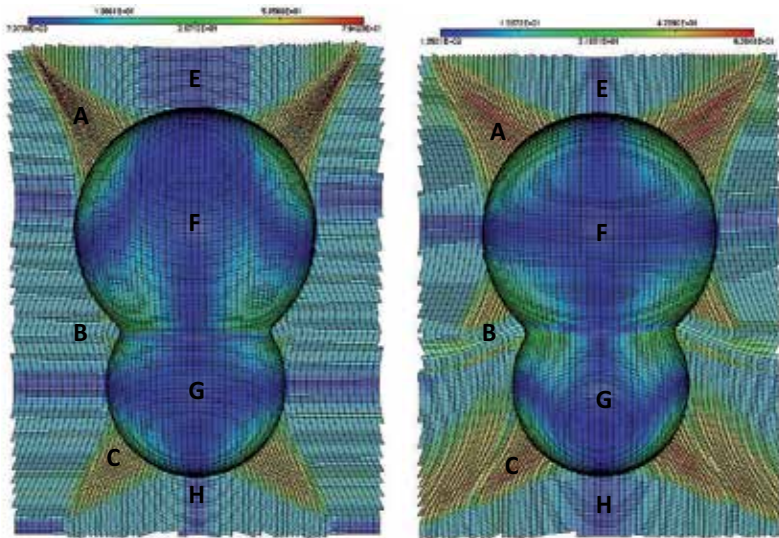


Figure 18. Shear angle of draped nonwoven fabric of drape D1 and drape D2

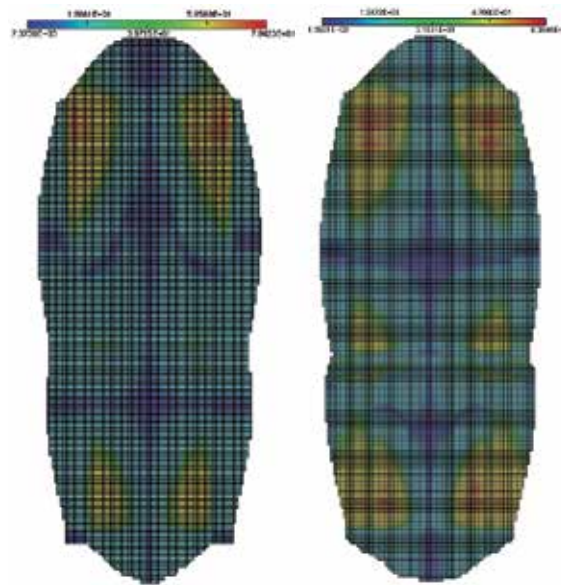


Figure 19. 2D Flat pattern results of drape D1 and drape D2

4. Conclusions

This paper presented several aspects of the draping of nonwoven fabric composite on complex mold geometry. The kinematic approach is well-adapted to preliminary design level. It is based on a modified MOSAIC algorithm, which is suitable to generate a regular quad mesh representing the draping of woven fabric on curved surfaces. In order to obtain suitable deformation of nonwoven during the draping operation, modified kinematic algorithm based on the shear angle criterion is proposed. This algorithm allowed step-by-step stretching of weaving yarns using iterative procedure. Some numerical examples concerning the draping of woven or nonwoven fabric are presented in order to demonstrate the efficiency of the proposed approach. They provide a good correlation with the experimental results.

Author details

Abel Cherouat* and Houman Borouchaki*

*Address all correspondence to: abel.cherouat@utt.fr; houman.borouchaki@utt.fr

University of Technology of Troyes, Charles Delaunay Institute/GAMMA-INRIA Project Team, Troyes, France

References

- [1] Bannister M. (2001), "Challenges for composites into the next millennium – a reinforcement perspective". *Composites Part A*, 32:901-10.
- [2] Laurenzi S., Casini A., Pucci D. (2014), "Design and fabrication of a helicopter unitized structure using resin transfer moulding", *Composites Part A: Appl Sci Manufact*, 67: 221-232.
- [3] Prodromou A.G, Chen J. (1997) "On the relationship between shear angle and wrinkling of textile composite preforms", *Composites Part A*, 28A, 491-503.
- [4] Hou M., Ye L., Mai Y.W. (1997), "Manufacturing process and mechanical properties of thermoplastic composite components". *J Mater Process Technol*, 63: 334-338.
- [5] Campbell F.C. (2004), *Manufacturing Processes for Advanced Composites*, Elsevier Advanced Technology, Oxford.
- [6] Trochu F., Ruiz E., Achim V., Soukane S. (2006), "Advanced numerical simulation of liquid composite molding for process analysis and optimization", *Composites Part A: Appl Sci Manufact*, 37: 890-902.
- [7] Ivanov D.S., Ivanov S.V. (2015), "Modelling the structure behaviour of 2D and 3D woven composites used in aerospace applications", *Polym Compos Aerospace Indus*, 21-52.
- [8] Mark C., Taylor H.M. (1956), "The fitting of woven cloth to surfaces", *J Text Inst*, 47: 477-488.
- [9] Breen D., House D., Wozny M. (1994), "A particle-based model for simulating the draping behavior of woven cloth". *Text Res J* 64, 11 663-685.
- [10] Trochu F., Hammami A., Benoit Y. (1996), Prediction of fibre orientation and net shape definition of complex composite parts. *Composites Part A*, 27:319-328.
- [11] Vandeurzen P., Ivens J., Verpoest I. (1996), "A three dimensional micro mechanical analysis of woven fabric composites: I. elastic analysis". *Compos Sci Technol*, 56:1317-1327.
- [12] Ben Boubaker B., Haussy B., Ganghoffer J.F. (2007), "Discrete woven structure model: yarn-on-yarn friction", *Comptes Rendus Mécanique*, 335(3):150-158.
- [13] Cordier F., Magnenat-Thalmann, N. (2002), "Real-time animation of dressed virtual humans". *Eurographics*, 21, 3.
- [14] Van Der Ween F. (1991), "Algorithms for draping fabrics on doubly curved surfaces", *Int J Numer Methods Eng*, 31:1414-1426.

- [15] Long A.C., Rudd C.D. (1994), "A simulation of reinforcement deformation during the production of preform for liquid moulding processes", *Proc Inst Mech Eng Part B J Eng Manuf*, 208: 269-278.
- [16] Hancock S.G., Potter K.D. (2005), "Inverse drape modelling—an investigation of the set of shapes that can be formed from continuous aligned woven fibre reinforcements", *Composites Part A: Appl Sci Manufact*, 36(7): 947-953.
- [17] Yin H., Peng X., Du T., Guo Z. (2014), "Draping of plain woven carbon fabrics over a double-curvature mold", *Composites Sci Technol*, 92(24): 64-69.
- [18] Ivanov I., Tabiei A. (2002), "Flexible woven fabric micromechanical material model with fiber reorientation", *Mech Adv Mater Struct*, 9: 37-51.
- [19] Kang T., Yu W. (1995), "Drape simulation of woven fabric by using the finite-element method", *J Text Instit*, 86(4): 635-648.
- [20] Kato S., Yoshino T., Minami H. (1999), "Formulation of constitutive equations for fabric membranes based on the concept of fabric lattice model", *Engin Struct*, 21: 691-708.
- [21] Boisse P., Cherouat A., Gelin J.C., Sabhi H. (1995), "Experimental study and finite element simulation of a glass fiber fabric shaping process", *Polym Compos*, 16(1): 83-95.
- [22] Duhovic M., Mitschang P., Bhattacharyya D. (2011), "Modelling approach for the prediction of stitch influence during woven fabric draping", *Composites Part A: Appl Sci Manufact*, 42: 968-978
- [23] Asthana R., Kumar A., Dahotre N.B. (2006), "Composites get in deep with new-generation engine", *Reinforced Plastics*, 50(11): 26-29.
- [24] Prodromou A.G., Stepan V. Lomov, Ignaas Verpoest (2011), "The method of cells and the mechanical properties of textile composites", *Compos Struct*, 93(4): 1290-1299.
- [25] Gatouillat G., Bareggi, Vidal-Sallé E., Boisse P. (2013), "Meso, modelling for composite preform shaping – Simulation of the loss of cohesion of the woven fibre network", *Composites Part A: Appl Sci Manufact*, 54: 135-144.
- [26] Gereke T., Döbrich O., Matthias Hübner, Chokri Cherif (2013), "Experimental and computational composite textile reinforcement forming": *Composites Part A: Appl Sci Manufact*, 46: 1-10.
- [27] Rozant O., Bourban PE., Manson JAE. (2000), "Drapability of dry textile fabrics for stampable thermoplastic preforms". *Composites: Part A*, 31: 1167-1177.
- [28] Cherouat A., Borouchaki H., Giraud-Moreau L. (2011), "Mechanical and geometrical approaches applied to composite fabric forming", *Int J Mater Form*, DOI 10.1007/s12289-010-0692-5.

- [29] Teik-Cheng Lim, Ramakrishna S. (2002), "Modelling of composite sheet forming: a review", *Composites Part A: Appl Sci Manufact*, 33: 515-537
- [30] Warby M.K., Whiteman J.R., Jiang W.-G., Warwick P., Wright T. (2003), "Finite element simulation of thermoforming processes for polymer sheets", *Math Compu Simul*, 61: 209-218.
- [31] Cherouat A., Borouchaki H., Billoët J.L. (2005), "Geometrical and mechanical draping of composite fabric", *Eur J Comput Mech*, 14 (6-7), 693-708.
- [32] ElHami A., Radi B., Cherouat A. (2009), "Treatment of the composite fabric's shaping using a Lagrangian formulation", *Math Compu Model*, 49(7-8):1337-1349.
- [33] Taha I., Abdin Y., Ebeid S. (2012), "Prediction of draping behavior of woven fabrics over double-curvature moulds using finite element techniques", *Int J Mater Mech Engin*, 1: 25-31.
- [34] Vanclooster K., Lomov S.V., Verpoest I. (2009), "Experimental validation of forming simulations of fabric reinforced polymers using an unsymmetrical mould configuration", *Composites Part A: Appl Sci Manufact*, 40(4): 530-539.
- [35] Potluri P., Sharma S., Ramgulam R. (2001), "Comprehensive drape modelling for moulding 3D textile preforms", *Composites Part A: Appl Sci Manufact*, 32(10): 1415-1424.
- [36] Xue P., Peng X., Cao J. (2003), "A non-orthogonal constitutive model for characterizing woven composites", *Composites Part A*: 34: 183-193.
- [37] Sharma S.B., Sutcliffe M.P.F. (2004), "A simplified finite element model for draping of woven material", *Composites Part A*, 35: 637-643.
- [38] Fan J.P., Tang C.Y., Tsui C.P., Chan L.C. and Lee T.C. (2006), "3D finite element simulation of deep drawing with damage development", *Int J Mach Tools Manufact*, 46(9): 1035-1044.
- [39] Heisley F., Haller, K. (1988) "Fitting woven fabric to surfaces in three dimensions". *J Text Instit* 2, 250-263.
- [40] Weëen, F. (1991), "Algorithms for draping fabric on doubly-curved surfaces". *Int J Numer Meth Engin*, 31: 1415-1426.
- [41] Robertson R., Hsiue E., Yeh G. (1984), "Fibre rearrangements during the moulding of continuous fibre composites", *Polym Composites*, 5: 191-197.
- [42] Cherouat A., Billoët J.L. (2001), "Mechanical and numerical modelling of composite manufacturing processes deep-drawing and laying-up of thin pre-impregnated woven fabrics", *J Mat Proc. Technol*, 118: 460-471.
- [43] Cherouat A., Borouchaki H. (2009), "Present state of the art of composite fabric forming: geometrical and mechanical approaches", *Mater* 2(4):1835-1857.

- [44] Vanclooster K., Lomov S.V., Verpoest I. (2009), "Experimental validation of forming simulations of fabric reinforced polymers using an unsymmetrical mould configuration", *Composites Part A: Applied Science and Manufacturing* 40 (4): 530-539.
- [45] De Luca, P., Lefébure, P., Pickett, A. (1998), "Numerical and experimental investigation of some press forming parameters of two fibre reinforced thermoplastics: APC2-AS4 and PEI-CETEX", *Composites Part A*, 29: 101-110.

Nonwoven Padding for Compression Management

Bipin Kumar

Additional information is available at the end of the chapter

<http://dx.doi.org/10.5772/61309>

Abstract

Nonwovens play an important and crucial role in the designing of appropriate structures for healthcare and hygiene products. One such application is the use of nonwoven padding in a multi-layer compression system recommended for the treatment of chronic venous disorders. Padding helps in ensuring uniform pressure distribution underneath the bandaging layer wrapped around the circumference of the limb. Apart from the pressure management, padding also facilitates body fluids' absorption and removal, and provides thermal and tactile comfort to ensure better compliance of the multi-layer compression system. This chapter analyses the different roles of padding in compression management. The importance of different nonwovens and their structure on the padding performance are also reviewed, using both experimental and theoretical analyses. Finally, some useful recommendations are provided for design considerations to develop optimized products.

Keywords: Padding, Nonwoven, Venous Ulcers, Pressure, Wadding, Multi-layer bandaging

1. Introduction

Today, nonwoven fabrics are the fastest growing area of the textile industry [1, 2]. As nonwoven fabrics are made directly from fibres, bypassing the large number of operations involved in assembling fibres first into yarn and then preparing the yarns suitably for the fabric formation process, tremendously decreases the labour cost, allows easier cutting and sewing for unskilled labour and reduces the lag time during production process [3]. Furthermore, nonwoven allows modifying its properties by selecting different fibres or binders and controlling the arrangement of the fibres in the web. Hence, they are successful in many

industrial and medical applications including geotextiles, diapers, wipes, draperies, furniture, mattress, mattress pads, apparel, etc. [4]. Each of these applications has different demands due to which the specific properties and characteristics of the nonwoven must be addressed carefully in order to design optimised fabric structure with maximum benefits. This chapter focuses on a particular end application for the nonwoven as a padding bandage used in multi-layer compression system recommended for chronic venous ulcers.

Nonwoven padding is an essential component in a multi-layer compression system [5, 6]. Padding lies underneath compression bandage or stocking through which substantial amount of pressure is exerted on the limb of patient. Padding plays two major functions: first it helps to maintain uniform pressure around the circumference of limb, and, second, it helps in proper exchange of moisture or air for improved comfort to the patient. This chapter addresses several issues related to padding: it begins by mentioning the medical problem, identifying the product requirements, describing the role of fibre and construction, attempting theoretical modelling to understand padding behaviour, examining the structure–property relationship and finally recommending the optimised product.

2. Chronic venous disorders

Chronic venous disorder occurs due to improper functioning of venous system, especially in the lower extremity, which makes it difficult for the venous reflux to return to the heart from the legs [7, 8]. Patients suffering from such disorders have poor quality of life due to consistent pain, limited mobility, physical function, depression, social isolation and high treatment cost [9]. It has been estimated that 1% of the general population (age group: 18–64) is suffering from chronic venous disorders [10]. This rate is further increased to 4% in people over the age of 65 [11]. Furthermore, it has been anticipated that the rate will increase significantly in future due to changing lifestyle and the growing aging population.

Chronic venous disorders such as varicose veins, deep vein thrombosis, oedema, ulcers, lymphoedema, etc., happen primarily in lower limbs when the veins are not able to pump enough blood back to the heart. This improper functioning is the result of venous hypertension [12]. In most cases, venous hypertension is caused by reflux through incompetent valves, but other causes include venous outflow obstruction and failure of the calf-muscle pump owing to obesity or leg immobility. Deep vein thrombosis is the condition where the blood clots (thrombus) inside the veins, which obstructs the smooth flow of blood toward the heart [13]. The blood trying to pass through these blocked veins can increase the blood pressure in the vein, which, in turn, will overload the valves. This can lead to damage to the valves, which can further worsen the problem as these incompetent values will not be able to prevent backflow of blood. This may result in pooling of blood in the surrounding tissues, which will cause swelling (also termed as oedema). Over time, this can worsen the condition and result in venous ulceration (Figure 1).

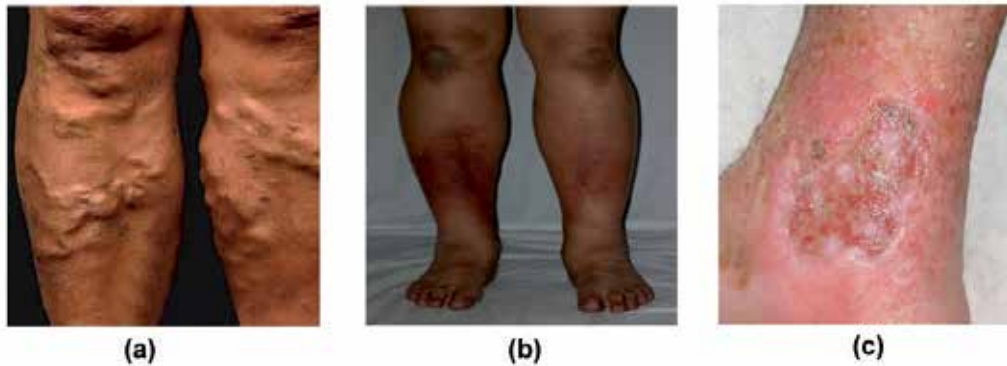


Figure 1. Different forms of chronic venous symptoms in lower leg (varicose veins, venous oedema and venous leg ulcers; from left to right)

2.1. Compression Therapy – Importance of External Pressure

Compression therapy is the cornerstone of treatment for phlebological and lymphatic conditions [7, 14-17]. The prime objective of compression therapy is to reduce the venous pressure in the affected limb region [13, 17, 18]. This finally serves several functions:

It reduces the venous diameter and increases the interstitial pressure in the surrounding, which increases the blood flow in the deep veins.

It restores the valve function by bringing the walls of the veins closer together.

It reduces blood pressure in the superficial venous system.

It reduces the pressure differences between the capillaries and the tissue to prevent backflow.

It increases the cutaneous microcirculation, favours white cell detachment from the endothelium and prevents further adhesion.

It reintegrates the interstitial liquids into the vessels.

The main parameter responsible for clinical efficiency is the interface pressure [19-26]. Interface pressure is defined as the pressure exerted by the compression system over the surface of skin. The Laplace's Law is used to predict the interface pressure (P), which is a function of the tension in the fabric, and the circumference of the limb [16, 21, 27]. This can be expressed as:

$$P = \frac{F}{r} \quad (1)$$

where F is the tension in the fabric per unit length, and r is the limb radius. The efficacy of the treatment is undoubtedly dependent on this interface pressure as this has to be quite accurate within certain limits and should not be below or above the prescribed level, otherwise it can

lead to certain complications during treatment [25, 28]. Low pressure will not have the benefit of external compression, and very high pressure impedes the arterial flow, which can cause discomfort. The optimal pressure necessary to overcome venous hypertension is not well known, but an external pressure of 35–40 mmHg at the ankle is necessary to prevent capillary exudation in legs affected by chronic venous insufficiency [11, 26].

2.2. Treatment Modalities – Need for Different Textile Materials

Several important factors must be present for a health practitioner to use compression systems, like knowing how to use different products, knowing the best available compression modalities available for the treatment, being able to identify the aetiology of the ulcer, and the willingness of the patient to agree to the commencement of compression treatment and for this to be sustained. Today, there exist several modes of compression devices. Table 1 lists some of the most common devices used for providing pressure. The basic constructions are woven or knitted. Woven construction consists of two sets of perpendicular yarns (also known as warp and weft yarns) that are interlaced together with the help of weaving process. Knitted construction consists of intersecting loops that are produced by a knitting process.

Medical Device	Advantages	Disadvantages
<i>Bandage</i>	<ul style="list-style-type: none"> √ Maintained compression √ Pressure can be adjusted √ Recommended for high level of compression (35–80 mmHg) 	<ul style="list-style-type: none"> √ Need to be applied by well-trained physicians and nurses √ Pressure variation and no measurement
<i>Stocking</i>	<ul style="list-style-type: none"> √ No trained physicians required √ Suitable for low pressure (20–40 mmHg) 	<ul style="list-style-type: none"> √ Difficult to put in √ Different stocking for different legs
<i>Extremity pump</i>	<ul style="list-style-type: none"> √ Augment venous return √ Effective for immobile patients 	<ul style="list-style-type: none"> √ Expensive, noisy, bulky √ Requires immobility for a few hours/day

Table 1. Pressure devices

Nonwoven is not used for generating compression. But it does play a very important role in compression and comfort management, which is discussed in the next section. Nonwoven is commonly used for the preparation of padding material for the multi-layer compression bandaging system. In a multi-layer compression system, there exist several layers of fabrics in addition to compression layer:

- *Wound contact layer:* It directly touches with wound portion of the skin and provides antimicrobial benefits.
- *Absorbent padding bandage:* It is applied from ankle to knee using a simple spiral technique and 50% overlap. This chapter primarily focus on this layer.
- *Compression bandage:* This is used over the padding layer. Its main function is to provide compression. It is applied from the ankle to the knee, using a figure of eight technique at 50% extension.

- *Flexible cohesive bandage*: This is the last layer which is used to secure all the innermost layers in place.

The roles of each of these layers are critical in the successful treatment of venous diseases.

3. Padding bandage

3.1. Role and function

In addition to compression layer, the role of padding is also critical in the successful treatment of chronic venous disorders. A suitable thickness of padding (~1–2.5 cm) is used between the bandage and skin layer for uniform pressure distribution [5, 29]. Padding is wrapped underneath the compression bandage and left over the wounded area for long period of time. In order to distribute pressure evenly around the limb, it is essential that high pressures created at the tibia and fibula regions are absorbed by the padding material. The normal pressure applied by the compression bandage gets absorbed and distributed within the structure of padding bandage. Some amount of pressure is dissipated in the structure, and the rest is transmitted through the thickness of the padding bandage to exert final absolute pressure on the patient's leg. Padding can also be used to reshape legs which are not narrower at the ankle than the calf. It helps to reshape the limb more like a cone-shape so that the pressure gradient can be achieved with more pressure at the ankle and less at the calf.

In addition to pressure management by padding, the other concern is to maintain good thermo-physiological comfort and to ensure better compliance for the patient during the course of compression treatment [30]. The thermo-physiological comfort concerns the heat and moisture transmission characteristics through clothing, that is, transmission of heat, air and moisture (liquid and vapour) [31, 32]. Multi-layer compression systems, such as 4-layer bandaging, are used for extended periods of time with minimum dressing change. This may cause overheating of the underlying tissues and, perhaps, excessive sweat production due to poor air or moisture exchange between the body and the surrounding [33]. Clearly, the removal of excess fluid or exudates is extremely important to avoid irritation and ensure comfort to the patients. Over-hydration or even maceration of the underlying tissues is likely to happen if the body fluids are not continuously removed from the affected region. Improper management of excessive wound exudates or other body fluids may delay healing and lead to other complications. The padding is used underneath the bandage and therefore is in direct contact with the skin. The interaction of fluids with the padding is therefore critical, as this determines the ability of padding to spread the liquid to a wider area and therefore helps in faster evaporation and prevention of excess moisture build-up. This will also provide better comfort to the patient. Furthermore, the surplus heat produced due to muscular activity should be discharged into the surrounding to facilitate wound healing. Several properties of padding including air permeability, moisture and thermal transmission, wicking, etc., are important here to finally ensure better thermo-physiological comfort of the compression product.

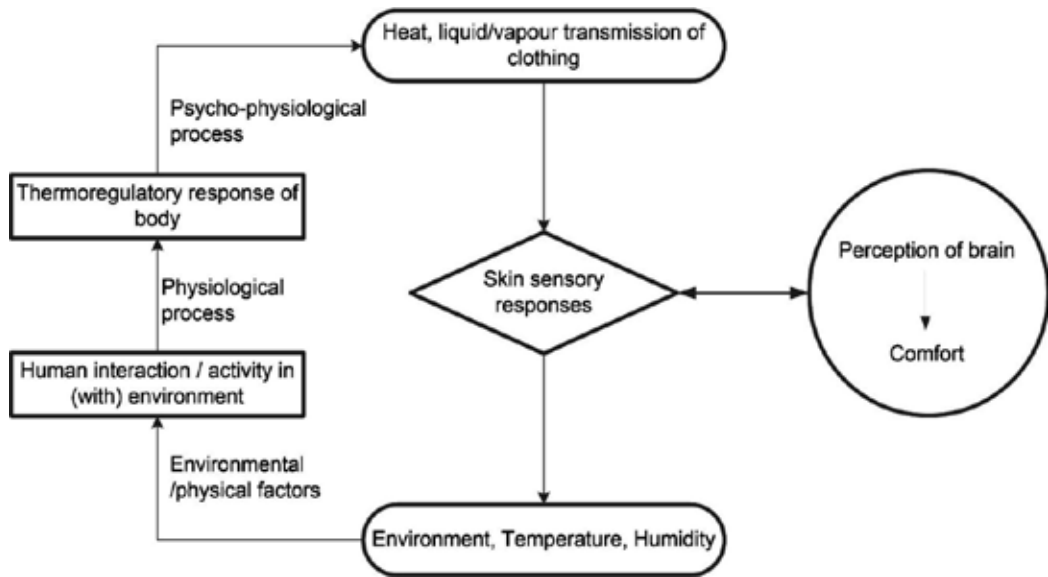


Figure 2. Important physical and physiological factors affecting padding comfort

Other comfort for padding includes the sensorial or tactile comfort which is related to the mechanical contact of the fabric with skin, that is, how a fabric or garment feels when it is worn next to the skin [31]. These are fabric handle or feel, softness, fullness, warm-cool touch, static charge generation, flexing, pricking, itching, etc. The physiological comfort, such as fitting, which is related to aesthetic properties of the fabric, that is, drape, lustre, colour, crease, pilling, staining, etc., are not our concern for the padding application. Figure 2 lists the important physical and physiological factors affecting padding comfort. Among all comfort characteristics, the most important factor is the movement of heat and moisture (liquid and vapour) through padding to maintain the thermal equilibrium between human body and the environment.

3.2. Material and structure

Nonwoven used for padding is developed either via needle-punching or thermal-bonding process. Needle-punched technology is where the entanglement of fibres is achieved via mechanical punching using needle beds. In thermal-bonding process, heat is used for the bonding of fibrous web. The fibres used for nonwoven padding is either single-component fibres (polyester, polypropylene, viscose, or cotton) or blend of fibres (polyester/viscose, polyolefin/viscose or polyester/cotton) in the structure [29]. In addition to nonwoven structure, the foam materials are also used as padding. The material used for foam padding is polyurethane and the common structure is open cell foam. Polyurethane foam materials have the advantage of not adhering to the wound or surrounding skin, which makes them attractive when treating fragile skin often found in the elderly [34]. Also these polyurethane materials absorb wound drainage four times more than hydrocolloid dressings of similar sizes. Foam

dressings are usually supplied as square pads of different sizes with steep edges. Hybrid structure can also be used as padding [30]. Laminating foams on the woven or knitted structure are being commercially used. Also, the combination of nonwoven and open cell elastic foam is also found where the foam is laminated on the filament-reinforced nonwoven.

3.3. Ideal padding

Several requirements must be met before considering a nonwoven as an ideal padding bandage. Some of critical needs are [6]:

- It should be light weight and easy to handle. Since multi-layer compression system has multiple layers, the overall system seems bulky and heavy to the patient. A light padding will not add too much weight and therefore is recommended for the therapy.
- It should be soft and impart cushioning effect to the limb. As the padding is in direct contact with the skin, so a soft padding will provide better sensorial or tactile comfort.
- It should be capable of distributing pressure at critical regions especially over bony prominence. This is important to prevent tissue damage.
- It should have good fluid absorptions and wicking properties. To tackle excess sweating or exudates, the padding should be able to transport these fluids to wider areas for faster evaporation.
- It should not produce irritation or any allergic reaction to the skin on prolonged contact.
- It should be cheap and easily available.
- It should tear easily by hand. The limb shape or size for different patients is different and therefore there are different requirements for the lengths and thicknesses of padding. Padding with high tearing strength will add more difficulties to nurses or health practitioners during wrapping.
- It should not be very stiff and should be easily conformable with the contour of the limb.

4. Measurement techniques

4.1. Pressure sensor/compression-recovery test

The measurement of interface pressure exerted by a compression device is of importance, for both efficacy and tolerability. Several instruments are available that can be used for pressure measurement directly on the leg. Most of them are air-filled devices such as Kikuhime[®] (Meditrade, Soro, Denmark; Figure 3a), SiGaT-tester[®] (Ganzoni-Sigvaris, St. Gallen, Switzerland), and Picopress[®] (Microlab, Padua, Italy) [35]. They are inexpensive, thin, flexible, adjustable and optimised for different applications and different measuring regimes. Picopress[®] and SiGaT-tester[®] allow continuous recording during dynamic tests and over longer time periods. Although direct pressure measurement on the limb is more relevant, there exist

several limitations of using *in vivo* measurement techniques. Especially, when comparing different padding performance on a leg, there exist unavoidable variation in application techniques and varying limb movement. Moreover, the location of pressure sensor at the critical sites especially over bony prominence is highly unstable, which may cause unnecessary noise or experimental error. The above facts indicate the need for a simple or alternative method to obtain pressure absorption ability of padding.

Compression load-recovery test is common to obtain the energy absorption ability of a nonwoven material. An Essediel thickness tester was used for measuring compression characteristics of textile materials (Figure 3b). The specimen was placed on a flat surface, and the transverse weight was applied using a pressure foot (20 mm diameter). The compressive pressure was increased from 20 to 200 kPa by applying additional dead weights during the compression cycle, and similarly in recovery the pressure was decreased in steps. The thicknesses were measured at different compressive loads during compression and recovery cycles. The initial thickness T_0 was taken for the initial pressure P_0 (~2 kPa), which was due to weight of the pressure foot without any applied external load. The works done during compression and recovery process can be obtained from the plot of thickness versus compressive pressure (Figure 6). These calculated energies can be further used to characterise padding performance as discussed in detail in the next section.

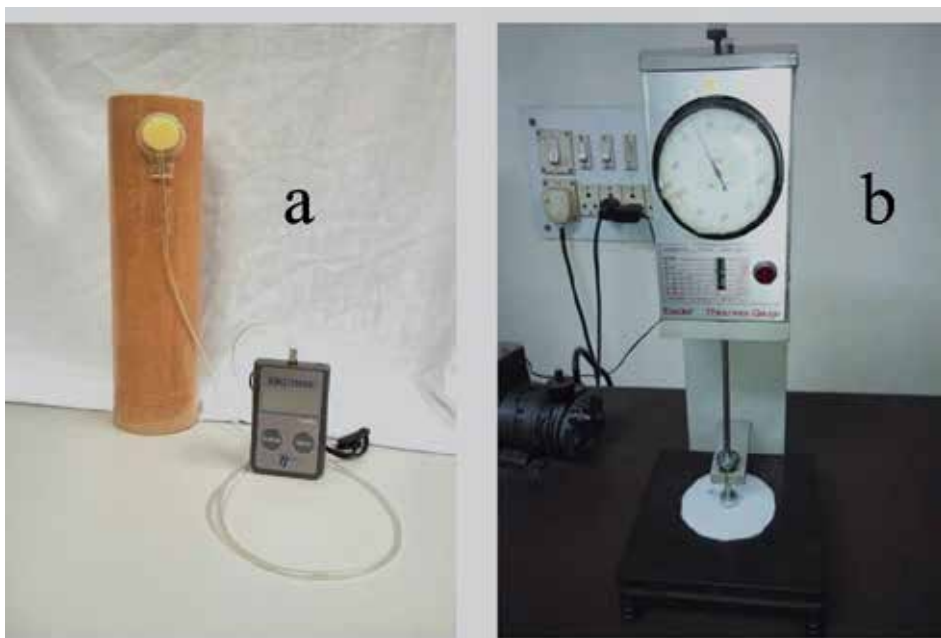


Figure 3. a) A simple prototype for the pressure measurement using Kikuhime® pressure sensor; b) An Essediel thickness tester for compression-recovery test

4.2. Comfort characterizations

Thermo-physiological wear comfort and skin sensational wear comfort are two main aspects of wear comfort of any clothing [31]. The first one concerns the heat and moisture transport properties of the fabric, while the latter one deals with the mechanical contact of the fabric with the skin, its softness and pliability in movement and its lack of prickle, irritation and cling when damp. The main properties of the fabric that influences the thermal comfort are: air permeability, water or moisture vapour permeability/transportation and heat transmission [36]. Air permeability is a measure of how well a fabric allows the passage of air through it. It is expressed as the volume of air (in cc) that passes in 1 s through 1 cm² of fabric under a pressure head of 1 cm of water. Figure 4a shows the photograph of a TEXTEST Air Permeability Tester (FX3300) to measure the air permeability at a standard atmosphere of 98 Pa. Similar to air permeability, the moisture vapour transmission indicates the breathability of the textile to allow water vapour to pass out from the skin surface through the textile. This is expressed as the steady water vapour flow in unit time through unit area of body, normal to specific parallel surfaces, under specific conditions of temperature and humidity at each surface. Figure 4b shows a Moisture Vapour Transmission Tester (Model CS-141), which offers an easy and fast method to obtain the moisture vapour transmission rate. Thermal comfort is related to the fabric's ability to maintain skin temperature and allow transfer of perspiration produced from the body. For the evaluation of thermal comfort, a very simple instrument Alambeta (Sensora) is available, which can measure thermal characteristics of textile such as thermal resistance, thermal conductivity and thermal absorptivity (Figure 4c).



Figure 4. (a) TEXTEST air permeability tester; b) moisture vapour transmission tester (Model CS-141); c) Alambeta (Sensora) for heat transmission

Apart from the above-mentioned comfort properties, liquid transport behaviour of padding is also critical. This helps in removing body fluids or exudates from the wounded portion to prevent excess moisture build-up that causes irritation or discomfort to the wearer. The measurement of fluid transport is essential to understand how padding behaves on interaction with the fluids and what should be ideal structure for the nonwoven to obtain more spreading of body fluids to promote faster evaporation or removal. Several vertical and in-plane wicking tester are available that can be used for easy assessment [37-41]. Vertical wicking is determined

by measuring the wicking height against gravity for a hanging fabric. An in-plane wicking deals with the transport behaviour in the horizontal plane of the fabric and describes several useful parameters such as the liquid flow anisotropy, the rate of movement, and the area of wet surface with time. Figure 5 shows the photograph of the computerized wicking tester for in-plane transport measurement [41].



Figure 5. Photograph of the instrumental set-up for measuring in-plane wicking

5. Theoretical insights into padding behaviour

5.1. Modelling of pressure loss

The magnitude of final pressure that appears on the surface of skin is more relevant in the compression treatment. Compression bandage applies a total pressure on the surface of padding which causes a pressure loss. This pressure loss is attributed to the significant changes in structure of the padding during compression, which results in its permanent thickness reduction, and significant energy loss. The absorbed energy by the padding during compressive load could be a good indicator of the pressure loss or absorption during the use of padding beneath compression bandage. The thickness change during compression-load-recovery test is used to obtain this energy loss or absorption in the nonwoven structure. The thickness changes in loading can be expressed as [42, 43]:

$$\frac{T}{T_0} = 1 - \alpha \ln\left(\frac{P}{P_0}\right) \quad (2)$$

where T is the thickness at arbitrary pressure P , T_0 is the initial thickness at pressure P_0 and α is the compressibility parameter. After loading to final pressure P_f , the thickness of the sample reduces to a lowest thickness T_f . During recovery case, the thickness T at arbitrary lower pressure $P (<P_f)$ can be expressed as:

$$\frac{T}{T_f} = \left(\frac{P}{P_f}\right)^{-\beta} \quad (3)$$

where β is the recovery parameter. Both α and β are dimensionless constants that could be easily obtained by a simple load-recovery test. Using these parameters, it is possible to characterise the compressional and recovery behaviour of different types of nonwoven fabrics. Figure 6 shows a typical thickness-pressure curve for a nonwoven fabric during loading and unloading. The shaded area under load and recovery curve represents the energy loss during a cycle. The work done during compression (E_c) can be obtained using Eq. (2) as:

$$E_c = \int_{T_0}^{T_f} PAdT = P_0A \int_{T_0}^{T_f} e^{\alpha\left(1-\frac{T}{T_0}\right)} dT \quad (4)$$

where A is the area of specimen; T_0 and T_f are initial and final thicknesses, respectively; and P_0 is the initial pressure. The potential energy recovered during release of load (E_r) taking into account Eq. (3), is given by:

$$E_r = \int_{T_f}^{T_r} PAdT = P_0A \int_{T_f}^{T_r} \left(\frac{T}{T_0}\right)^{\frac{-1}{\beta}} dT \quad (5)$$

where T_r is the recovered thickness after load removal. Using these potential energies (E_r and E_c), it is possible to calculate the energy loss (EL) of the fabric during the compression recovery cycle:

$$EL = \frac{E_c - E_r}{E_c} \quad (6)$$

The lower the value of EL (energy loss), the poorer is the performance of padding in energy absorbance. Padding bandage lies underneath the compression bandage that applies signifi-

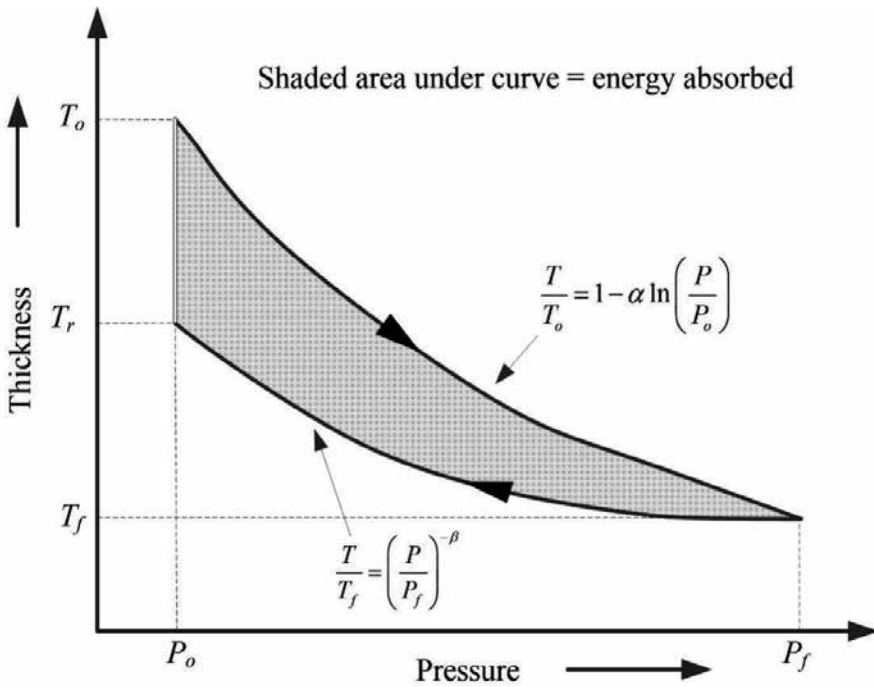


Figure 6. A typical curve of pressure-thickness data for a nonwoven

cant amount of interface pressure in the range from 10 to 50 mmHg, depending on severity of venous disease. The applied pressure by the compression bandage on the padding has two components: first, the pressure that is transferred through padding and finally appears on the skin; second, the pressure loss in the padding structure. This pressure loss can be related to the energy loss EL as described in Eq. (6). So, the pressure results can be expressed as:

$$P_f = P_T - P_l = P_T - f(EL) \times P_T = \frac{F}{r} (1 - f(EL)) \tag{7}$$

where, P_f is the final pressure on the surface of skin, F is the applied force to the compression bandage which generates total pressure P_T on the padding, r is the radius of the limb and P_l is the pressure loss that can be related to EL . Using a set of experimental results, one can easily obtain the function relating pressure loss and energy loss for a given padding sample. Once expressed, it would be easy to obtain the final pressure at any given applied force (F). The measurement of applied force is difficult to judge during wrapping but the applied extension ϵ is easy to measure. The applied force F is related to the extension applied in the compression bandage during wrapping:

$$F = \tau \times \epsilon \tag{8}$$

where τ is the tensile modulus of the compression bandage. So, using the experimental results of tensile test for the compression bandage and the load-recovery tests for padding bandage, it is possible to predict the pressure results of the multi-layer compression system. Both these experiments can be done in the laboratory and therefore provide a simple method to access multi-layer bandaging performance.

5.2. Understanding Liquid Transport

Liquid transport, that is, wicking, happens due to capillary action that occurs when the fibrous network is completely or partially immersed in a liquid or in contact with a limited amount of liquid from an infinite (unlimited) or limited (finite) reservoir [39]. During transport, the liquid in a nonwoven structure can transmit through the thickness of the sample, that is, transverse wicking, or it can move along the plane of the fabric, that is, longitudinal or in-plane wicking [39, 44-46]. The thickness of padding is small as compared to other dimensions; and therefore, the liquid transmission in the plane of padding is more relevant for the present case. The basic theory in the field of non-homogeneous flows was proposed by Young and Laplace, which is related to the equation of capillarity as [44, 47]:

$$\Delta P = -\gamma \nabla \hat{n} \quad (9)$$

where ΔP is the pressure difference across the fluid interface, γ is the surface tension (or wall tension) and \hat{n} is the unit normal pointing out of the surface. This describes the capillary pressure difference sustained across a curved interface between two immiscible fluids, such as water and air, due to the phenomenon of surface or wall tension. Lucas and Washburn further extended their work on capillary-driven non-homogeneous flows, which has been frequently used in textile areas [45, 47-49]. The Lucas–Washburn theory relates the rate of fluid flow into a circular tube via capillary action. This theory is a special form of a laminar viscous flow of a Newtonian liquid in a cylindrical type as expressed by Hagen–Poiseuille law [50]:

$$\frac{dV}{dt} = \frac{\pi r^4 (p_a - p_b)}{8l\mu} \quad (10)$$

$\frac{dV}{dt}$ is the volume flow rate of the Newtonian fluid, $p_a - p_b$ is the pressure difference between the tube ends, r and L are the radius and length of the tube, respectively, and μ is the viscosity of the fluid. The structure of a nonwoven resulted in complex network of pores in a three-dimensional (3D) network. For simplification, a capillary or pore in the network is assumed as a cylindrical tube (radius r) in which the distance travelled by the liquid along the capillary axis is l (Figure 7a). The capillary pressure (P_a) and the hydrostatic pressure (P_b) can be expressed as:

$$p_a = \frac{2\gamma \cos \theta}{r} \tag{11}$$

$$p_b = l\sigma g \cos \beta \tag{12}$$

where θ is the contact angle between the liquid surface and the capillary wall and β denotes the angle between the tube and the vertical axis (Figure 7a).

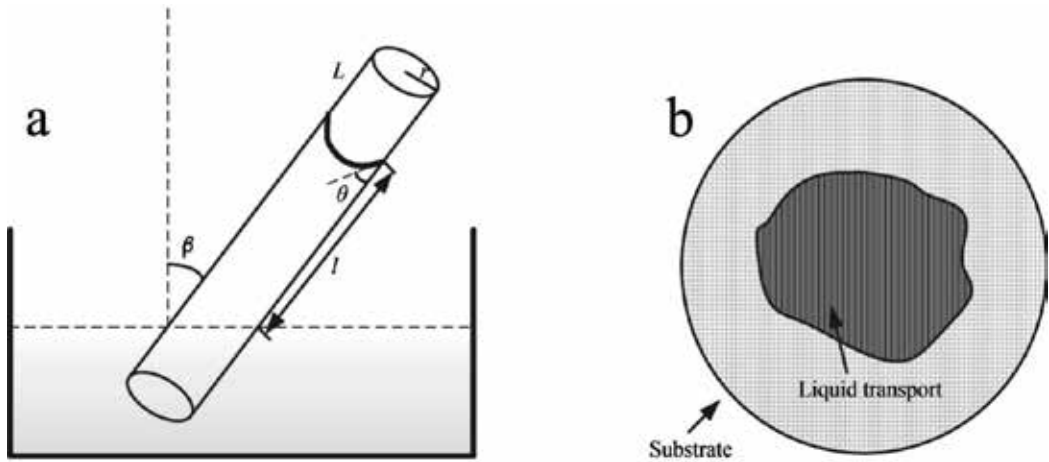


Figure 7. a) A tube (L) of a radius r is suspended in a liquid source. The distance travelled by the liquid along the capillary axis is l . (b) Liquid transport on the surface of a textile substrate

Substituting Eqs. (11) and (12) in Eq. (10) and expressing the volume V as $\pi r^2 l$, we can obtain the Lucas–Washburn equation to express the flow rate as:

$$\frac{dl}{dt} = \frac{r\gamma \cos \theta}{4\mu l} - \frac{r^2 \sigma g \cos \beta}{8\mu} \tag{13}$$

The parameters, r , γ , θ , μ , σ , g and β remain constant for a given system, so Eq. (5) can be simplified to:

$$\frac{dl}{dt} = \frac{a}{l} - b$$

where a and b are constants. When the penetration of liquid is horizontal ($\beta = 90^\circ$), the effects of the gravitation field are negligible and the acceleration g vanishes and therefore the second term (b) can be neglected. Finally, the wicking length (l) can be solved as [47, 48]:

$$l = (2at)^{1/2} \quad (14)$$

The above equation can be used for our case where the liquid from a point source is poured at the centre of a textile substrate and the spreading occurs radially outward in horizontal plane (Figure 7b).

6. Structure–property relationship

Although different nonwoven materials such as needle-punch, melt spun, thermal bonded, etc. are used as padding, this chapter focuses more on the needle-punch structures. A needle-punch structure is obtained from the entanglement of fibres which is achieved via mechanical punching using needle beds [3, 4]. The structure is decided by the fibres and the processing parameters, for example, fibre size and distribution, depth of needle penetration, amount of feed, layering factor, and needle punching frequency. As an example, the results of a set of nonwoven samples made from 100% polypropylene fibres are described. The varying parameters are the fibre linear density (expressed as denier @ weight of 9000 m length of fibre), mass per square meter (g/m^2) and needling density (punches/ m^2) of the nonwoven. Three levels of fibre denier (2.5, 6 and 15) are taken for comparison. The gram per unit area and needling density (punches/ m^2) of the nonwoven samples can be obtained by changing the machine parameters. The effect of different levels for the mass per square meter (100, 200, 300 and 400 g/m^2) and needling density (50E4, 130E4 and 210E4 punches/ m^2) is explained on the pressure and comfort performance of padding product.

6.1. Energy or pressure absorption

Energy or pressure absorbed (%) by padding decreases with increase in mass per unit area of padding (Figure 8a). This is due to the fact that the increase in mass per unit area leads to availability of more number of fibres for sharing the compressive load. Availability of more fibres increases entanglement during preparatory methods, and this causes more frictional resistance to prevent fibre-to-fibre slippage during compression load-recovery test. Reduction of fibre slippages minimizes the permanent deformation in compression-load recovery test. Therefore, lower energy absorption is obtained for higher mass per unit area of padding. Furthermore, the amount of energy loss decreases with increasing needling density (Figure 8b). Increase in needling density also stimulates more entanglement of fibres, which causes the compact and stiff structure of padding [42, 43]. This avoids fibre-to-fibre slippages during compression; hence, there will be low energy or pressure absorption for a stiff padding compared to soft padding. In real scenario, the use of a heavy and stiff padding should be avoided as it would not be able to absorb the excess pressure at critical regions. If comparing different fibres, it can be concluded that the energy absorbed is less for padding composed of thinner fibre than coarser fibre (Figure 8c). Thick or coarse fibre has less specific area compared to thin fibre, due to which the frictional resistance within the porous network of padding will

be lesser for thick fibre compared to thin fibre. Moreover, padding made from coarser fibre has more porous structure. This all results in more energy absorption and therefore more pressure reduction for the padding made from higher fibre linear density compared to lower fibre linear density.

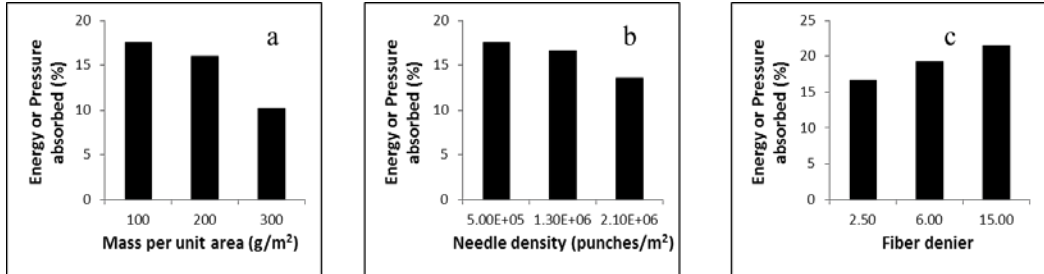


Figure 8. Effect of structural parameters of nonwoven on pressure absorbency: (a) effect of mass per unit area (50E4 punches/m²; 2.5 denier); (b) effect of needling density (100 g/m²; 2.5 denier); (c) effect of fibre denier (100g/m²; 130E4 punches/m²)

6.2. Thermo-physiological comfort

The effect of structural parameters is same on the air permeability and moisture vapour transmission rate (MVTR). Air permeability and MVTR decreases with increasing the level of both mass per unit area and needle density (Figures 9a, 9b, 10a & 10b). This is due to decrease in size of the air-conducting channels during more punching process and also due to availability of more fibres for the entanglement, which decreases the permeability of the air or moisture to the padding. The effect is opposite for the fibre denier where both increase with increase in the fibre denier (Figure 9c & 10c). The density of the padding bandages decreases with increase in fibre denier due to which there is increase in the size of the air channels which provide easy air or moisture flow.

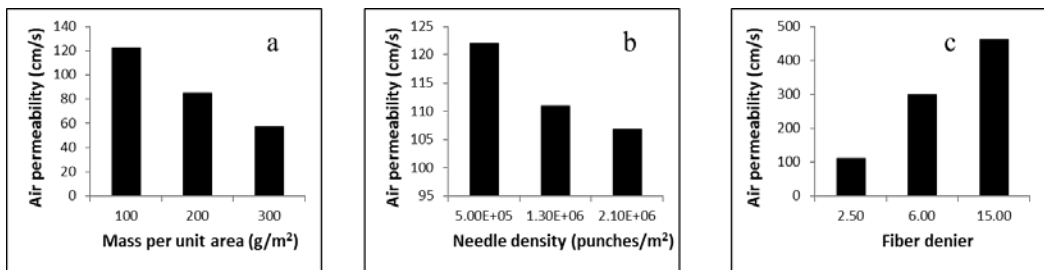


Figure 9. Effect of structural parameters of nonwoven on air permeability: (a) effect of mass per unit area (50E4 punches/m²; 2.5 denier); (b) effect of needling density (100 g/m²; 2.5 denier); (c) effect of fibre denier (100g/m²; 130E4 punches/m²)

For thermal results, the thermal resistance increases with increase in mass per unit area for same level of needling density (Figure 11a). This is because thickness of samples increases with

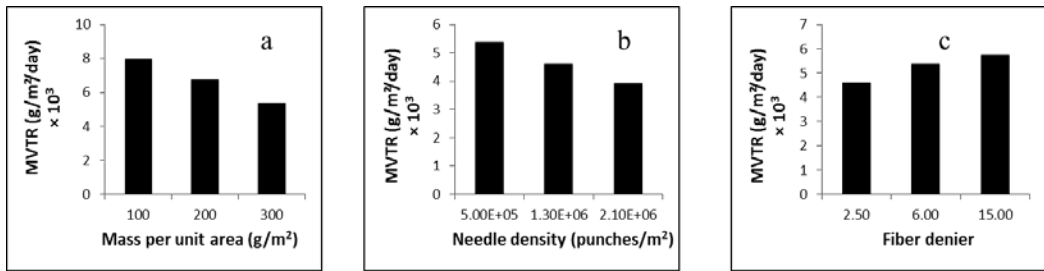


Figure 10. Effect of structural parameters of nonwoven on moisture vapour transmission rate (MVTR): (a) effect of mass per unit area (130E4 punches/m²; 6 denier); (b) effect of needling density (300 g/m²; 2.5 denier); (c) effect of fibre denier (300g/m²; 130E4 punches/m²)

increase in mass per unit area. Also the thermal resistance of padding decreases with increase in needling density (Figure 11b). For the liquid transport (Figure 7b), the spreading time is lower for the samples having more free spaces in the capillary network. Increasing mass per unit area and needling density reduces the porosity, and stimulates lower rate for fluid transport and takes more time (Figure 12a & 12b). Nonwoven made from coarser fibres results in larger capillaries and shows faster spreading rate and takes lower time (Figure 12c).

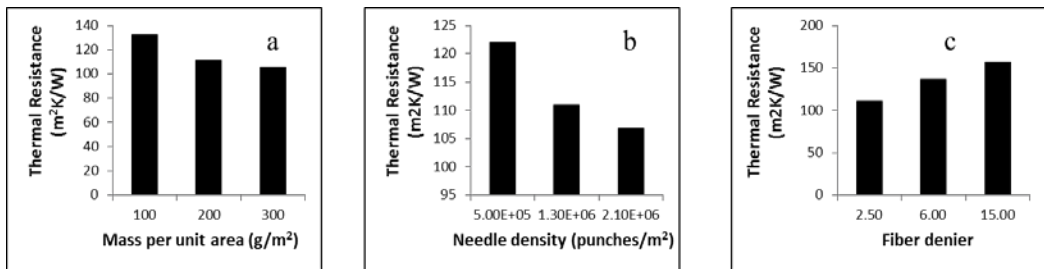


Figure 11. Effect of structural parameters of nonwoven on thermal resistance: (a) effect of mass per unit area (50E4 punches/m²; 2.5 denier); (b) effect of needling density (100 g/m²; 2.5 denier); (c) effect of fibre denier (100g/m²; 130E4 punches/m²)

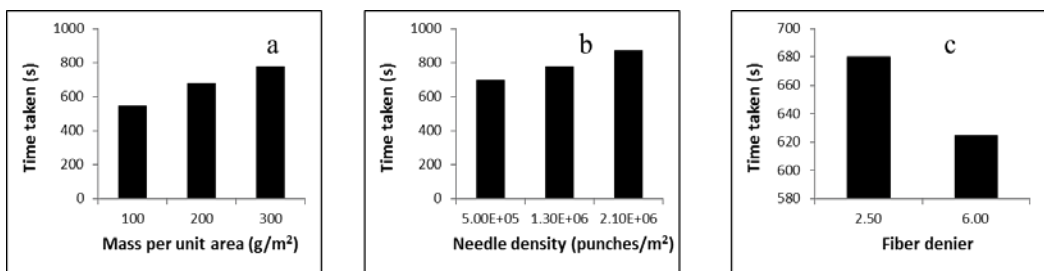


Figure 12. Effect of structural parameters of nonwoven on liquid transport (time taken represents the total period taken by liquid to cover an area 380 cm² of a circular specimen as shown in Figure 7b): (a) effect of mass per unit area (1300E4 punches/m²; 2.5 denier); (b) effect of needling density (300 g/m²; 2.5 denier); (c) effect of fibre denier (200g/m²; 130E4 punches/m²)

6.3. Design consideration

Several inferences can be drawn based on the above results of needle-punched padding:

- Padding materials should be made as isotropic as possible, for any anisotropy will lead to behaviour variations at different directions, thus causing non-uniform pressure performance and less effective fluid absorption or transmission properties in certain directions.
- It is recommended that padding with more porosity and larger pore size could help in better management of liquid exudates, air or moisture exchange. To achieve that the mass per unit area and needling density of the nonwoven has to be decreased which results in more porosity. This will accelerate the evaporation and thereby prevent excess moisture build-up. Moreover, fibres with higher linear density should be selected for the preparation of padding to get bigger pore size that is more suitable for faster spreading.
- In general practice, a heavier or thicker padding is recommended in order to obtain maximum pressure reduction especially at critical regions over bony prominences such as tibia or fibula. However, a heavier padding will be more obstructive in liquid flow. So, a balance should be made to get optimum pressure performance with good transport/transmission characteristics.

All the above points should be taken into consideration to design or develop suitable padding structure for maximum performance.

7. Future study

Padding is critical in compression management; it serves several functions including pressure or comfort management. Padding can have different fibrous materials or structure due to which it can have different mechanical responses while it is being used. Understanding of all these parameters is essential to have improved understanding of the role of textile material or structure for the designing or engineering of optimised products. This chapter introduces the structure–property relationship of nonwoven padding. However, there exist several gaps in the literature which should be systematically examined for further improvement. Some future outlooks could be as follows:

1. All the above description is based on the single padding layer. However, the padding is just one of the parts of the multi-layer compression system. The system has multiple layers of different fabrics once wrapped over the limb. These include cohesive, padding, compression and wound layers. Each of these layers performs a different role or function. The performance of overall assemblies should also be assessed for better judgement.
2. Padding bandage lies underneath the bandage that applies significant amount of interface pressure in the range from 10 to 50 mmHg to the leg. Under external compression, the porosity or indeed the wicking performance of the padding will change significantly; so it is expected that the liquid transport or other transmission behaviour of the same padding material will vary when exposed to different levels of normal compression.

Clearly, the effect of the external pressure has to be accounted for in future analysis. Also the model for fluid transport should be modified accordingly to account for porosity change due to external pressure.

3. This chapter focuses more on the performance of only needle-punched samples. Study should be conducted for other nonwovens such as thermal-bonded and melt-spun. The performance of other fibres such as PET, cotton, wool and viscose should also be examined.
4. The patients using compression treatment can have dynamic or static nature. Especially old patients prefer to sit for longer period of time, and the limb is therefore under static state. On the other hand, there may be some group of patients who are still active or working even under compression treatment. Under such circumstances, the limbs can undergo active movement. The assessment of padding should be done for both static and dynamic cases.
5. Although the present study is based on lab-based measurement, it may be possible to have different results once used on the real leg. More sophisticated approaches are needed to do an *in vivo* study to compare it with *in vitro* results.
6. Textiles give us a lot of flexibility in choosing an appropriate structure or weave for a particular application. Although the nonwoven is primarily used in the padding for so long, but there is still possibility to look for other textile structure. The spacer fabric (3D warp knitted structure) could have more potential in compression and comfort outcomes. The comparisons of the nonwoven with other textile structures should also be examined.
7. Compression system is usually worn for an extended period of time. This chapter only reveals the immediate response of the padding. Further study should be conducted on evaluating the time dependence performance.

8. Summary

This chapter introduces the basics of a medical problem related to venous disorders and related compression modalities. The need and role of different fibrous materials in compression management are presented. More focus is given in describing the critical functions of the padding. Padding is used for the pressure redistribution on the limb. Furthermore, it helps to ensure proper comfort to the wearer due to proper management of heat, moisture, air, liquid, etc. Herein, the nonwoven paddings have been evaluated for the compression and different comfort properties including air permeability, moisture transmission, heat flow and liquid transport. The importance of different nonwovens and their structures are reviewed, which could affect padding performance. Based on the observed results, it has been recommended that padding with more porosity and larger pore size results in more pressure absorption and good transmission (air/moisture/liquid). Padding with low mass per unit area and needling density results in more porosity and therefore can help in faster transport of fluids, air or moisture to a larger area. Moreover, fibres with higher linear density should be selected for

the preparation of padding to get bigger pore size, which is more suitable for faster transmission and more pressure absorption. This can further help in deciding the optimum structure or material for an ideal product. Some useful theoretical insights are also provided to relate the structure–property relationship to access different padding performance using model parameters. In conclusion, this chapter could serve as a complete package to readers regarding nonwoven product development and optimization. Some future goals are also listed, demanding more innovative solutions or approaches to overcome the limitations of the existing problems, and exploiting the existing features and capacity of nonwoven padding.

Author details

Bipin Kumar*

Address all correspondence to: bipiniitd18@gmail.com

Division of Textiles, Biological & Agricultural Engineering, The University of California at Davis, USA

References

- [1] Rupp, J., Nonwovens: Challenges & trends, environmental factors. *Textile World*, 2009. 159(6): p. 34-6.
- [2] Russell, S., *Handbook of nonwovens*. 2006, Cambridge, England: Woodhead Publishing Ltd., p. 1-15
- [3] Banerjee, P.K., *Principles of Fabric Formation*. 2015, Boca Raton, FL 33487-2742: CRC press, p. 9-19
- [4] Batra, S.K. and B. Pourdeyhimi, *Introduction to Nonwovens Technology*. 2012, Lancaster, Pennsylvania 17602 USA: DEStech Publications, Inc., p. 3-11
- [5] Rajendran, S. and S. Anand, Developments in medical textiles. *Textile Progress*, 2002. 32(4): p. 1-42.
- [6] Anand, S.C., et al., *Medical and Healthcare Textiles*. 2010: Elsevier, p. 257-262
- [7] Partsch, H., Compression therapy in leg ulcers. *Rev Vasc Med*, 2013. 1(1): p. 9-14.
- [8] Kumar, B., A. Das, and R. Alagirusamy, Effect of material and structure of compression bandage on interface pressure variation over time. *Phlebology*, 2013. 29(6): p. 376-385.
- [9] Reich-Schupke, S., et al., Quality of life and patients' view of compression therapy. *Int Angiol*, 2009. 28(5): p. 385-93.

- [10] Evans, C.J., et al., Prevalence of varicose veins and chronic venous insufficiency in men and women in the general population: Edinburgh Vein Study. *J Epidemiol Comm Health*, 1999. 53(3): p. 149-153.
- [11] Patel, N.P., N. Labropoulos, and P.J. Pappas, Current management of venous ulceration. *Plast Reconstruct Surg*, 2006. 117(7): p. 254s-260s.
- [12] Bergan, J.J., et al., Mechanisms of disease: Chronic venous disease. *N Eng J Med*, 2006. 355(5): p. 488-498.
- [13] Partsch, H., Compression therapy for deep vein thrombosis. *Vasa-Eur J Vasc Med*, 2014. 43(5): p. 305-307.
- [14] Dennis, M., et al., Effectiveness of thigh-length graduated compression stockings to reduce the risk of deep vein thrombosis after stroke (CLOTS trial 1): a multicentre, randomised controlled trial. *Lancet*, 2009. 373(9679): p. 1958-65.
- [15] Kumar, B., A. Das, and R. Alagirusamy, An approach to determine pressure profile generated by compression bandage using quasi-linear viscoelastic model. *J Biomech Engin-Trans Asme*, 2012. 134(9).
- [16] Kumar, B., A. Das, and R. Alagirusamy, Prediction of internal pressure profile of compression bandages using stress relaxation parameters. *Biorheology*, 2012. 49(1): p. 1-13.
- [17] Kumar, B., A. Das, and R. Alagirusamy, Study on interface pressure generated by a bandage using in vitro pressure measurement system. *J Textile Instit*, 2013. 104(12): p. 1374-1383.
- [18] Kumar, B., A. Das, and R. Alagirusamy, *Science of Compression Bandages*. 2014: WPI India, p. 41-55
- [19] Hafner, J., et al., Instruction of compression therapy by means of interface pressure measurement. *Dermatol Surg*, 2000. 26(5): p. 481-486.
- [20] Partsch, H., Compression for the management of venous leg ulcers: which material do we have? *Phlebology*, 2014. 29: p. 140-145.
- [21] Thomas, S., The production and measurement of sub-bandage pressure: Laplace's Law revisited. *J Wound Care*, 2014. 23(5): p. 234-246.
- [22] Zarchi, K. and G.B.E. Jemec, Delivery of compression therapy for venous leg ulcers. *Jama Dermatol*, 2014. 150(7): p. 730-736.
- [23] Kumar, B., A. Das, and R. Alagirusamy, *An approach to examine dynamic behavior of medical compression bandage*. *J Textile Instit*, 2013. 104(5): p. 521-529.
- [24] Kumar, B., A. Das, and R. Alagirusamy, Analysis of factors governing dynamic stiffness index of medical compression bandages. *Biorheology*, 2012. 49(5-6): p. 375-384.

- [25] Kumar, B., A. Das, and R. Alagirusamy, *Analysis of sub-bandage pressure of compression bandages during exercise. J Tissue Viability*, 2012. 21(4): p. 115-124.
- [26] Das, A., et al., Pressure profiling of compression bandages by a computerized instrument. *Ind J Fibre Textile Res*, 2012. 37(2): p. 114-119.
- [27] Basford, J.R., The Law of Laplace and its relevance to contemporary medicine and rehabilitation. *Arch Phys Med Rehabil*, 2002. 83(8): p. 1165-70.
- [28] Mosti, G. and H. Partsch, High compression pressure over the calf is more effective than graduated compression in enhancing venous pump function. *Eur J Vasc Endovasc Surg*, 2012. 44(3): p. 332-336.
- [29] Rajendran, S. and S.C. Anand, Contribution of textiles to medical and healthcare products and developing innovative medical devices. *Ind J Fibre Textile Res*, 2006. 31(1): p. 215-229.
- [30] Fauland, G., et al., Assessment of moisture management performance of multilayer compression bandages. *Textile Res J*, 2012. 83(8): p. 871-880.
- [31] Das, A. and R. Alagirusamy, *Science in Clothing Comfort*. 2010: Woodhead Publishing India Pvt Ltd, p 17-39
- [32] Kumar, B., A. Das, and P.A. Singh, Studies on elastane-cotton core-spun stretch yarns and fabrics: Part III-Comfort characteristics. *Ind J Fibre Textile Res*, 2014. 39(3): p. 282-288.
- [33] Cutting, K.F. and R.J. White, Avoidance and management of peri-wound maceration of the skin. *Prof Nurse*, 2002. 18(1): p. 33, 35-36.
- [34] Al-Muhairi, A. and T. Phillips, Surgical pearl: A wound dressing tip for venous ulcers. *Wounds Compend Clin Res Pract*, 2006. 18(6): p. 158-161.
- [35] Partsch, H. and G. Mosti, Comparison of three portable instruments to measure compression pressure. *Int Angiol: J Int Union Angiol*, 2010. 29(5): p. 426-430.
- [36] Das, A., V.K. Kothari, and A. Sadachar, Comfort characteristics of fabrics made of compact yarns. *Fibers Polym*, 2007. 8(1): p. 116-122.
- [37] Kumar, B. and A. Das, Vertical wicking behavior of knitted fabrics. *Fibers Polym*, 2014.
- [38] Raja, D., et al., Comparison of different methods to measure the transverse wicking behaviour of fabrics. *J Indus Textiles*, 2014. 43(3): p. 366-382.
- [39] Kumar, B., et al., Characterization of liquid transport in needle-punched nonwovens. I. Wicking under infinite liquid reservoir. *Fibers Polym*, 2014. 15(12): p. 2665-2670.
- [40] Kumar, B. and A. Das, Vertical wicking behavior of knitted fabrics. *Fibers Polym*, 2014. 15(3): p. 625-631.

- [41] Kumar, B. and A. Das, Design and development of a Computerized Wicking Tester for longitudinal wicking in fibrous assemblies. *J Textile Instit*, 2014. 105(8): p. 850-859.
- [42] Kothari, V.K. and A. Das, Compressional behavior of layered needle-punched nonwoven geotextiles. *Geotext Geomemb*, 1993. 12(2): p. 179-191.
- [43] Kothari, V.K. and A. Das, Compressional behavior of nonwoven geotextiles. *Geotext Geomemb*, 1992. 11(3): p. 235-253.
- [44] Kissa, E., Wetting and wicking. *Textile Res J*, 1996. 66(10): p. 660-668.
- [45] Pan, N. and W. Zhong, Fluid Transport Phenomena in Fibrous Materials. *Textile Progress*, 2006. 38(2): p. 1-93.
- [46] Patnaik, A., et al., Wetting and Wicking in Fibrous Materials. *Textile Progress*, 2006. 38(1): p. 1-105.
- [47] Mhetre, S. and R. Parachuru, The effect of fabric structure and yarn-to-yarn liquid migration on liquid transport in fabrics. *J Textile Instit*, 2010. 101(7): p. 621-626.
- [48] Lukas, D., et al., Computer simulation of 3-D liquid transport in fibrous materials. *Simulat-Transact Soc Modeling Simulat Int*, 2004. 80(11): p. 547-557.
- [49] Zhu, L., et al., Static and dynamic aspects of liquid capillary flow in thermally bonded polyester nonwoven fabrics. *J Adhesion Sci Technol*, 2008. 22(7): p. 745-760.
- [50] Landau, L.D. and E.M. Lifshitz, *Fluid Mechanics*, Second Edition: Volume 6 (Course of Theoretical Physics S). 1987, Moscow: Nauka, p. 47-98.

Non-Woven Textiles in the Indoor Environment

Radostina A. Angelova

Additional information is available at the end of the chapter

<http://dx.doi.org/10.5772/61324>

Abstract

The chapter presents the basic metrics of the indoor environment that are used to assess the quality of living and working, together with the risk factors and pollutants indoors. From this point of view the non-woven textiles are presented and discussed. Different groups of non-woven materials are considered: floor coverings, wallcoverings, upholstery and furniture textiles, filters of the HVAC systems, etc. Their particular application on the indoor environment is presented and their effect on the metrics of the Indoor Environmental Quality (IEQ) is analyzed.

Keywords: Non-woven, indoor environment, textiles, indoor environmental quality

1. Introduction

Nowadays, people in urban areas spend more than 90% of their life in enclosures – homes, offices, public buildings, and means of transport [1, 2]. Therefore, the Indoor Environmental Quality (IEQ) is of a particular importance for people's comfort, health, and productivity.

Textiles are part of every indoor environment and influence its basic metrics. Textiles and clothing are an excellent tool to maximize comfort and personification of the working and living environment. Textiles affect the comfort of people in the indoor environment as [3]:

- *A direct insulation layer* between the human body and the indoor environment: clothing, bedding, textiles for furniture
- *An indirect insulation layer* between the human body and the indoor environment: floor coverings, wall coverings, curtains, etc.

Unlike clothing that can be changed, and linen, which is easy to replace, the other textile items in the indoor environment are relatively constant and their correct selection is essential for IEQ.

Non-woven textiles are an important part of textiles in the indoor environment. Different groups of non-woven materials can be found in buildings and means of transport: floor coverings, wallcoverings, upholstery and furniture textiles, filters, etc. Depending on their application, they can be classified as:

- *Hidden non-woven textiles* as part of clothing, bedding, furniture, and heating, ventilation, and air-conditioning (HVAC) systems;
- *Visible non-woven textiles* as part of floor coverings, wallcoverings, and furniture systems.

The purpose of the chapter is to discuss the application of non-wovens indoors from the point of view of the basic metrics of the indoor environment used to assess the quality of living and working. Different types of applications are considered: non-woven textiles, used as floor coverings, bedding, furniture, wallcoverings, walls, and curtains, as well as non-woven textiles, applied in cars. The influence of the non-woven materials on Indoor Air Quality (IAQ), Indoor Thermal Quality (ITQ), Indoor Lighting Quality (ILQ), Indoor Sound Quality (ISQ), Indoor Odor Quality (IOQ), and Indoor Vibration Quality (IVQ) is presented. The risk factors, related with the use of non-wovens indoors and their possible role as sources of pollutants are also detailed.

2. Indoor environment

2.1. Basic metrics of the indoor environment

Indoor Environmental Quality (IEQ) is a complex term in the field of indoor climate engineering, which reflects the combined impact of the different characteristics of the indoor environment on the basic senses of the human body. Figure 1 summarizes the basic metrics of the IEQ: Indoor Air Quality (IAQ), Indoor Thermal Quality (ITQ), Indoor Lighting Quality (ILQ), Indoor Sound Quality (ISQ), Indoor Odor Quality (IOQ), and Indoor Vibration Quality (IVQ). Textile and particularly non-woven textiles may contribute to all these characteristics of the indoor environment.

The review article [4] discusses the difficulty to assess which of the basic metrics and particular characteristics of the indoor environment plays the most important role for the quality of life and work of the inhabitants. The authors attribute that fact to concomitant problems of investigations cited in their work: problems with the studies' settings, the percentage of respondents, or the analysis of the data obtained.

A later study [5], however, has already reported such results. According to their analysis, the *five* main characteristics of the IEQ, which are important for the occupants (taken as absolute values of the regression coefficients for positive/negative effects) are:

- Amount of space
- Visual privacy



Figure 1. Basic metrics of the Indoor Environmental Quality (IEQ)

- Noise level
- Colors and textures
- Comfort of furnishing

The first two characteristics are related with the ergonomics of the working and living environment, but at the same time they influence basic metrics of the IEQ like Indoor Air Quality (IAQ). Noise level contributes to Indoor Sound Quality (ISQ). The last two characteristics are also related with the ergonomics, but at the same time they are relevant to Indoor Thermal Quality (ITQ), Indoor Lighting Quality (ILQ), and Indoor Sound Quality (ISQ).

Non-woven textiles in the indoor environment can contribute to the amount of space and visual privacy being used as freestanding constructions that divide the indoor space into smaller areas. Non-wovens, as all textile materials, decrease the noise in the built environment and car compartments. All visible non-woven textiles (floor coverings, wallcoverings, upholstery textiles, etc.) influence people's comfort through their colors and textures. At the same time, both visible and hidden non-woven textiles in furniture systems, car seats and compartments influence the comfort of people, which is related to furnishing convenience.

2.2. Human comfort in the indoor environment

Comfort is a relative and subjective category, but when it is associated with the interaction between the human body and textiles it can be considered as physical, physiological, and psychological comfort. Figure 2 summarizes the main factors related to textiles and clothing, which define human comfort in the indoor environment.

The *physical comfort* is largely a subjective factor: although influenced by receptors that are common to the human body, individuals have varying degrees of sensitivity. The physical

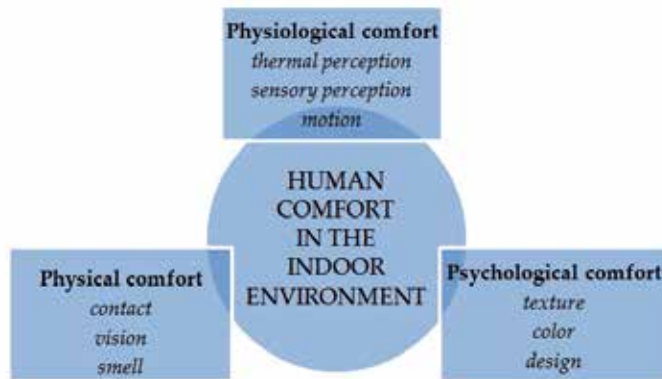


Figure 2. Factors that determine human comfort in the indoor environment, related to textiles and clothing

comfort is preconditioned by the contact between the human skin and the textiles, the presence of odors and the stimuli for the eyes. Ensuring physical comfort is a task of both the engineering aspect and the design aspect of the textiles production.

The *physiological comfort*, though again dependent on individual reactions and perceptions, is preconditioned to a high degree by the textiles design and engineering: from the selection of materials and structures, through their production and finishing, to their incorporation in the indoor environment as single items (floor covering, curtains) or parts of complex structures (bedding, furniture). It is predetermined mainly by the sensors for warmth/cold in the body, which are susceptible to thermal environment, presence of room airflow (draft), temperature asymmetry, etc.

The *psychological comfort* – not less subjective – depends largely on the textile design, fashion trends, and other factors, mainly related to art.

2.3. Risk factors in the indoor environment

The concept of Sick Building Syndrome (SBS) was developed in the 1970s. Nowadays, it is associated with the negative attributes of the Indoor Environmental Quality (IEQ). The SBS concept summarizes the dissatisfaction of the occupants from IEQ and series of clinical complaints, related to the stay of people in buildings. However, traditional clinical studies have not completely identified the causes of those complaints. Female subjects and elderly people are more sensitive to IEQ, but the mechanisms by which such sensitivity occurs, remain unspecified enough [6]. SBS is still a subject of clinical, chemical, and engineering studies; for the past decades, significant knowledge about the factors that determine SBS has been accumulated.

The main risk factors, related to indoor air quality (IAQ), which can provoke dissatisfaction among the inhabitants have been summarized in [7]. The results from that research are visually presented in Figure 3.

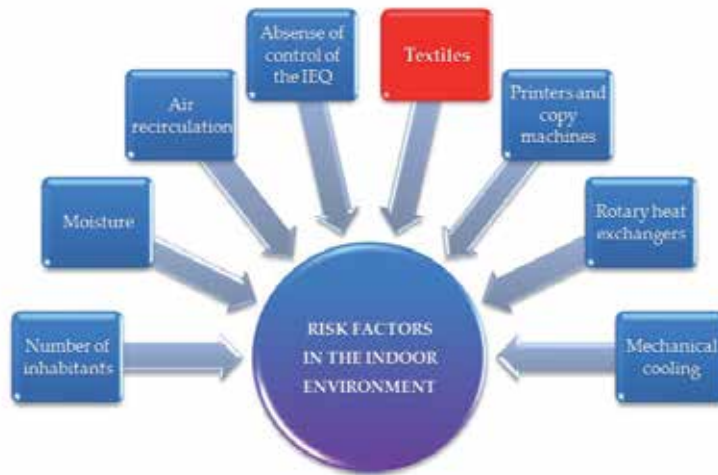


Figure 3. Risk factors for IAQ: summary of data from [7]

Textiles are among the risk factors for the quality of the indoor environment. Their influence on the IEQ is related with the ability of the textile surfaces to accumulate dust and odors, to emit dust and odors, to play the role of insulation layer thus affecting the thermal environment, to have influence upon the acoustics and lighting, etc. The type of the textiles macrostructure: woven, non-woven, or knitted, is also very important, as it determines the application of the particular textile in the indoor environment and its possible contribution to the IEQ.

2.4. Pollutants in the indoor environment

The up-to-date knowledge on the airborne pollutants in the indoor environment differentiates between the following pollutants of the indoor environment:

- Volatile Organic Compounds (VOCs)
- Microbial Volatile Organic Compounds (MVOCs)
- Particulate matter
- Inorganic compounds – CO₂, CO, O₃
- Semi-Volatile Organic Compounds (SVOCs)

Volatile Organic Compounds (VOCs) (formaldehyde, pesticides, ingredients of paints, dyes, etc.) are the most widely discussed pollutants that impair indoor air quality [7-9]. The highest levels of VOCs emissions indoors are measured immediately after building finishing or installation of furniture, flooring, etc. Due to their absorption ability textiles should not be installed in the indoor environment during the intensive release of VOCs from other items. The period of VOCs emissions can last from days to months, depending mainly on ventilation (natural or HVAC system), temperature, and humidity [10].

Semi-Volatile Organic Compounds (SVOCs) are associated with the presence of phthalates, pesticides, and flame retardants, which can be frequently found on textile surfaces in the indoor environment [11]. Microbial volatile organic compounds (MVOCs) are formed in the metabolism of fungi and bacteria [12]; therefore, they can be found in the indoor environment due to presence of moisture and mold growth.

A recent work [13] has summarized the state of the art in the field of the Very Volatile Organic Compounds (VVOCs) – an important subgroup of indoor pollutants that involves a wide spectrum of chemical substances. However, there is still no clear definition of VVOCs and techniques for their assessment.

3. Non-woven textiles in the indoor environment

Needle-punched non-woven textiles can be found as backing of carpets and wall coverings, and also as low-quality blankets, hidden layers in furniture systems, and wadding/padding. Spunlaced/hydroentangled non-woven materials are used in furnishing and bedding, as coverings and sheets. Spunbonded non-wovens are applied as a backing layer for wallcoverings, carpets, curtains, and furniture. They are also used as upholstery layers, filters, and tablecloths. Tablecloths are also made of wet-laid and spunlaced non-wovens. Chemically bonded non-woven textiles are applied as wadding and padding. The same is the application of the thermally bonded non-wovens, which are also applied in carpets underlying and furniture systems, including as upholstery textiles. The tufting technology is used for production of carpets for both built environment and car interiors.

Table 1 summarizes the main applications of different types of non-wovens in the indoor environment.

Several specific requirements have to be taken into account when designing non-wovens for application in the indoor environment. These requirements are related with both the product in question and its particular function: strength, dimensional stability, volume density, wear resistance, air-permeability, etc. There are other design considerations, however, related to the basic metrics of IEQ, which should be taken into account.

Non-wovens influence all basic metrics of IEQ. They may be used for sound control in residential and public buildings, or for glare reduction. As many textiles in public places, non-wovens are required to be flame-resistant. This additional treatment may be in a conflict with the demands for indoor air quality. The maintenance of the textiles surfaces is related to their ability to accumulate dust; therefore, the cleaning of the visible non-woven textiles in the indoor environment has to be easy. The last is also related with the products, as the cleaning agents themselves could frequently be sources of airborne pollutants.

Non-wovens have very good insulation abilities, used as floor coverings, wallcoverings, upholstery textiles (hidden layers or outer, visible layer), bedding, and they influence the indoor thermal quality. At the same time they can be a source of unpleasant odors, decreasing the indoor odor quality, especially in the case of floor coverings, including carpet backing. The

Nonwovens Indoors application	Needle punched	Spunlaced / Hydro- entangled	Spunbonded	Chemically bonded	Thermally bonded	Wet-laided	Tufted
Backing for wallcoverings		+	+				
Bedding coverings		+	+				
Bedsheets		+					
Blankets	+						
Carpet underlay/ backing	+		+		+		
Curtain backing			+				
Filters	+		+				
Floor covering	+						+
Furniture backing			+		+		
Tablecloths		+	+			+	
Upholstery	+	+	+		+		
Wadding and padding	+			+	+		

Table 1. Application of non-wovens in the indoor environment of buildings

sources of unpleasant odors could be either the non-woven item itself or the adhesive materials used for fixing the carpet to the floor.

4. Influence of the non-woven textiles on the indoor environmental quality

4.1. Non-woven textiles as floor coverings

Non-woven textiles, used as floor coverings in the indoor environment, increase the aesthetic comfort of the inhabitants. At the same time they influence thermal, acoustic, visual and odor environment, as well as indoor air quality.

Textile floor coverings have several advantages over other types of flooring (tiles, cement, wood, linoleum, bamboo, etc.) [9]. They increase the quality of the thermal environment; their insulation varies between 0.1 m²K/W and 0.3 m²K/W [14]. The insulation abilities are even better if a combination between hard flooring and textile floor covering is used.

Non-woven carpets influence the quality of the acoustic environment as they reduce noise levels indoors. They absorb the sound of steps and dropped objects and the absorption is higher when a pile carpet (tufted carpet) is used. At the same time, the quality of desired sound (music, speech) remains constant.

From economical point of view, the use of textile floor covering indoors can decrease or even eliminate the costs for sound and thermal insulating materials, especially in residential buildings.

Textile floor coverings do not reflect light; therefore, they can be used for glare reduction in the indoor environment, especially when hard flooring is also applied. The contact between sunlight and the textile fibers (mainly wool) leads to photobleaching effect, which requires additional treatment. However, all treatments of carpets, including those for stain blocking, fire resistance, moths blocking, etc., may affect negatively the indoor air quality (IAQ).

Several authors report and analyze the connection between IAQ and wall-to-wall non-woven carpets. Tufted carpets release Volatile Organic Compounds (VOCs) weeks after their installment in the indoor environment, due to the adhesives used for their fixation [15]. The cleaning of the near-wall zones is also very important, as they are a big source of airborne pollutants due to difficulty of access [16].

The surface pile of tufted carpets is indicated as a very important source of airborne pollutants in the indoor environment [15, 17-19]. The pile accumulates dust and particles, thus converting the tufted carpet into a "reservoir" for pollutants [9]. In addition, wool fibers can absorb formaldehyde, oxides of nitrogen and other toxic pollutants from the air [14]. Regular vacuum cleaning and wet extraction with cleaning products is a way of reducing the VOCs absorbed in the floor covering, but the cleaning products themselves are also a source of VOCs [9].

Tufted and needle-punched floor coverings can also be a source of VOCs and SVOCs in the indoor environment because of the backing. Tufted carpets need more complex finishing than woven carpets to obtain dimensional stability [20]. Synthetic latex is applied for backing of both needled and tufted floor coverings, which can be associated with airborne pollutants and unpleasant odors.

At the same time, Whitefoot [14] has reported the absence of scientific evidence that the removal of carpet alone has a proven effect on the health of the inhabitants. The author has discussed the advantage of pile carpets, including non-woven carpets, the surface of which can trap airborne pollutants and allergens, thus decreasing health problems related to allergy and asthma.

The study by Kidesø et al. [21] has concluded that heavy-weight needle-punched and tufted carpets from polypropylene and polyamide are particularly appropriate for residential buildings. The authors especially have underlined the requirement for smooth surface or surface with very low pile. The use of floor coverings with synthetic fibers, however, increases the risk of Microbial Volatile Organic Compounds (MVOCs) in the air. The higher humidity of the indoor air may provoke the development of mold and mildew; as a result, the carpet becomes a source of microbial airborne pollutants. Regular cleaning and use of antimicrobial

additives is a solution against MVOCs, especially in indoor environments with high traffic and high humidity [22]. At the same time, antimicrobial treatment (applied on the carpet fibers, the carpet backing, etc.) must exclude volatile organic chemicals (VOCs and SVOCs), toxins, allergens, carcinogens, and other substances that are dangerous for humans and animals [23].

4.2. Non-woven textiles as bedding

Bed linen and blankets are mainly related to two types of hazards in the internal environment: Microbial Volatile Organic Compounds (MVOCs) and particulate matter. In specific cases, Semi-Volatile Organic Compounds (SVOCs) can be also detected, usually for relatively short periods of time.

The main task of bedding in the indoor environment is to provide thermophysiological comfort for the person at rest [24]. Since at rest the human body produces minimal heat energy, higher requirements are demanded for the thermal insulation capacity of textiles for bedding [25]. Like the fabrics for clothing, textiles for bedding and blankets should absorb and transport water vapor emitted by the human body during rest and sleep. The role of bedding is critical for bedridden patients, adults with a high degree of immobility, and infants, because they spend a substantial part of their time in bed [26,27]. To avoid discomfort and getting bedsores, bedding items as material, structure, and finishing, should ensure the thermophysiological comfort by transferring air, heat, and moisture and not be a cause of allergic reactions.

Bed linen and blankets are serious battery of particulate matter. That, in a combination with high humidity and improper ventilation, leads to the development of MVOCs and microorganisms that cause allergic diseases. Non-wovens are excellent barrier against microorganisms (dust mites) because of their low porosity: with an average size of mites around 10 μm , the average pore size in fabrics for bedding has to be 6 μm or less. Non-woven mattress covers create impenetrable layer against microorganisms. Another solution is the use of textiles with zero permeability, but they do not provide breathability and reduce the comfort in general; they are also unsuitable for people with sensitivity to synthetic materials.

Non-woven textiles participate as visible or hidden elements in textile mattress pads, where a non-woven web is usually quilted between two woven or non-woven layers. Spunbonded polyester is used as face cloth because of its high wear resistance and resistance to washing.

An essential characteristic of the non-woven textiles for bedding is their ability to be subject to antimicrobial treatment [28]. Thus, the amount of MVOCs and unpleasant odors in the indoor environment is reduced by inhibiting the growth of mold, mildew, etc. The antimicrobial treatment, which can involve both antibacterial and antifungal treatments, is performed as part of the finishing of the non-wovens textiles (i.e., coating and spraying) or by adding additives directly to the fiber spinning dope.

Non-woven webs and fiber fills are frequently used in the production of pillows, quilts, and duvets. The use of hollow fibers increases the insulation abilities of fiber fills. Polypropylene spunbonds of around 50 g/m² replace the tightly woven fabrics, used as a nonremovable pillow cover [29]. Non-woven textiles are also applied as outer covering of economical quilts and duvets. Cheaper needle-punched blankets are produced from regenerated fibers for disposable

and emergency use, though high-quality needle-punched blankets are also produced from natural and synthetic fibers [30].

4.3. Non-woven textiles in furniture

The comfort, related with upholstery textiles, is generally associated with their touch [31,32]. In fact, the touch of the textiles is one of the factors for physical and neurophysiological comfort of the individual. However, the comfort of furniture, covered with fabrics, is determined by the thermophysiological comfort of the person. The thermophysiological comfort, in turn, depends on the behavior of the textile barrier between the body and the piece of furniture [33].

Non-woven textiles are applied in 80–90% of foambacked furniture systems and mattresses [34]. They are the outermost layer of the system (being the upholstery layer) or are used to provide support for the upholstery fabric. Currently, there is a trend of replacing the traditional woven covers of mattresses, made of cotton yarns, with filament non-wovens made of polyester and polypropylene.

Different types of non-woven coverings are in use [34]:

- Bonded polyester non-wovens as the outermost layer of furniture systems, which are not subjected to high loads
- Thermobonded non-wovens as the outermost layer of foambacked upholsters
- Laminated or quilted non-wovens as the outermost layer of foambacked upholstery with high dimensional stability

Inside furniture systems, non-wovens are used for support, insulation, and comfort. Needle-punched waddings and paddings, made from natural and chemical fiber that are recycled from textile production waste, or virgin fiber from acrylic, polypropylene, and polyethylene terephthalate are among the most commonly used [35]. The non-wovens replace the polyurethane foams in furniture systems and mattresses. These are products, based on stitch-bonding technologies, which provide thermal insulation and reduce noise and vibration during operation of furniture and mattresses. Composite non-woven textiles, produced by a web from bi-component fibers, are also in use. They have the same quality as foam of the same thickness [34], but demonstrate higher air permeability, which is important for ensuring both the thermophysiological comfort and the retention of MVOCs.

There is no risk for the Indoor Air Quality (IAQ) in terms of gas emissions from the upholstery textiles [36]. The upholstery surface, however, creates the same problems of accumulation of dust and particulate matter as the floor coverings. Therefore, furniture systems can be a source of VOCs, MVOCs, etc. due to accumulation of dust and allergenic particles from other sources of harmful substances in the indoor environment.

A solution of that problem is the use of synthetic leather as outermost layer of furniture pieces. Non-wovens are successful substitute for genuine leather. Different materials and technologies are applied for the production of synthetic leather. At the same time, synthetic leathers are an excellent substitute for both woven and knitted upholstery fabrics, which positively influences

the IAQ of the indoor environment. Synthetic leather does not accumulate dust as woven and knitted textiles; it is not permeable toward the inner layers of the furniture system and can be cleaned more easily compared to traditional textiles.

4.4. Non-woven textiles as wallcoverings

Non-woven textiles are used more as commercial wallcoverings, applied in the interiors of public buildings (hotels, offices, hospitals). They must meet a series of requirements for flammability, abrasion resistance, washability and stain resistance, tear strength, etc.

The application of non-woven textiles for wallcoverings in the indoor is developing in two main directions: backing for wallcoverings and wallcoverings.

Non-wovens are used in fabric-backed vinyl wallcoverings, where a non-woven substrate is laminated to form a decorative surface of solid vinyl. Light or medium weight wallcoverings are produced with a non-woven backing. Traditional wallcovering substrates are produced with a non-woven backing: needle-punched or stitch-bonded layers [34].

Non-woven wallcoverings influence the IAQ as they can accumulate dust and are used in big areas in the indoor environment. Certainly, their effect on accumulation of dust and particles, released from other sources in the indoor environment is much lower than in the case of carpets and upholstery. Flocked wallcoverings, which have velvet appearance or 3D effects, require special attention. Being overlaid with very fine fibers of cotton, silk, or man-made fibers, the flocked wallcoverings must be subjected to frequent cleaning.

Non-wovens are applied for the production of textile wallcoverings with a variety of designs and textures. Products from synthetic/polyolefin fibers are additionally treated for higher abrasion and stain resistance. Polyolefin and polyester fibers are also applied for the production of acoustic wallcoverings. They have different levels of sound absorption, thus influencing the Indoor Sound Quality (ISQ).

4.5. Non-woven textiles as filters

Non-woven textiles are used as filters in Heating, Ventilation, and Air-Conditioning (HVAC) systems in buildings. HVAC systems provide clean air for the inhabitants in public and residential built environment, including buildings where natural ventilation is not possible (i.e., due to closed glass facades). They also provide clean air for sensitive work places, which require zero dust and microbial emissions: operating rooms in hospitals, pharmaceutical production lines, production of electronic components and devices, research laboratories, etc.

Six types of non-woven filters used in residential buildings have been identified [37]. Five of them contain non-woven media: fiberglass filters, pleated filters with non-woven mats, reusable filters, electret filters, and deep pleated filters. All require regular change or cleaning: from one month in periods of normal use (for fiberglass filters) to once a year (for deep pleated filters).

Non-wovens are also used in air purifiers: portable units in the indoor environment, aimed to remove particles and odors and provide clean air for the occupants. Pleated and electret filters

are used, like Technostat® needle-punch felt media [38]. Glass microfiber HEPA filters, filter media of blends between synthetic and glass fibers, as well as composites with non-woven media are also in use. Non-woven felts from a mixture of natural and synthetic fibers are applied for a backing support [38].

In their role of filter media non-woven materials can influence the Indoor Air Quality (IAQ) and indoor odor quality (IOQ). HVAC systems and air purifiers increase the quality of the indoor environment when working properly and maintained correctly. Noncompliance with the requirements for cleaning or replacement of the particular filter media can lead to change of the indoor environmental quality for the worse. The main reasons are either the incapacity of the filters to retain dust and particles, or the growth of airborne microbial contaminants, which are spread from the filter media to the air of the enclosure, leading to increment of VOCs, MVOCs, and other pollutants of the indoor environment.

4.6. Non-woven textiles in cars

The use of non-woven textiles in the sector of transportation is growing and the car industry is leading this trend. A number of applications of non-wovens in car construction are described in details in [39,40]: lining of doors boot and hoodcase, seat construction (including upholstery cover), filters, engine housing, etc. The requirements for the types of the non-wovens used and their characteristics depend on the particular application and related stresses and loads, as well as the long-term effect from their application for example, specific requirements for the non-woven items in car construction are their light resistance and temperature resistance [40].

Non-woven textiles in cars and other means of transport may influence all six basic metrics of the Indoor Environmental Quality, including the Indoor Vibration Quality (IVQ), which is rarely discussed in the case of built environment. The way the non-woven items in cars affect the IEQ is similar to the application of non-woven textiles in buildings, where they are used as upholstery coverings, floor coverings, backing, etc.

The level of emissions from all items in the interior of the car, including the non-wovens, is important for both the IEQ and the fogging, which may occur. All non-wovens have to be environmental friendly with low emissivity, including in cases of extreme indoor temperatures. Therefore, the car industry takes special care to use materials that have low emission potential, either as release of volatile chemicals (VOCs, SVOCs, VVOCs) or as reaction products. The last is closely related with the temperature and partial pressure drop.

The Indoor Odor Quality (IOQ) in cars is influenced by the non-wovens applied and is preconditioned in many cases by the emission of substances that influence the IAQ [41,42]. The emissions frequently occur at high temperatures only, but due to condensation on flat surfaces (mainly the windscreen and side windows) they form unacceptable fogging.

Non-woven materials in the car are used for thermal and acoustic insulation, thus improving the Indoor Thermal Quality and Indoor Sound Quality not only in the car compartment, but also in the boot and the engine housing. The main insulated parts are the dashboard, the roof, and the floor, the side walls and the rear wall, the parcel shelf, the doors, the tailgate, the ABC pillars, the boot sides, the air-conditioning conduit, etc. [39]. Non-woven textiles made of

recycled natural fibers are still competing with polyurethane foams for being used as insulation materials in cars. Chemically bonded fiber webs with volume densities from 50 to 150 kg/m³ are used for acoustic insulation [39]. At the same time, high-density webs are applied for production of car components like the roof or the parcel shelf, which can emit strong-smelling amines immediately after the installment. According to the study in [42], these emissions decrease rapidly after days, eliminating their negative effect on the IOQ.

Thermally bonded non-wovens with volume densities from 40 to 130 kg/m³ from polypropylene fibers have been developed in order to replace the chemically bonded cotton webs and to avoid the undesired emission inside the cars [39]. These non-woven insulations demonstrate less fogging capacity and lower emissions.

Thermally bonded non-wovens with special shape of the fiber cross section (triangular, star-shaped, etc.) are also used to improve the Indoor Sound Quality.

Non-woven textiles of different type are widely used as covers in car compartments: needle-punched, spunbonded with reinforcement, thermally bonded, or meltblown non-wovens. Tufted fabrics are applied as floor coverings and light non-woven webs are also used as backing of the tufted floor coverings. Needle-punched fabrics are also in use, but for cheaper car models. In any case, cut pile of the tufted floor coverings are preferable than the loop pile, which accumulates more dust and particulate matter.

The analysis of the market and the research in the field, including the patents, show that much more effort, know-how, and economical support are put in the development of non-woven fabrics for car interiors than for the interior of buildings. Therefore, new materials and blends, methods for bonding, lamination, and new composite materials can be found much more in the car production industry than in the construction of buildings. The driving force of one of the biggest industries in the world – the automotive industry – is of particular importance for the advances in the field of non-woven textiles.

4.7. Other applications of non-woven textiles in the indoor environment

Non-woven walls: Non-woven textiles are used for building of flexible freestanding constructions for partition of open indoor spaces. Special polyethylene Tyvek® is applied for the production of the non-woven walls, which includes 10–15% recyclable content [43]. Non-woven flexible walls influence the ILQ and ISQ, as they can sculpt the light of the indoor environment and dampen the sound.

Non-woven curtains: Similar to floor coverings, non-woven textiles are used in the indoor environment either as the outer fabric or as the reinforcing lining of blinds and curtains. When visible, and in contact with the indoor air, non-woven textiles can affect the metrics of the indoor environmental quality in a similar way as the wallcoverings. Non-woven curtains reduce sound from the outdoor environment and affect the Indoor Light Quality (ILQ). Synthetic materials dominate over natural fibers as they are easy to maintain and have good resistance to UV rays. Like non-woven upholstery textiles, curtains and screens accumulate odors and particulate matter and need regular cleaning.

5. Conclusions

Textiles are an important factor for Indoor Environmental Quality (IEQ). The increasing application of non-woven textiles in the built environment and means of transport requires more research to be performed for the estimation of the particular influence of non-woven textiles of different types on the metrics of the indoor environment. Every step for improvement of IEQ will increase the human comfort, will improve human health, and will support higher productivity and school work performance.

Author details

Radostina A. Angelova

Address all correspondence to: joy_angels@abv.bg

Technical University of Sofia, Bulgaria

References

- [1] Leech J.A., Wilby K., McMullen E., Laporte K. 1997. The Canadian human activity pattern survey: report of methods and population surveyed. *Chronic Dis Can* 17(3): 118-23.
- [2] Klepeis N.E., Nelson W.C., Ott W.R., Robinson J.P., Tsang A.M., Switzer P., et al. 2001. The national human activity pattern survey (NHAPS): a resource for assessing exposure to environmental pollutants. *J Expo Anal Environ Epidemiol* 11(3):231-52.
- [3] Angelova R.A. 2015. Textiles and human thermophysiological comfort in the indoor environment, CRC Press, NY: 11-19.
- [4] Frontczak M., Wargocki P. 2011. Literature survey on how different factors influence human comfort in indoor environments. *Build Environ* 46(4): 922-937.
- [5] Kim J., de Dear R. 2012 How does occupant perception on specific IEQ factors affect overall satisfaction?, Proceedings of 7th Windsor Conference: The changing context of comfort in an unpredictable world Cumberland Lodge, Windsor, UK, 12-15 April 2012. London. Available at: nceub.commoncense.info/uploads/W1215%20Kim.pdf
- [6] Wyon D. 1994. Current indoor climate problems and their possible solution. *Indoor Built Environ* 3: 123-129.
- [7] Boestra A.C., Leyton J.L. 1997. Diagnosing problem buildings: The risk factor approach. *Indoor Air* 2: 278-283.

- [8] Levin H. 1989. Building materials and indoor air quality. In *State of the Art Reviews in Occupational Medicine* (eds.) M. Hodgson and J. Cone, Philadelphia, PA: Hanley and Belfus: 667-693.
- [9] Smith B., Bristow V. 1994. Indoor air quality and textiles: An emerging issue. *Am Dyestuff Rep* 83: 37-46.
- [10] Guo H., Murray F. 2000. Modelling of emissions of total volatile organic compounds in an Australian house. *Indoor Built Environ* 9: 171-181.
- [11] Järnström H., Vares S., Airaksinen M. 2009. Semi volatile organic compounds and flame retardants: occurrence in indoor environments and risk assessment for indoor exposure, VTT Technical Research Centre of Finland. Available at: <http://www.vtt.fi/inf/pdf/tiedotteet/2009/T2486.pdf>
- [12] Korpi A., Järnberg J., Pasanen A.-L. 2009. Microbial volatile organic compounds. *Crit Rev Toxicol* 39, 139–193.
- [13] Salthammer T. 2014. Very volatile organic compounds: an understudied class of indoor air pollutants, *Indoor Air* 2014, DOI: 10.1111/ina.12173
- [14] Whitefoot D. 2009. Carpet types and requirements, In *Advances in Carpet Manufacturing*, ed. K. K. Goswami, Woodhead Publishing Ltd., CRC Press: 1-18.
- [15] Catalli V. 1995. Choosing carpets for good IAQ, *Proc Peace Environ*, 6: 235-239.
- [16] MirafTAB M., Horrocks R., Woods C. 1999. Carpet waste, an expensive luxury we must do without! *AUTEX Res. J.* 1: 1–7.
- [17] Lewis R.G., Fortmann R.C., Camann D.E. 1994. Evaluation of methods for monitoring the potential exposure of small children to pesticides in the residential environment. *Arch Environ Con Tox* 26.1: 37–46.
- [18] Pluschke P. (ed.). 2004. *The Handbook of Environmental Chemistry: Indoor Air Pollution*, Part F, Berlin, Germany: Springer-Verlag: 14-30.
- [19] Roberts B.C., Waller T.M., Caine M.P. 2007. Thermoregulatory response to baselayer garments during treadmill exercise. *Int J Sports Sci Eng* 1: 29–38.
- [20] Carr W., Dong H., Lee H.S., Developments in the thermal processing of carpets. In *Advances in Carpet Manufacturing*, ed. K. K. Goswami, Woodhead Publishing Ltd., CRC Press, 2009: 291-309.
- [21] Kidesø J., Vinzents P., Schneider T. 1999. A simple method for measuring the potential resuspension of dust from carpets in the indoor environment. *Text Res J* 69: 169–75.
- [22] White W.C., Monticello R., Soens H. 2002. Microbiological Problems Associated With Carpeting, in Proc. Of Unitex First World Congress – Carpets, May, Belgium: 100-119.

- [23] Moody W., Needles H. L. 2004. *Tufted Carpets*, William Andrew, Inc., USA: 145-154.
- [24] Mizuno O.K., Tsuzuki K., Ohshiro Y., Mizuno K.. 2005. Effects of an electric blanket on sleep stages and body temperature in young men. *Ergonomics* 48: 749–57.
- [25] Muzet A., Libert J.P., Candas V. 1984. Ambient temperature and human sleep. *Cell Mol Life Sci* 40: 425–29.
- [26] Worfolk J. 1997. Keep elders warm. *Geriatr Nurs* 18: 7–11.
- [27] Holland E.J., Wilson C.A., Niven B.E. 1999. Microclimate ventilation of infant bedding. *Int J Cloth Sci Tech* 11: 226–39.
- [28] Kane F. 2010. Nonwoven textiles for residential and commercial interiors. In *Applications of Nonwovens in Technical Textiles*, ed. R Chapman, Woodhead Publ. Ltd.: 136-158.
- [29] Yeager J. I., Teter-Justice L.K. 2000. *Textiles for Residential and Commercial Interiors*, 2nd Edition, Fairchild Publications, New York: 452-474.
- [30] Kittelmann W., Dilo J. P., Gupta V. P., Kunath P. 2002. Web bonding. In *Nonwoven Fabrics, Raw Materials, Manufacture, Applications, Characteristics, Testing Processes*, Albrecht W., Fuchs H., Kittelmann W. (eds.), Wiley-Vech, Weinheim, Germany: 269-398.
- [31] Pierce F. 1930. The handle of cloth as a measurable quantity. *Shirley Inst Mem* 9:83–122.
- [32] Howorth W.S., Oliver P.H. 1958. The application of multiple factor analysis to the assessment of fabric handle. *J Text I* 49: T540–53.
- [33] Barker, R.L. 2002. From fabric hand to thermal comfort: The evolving role of objective measurements in explaining human comfort response to textiles. *Int J Cloth Sci Tech* 14: 181–200.
- [34] Stein W., Slovacek J. M. 2002. Nonwovens for home textiles. In *Nonwoven Fabrics, Raw Materials, Manufacture, Applications, Characteristics, Testing Processes*, Albrecht W., Fuchs H., Kittelmann W. (eds.), Wiley-Vech, Weinheim, Germany: 515-522.
- [35] Anand S. C., Brunnschweiler D., Swarbrick G., Russell S. J. 2007. Mechanical bonding. In *Handbook of Nonwovens*, Russell, S. J. (ed.), Woodhead Publ. Ltd. Cambridge: 201-297.
- [36] McCullough E.A., Olesen B.W., Hong S. 1994. Thermal insulation provided by chairs. *ASHRAE Tran* 100: 795–802.
- [37] Kinzer K.E., Moreno R.C. 1997. Performance characteristics of residential in-duct air cleaning devices. *AFSS Adv Filtr Sep Technol* 11: pp. 252-263.
- [38] Hutten I. 2007. *Handbook of Non-Woven Filter Media*, Elsevier Science & Technology Books: 71-102.

- [39] Schmidt G. 2003, The motor vehicle industry. In *Nonwovens for Technical Applications* (eds.) W. Albrecht, H. Fuchs, W. Kittelmann, WILEY-VCH Verlag GmbH & Co. KGaA, Weinheim: 545-628.
- [40] Russell S.J., Tipper M.J. 2008. Nonwovens used in automobiles, in *Textile advances in the automotive industry*. (ed.) R. Shishoo, Woodhead Publ. Ltd. and CRC Press LLC: 63-85.
- [41] Eisele D. 1992. Emissionspotential am Beispiel eines mit PVC beschichteten Polvliesbelages. *Melliand Textilber* 73, 1: 84-87.
- [42] Marutzky R., Meyer B. 1992. Emissionen aus duroplastisch gebundenen Formteilen für den Kfz-Innenraum, Konf Einzelber: Anwendungen von duroplastischen Kunststoffen im Automobilbau, SKZ-Fachtag, Süddeutsch Kunststoff-Zentrum Würzburg: 215-229.
- [43] www.molodesign.com

Medical Application of Nonwoven Fabrics - Intra-abdominal Spacers for Particle Therapy

Ryohei Sasaki, Hiroaki Akasaka, Yusuke Demizu, Sachiko Inubushi, Tianyuan Wang and Takumi Fukumoto

Additional information is available at the end of the chapter

<http://dx.doi.org/10.5772/61787>

Abstract

The authors aimed to introduce a medical application for nonwoven fabric as spacers in particle therapy. Particle therapy, exhibiting more focused effects on target tissues, has emerged as a promising treatment modality. However, close proximity of tumor tissue and adjacent organs makes delivery of curative doses to the tumor difficult because severe radiation morbidities might occur. A method using surgically placed GORE-TEX sheets as a spacer has been reported. Although this method provides for separation of adjacent organs, the material is not resorbed. To overcome these anatomical and therapeutic difficulties, and to deliver effective radiation doses to treat upper abdominal tumors, we have developed a nonwoven fabric spacer composed of bioabsorbable suture material. The absorbable polyglycolic acid (PGA) spacer had water-equivalent, biocompatible, and thickness-retaining properties. Although further evaluation is warranted in a clinical setting, the PGA spacer may be effective to block particle beams and to separate normal tissues from the radiation field. These findings suggest that the nonwoven-fabric PGA spacer might become a useful device in particle therapy.

Keywords: Spacer, polyglycolic acid, pancreatic cancer, particle therapy, bioabsorbability

1. Introduction

Two of the properties of nonwoven fabrics that have justified previous use in medical products are economic viability in single-use scenarios and reliable performance [1]. The design and

performance characteristics of these products—which come into close contact with the human body—are driven by their end use, which determines the desired function and barrier, absorption, and strength properties, and the fact that any chemical additives need to be biocompatible. Nonwoven products remain the component of choice for providing appropriate protection because of their ability to create barriers due to either the structure of the nonwoven material itself or an additional active coating for personal protective apparel. Nonwoven materials are also beginning to play a role in extracorporeal devices, such as artificial lungs, hearts, and kidneys, as well as in ligament repairs and other skeletal scaffolds, yet these uses are still rare compared with their other uses [2].

Radiotherapy is one of the strategies used against several cancers, and X-ray or particle beams are mainly used for cancer treatment. Particle therapy, exhibiting more focused effects on target tissues, has emerged as a promising treatment modality. Several systematic reviews associated with proton or carbon-ion beam therapy discuss the extensive use of particle therapy to treat various malignant tumors, including chordoma, ocular melanoma, and prostate cancer [3–5]. Several studies have indicated the efficacy of proton therapy for the treatment of hepatocellular carcinoma or pancreatic cancer [6–9]. However, in certain cases, it is difficult to deliver curative doses of radiation to treat upper abdominal tumors without damaging adjacent radiosensitive organs, such as the duodenum, jejunum, and stomach. To overcome these anatomical difficulties and to deliver effective radiation doses to treat upper abdominal tumors, nonwoven fabric barriers have been applied as spacers to separate tumors and adjacent organs [10, 11].

2. Medical application of nonwoven fabric spacers

Nonwoven fabric is a fabric-like material manufactured from long fibers bonded together by chemical, mechanical, heat, or solvent treatment. The performance characteristics of nonwoven fabrics vary according to the material components and the manufacturing process. A characteristic of nonwoven fabrics is not to have directionality for strength or growth. In addition, specific features of nonwoven fabrics include “water absorbency,” “chemical resistance,” “breathability,” “abrasion resistance,” and “flexibility.” These characteristics of nonwoven fabrics support their use as surgical gowns and hats, masks, drapes, water-absorbing mats, and machine covers. The GORE-TEX sheet is a waterproof, breathable fabric membrane and has been widely used in permanent implants, including the artificial blood vessel, for many years. The GORE-TEX sheet was the first nonwoven fabric to be applied as a spacer in the field of particle therapy [10–12] (Figure 1). The use of this spacer allows the application of particle therapy in cases in which particle therapy may result in severe incurable damage to adjacent organs. However, although the GORE-TEX spacer is useful during the period of particle therapy, it becomes a foreign body after the therapy [12]. Problems related to the ongoing presence of the spacer may be avoided by removal during a second surgery, but repeated operations might be a risk for the patient.

3. Usefulness of nonwoven fabric spacers in the treatment of pancreatic cancer

Despite recent progress in treatment options for pancreatic cancer, survival rates have failed to show any significant improvement [13]. Among these modalities, resection is the only curative treatment for pancreatic cancer, but only 10%–15% of patients have operable tumors [14, 15]. The remaining patients cannot undergo resection because of local invasion or distant metastasis at the time of diagnosis [16]. Local invasion is found in approximately 40% of patients with pancreatic cancer at the time of presentation and most commonly includes the superior mesenteric vessels or the celiac trunk [17].

Chemoradiotherapy with concurrent 5-fluorouracil was historically considered the standard therapy for locally advanced pancreatic cancer [18]. Recently, successful results have been reported with the use of a combination of gemcitabine and proton therapy to treat this type of advanced pancreatic cancer. However, reductions of the irradiation doses and target fields were necessary because approximately 10% of the patients subsequently developed Grade 3 or higher gastric ulcers several months after completing the therapy [9]. In such cases, surgical placement of a spacer between the pancreas and the gastrointestinal tract might be an effective option to reduce gastrointestinal toxicity and allow the continued use of high doses of radiation.

Among pancreatic cancers in various regions, good candidates for spacer placement are unresectable pancreatic body and tail cancers. Pancreatic head cancer is not amenable to this treatment strategy because the pancreatic head cannot be separated from the duodenum.

The treatment strategy aims to keep the gastrointestinal tract away from the irradiation field by spacer placement and to allow the application of proton-beam radiotherapy with curative intent. The GORE-TEX sheets and the omentum are superimposed and applied as a spacer to maintain a safety margin of approximately 10 mm from the gastrointestinal tract. The spacer is finely fixed to the retroperitoneum, peritoneum, stomach, and surrounding tissues using 4-0 nylon to avoid hernia formation. The use of absorbable sutures for the fixation must be avoided because it leads to migration of the spacer. In the treatment of pancreatic body and tail cancers, target gastrointestinal tract components to be protected by spacer placement include the stomach, duodenum, small, jejunum, and colon. Of note, the protection of the duodenal bulb and horizontal part of the duodenum in the region of the Treitz ligament is of particular importance. The spacer placement surgery is a first step to allow proton-beam radiotherapy, and no part of the tumor is resected during this procedure.

Until the end of 2013, 8 patients with unresectable pancreatic body and tail cancers were treated by spacer placement and particle therapy as phase I and phase II trials. One-year and 2-year survival rates were 87.5% and 43.8%, respectively. These patients were free from complications associated with the gastrointestinal tract.

We believe that surgical spacer placement can be used to maintain a safety margin around the gastrointestinal tract. In consequence, full-dose particle-beam radiotherapy for pancreatic body and tail cancers can be achieved without serious toxicities.

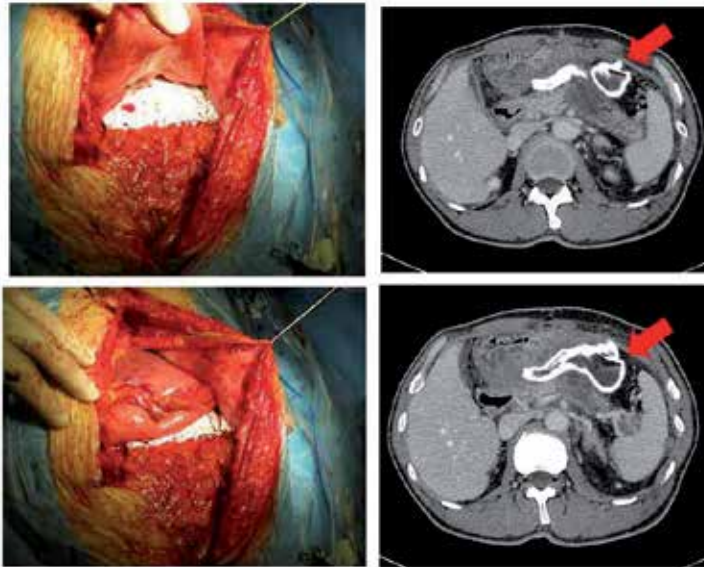


Figure 1. A case of pancreatic body cancer in which a GORE-TEX spacer was placed before the application of proton-beam therapy. The left panels show perisurgical images during the placement of the GORE-TEX spacer. The right panels show computed tomography images, including tumors, liver, adjacent organs, and the GORE-TEX spacer (arrows) after the surgery.

4. Novel nonwoven fabric bioabsorbable spacer for particle radiotherapy

The purpose to produce a bioabsorbable nonwoven fabric spacer is to overcome problems associated with nonabsorbable GORE-TEX spacer [19]. The nonabsorbable GORE-TEX spacer might cause serious complications after the completion of particle therapy. On the other hand, although previous investigators have reported usefulness of gel spacers for separation of prostate and rectum [20, 21], those spacers are inappropriate for the upper abdomen, which contains lots of free space. Therefore, at present, a nonwoven fabric bioabsorbable spacer is necessary and appropriate for the separation of tumor and adjacent organs of upper abdomen malignancies.

The process for producing the nonwoven fabric involves entangling threads in 3 dimensions with a needle-punching process and other methods [22, 23]. Spacer placement during radiotherapy is a promising method designed to allow increased tumor dose while limiting radiation exposure to adjacent organs. The spacer exhibits excellent properties related to bioabsorbability, biocompatibility, thickness retention, and water equivalency according to physical and animal experiments (Figure 2). The reason and the advantage for the use of PGA to construct this nonwoven fabric spacer are that PGA is one of the most widely studied polymers and has excellent mechanical properties and biological affinity [24, 25]. Historically, PGA has played a central role in surgery since its development as the first synthetic absorbable

suture material in 1962 [26]. The PGA is absorbed in 60–90 days after insertion in the body. It is hydrolyzed without any phagocytosis, which results in a weaker immune response than that of absorbable organic sutures [27]. The degradation of PGA generally involves random hydrolysis of their ester bonds. Under physiologic conditions, PGA is also degraded by certain enzymes, especially those with esterase activity [28, 29]. The attractiveness of PGA as a biodegradable polymer in medical application is that its degradation product glycolic acid is a natural metabolite [29]. The glycolic acid is nontoxic and can enter the tricarboxylic acid cycle, after which it is excreted as water and carbon dioxide. Part of the glycolic acid is also excreted in urine [26, 28].

As for PGA sutures, Chu et al. have reported a simple degradation mechanism via homogeneous erosion [30–32]. The degradation process occurs in two stages, the first involves the diffusion of water into the amorphous regions of the matrix and simple hydrolytic chain scission of the ester groups. The second stage of degradation involves largely the crystalline areas of the polymer, which becomes predominant when the majority of the amorphous regions have been eroded. It is important to note that PGA nonwoven fabric spacer is comprised of the PGA suture mainly with a 3-dimensional needle-punching process. Therefore, the degradation mechanism of the content of the PGA spacer could be same as PGA sutures. However, it is possible that because the volume of PGA polymers in the PGA spacer is quite large, inflammatory biological responses might be different from that of relatively small volume of PGA suture (Figure 3).

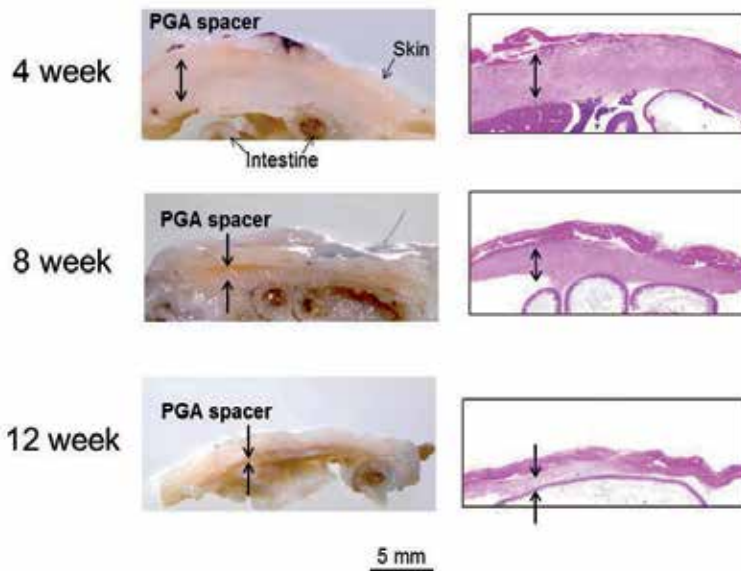


Figure 2. Macroscopic features of a novel nonwoven-fabric bioabsorbable spacer composed of surgical polyglycolic acid (PGA) sutures in the rat abdomen. The left panels show images of formalin-fixed specimens showing the abdominal wall, implanted PGA spacer, and adjacent intestines. The right panels show images of the same specimens stained with hematoxylin and eosin (HE). These images indicate that the PGA spacer was absorbed gradually.

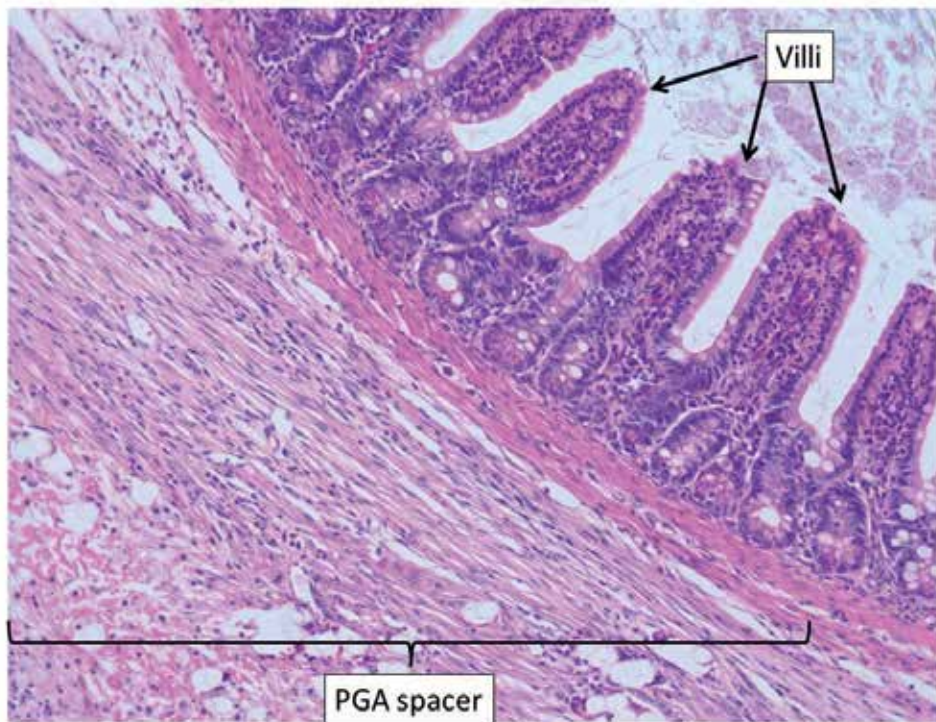


Figure 3. Microscopic features of the PGA bioabsorbable spacer implanted in the rat abdomen. In the surface of the PGA spacer, inflammatory response was observed. There were degraded PGA fibers, lymphocyte, and macrophage observed in the surface. Interestingly, very few cell infiltrations were observed in the body of the PGA spacer

Although there is no clear definition of a bioabsorbable nonwoven fabric spacer reported, an optimal bioabsorbable spacer must have thickness-retaining and water-equivalency properties according to treatment duration [19]. In particle therapies, because treatment protocols take 2–7 weeks [5, 33], a spacer that maintains its thickness for the duration of or slightly longer than the treatment period seems to be ideal. From our investigation, the percentage of thickness retention of the PGA spacer varies according to the concentration of the PGA sutures. The PGA spacer product with 0.2 g/cm^3 of PGA sutures retains more than 90% thickness for 8 weeks. Therefore, this PGA spacer could be applied in various protocols in particle therapy. The bioabsorbable PGA spacer might become a useful device and expand indications for particle therapy.

5. Future direction of medical application of bioabsorbable nonwoven fabric spacers

Adhesions after surgery might lead to serious complications [34, 35]. In the pelvic and abdominal sites, these complications might lead to small-bowel obstruction, infertility, chronic

pelvic pain, and difficulty with further surgical access. Therefore, regarding spacer placement, it is necessary to minimize adhesions between the spacer and surrounding organs. In our preclinical study, the efficacy and the safety of a bioabsorbable spacer composed of PGA sutures were investigated in several animal models [19]. The PGA nonwoven fabric spacer exhibited excellent properties, no toxic effects in the animals, and negligible adhesion formation. However, different conditions between experimental animals and clinical settings might affect outcomes, and adhesion formation may be different in the presence of malignant tumors.

Therefore, if it is necessary to improve properties of the nonwoven fabric PGA spacer, next-generation spacers are expected to avoid adhesion as far as possible. A promising method might be to combine an anti-adhesion material with the PGA spacer. In our recent observation using a healthy rat model, adhesion was significantly decreased, and no exceptional toxicity risk was observed compared with the control group. In the future, less-invasive methods, including endoscopic surgery, might be applied for implantation of the spacer.

6. Conclusion

The absorbable PGA spacer had water-equivalent, biocompatible, and thickness-retaining properties. Although further evaluation is warranted in a clinical setting, the PGA spacer may be effective to block particle beams and to separate normal tissues from the radiation field. These findings suggest that the nonwoven fabric PGA spacer might become a useful device in particle therapy.

Author details

Ryohei Sasaki^{*}, Hiroaki Akasaka¹, Yusuke Demizu², Sachiko Inubushi¹, Tianyuan Wang¹ and Takumi Fukumoto¹

^{*}Address all correspondence to: rsasaki@med.kobe-u.ac.jp

¹ Divisions of Radiation Oncology and of Hepato-Biliary-Pancreas Surgery, Kobe University Graduate School of Medicine, Kobe City, Hyogo, Japan

² Department of Radiology, Hyogo Ion Beam Medical Center, Hyogo, Japan

References

- [1] Ziegenfus T. Maintaining specialty textiles quality. *Textile World*. 2005;4:155.

- [2] Visser LC, Arnoczky SP, Caballero O, et al. Growth factor-rich plasma increases tendon cell proliferation and matrix synthesis on a synthetic scaffold: an in vitro study. *Tissue Engineering Part A*. 2010;16:1021–1029.
- [3] Brada M, Pijls-Johannesma M, De Ruyscher D. Proton therapy in clinical practice: current clinical evidence. *Journal of Clinical Oncology*. 2007;25:965–970.
- [4] De Ruyscher D, Mark Lodge M, Jones B, et al. Charged particles in radiotherapy: a 5-year update of a systematic review. *Radiotherapy and Oncology*. 2012;103:5–7. DOI: 10.1016/j.radonc.2012.01.003
- [5] Tsujii H, Kamada T. A review of update clinical results of carbon ion radiotherapy. *Japanese Journal of Clinical Oncology*. 2012;42:670–685. DOI: 10.1093/jjco/hys104
- [6] Nakayama H, Sugahara S, Fukuda K, et al. Proton beam therapy for hepatocellular carcinoma located adjacent to the alimentary tract. *International Journal of Radiation, Oncology, Biology, Physics*. 2011;80:992–995. DOI: 10.1016/j.ijrobp.2010.03.015
- [7] Mizumoto M, Okumura T, Hashimoto T, et al. Proton beam therapy for hepatocellular carcinoma: a comparison of three treatment protocols. *International Journal of Radiation, Oncology, Biology, Physics*. 2011;81:1039–1045. DOI: 10.1016/j.ijrobp.2010.07.015
- [8] Klein J, Dawson LA. Hepatocellular carcinoma radiation therapy: review of evidence and future opportunities. *International Journal of Radiation, Oncology, Biology, Physics*. 2013;87:22–32. DOI: 10.1016/j.ijrobp.2012.08.043
- [9] Terashima K, Demizu Y, Hashimoto N, et al. A phase I/II study of gemcitabine-concurrent proton radiotherapy for locally advanced pancreatic cancer without distant metastasis. *Radiotherapy and Oncology*. 2012;103:25–31. DOI: 10.1016/j.radonc.2011.12.029
- [10] Komatsu S, Hori Y, Fukumoto T, et al. Surgical spacer placement and proton radiotherapy for unrespectable hepatocellular carcinoma. *World Journal of Gastroenterology*. 2010;16:1800–1803.
- [11] Fukumoto T, Komatsu S, Hori Y, et al. Particle beam radiotherapy with a surgical spacer placement for advanced abdominal leiomyosarcoma results in a significant clinical benefit. *Journal of Surgical Oncology*. 2010;101:97–99. DOI: 10.1002/jso.21417
- [12] Ogino T, Sekimoto M, Nishimura J, et al. Intraluminal migration of a spacer with small bowel obstruction: a case report of rare complication. *World Journal of Surgical Oncology*. 2012;10:30. DOI: 10.1186/1477-7819-10-30
- [13] Hidalgo M. Pancreatic cancer. *New England Journal of Medicine*. 2010;362:1605–1617.

- [14] Conlon KC, Klimstra DS, Brennan MF. Long-term survival after curative resection for pancreatic ductal adenocarcinoma. *Clinicopathologic analysis of 5-year survivors. Annals of Surgery.* 1996;223:273–279.
- [15] Chua YJ, Cunningham D. Adjuvant treatment for resectable pancreatic cancer. *Journal of Clinical Oncology.* 2005;23:4532–4537.
- [16] D’Souza MA, Shrikhande SV. Pancreatic resectional surgery: an evidence-based perspective. *Journal of Cancer Research and Therapy.* 2008;4:77–83.
- [17] Mancuso A, Calabrò F, Sternberg CN. Current therapies and advances in the treatment of pancreatic cancer. *Critical Reviews in Oncology/Hematology.* 2006;58:231–241.
- [18] Moertel CG, Frytak S, Hahn RG, et al. Therapy of locally unresectable pancreatic carcinoma: a randomized comparison of high dose (6000 rads) radiation alone, moderate dose radiation (4000 rads + 5-fluorouracil), and high dose radiation + 5-fluorouracil: the Gastrointestinal Tumor Study Group. *Cancer.* 1981;48:1705–1710.
- [19] Akasaka H, Sasaki R, Miyawaki D, et al. Preclinical evaluation of bioabsorbable polyglycolic acid (PGA) spacer for particle therapy. *International Journal of Radiation, Oncology, Biology, Physics.* 2014;90:1177–1185. DOI: 10.1016/j.ijrobp.2014.07.048
- [20] Susil RC, Mcnutt TR, Deweese TL, et al. Effects of prostate-rectum separation on rectal dose from external beam radiotherapy. *International Journal of Radiation Oncology, Biology, Physics.* 2010;76:1251–1258.
- [21] Pinkawa M, Corral NE, Caffaro M, et al. Application of a spacer gel to optimize three-dimensional conformal and intensity modulated radiotherapy for prostate cancer. *Radiotherapy and Oncology.* 2011;100:436–441.
- [22] Gunatillake PA, Adhikari R. Biodegradable synthetic polymers for tissue engineering. *European Cells and Materials.* 2003;5:1–16.
- [23] Williams DF. *Clinical Implant Materials, 2.* Boca Raton, FL: CRC Press; 1981.
- [24] Larobina D, Mensitieri G, Kipper MJ, et al. Mechanistic understanding of degradation in bioerodible polymers for drug delivery. *AIChE Journal.* 2002;48:2960–2970.
- [25] Park TG, Cohen S, Langer R, et al. Poly(L-lactic acid)/pluronic blends: characterization of phase separation behavior, degradation, and morphology and use as protein-releasing matrices. *Macromolecules.* 1992;25:116–122.
- [26] Singh V, Tiwari M. Structure-processing-property relationship of poly(glycolic acid) for drug delivery systems 1: synthesis and catalysis. *International Journal of Polymer Science.* Volume 2010. Article ID 652719, 23.
- [27] Craig PH, Williams JA, Davis KW, Magoun AD, Levy AJ, Bogdansky S, et al. A biologic comparison of polyglactin 910 and polyglycolic acid synthetic absorbable sutures. *Surgery, Gynecology, and Obstetrics.* 1975;141:1–10.

- [28] Williams DF, Mort E. Enzyme-accelerated hydrolysis of polyglycolic acid. *Journal of Bioengineering*. 1977;1(3):231–238.
- [29] Gunatillake PA, Adhikari R. Biodegradable synthetic polymers for tissue engineering. *European Cells and Materials*. 2003;5:1–16.
- [30] Chu CC. An in-vitro study of the effect of buffer on the degradation of poly(glycolic acid) sutures. *Journal of Biomedical Materials Research*. 1981;15: 19–27.
- [31] Chu CC. The *in-vitro* degradation of poly(glycolic acid) sutures—effect of pH. *Journal of Biomedical Materials Research*. 1981;15: 795–804.
- [32] Chu CC. Hydrolytic degradation of polyglycolic acid: tensile strength and crystallinity study. *Journal of Applied Polymer Science*. 1981;26: 1727–1734.
- [33] Klein J, Dawson LA. Hepatocellular carcinoma radiation therapy: review of evidence and future opportunities. *International Journal of Radiation, Oncology, Biology, Physics*. 2013;87:22–32.
- [34] Al-Jaroudi D, Tulandi T. Adhesion prevention in gynecologic surgery. *Obstetrical and Gynecological Survey*. 2004;59:360–367.
- [35] Fazio VW, Cohen Z, Fleshman JW, et al. Reduction in adhesive small-bowel obstruction by Seprafilm® adhesion barrier after intestinal resection. *Diseases of the Colon and Rectum*. 2006;49:1–11.

Plasma Surface Treatments of Nonwovens

Burçak Karagüzel Kayaoğlu

Additional information is available at the end of the chapter

<http://dx.doi.org/10.5772/61307>

Abstract

Plasma treatment has been used for surface activation and modification of textiles. The ionized, highly reactive species, such as ions, electrons, and radicals, in plasma modify the surface of the substrate material, and the composition of plasma depends on the gas used. Plasma technology is an environmentally friendly process and resource-efficient in nature. There is no solvent emission or wastewater in the process and drying processes with high energy and time consumption are not required. The textile applications of plasma include sterilization, wettability and hydrophobicity, dyeability enhancement, flame-retardant finishing, and antimicrobial properties. Plasma surface modification applied to fiber is a way to add value to a nonwoven fabric and enhance the functional performance of the final product. This chapter provides an overview of the plasma treatments of nonwovens that enhance their surface-related properties.

Keywords: nonwoven, plasma, surface modification, coating, functionalization

1. Introduction

1.1. Surface functionalization of nonwovens by plasma techniques

Nonwoven fabrics are produced by bonding or interlocking of fibers by different means such as mechanical, chemical, thermal, or physical. These fabrics may be designed to have a limited lifetime or as single-use fabrics, or very durable ones. The technologies enable the production from simple roll-goods to micro- and nanofiber webs. The structure of a typical nonwoven made from polypropylene fibers by melt-extrusion technologies is shown in Fig. 1. Nonwovens have been used in a wide range of products such as wipes, baby diapers, filtration media, garment interlinings, furniture padding, and many others. The end-use properties of nonwovens are determined by the properties of the fibers they are made from, the fabric structure, and other functionalities, such as absorbency, hydrophobicity, wettability, and antimicrobial

property, imparted by potential modifications. Surface modification applied to the fiber is a way to add value to the nonwoven fabric and enhance the functional performance of the final product.

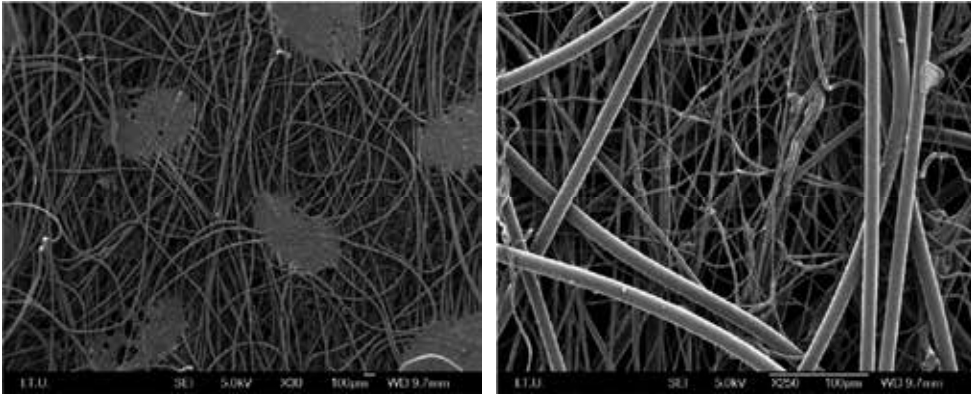


Figure 1. Scanning electron microscopy images showing the surface texture of a nonwoven fabric

Plasma is the mixture of partially and fully ionized gas, photons, free electrons, and chemically reactive atoms and radicals [1]. Plasma is generated by raising the energy content of matter through different methods such as dielectric barrier discharge, glow discharge, corona discharge, or the application of a high electric field.

The gas molecules become ionized when the kinetic energy of gas molecules exceeds their ionization energy. The active species in plasma only interact with the outermost surface of the substrate, approximately 10 nm in depth, without altering the bulk properties of the substrate [2].

Plasma treatment has been recognized as an alternative ecological surface treatment to conventional liquid-based textile-coating treatments, which use solvents, additives, and organic reagents and produce large volumes of liquid waste.

Plasma treatment can be used to modify the surface properties of nonwovens for:

- Enhancement of surface energy, thereby improving wettability and adhesion properties of nonwovens
- Improvement of the surface properties of natural and synthetic fibers to improve wettability, printability, and dyeability of nonwovens
- Hydrophobization, oleophobization (dirt- and oil-repellent effect), and functional and bioactive coatings (antibacterial, fungicidal)

With plasma, different reactions such as surface cleaning, etching, deposition, cross-linking, surface roughening, and grafting are possible [2]. Polymer surfaces can be cleaned or etched, mostly using nonpolymerizable gases such as O_2 , N_2 , H_2 , the noble gases, or gas mixtures [3].

Plasma etching has been used to remove contaminations such as lubricants, oils, surfactants from textile fibers and also to increase the wettability of the surface by changing the surface roughness [3].

1.2. Plasma reactions

1.2.1. Plasma grafting

Surface properties of polymer materials such as nonwovens can be tailored by wet chemical treatments or physical techniques such as glow discharge plasma treatment [2, 3, 4, 5].

Grafting is a method to modify and functionalize fibrous surfaces and it leads to a thin film coating on the substrates (Fig. 2). In surface grafting, a second polymer is attached to the polymer backbone of the fibrous surface through covalent bonding. Properties of the surface, such as wettability, hydrophobicity, adhesion, and friction, can be dramatically changed by this method [2, 3].

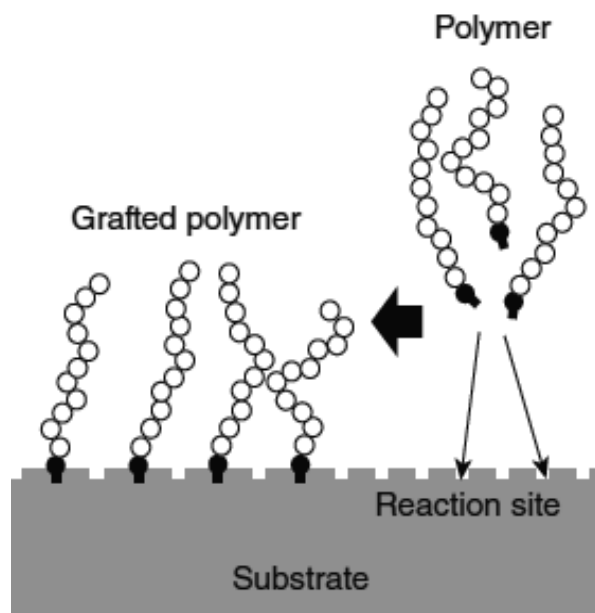


Figure 2. Schematic of surface grafting of a polymer on a substrate [2]

Plasma glow discharge is a method used for surface grafting reaction, where radio frequency energy is applied to an electrode (Fig. 3) pair in order to excite a gas such as oxygen, air, helium, or argon at low pressure (0.1 - 1.0 torr). Free radicals are generated at high energy levels through stripping of electrons from the gas particles. Then polymerization starts with the introduction of one or more types of monomer gases such as acrylic acid, carboxyl and amino groups into the plasma treatment chamber where the radicals react with monomer gases [2, 3, 6].

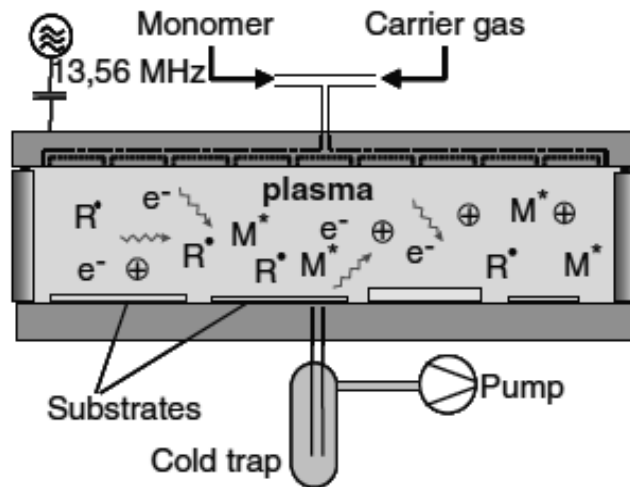


Figure 3. Schematic of plasma treatment reactor for surface modification and deposition [3]

Plasma conditions are controlled by plasma parameters such as plasma power, frequency, duration, carrier gas, gas pressure, flow rate, and monomer types [3].

Corona discharge is commonly used for surface treatment of polyethylene and polypropylene having low surface energy. In this method, an electrode at a high electric potential (of 15 kV at 20 kHz) ionizes the surrounding gas which generates a corona discharge (Fig. 4). While the fabric passes between the high-potential electrode and a grounded electrode, chemical reactions occur between some of the ionized gas particles and the surface of the substrate. During this process, surface roughening and addition of functional groups such as carbonyls, hydroxyls, carboxylic acids, and unsaturated bonds to the fabric surface take place. Oxidation of the substrate surface occurs when corona discharge is performed at atmospheric pressure in air, which oxidizes the surface [6].

1.2.2. Thin film deposition

Plasma polymerization includes the formation and deposition of thin polymeric films on the surface of substrates with the influence of plasma generated by some kind of electrical discharge [6].

Plasma polymerization process includes fragmentation of vapor-type organic, organosilicone, or organometallic monomer molecules, the formation of reactive radicals, and recombination of the activated fragments in which the treatment time influences the thickness of the applied coatings [6].

Thin films of metals and metal oxides have been applied to nonwoven substrates using different thin film deposition techniques such as ionized gas treatments, plasma treatment,

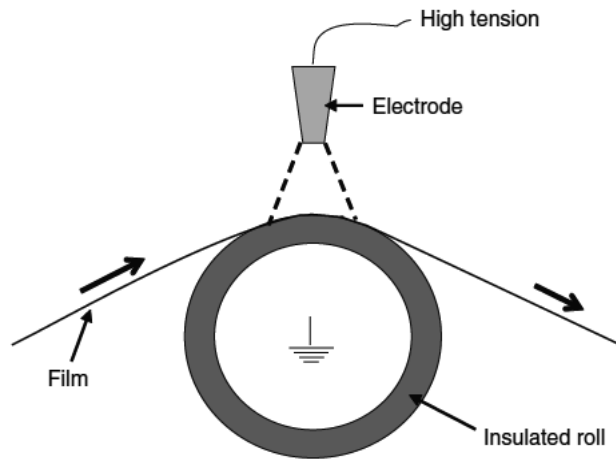


Figure 4. Schematic of corona discharge treatment process [6]

chemical vapor deposition (CVD), physical vapor deposition (PVD), surface grafting, and layer-by-layer deposition [2, 7, 8, 9, 10, 11, 12, 13].

In physical vapor deposition (PVD), vaporized material is deposited on the substrate surface uniformly as a thin film in a vacuum environment where the use of different coating materials is possible [14]. Coatings on polymeric materials by PVD methods have been found to improve the surface properties without altering the bulk properties [15, 16, 17, 18]. PVD techniques offer advantages over conventional textile coating [10, 12, 16, 19, 20, 21], since it is an environmentally friendly, solvent-free process without any need to dispose of any liquid waste. Moreover, a strong bonding is achieved between the fibrous substrate and coating layer.

PVD techniques are commonly used for coating very thin metallic or ceramic films on different substrates. Sputtering is a PVD technology in which atoms are ejected from a solid target material through bombarding the target by energetic ions in a plasma confinement. These atoms condense on the substrate and form a thin film. Sputtering techniques include direct current (DC) sputtering, radio frequency (RF) sputtering, reactive sputtering, and magnetron sputtering [12].

Wei et al. [22] studied the interfacial bonding between polypropylene (PP) fibrous nonwoven substrate and sputter-coated copper. Adhesion of the coating layer to the PP fibrous substrate was found to be affected from plasma treatment and heat during the sputtering process. PP nonwoven showed the lowest abrasion resistance among the tested materials, whereas the sputtered copper coating significantly improved its abrasion resistance further.

Deposition of layers onto the substrates by chemical vapor deposition (CVD) is achieved by chemical reactions in a gaseous medium [23]. A thin film is deposited on the substrate surface through decomposing and/or reacting one or more volatile precursor materials using plasma energy [2]. Different monomers such as methane, hexamethyldisiloxane, tetramethylsilane, hexafluoropropylene ethylene, butadiene, hydroxyethylmethacrylate, and *N*-vinylpyrrolid-

done have been used in plasma-enhanced chemical vapor deposition processes to obtain surface coatings with different functionalities such as oleophobic, hydrophobic, and corrosion-resistant [24].

1.2.2.1. Industrial-scale production-line application

Atmospheric pressure plasma CVD (APCVD) offers a continuous processing opportunity in textile production. The disadvantages such as costs and operating difficulties related to high vacuum equipment are eliminated and the need to interrupt the line is avoided since a continuous coating process is possible instead of a batch process. An atmospheric pressure plasma CVD system is schematically shown in Fig. 5.

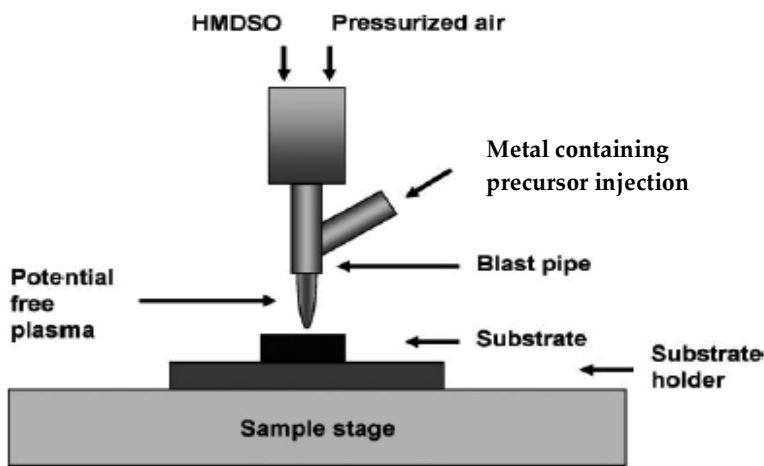


Figure 5. Schematic view of the APCVD system [25]

On a commercial scale, reactor geometry, gas feed, heat distributions are important for delivering coatings that are uniform across the substrate [12].

Oxidative chemical vapor deposition (OCVD) is a novel technique to obtain uniform polymer layers on a variety of flexible and rigid substrates that does not require any solvent to be processed while depositing uniform, thin polymer layers on various substrates [26].

ALD (atomic layer deposition) is another vapor phase vacuum film deposition technique that can generate thin conformal deposited layers by successive surface reactions of a precursor and a reactive gas [27, 28]. This technique has the advantages of precise thickness control and uniformity and conformability of the deposited layer on the substrate [27]. Metallic, nitride, or oxide films such as aluminum oxide can be deposited on nonwovens by this technique [28]. In comparison to the regular thermal ALD, in plasma-enhanced ALD, the reactant gas flows through a plasma source providing shorter deposition time, and lower deposition temperatures allow coating on heat-sensitive fibers and denser films can be produced [28].

2. Plasma treatment for improvement of wettability, printability, and dyeability of nonwovens

Plasma treatment, depending on the type of process gas, changes not only the surface morphology but also leads to a change in chemical composition of the surface. For instance, when oxygen is used as process gas, different oxygen-containing functional groups, such as $-OH$, $-C=O$, $-COOH$, are introduced onto the surface of the nonwoven [3, 29]. Therefore, oxygen plasma treatment was found to increase the dye-uptake and printability of textiles [3].

DuPont's Tyvek® is a flash-spun and calendered nonwoven substrate made of high-density polyethylene fibers. It is a paper-like, dense substrate providing a smooth medium for printing signs, banners, and other graphics. Tyvek® has a corona discharge treatment on one side. SEM cross-sectional image (Fig. 6) shows the micropores created on the treated side where the ink is wicked through [30]. Electronic charging during corona treatment of the substrate oxidizes the surface and increases the wettability of the substrate. This improves adhesion of ink, adhesive, and coating to Tyvek® [31].

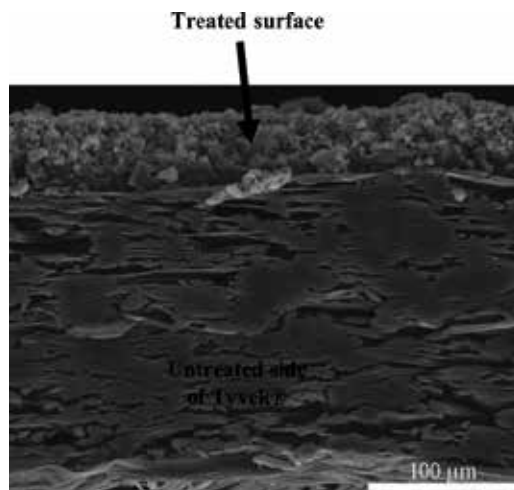


Figure 6. SEM cross-sectional image of plasma surface treated Tyvek® [30]

Enercon Industries Corp. [32] manufactures industrial atmospheric plasma treatment systems for nonwovens operating at low temperature and atmospheric pressure.

3. Plasma treatment for enhancement of adhesion properties of nonwovens

Surface modification of textiles by plasma treatment has been used for the adhesion enhancement of fibers and fabrics. Introduction of functional groups at the fiber surface helps to form affinity or chemical bonds with a coating material leading to an adhesion improvement [33,

34, 35]. For instance, Šimor et al. [36] used atmospheric-pressure nitrogen plasma as a pre-treatment to render the surface of polyester nonwoven fabric hydrophilic for subsequent electroless nickel plating.

However, bonding should be immediately performed following plasma treatment, since storage may result in a reduction or loss of adhesion to the treated surface [6].

Rombaldoni et al. [33] used low-temperature oxygen plasma treatment to enhance the adhesion between polypropylene nonwoven and poly(ethylene oxide) and polyamide-6 nanofibrous mats deposited onto polypropylene nonwoven. Improvement of adhesion between the nonwoven and the nanofibrous coatings was reported, which was attributed to the increased wettability of the supporting polypropylene fabric and polar functional groups introduced by plasma treatment allowing a stronger interaction between the treated fabric and coatings [33, 35].

Li et al. [37] fabricated a high-performance battery separator where they used polypropylene nonwoven as the support material. A fluorinated polymer, octafluoropentyl methacrylate, was grafted onto the surface of the polypropylene nonwoven by plasma treatment to improve the nonwoven's adhesion with poly(vinylidene fluoride-co-hexafluoropropylene).

The adhesion (peel bond) strength between two layers of polypropylene spun-bonded nonwovens, plasma treated and laminated by polyurethane-based adhesive, was improved by up to 150% compared to that of the untreated laminated samples [38, 39]. This was attributed to the increased surface roughness of the polypropylene fibers due to the etching effect of the plasma treatment (Fig. 7), leading to enhanced mechanical adhesion between the laminated layers.

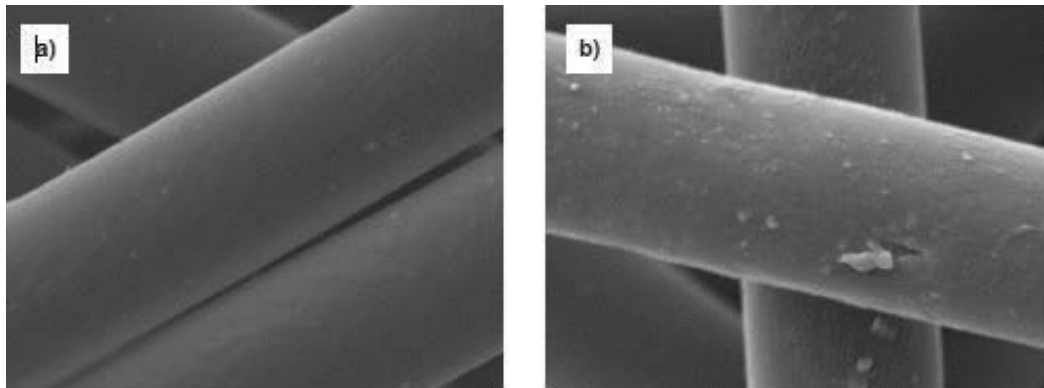


Figure 7. SEM images of PP fibers, (a) untreated ($\times 5060$) and (b) treated by argon plasma at 80 W for 10 min ($\times 5490$) [38]

The plasma-induced changes in surface morphology of polypropylene fibers of a spun-bonded nonwoven on the nanometer scale was demonstrated by [40] via AFM (atomic force microscopy) analysis (Fig. 8). It was found that plasma treatments increased the fiber surface area

and surface roughness due to fiber etching by the bombardment of the fiber surface by plasma-generated energetic particles and reactive particles.

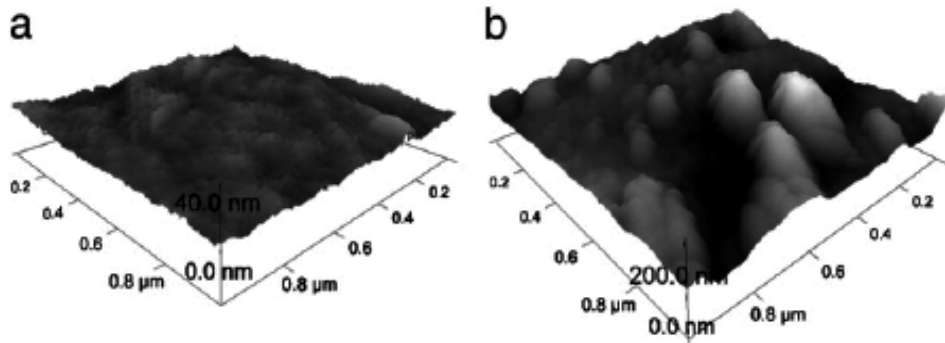


Figure 8. AFM images of (a) untreated and (b) dielectric barrier discharge plasma-treated spun-bonded polypropylene fabric [40]

Armağan et al. [29] reported about 28–60% improvement in the adhesion (peel-off) strength of oxygen plasma pretreated and laminated cotton/polypropylene fabrics using an acrylic-based adhesive compared to untreated laminated samples. After 40 washing cycles, an improvement in peel-off strength of plasma pretreated and laminated samples compared to that of untreated laminated samples was also reported. The improvement was attributed to the increased wettability of the surfaces with oxygen plasma treatment contributing to the adequate wetting of the surface by the adhesive. Functional groups introduced to the fiber surface resulted in better interaction between the adhesives and the plasma-pretreated fabric surface.

The change of the functional side groups on a polypropylene spun-bonded nonwoven after oxygen plasma treatment was determined by high-resolution XPS analysis of C1s peaks [29]. It was observed that the amount of C–C/C–H group decreased, while the amount of oxygen-related groups increased (Fig. 9) after the plasma treatment, rendering the fabric surface more wettable.

4. Plasma coating of nonwovens for functional and bioactive coatings

Plasma coating techniques have been utilized to obtain functional and bioactive coatings on nonwovens to improve surface hydrophilicity, hydrophobicity, electrical conductivity, UV and electromagnetic shielding, and antibacterial properties.

Polypropylene nonwoven fabrics are commonly used for hygienic and disposable absorbent products such as diapers, feminine care products, wound dressings, and wipes. In all these applications, nonwoven needs to be wettable by water or aqueous-based liquids [41, 42]. This is usually obtained by coating the fabric with a surfactant solution lowering surface tension of

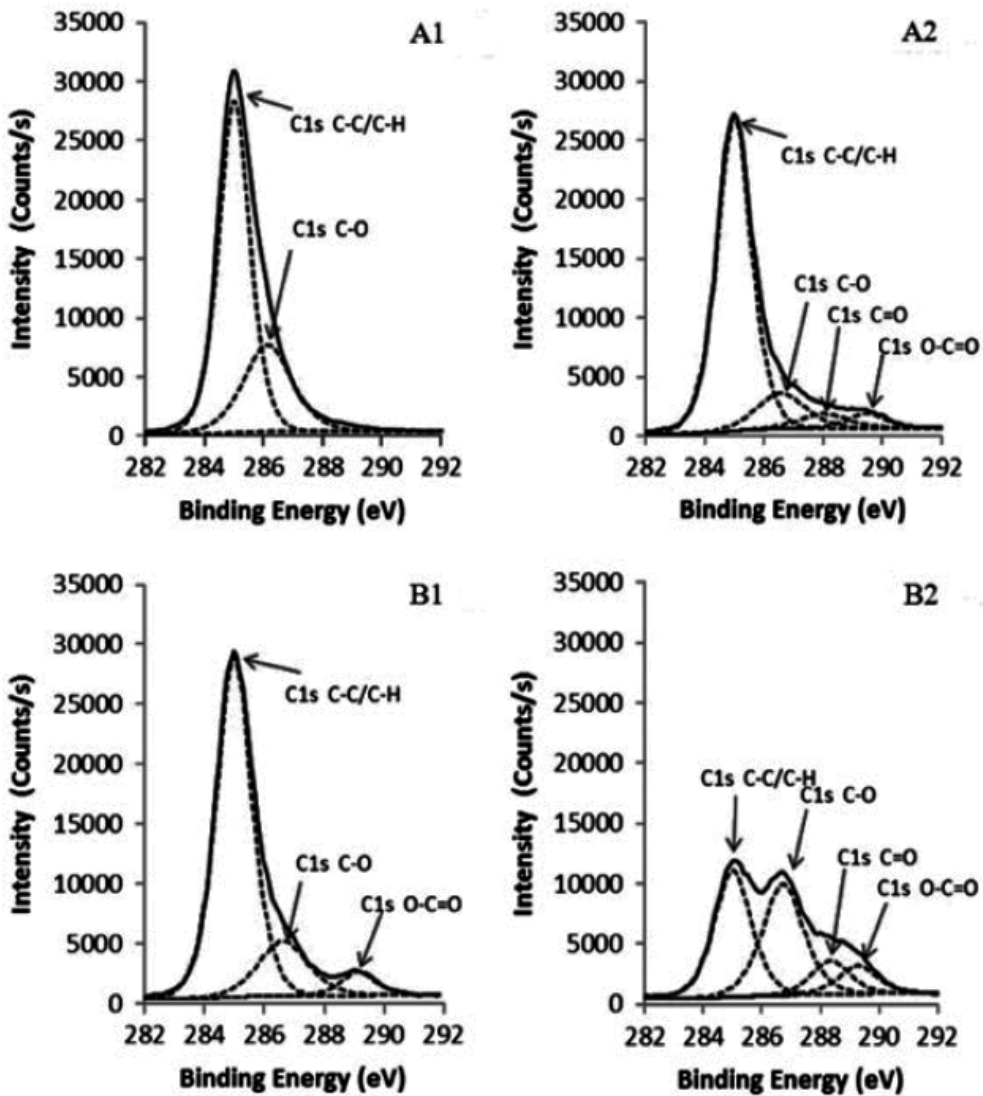


Figure 9. C1s peak of untreated and oxygen plasma treated sample at 80 watt and 10 minutes, (A1) PP untreated, (A2) PP oxygen plasma treated, (B1) cotton untreated, (B2) cotton oxygen plasma treated [29]

the aqueous liquid and subsequent drying of the fabric. In such case, the surfactants are effective in rendering the fabric wettable for a limited time during the use of the product. Surface treatment of nonwoven fabrics using plasma is an alternative method to improve their wettability [41].

Behary et al. [43] activated the surface of a carded and hydroentangled PET (polyethylene terephthalate) nonwoven by an air–dielectric barrier discharge atmospheric plasma. The wettability of the PET nonwoven was enhanced due to plasma treatment which was evident

from considerable decrease in water contact angle results and increase in the proportion of polar groups, in particular carboxyl $-O-C=O-$ groups.

On the other hand, super-hydrophobic, self-cleaning nonwoven surfaces have been produced by imparting of oxides such as TiO_2 and a polymethylsiloxane coating on cellulose via CVD technique [12]. Sobczyk-Guzenda et al. [44] used radio frequency plasma-enhanced chemical vapor deposition technique to deposit thin TiO_2 film (Fig. 10) on cotton fabric to impart a self-cleaning effect under UV illumination through a photooxidizing activity.

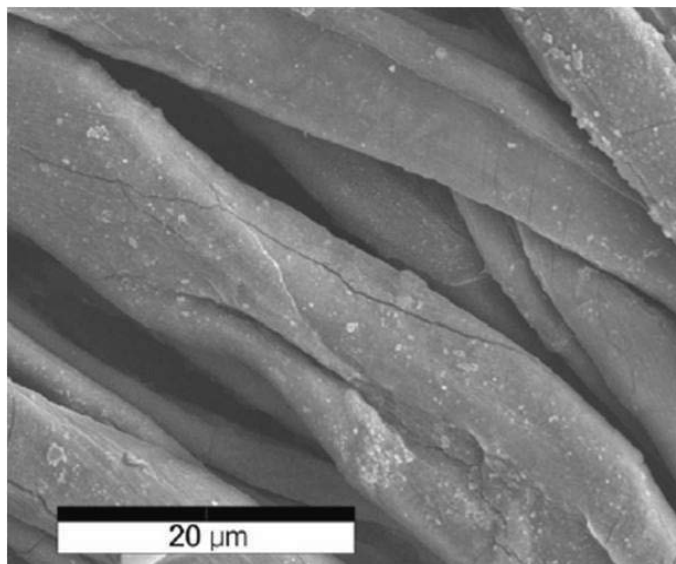


Figure 10. Scanning electron microscope picture of plasma deposited TiO_2 coating on cotton fabric [44]

The surface wetting of the nonwoven materials was changed by deposition of different materials through sputtering. Wei et al. [10] performed the deposition of copper, zinc oxide (ZnO), and polytetrafluoroethylene (PTFE) on the surface of polypropylene meltblown nonwoven through sputtering. While copper coating improved the surface conductivity of the material, ZnO coating significantly increased the UV absorption of the material necessary for UV shielding. Both Cu and ZnO coating rendered the nonwoven surface hydrophilic. Deposition of PTFE provided surface hydrophobicity on the nonwoven material due to increase in surface contact angle and roughness [10]. Sputter coatings of copper and silver on spun-bonded polypropylene nonwovens provided reduced transmittance both in UV and visible light ranges [20].

Deng et al. [45] and Wei et al. [46] reported a decrease in electrical resistance of aluminum and copper sputtered polypropylene spun-bonded nonwovens. Aluminum-doped zinc oxide (AZO) and doped indium oxide (ITO) films were deposited onto the polypropylene nonwo-

vens by magnetron sputtering. For the same thickness, nonwoven materials coated with ITO showed a lower electrical resistance than those coated with AZO. The nanoscale AZO coating on nonwoven provided better UV protection than ITO coating for the same thickness [20]. Jianfeng et al. [47] studied the electromagnetic shielding efficiency of PET nonwovens by sputtering of nanoscaled Cu, Ag, Ag/Cu, and Ag/Cu/Ag films.

In another study, Baek et al. [48] used microwave-induced argon plasma to modify and sputter-coat the surface of nanofibrous silk fibroin scaffolds with gold/platinum to enhance the attachment and proliferation of the human articular chondrocyte cultures.

Nonwovens currently find applications in various industries such as medical and hygiene, home textiles such as mattresses, floor coverings, and shoe linings. A suitable environment for infection by microorganisms is created especially in nonwoven products used in hospitals, hotels, and the clothing of the personnel. Nonwovens made from natural fibers such as cotton are more susceptible to bacterial proliferation than synthetics due to the moisture content of natural fibers.

Antibacterial property has been imparted to nonwovens by the application of antibacterial finishes such as metallic ions of silver [40, 49], copper, and their compounds, also phenols, quaternary ammonium salts, and organosilicones. Nontoxicity of the antibacterial agent becomes critical depending on the end-use of the product.

Mazlounpour et al. [50] used atmospheric pressure glow discharge plasma to impart antimicrobial properties to a polypropylene spun-bond nonwoven. A durable antimicrobial property was achieved on the nonwoven by plasma grafting of diallyldimethylammonium chloride (DADMAC) in the presence of a cross-linker.

Several studies showed metal, that is, silver, sputtering onto polypropylene and polyester nonwovens and polyacrylonitrile electrospun nonwovens to impart antibacterial property [51, 52, 53]. Shahidi et al. [16] deposited copper onto the surface of cotton fabric samples by DC magnetron sputtering for antibacterial effect and found that duration of the application process was shorter compared to conventional application processes using nonionic detergent and metallic salts. The obtained antibacterial effect was found to be durable against 30 washing cycles.

Plasma deposition has also been used to impart flame retardancy to nonwovens. Acrylate monomers containing phosphorus have been plasma grafted on cotton and PET/cotton fabrics. Plasma enhanced chemical vapor deposition of an organosilicon thin film on polyamide 6 has been performed using the cold remote nitrogen plasma process [54].

5. Conclusion

Nonwoven fabrics have a wide variety of applications such as cleaning cloths, wipes, filters, disposable gowns and drapes, baby diapers, mattress coverings, shoe linings, insulating materials, and many others. According to EDANA [55], a trade organization in Europe, around

1,954 million tons of nonwovens (roll goods) were produced in 2012. There has been a significant growth for nonwovens market and between 2013 and 2018; a significant growth rate of 7.6% (tonnage) is predicted for global nonwovens market according to a market report by Smithers Apex [56].

Nonwoven technologies offer the ability to easily manipulate fabric properties such as porosity, weight, mechanical strength, and surface textures much more cost-effectively than their woven or knitted counterparts. Additional functionalities can be added to nonwovens by padding and coating treatments; therefore, functional performance of the final product can be enhanced. The conventional methods for coating application include wet chemical processes where there is use of large quantities of chemicals, solvents, water, and energy. There are major drawbacks for conventional wet processes such as use of toxic solvents that are harmful to human health and environment, large quantities of energy and water consumption, and disposal of chemicals.

Plasma surface treatments have been shown to have unique advantages including environment-friendly process, low production cost, and modification of only the upper molecular layers of the substrates without changing the material's bulk properties. Plasma treatment has been recognized as an alternative ecological surface treatment to conventional wet textile coating and finishing treatments.

Plasma-based techniques offer many opportunities to obtain different surface functionalizations on various substrates. Surface properties of nonwovens can be engineered from hydrophilic to super-hydrophobic with plasma treatments. Plasma techniques provide many surface treatment possibilities such as surface cleaning, surface activation, etching, surface roughening, thin film deposition at nanoscale and grafting. With plasma coating techniques, tailor-made surfaces can be created with specific functions such as flame retardancy, electrical conductivity, antibacterial, or self-cleaning effects.

The low surface energy fibers such as polypropylene and polyester are widely used in many nonwoven applications and inherently they are hydrophobic, so their wettability is generally achieved by a hydrophilic surface treatment such as a wet-chemical treatment. Plasma processes have been successfully applied to improve the wettability of inherently hydrophobic surfaces. Moreover, plasma treatment has been recognized as a pretreatment technique for enhancement of the adhesion of a nonwoven surface to another or a coating layer to a nonwoven substrate. The addition of oxygen-containing functional groups, such as $-OH$, $-C=O$, $-COOH$, on surfaces through plasma treatment was found to increase the dye-uptake and printability of nonwoven substrates.

Plasma technology continues to offer opportunities to tailor the surface properties of nonwovens and impart unique characteristics to the fabrics; yet there are still challenges in the integration of the plasma systems to industrial-scale roll-to-roll production lines. Although there are available industrial atmospheric plasma treatment systems, particularly the incorporation of plasma thin-film deposition to industrial roll-to-roll processes is still at an evolving stage.

Author details

Burçak Karagüzel Kayaoğlu

Address all correspondence to: bkayaoglu@itu.edu.tr

Istanbul Technical University, Faculty of Textile Technologies and Design, Department of Textile Engineering, Istanbul, Turkey

References

- [1] Yang Q., Yu L., Wang Y., Wei Q., Functionalization of textile materials by plasma enhanced modification, *J Indus Textiles* 2007, 36(4): 301-309.
- [2] Shim E., Chapter 3. 'Smart surface treatments for textiles for protection' in Chapman R., *Smart Textiles for Protection*, Woodhead Publishing Limited 2013, 87-126.
- [3] Vohrer, U., Chapter 8. 'Interfacial engineering of functional textiles for biomedical applications' in Shishoo, R., *Plasma Technologies for Textiles*, Woodhead Publishing Limited 2007, 202-227.
- [4] Shufang, L.I., Surface treatment of PET nonwovens with atmospheric plasma, *Plasma Sci Technol* 2013, 15, 1: 82-85.
- [5] Tsai, C.-Y., Wei, T.-C., Chen, K.-S., Juang, R.-S., Huang C., Tailoring surface properties of nonwoven polypropylene by cyclonic atmospheric pressure plasma 2014, *IEEE Transact Plasma Sci*, 42, 12: 3668-3673.
- [6] Troughton, M. J., Chapter 17. 'Adhesive bonding' in *Handbook of Plastics Joining: A Practical Guide*, Second Edition, William Andrew Inc. TWI, Norwich, NY, USA, 2008, 145-173.
- [7] Deng, B., Yan, X., Wei, Q., Gao, W., AFM characterization of nonwoven material functionalized by ZnO sputter coating, *Mater Character* 2007a, 58: 854-858.
- [8] Xu, Y., Wei, Q. F., Wang, Y. Y., Huang, F. L., Preparation of TiO₂ coated on fabrics and their photocatalytic reactivity, *J Donghua Univ* 2007, 24: 333-336.
- [9] Jiang, S.X., Qin, W.F., Guo, R.H., Zhang, L., Surface functionalization of nanostructured silver-coated polyester fabric by magnetron sputtering, *Surf Coat Technol* 2010, 204: 3662-3667.
- [10] Wei, Q., Yu, L., Hou, D., Huang, F., Surface characterization and properties of functionalized nonwoven, *J Appl Polymer Sci* 2008a, 107: 132-137.
- [11] Wei, Q., Yu, L., Wu, N., Hong, S., Preparation and characterization of copper nanocomposite textiles, *J Indus Textiles* 2008b, 37(3): 275-283.

- [12] Wei, Q., Chapter 3. 'Textile surface functionalization by physical vapor deposition (PVD)' in *Surface Modification of Textiles*, Woodhead Publishing in Textiles, The Textile Institute 2009a, 58-79.
- [13] Spagnola J.C., *Atomic layer deposition on fiber-forming polymers and nonwoven fiber structures*. PhD Thesis, Raleigh, North Carolina State University 2010, 7-12.
- [14] Mattox D.M., Chapter 7. 'Physical sputtering and sputter deposition (sputtering)' in *Handbook of Physical Vapor Deposition (PVD) Processing*, Westwood, NJ, Noyes Publications 1998, 237-286.
- [15] Wei, Q., Wang, Y., Wang, X., Huang, F., Yang, S., Surface nanostructure evolution of functionalized polypropylene fibers, *J Appl Polym Sci* 2007, 106: 1243-1247.
- [16] Shahidi, S., Ghoranneviss, M., Moazzenchi, B., Rashidi, A., Mirjalili, M., Investigation of antibacterial activity on cotton fabrics with cold plasma in the presence of a magnetic field, *Plasma Process Polym* 2007, 4: S1098-S1103.
- [17] Dietzel, Y., Przyborowski, W., Nocke, G., Offermann, P., Hollstein, F., Meinhardt, J., Investigation of PVD arc coatings on polyamide fabrics, *Surf Coat Technol* 2000, 135: 75-81.
- [18] Körner, E., Rupper, P., Lübben, J.F., Ritter, A., Rühle, J., Hegemann, D., Surface topography, morphology and functionality of silver containing plasma polymer nanocomposites, *Surf Coat Technol* 2011, 205: 2978-2984.
- [19] Wei, Q. F., Wang, X.Q., Gao, W. D., AFM and ESEM characterization of functionally nanostructured fibers, *Appl Surf Sci* 2004, 236, 456-460.
- [20] Wei, Q., Shao, D., Deng, B., Xu, Y., Comparative studies of polypropylene nonwoven sputtered with ITO and AZO, *J Appl Polym Sci* 2009b, 114: 1813-1819.
- [21] Xu, Y., Wu, N., Wei, Q., Pi, X., Preparation and the light transmittance of TiO₂ deposited fabrics, *J Coat Technol Res* 2009, 6 (4): 549-555.
- [22] Wei, Q., Xu, Q., Cai, Y., Wang, Y., Evaluation of the interfacial bonding between fibrous substrate and sputter coated copper, *Surf Coat Technol* 2008c, 202, 4673-4680.
- [23] Bhat D.G, Chapter 32. 'Chemical Vapor Deposition', in Satas D. and Tracton A.A, *Coatings Technology Handbook*, New York, Marcel Dekker, Inc. 2001, 313-325.
- [24] Kaplan, S., Plasma processes for wide fabric, film and non-wovens, *Surf Coat Technol* 2004, 186: 214-217.
- [25] Zimmermann, R., Pfuch A., Horn, K. Weisser, J., Heft, A. Röder, M., Linke, R., Schnabelrauch, M., Schimanski, A., An approach to create silver containing antibacterial coatings by use of atmospheric pressure plasma chemical vapour deposition (APCVD) and combustion chemical vapour deposition (CCVD) in an economic way, *Plasma Process Polym* 2011, 8: 295-304.

- [26] Bashir, T., Skrifvars, M., Persson, N.K., Production of highly conductive textile viscose yarns by chemical vapor deposition technique: a route to continuous process, *Polym Adv Technol* 2011, 22, 2214-2221.
- [27] George, S.M., Atomic layer deposition: an overview, *Chemic Rev* 2010, 110(1): 111-131.
- [28] Musschoot, J., Dendooven, J., Deduytsche, D., Haemers, J., Buyle, G., Detavernier, C., Conformality of thermal and plasma enhanced atomic layer deposition on a non-woven fibrous substrate, *Surf Coat Technol* 2012, 206: 4511-4517.
- [29] Armağan O.G., Karagüzel Kayaoğlu B., Canbaz Karakaş H., Plasma-induced adhesion improvement of cotton/polypropylene-laminated fabrics, *J Adhesion Sci Technol* 2013b, 27, 21: 2326-2339.
- [30] Karaguzel, B., Tafreshi H. V., Pourdeyhimi B., Potentials and challenges in jetting microdroplets onto nonwoven fabrics, *J Textile Instit* 2008, 99(6): 581-589.
- [31] <http://www.materialconcepts.com/products/tyvek> (date of access: June, 25, 2015)
- [32] <http://www.enerconind.com/treating/index.aspx> (date of access: June, 26, 2015)
- [33] Rombaldoni, F., Mahmood, K., Varesano, A., Songia, M.B., Aluigi, A., Vineis, C., Mazzuchetti, G., Adhesion enhancement of electrospun nanofiber mats to polypropylene nonwoven fabric by low-temperature oxygen plasma treatment, *Surf Coat Technol* 2013, 216: 178-184.
- [34] Xin, Z., Yan, S., Ding, J., Yang, Z., Du, B., Du, S., Surface modification of polypropylene nonwoven fabrics via covalent immobilization of nonionic sugar-based surfactants, *Appl Surf Sci* 2014, 300: 8-15.
- [35] Colmenares, J.C., Kuna, E., Jakubiak, S., Michalski, J., Kurzydłowski, K. Polypropylene nonwoven filter with nanosized ZnO rods: Promising hybrid photocatalyst for water purification, *Appl Catalys B: Environment* 2015, 170-171: 273-282.
- [36] Šimor, M., Ráhel, J., Černák, M., Imahori, Y., Miloslav Štefečka, M., Kando, M., Atmospheric-pressure plasma treatment of polyester nonwoven fabrics for electroless plating, *Surf Coat Technol* 2003, 172: 1-6.
- [37] Li, X., He, J., Wu, D., Zhang, M., Meng, J., Ni, P., Development of plasma-treated polypropylene nonwoven-based composites for high-performance lithium-ion battery separators, *Electrochim Acta* 2015, 167: 396-403.
- [38] Armağan O.G., Karagüzel Kayaoğlu B., Canbaz Karakaş H., Güner F. S., Improving the adhesion strength of polypropylene nonwoven laminated fabrics using low-pressure plasma, *Fibres Textiles East Eur* 2013, 21, 3(99): 96-101.
- [39] Armağan O.G., Karaguzel Kayaoglu B., Canbaz Karakas H., Guner F. S., Adhesion strength behaviour of plasma pre-treated and laminated polypropylene nonwoven fabrics using acrylic and polyurethane-based adhesives, *J Indus Textiles* 2014, 43(3): 396-414.

- [40] Radić, N., Obradović, B.M., Kostić, M., Dojčinović, B., Kuraica, M.M., Černák, M., Deposition of silver ions onto DBD and DCSBD plasma treated nonwoven polypropylene, *Surf Coat Technol* 2012, 206: 5006-5011.
- [41] Ráhel, J., Šimor, M., Černák, M., Štefečka, M., Imahori, Y., Kando, M., Hydrophilization of polypropylene nonwoven fabric using surface barrier discharge, *Surf Coat Technol* 2003, 169-170: 604-608.
- [42] Chen, K.-S., Ku, Y.-A., Lee, C.-H., Lin, H.-R., Lin, F.-H., Chen, T.-M., Immobilization of chitosan gel with cross-linking reagent on PNIPA Am gel/PP nonwoven composite surface, *Mater Sci Engin* 2005, C 25: 472-478.
- [43] Behary, N., Perwuelz, A., Campagne, C., Lecouturier, D., Dhulster, P., Mamede, A.S. Adsorption of surfactin produced from *Bacillus subtilis* using nonwoven PET (polyethylene terephthalate) fibrous membranes functionalized with chitosan, *Coll Surf B: Biointerfaces* 2012, 90: 137-143.
- [44] Sobczyk-Guzenda, A., Szymanowski, H., Jakubowski, W., Błasińska, A., Kowalski, J., Gazicki-Lipman, M., Morphology, photocleaning and water wetting properties of cotton fabrics, modified with titanium dioxide coatings synthesized with plasma enhanced chemical vapor deposition technique, *Surf Coat Technol* 2013, 217: 51-57.
- [45] Deng, B.Y., Wei, Q. F., Gao, W. D., Yan, X., Surface functionalization of nonwoven by aluminum sputter coating, *Fibres Textiles East Eur* 2007b, 15, 4: 90-92.
- [46] Wei, Q., Xiao, X., Hou, D., Ye, H., Huang, F., Characterization of nonwoven material functionalized by sputter coating of copper, *Surf Coat Technol* 2008d, 202: 2535-2539.
- [47] Jianfeng, D. I., Wenqin, D. U., Fei, Y.U., Honjin, Q.I., Multi-functional nanoscaled film deposited on pet non-woven by sputtering, *Adv Mater Res* 2009, 79-82:557-560.
- [48] Baek, H.S., Park, Y.H., Ki, C.S., Park, Y.C., Rah, D.K., Enhanced chondrogenic responses of articular chondrocytes onto porous silk fibroin scaffolds treated with microwave-induced argon plasma, *Surf Coat Technol* 2008, 202: 5794-5797.
- [49] Amberg, M., Grieder, K., Barbadoro, P., Heuberger, M., Hegemann, D., Electromechanical behavior of nanoscale silver coatings on PET fibers, *Plasma Process Polym* 2008, 5: 874-880.
- [50] Mazloumpour, M., Malshe, P., El-Shafei, A., Hauser, P., Conferring durable antimicrobial properties on nonwoven polypropylene via plasma-assisted graft polymerization of DADMAC, *Surf Coat Technol* 2013, 224: 1-7.
- [51] Scholz, J., Nocke, G., Hollstein, F., Investigation on fabrics coated with precious metals using magnetron sputtering technique with regard to their anti-microbial properties, *Surf Coat Technol* 2005, 192: 252-256.
- [52] Wang, H.B., Wang, J. Y., Wei, Q. F., Hong, J. H., Zhao, X. Y., Nanostructured antibacterial silver deposited on polypropylene nonwovens, *Surf Rev Lett* 2007a, 14: 533-557.

- [53] Wang, H., Wang, J., Hong, J., Wei, Q., Gao, W., Zhu, Z., Preparation and characterization of silver nanocomposite textile, *J Coat Technol Res* 2007b, 4 (1): 101-106.
- [54] Duquesne S. and Bourbigot, S., Chapter 4. 'Flame retardant nonwovens' in Chapman R., *Applications of Nonwovens in Technical Textiles*, Woodhead Publishing Limited 2010, 65-84.
- [55] <http://www.edana.org/discover-nonwovens/facts-and-figures> (date of access: July, 01, 2015)
- [56] <http://www.smithersapex.com> (date of access: June, 28, 2015)

Damage Prediction in Woven and Non-woven Fabric Composites

Masoud Haghi Kashani and Abbas S. Milani

Additional information is available at the end of the chapter

<http://dx.doi.org/10.5772/61511>

Abstract

This chapter presents a step-by-step review on different damage prediction approaches for woven and non-woven fabric composites. First, the characteristics of woven and non-woven fabrics are distinguished one from another, suggesting more complex analyses required for non-woven fabrics. Then, the subsequent sub-sections are geared toward a comparison of different approaches utilized in predicting the mechanical behavior and damage mechanisms of these composites at various material scales including micro, meso, and macro. The merits and demerits of each approach with regard to practicality, accuracy, effectiveness, and characterization expense are discussed. Moreover, using recent experimental evidences, the chapter aims to highlight a number of inherent complexities in the interlaced architecture of woven composites, which may not be precisely taken into account by the damage models originally developed for non-woven and unidirectional composites. Finally, two illustrative examples on the effect of the aforementioned complexities on the mechanical behavior of woven composites are presented in more detail, through some recent works of the authors.

Keywords: Fabric reinforced composites, Damage mechanisms, Prediction models, Advanced characterization

1. Introduction

Several decades ago, composite materials were introduced with a great potential to replace conventional monolithic materials, primarily metals, due to two main features:

- Much higher ratios of stiffness and strength to weight
 - Anisotropy of material properties, providing designers with more flexible design options
-

Since the dawn of composite materials (1937), “unidirectional” (UD) fiber reinforced composite materials caught most of the designers’ attention for several years, primarily due to their high specific stiffness ratios as well as simplicity in their analyses/design. Nevertheless, woven fiber reinforced composites gradually became a decent alternative to traditional UD composites in specific industries [1]. Woven fabric reinforcement in essence can be defined as interlaced warp and weft fibers in a repetitive pattern or weave style such as plain, twill, satin, etc. Woven composites can enjoy numerous inherent characteristics—all of which arising from their interlaced fibrous structure [1]:

- Laminated composites comprised of UD architecture are often inclined toward experiencing delamination, which in turn can decrease their stiffness and yield low damage tolerance. Instead, interlaced yarns in two directions of woven fabric reinforced composites can decrease the mismatch between laminate layers, and hence helping the material system resist de-bonding and its propagation in a superior manner.
- The undulation of yarns, resulting from the interlacing yarns, induces an out-of-plane reinforcement state in woven textile composites, whereas UD composites generally suffer from a weak resistance through the thickness direction.
- The manufacturing process of woven fabric composites is generally easier than the UD. This is mainly because of the yarns entanglement, easing the draping and molding process of the material for producing near-net shapes.
- Woven fabric plies, due to their bi-directional reinforcement, can show a much more balanced behavior than the UD under complex loading modes in service.

In addition to woven fabrics, there exists another main type of fabric reinforcement known as ‘non-woven’ fabrics, which also include ‘felts’. Non-woven fabrics are sheets or web structures comprised of chopped or long fibers or filaments arranged in a rather disordered architecture and consolidated by bonds of different nature, such as chemical, mechanical (e.g., stitching), or thermal bonding, rather than geometrical weaving or knitting. According to this definition, the distinct differences between woven and non-woven fabrics are the fibers arrangement at the microstructural level and the type of bonding. Woven fabrics have an ordered architecture of fibers interlaced to one another, whereas there is more randomness in the fibrous architecture of non-woven fabrics. Recently, in light of lower processing cost of non-woven composites, and easier recyclability in some cases, the use of these materials is being increased in several industrial applications such as fireproof layers, thermal insulations, ballistic protections, liquid-absorbing textiles, and geotextiles for soil reinforcement [2]. Owing to the aforementioned inherent geometrical differences between woven and non-woven fabrics, their mechanical performances are also expectedly different. In general, woven composites enjoy higher stiffness and strength in comparison with non-woven felts. However, the ultimate deformation and absorbed energy values in non-woven fabrics are often higher than woven fabrics [2].

Thanks to defined standards by most governments and related safety authorities, risk-sensitive industries in general, and aerospace and transportation in particular, as the main sectors of the composite world, are expected to satisfy certain requirements before a product can be

brought to service. By flourishing the use of composites more and more, so crucial is the possession of a comprehensive knowledge on their underlying damage mechanisms upon which the ultimate load bearing capacity and deformation of structures can be predicted. As a matter of fact, the design of a composite structure with highest safety and at the same time the lightest possible *weight* cannot be accomplished without a profound knowledge on its damage behavior. Regarding the damage modeling of composite materials, to date there have been much more research activities in the area of UD composites, rather than woven and non-woven fabrics. As an example, according to the World Wide Failure Exercise [3], there are nearly 20 failure theories derived for UD composite materials, while there is a very limited explicit failure criterion specifically developed and standardized for woven composites. Actually, using some assumptions and modifications, the common failure models of UD composite materials, for example the maximum stress criterion, are being used by some practitioners for the damage analysis of woven materials. This practice is despite the fact that none of such failure theories has been originally developed to mimic the woven nature of reinforcing material in consolidated laminate. The fact is, although woven composites are endowed with some advantages in comparison with UD on account of their enhanced fibrous architectures, some intrinsic complications can cause their analysis to be cumbersome and very different from UD. These complexities are briefly introduced in this section and will be further discussed in the next sections of the chapter. One of these difficulties is the change in cross-section of woven yarns over their longitudinal axes. Another one is that fibers are not straight in woven yarns similar to fibers in UD tows. In fact, yarns can have in-plane waviness (misalignment) and out-of-plane waviness (crimping) in woven laminates, which considerably affect their tensile and bending behaviors. Moreover, interaction between the warp and weft yarns may affect the effective mechanical behavior of woven laminates, especially under multi-directional/combined loading modes, similar to its significant effect on the mechanical behavior of dry fabrics. Furthermore, owing to a cellular reinforcement architecture, failure modes such as matrix cracking is restricted between weave cells in woven composites and cannot propagate as fast as it would in UD. Another point is that the interlacement of yarns can cause local stress concentrations at meso-level. More severe complications come in the behavior of non-woven fabrics due to their rather random architecture and complex contact between fibers. Fiber re-orientation, fiber sliding, non-linear bond failure, fiber fracture, and continuous rearrangement of fibrous network are among other difficulties encountered in the analysis of non-woven fabrics [2].

The rest of this chapter attempts to review the methods employed by different researchers to investigate the mechanical behavior of woven and non-woven fabric composites in general, and their damage mechanisms in particular. Benefits as well as disadvantages of each approach are discussed by relating to the above-described inherited complexities in fabric composites. In addition, the validity of presumed assumptions for each approach is argued. For woven composites, different approaches will be discussed in sub-sections 2.1.1–2.1.3, and the approaches employed to predict the mechanical behavior of non-woven fabrics, which are methodically similar to those of woven composites, are reviewed in section 2.2. Thereafter, the above-addressed incompatibility of previous damage models of UD to accurately anticipate the mechanical behavior of fabric composites is assessed. In particular, it is argued that owing

to complex reinforcement architecture in woven composites, new enhanced damage models need to be driven. In order to further underscore this need, some recent experimental evidences by the authors regarding the influence of in-plane and out-of-plane waviness of yarns upon the mechanical behavior of a typical woven composite is presented. The last section of the chapter outlines the main conclusions and the anticipated future work developments.

2. Damage modeling approaches for fabric composites

Preparatory to discussing the damage mechanisms of woven and non-woven fabrics, a definition for an appropriate damage model should be provided. Generally, a comprehensive and accurate damage model for a given material would embrace three features:

- **Damage initiation:** Exploiting precise and reasonable failure criteria to predict the onset of various failure modes is the primary part of any damage model.
- **Degradation of material properties:** On account of any damage in a material, it cannot provide stiffness and strength as high as its undamaged state. Anticipating a reasonable pattern to reduce the mechanical properties of the material upon damage is another critical aspect of a full-scale damage model.
- **Damage propagation:** How an induced damage grows is perhaps the most controversial part of any damage model. Forecasting the rate of damage growth with an acceptable accuracy imparts the post-damage behavior and tolerance of a manufactured structure/product during service.

The studies investigating damage in woven and non-woven fabric materials can be classified in different ways. One categorization may be with respect to the group of studies on each of the three aforementioned features of a damage model. Another classification is based on the investigations methodology. Researchers have performed analytical, numerical, and experimental methods in order to study the damage behavior of fabric composite materials. The numerical and analytical studies are in turn divided to micro, meso, and macro. The latter type of classification is the one opted here for the subsequent review sections.

2.1. Damage models for woven fabric composites

2.1.1. *Micro/meso level analyses*

Despite the fact that composite materials are predominantly regarded as homogeneous orthotropic materials, notably in industrial projects, they are not as homogeneous as conventional materials such as metals. Composites are comprised of fibers and matrix constituents and therefore the mechanical properties of different points of the material medium are not necessarily the same. In fact, it is this specific feature of composite materials that distinguishes their global behavior. As an illustration, when a visible macro-damage is observed in a composite specimen under loading, failure has already initiated and propagated in the micro/meso level of the specimen before it appears at macro level. As a consequence, one of the ways

to study the failure mechanism of fabric composite materials is to conduct an investigation into the micro/meso levels. However, studying full scale structures/specimens at these levels is more arduous and expensive in comparison to the macro level. In order to carry out the micro/meso level analyses of composite materials in a cost-effective manner, the smallest segment of a whole specimen is sometimes defined such that it is the representative of the whole specimen. That is, the whole specimen should be reproducible by repeating this representative volume element (RVE). Homogenization—the main basic rule in the RVE approach—is then employed to define the effective mechanical properties of the RVE based on the mechanical properties of its constituents, namely fibers and matrix. The effectiveness of the micro/meso-level investigation for woven composite materials is deemed to be more, when compared to unidirectional composites, in that the micro-structure of woven architectures is more complicated and may not be idealized at macro-levels.

The woven composite RVEs can be mainly studied in two ways. The first method is to model yarns in warp as well as fill directions and matrix in a detailed numerical model with shell or solid elements. In this approach, the yarns and matrix are considered explicitly. In one of the first study of this kind, Blacketter et al. presented a meso-level model for woven composite materials using solid elements [4]. In their simulations, the mechanical properties of yarns, which included fibers and resin, were found based on the micromechanical homogenization approach and the mechanical properties of constituents. The volume fraction of fibers in the yarns and in the unit cell was selected 70% and 60%, respectively. The failure occurrence in the matrix, which was considered isotropic, was based on a maximum stress criterion. In addition, damage degradation was taken into account by decreasing the corresponding Young's modulus of the Gaussian integration points in an element by 99%. Regarding the yarns modeled as orthotropic materials, two failure modes in the longitudinal and transverse directions were assumed. The results of experimental and numerical studies were rather comparable.

In another study, Tang and Withcomb assumed a failure criterion and a linear degradation model for different woven architectures in order to compare their damage mechanisms [5]. They modeled warps, wefts, and matrix pockets of an RVE in a detailed 3D fashion. The maximum stress failure criterion was utilized. The obtained results showed that the weave architecture can have a considerable impact on the composite's progressive damage behavior, even if the volume fraction of fibers, tow waviness, and tow cross-sections of the specimens were the same. Jia et al. established a micro-meso scale model for the repeating unit cells of a 3D woven composite material, in which there were yarns in three principal directions [6]. The yarns in the meso level simulation were composed of repeating micro representative unit cells (RUC) consisting of fibers and matrix. The maximum strain and stress values were monitored as the failure criteria for the damage in the matrix and fibers. As to post-damage behavior, they presumed that the corresponding stress becomes zero instantly. A quadrilateral cross section was employed for the yarns. The results for one tensile testing demonstrated that there is an agreement regarding the ultimate strength prediction by the model; however, there were disagreements between numerical and experimental results at each time step (i.e., different stages of deformation before the final failure). In another research project by the same authors,

the behavior of woven composite materials under three-point bending was investigated at a multi-scale (micro-meso-macro) level [7].

In each of the aforementioned studies, only a fabric cell was modeled, as a periodic boundary condition was used instead of repeating cells to create the whole specimen geometry. In general, there are two types of periodic boundary conditions known as parallel and series models. In a parallel model, it is assumed that the displacement of all constituents (cells) is the same and the load is shared between them. On the other hand, the stress is presumed to be the same in all cells in a series model, and the general displacement is the sum of that of each cell. In order to avoid such boundary assumptions, some researchers have opted to create the whole specimen meso-model by reproducing a large number of cells adjacent to each other. A good example of such approach is the simulation conducted by Chandekar and Kelkar [8]. Making use of LS-DYNA, they investigated the low velocity impact of glass and carbon woven composite materials [8]. The mosaic pattern was chosen to repeat the unit cells so as to produce the whole plate geometry. Although comparable results were observed between numerical and experimental results, running such simulations normally takes a considerable time, comprising their effectiveness for large scale industrial simulations.

In order to reduce computational time in meso-level modeling of woven composites, a second RVE methodology has been introduced. In this approach, the RVE is divided into several sub-cells, instead of a great number of elements. Where one level of homogenization was considered in the first RVE modeling approach, two levels of homogenizations are performed in the second approach; the first of which is to find the general mechanical properties of sub-cells and the second is to determine the general mechanical behavior of the whole cell. The first research in this area was performed by Ishikawa and Chou [9]. Employing the classical laminate theory, they studied the elastic behavior of woven fabric materials in three models, including mosaic, undulation, and bridging models [9]. In the mosaic pattern, the fiber continuity and its crimping were not taken into account. However, these factors were considered in the undulation model. One of the main limitations of this model was that two UD layers were assumed instead of one interlaced layer. After this work, some researchers attempted to conduct investigations into the failure behavior of woven fabric materials using the sub-constituents method [10–12]. In one of the latest papers in this area, Li et al. predicted the stiffness matrix, strength, and damage evolution of woven fabric materials using Abaqus [13]. They used parallel-series assumption for the two-level homogenization. Six failure variables referring to six failure modes, including longitudinal, transverse, and out-plane failures, besides shear failure in 12, 23, and 13 directions, were taken into account. The maximum stress was chosen as the failure criterion of both fibers and matrix. The numerical results were comparable with the experimental data of tensile tests on a glass epoxy woven composite.

Although using RVEs as representatives of woven fabric materials could help designers predict the general behavior of these materials with some accuracy, this method relies on some limiting assumptions. For instance, a common assumption is that fibers and matrix have perfect contact with each other. In other words, the interface between yarns and matrix is assumed to be bonded perfectly under arbitrary deformation conditions. In reality, however, voids which arise during manufacturing processes are inevitable. On top of that, even by assuming perfect

curing/consolidation, the genuine contact between fibers and matrix is similar to a 'tiebreak' contact, rather than a tied contact. In a tiebreak contact, components are bonded to each other until an ultimate interface stress is reached [14], which debonds fibers and matrix. As stated earlier, another drawback of the RVE approaches may be that the simulations in micro as well as meso levels normally takes a great amount of time/cost; therefore, they are not always feasible to use for industrial applications. The last, and perhaps the most debatable, point is that in reality the failure starts in one point of a specimen and propagates to other points, whereas it is assumed in the RVE approach that when a failure mode occurs within one RVE, it arises in all the RVEs. In other words, damage localization cannot be captured in most RVE approaches. The most useful information that can be obtained from such analysis, however, is the extent of stress concentration in the meso/micro level due to the specific architecture of woven fabric materials; specially knowing that the stress applied to the composite constituents can be much higher than the global stress applied to the specimen at macro level [15].

2.1.2. Macro level analyses

As a general characteristic, macro level analyses do not take into account the micro failures in the composite specimens. Although macro level analysis of damage mechanism in woven fabric materials is not as complex as its micro/meso level counterparts, it is more practical (cost-effective) for large scale simulations. The published works in this area can be divided into three categories as follows.

2.1.2.1. Failure criteria-based approach

In this method, specific relationships based on either stress or strain components are introduced for the onset of failure modes. One fashion for the presentation of this method is the use of a single relationship to represent all the failure modes collectively. A case in point is the Tsai-Wu failure criterion [16] which offered a response surface for damage in stress or strain space. This approach is not able to distinguish between individual failure modes. Moreover, it is not meant to consider the degradation mechanism of composites. In order to propose a precise degradation mechanism, the induced failure modes have to be identified individually so that the corresponding stiffness coefficients can be decreased gradually.

There is another presentation type under this approach which offers a distinct relationship for each failure mode. Perhaps the most popular models of this kind are those proposed by Chang-Chang [17] and Hashin [18]. Nevertheless, all of the aforementioned failure criteria have been developed for UD composite materials, rather than woven fabric composites. In these failure criteria, the authors have assumed that failure in the longitudinal and transverse directions correspond to failure in fibers and matrix, respectively. As an example, Table 1 [14] shows the introduced failure criterion for each failure mode by Chang-Chang. For the Hashin failure criteria, β in the first equation is 1. According to this table, the failure modes of UD composites are classified as compression as well as tension in both fibers and matrix (longitudinal and transverse) directions, whereas in woven composite materials, fibers (wefts and warps) are spread in both longitudinal and transverse directions.

Tensile fiber mode	$e_f^2 = \left(\frac{\sigma_{aa}}{X_t}\right) + \beta \left(\frac{\sigma_{ab}}{S_c}\right) - 1 \begin{cases} \geq 0 & \text{failed} \\ < 0 & \text{elastic} \end{cases}$
Compressive fiber mode	$e_c^2 = \left(\frac{\sigma_{aa}}{X_c}\right)^2 - 1 \begin{cases} \geq 0 & \text{failed} \\ < 0 & \text{elastic} \end{cases}$
Tensile matrix mode	$e_m^2 = \left(\frac{\sigma_{bb}}{Y_t}\right)^2 + \beta \left(\frac{\sigma_{ab}}{S_c}\right)^2 - 1 \begin{cases} \geq 0 & \text{failed} \\ < 0 & \text{elastic} \end{cases}$
Compressive matrix mode	$e_d^2 = \left(\frac{\sigma_{bb}}{2S_c}\right)^2 + \left[\left(\frac{Y_c}{2S_c}\right)^2 - 1\right] \frac{\sigma_{bb}}{Y_c} + \left(\frac{\sigma_{ab}}{S_c}\right)^2 - 1 \begin{cases} \geq 0 & \text{failed} \\ < 0 & \text{elastic} \end{cases}$

Table 1. Chang-Chang failure criteria [14].

Another notable point is that in the former type of ‘surface’ failure criteria (also called failure ‘envelope’), some terms of both longitudinal and transverse stresses appear in the corresponding relationships, meaning that the stress values in both principal directions can accelerate the failure occurrence. On the other hand, in the second category, no terms of transverse (longitudinal) stresses are observed in the presented relationship corresponding to the failure in longitudinal (transverse) direction, as shown in Table 1. In other words, the latter technique of failure introduction assumes that the transverse stresses do not affect the failure in the longitudinal direction, and vice versa. The validity of such presumption should be challenged particularly for consolidated fabric composites, as there have been recent evidences of influence of coupling between warp and weft yarns in dry and coated fabrics [19–22] as will be further expanded on in section 2.1.3.1 Furthermore, as indicated earlier, both of these modeling types can forecast the initiation of damage and not the damage growth. In fact, after fulfillment of such relationships, the corresponding stiffness coefficients decrease to zero.

Recently, Materials Science Corporation (MSC) presented a model for woven composite materials by generalizing the Hashin failure criteria [14]. They assumed tensile and compression in both warp and fill directions, crushing failure, shear failure due to matrix cracking without fiber breakage, and tensile matrix failure in the out of plane direction. However, for failure in the warp and fill directions—the most common and predominant failure mode in woven composites—the relationship was analogous to that of Hashin’s. That is, the effect of stress in the second main direction is not seen in the relationship for the first main direction.

2.1.2.2. Plasticity-based approach

Unidirectional composite materials are predominantly known as brittle materials showing an elastic and linear response until failure. However, woven composite materials can show a non-linear response even in the early stage of a tensile test in the fibers' direction [23]. Some facts, such as wavy architecture of woven composites, visco-elastic behavior of matrix, and matrix cracking, can be postulated as the reasons of such non-linearity. Although earlier studies [23] showed that matrix cracking in woven composites can partially cause a non-linear tensile behavior, there has not been a full-scale investigation into discriminating all different sources and understand their effects. One of the easiest modeling methods to take the non-linear behavior of woven composites into account is the plasticity approach, in which the non-linear

behavior of the composite is equivalently modelled as a plastic material behavior, regardless of the reason of non-linearity. In the first study in this area, Hill introduced a plastic model for anisotropic materials [24]. Vaziri et al. proposed a comprehensive plasticity model for fiber reinforced composite plies based on a rate-independent orthotropic plasticity theory [25]. In this method, a relationship known as flow rule is considered between the effective strain and the effective stress. The coefficients of the flow rule are obtained using several tensile tests. Although this approach is very suitable to prediction loading regimes, it is not as accurate for events containing loading and unloading regimes, such as impact events, especially after the occurrence of some damage. The loading-unloading response of damaged woven composites has not been fully characterized in the literature yet. Each of the aforementioned non-linearity sources in woven composites probably has a different influence on the unloading behavior of these materials. In addition, in woven composites under tensile loading, the first failure mode is matrix cracking, decreasing the stiffness in a non-linear manner and causing a non-linear global response as illustrated in Figure 1 [23]. However, there is a fact known as 'crack saturation' in which crack growth is saturated and stopped. After crack saturation, a linear response is seen until yarn breakage. As a result, in some cases after damage initiation, some linear responses are observed in reality, which cannot be modeled by the plasticity approach. Another point regarding the limitation of the plasticity approach is that the behavior of composite materials in general, and their stress-strain responses in particular, under compression are not the same as that of tensile loading. This fact can be interpreted in a way that fiber yarns in composites, which may be comparable to thin beams, are more endangered with compression loading—buckling—rather than tensile loading. As a result, the ultimate compression strength of composite materials is predominantly less than their maximum tensile strength [26]. Also, the non-linearity in tensile loading of textile composites does not necessarily exist in compression loading. Hence, the plasticity method may not be fully applicable to simulate the behavior of woven composites under real-life loadings such as crashes in which some regions of the structure undergo compression. Finally, the effect of stress in one yarn direction upon the failure in the other yarn direction (coupling effect) cannot be considered in the plasticity approach.

2.1.2.3. Continuum damage mechanics-based approach

The continuum damage mechanics covers the initiation as well as propagation of various failure modes, including matrix cracking, delamination, and fiber fracture under tension as well as compression. This approach was introduced by Kachanov [27] and developed for composite materials by Frantziskonis [28]. Basically, the method employs a set of damage variables each of which representing a certain failure mode and varying from zero to one, covering no damage, partial damage, and complete damage states in a material element. Frantziskonis also defined the damage variable, r , as the ratio of damaged volume to the total volume. It was assumed that the strain for the damaged and undamaged part is the same, and then the stress was calculated employing the mixed rule.

In another work under continuum damage mechanics-based approach, Feng et al. introduced a damage model for woven fabric materials [29]. Due to the stress concentration in textile

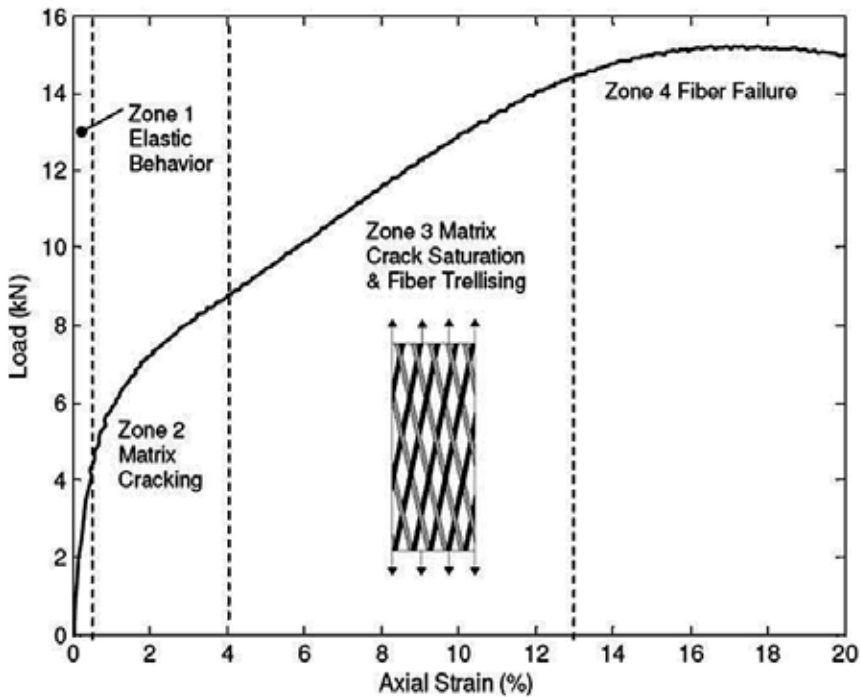


Figure 1. Tensile behavior of a woven composite sample [23].

composites arising from their complex fibrous architectures as proven in the micromechanical approaches using FEM [15], such materials can experience damage in early stages of deformation. Therefore, Feng et al. employed a stress variation factor (SVF) to correct the stress value by multiplying the nominal stress by the defined SVF. In their study, a woven lamina was assumed as two unidirectional (cross-ply) layers. Hashin failure criteria were utilized to predict the damage occurrence in each ply. For degradation mechanism, the corresponding stiffness coefficients were instantaneously reduced to zero. They compared the numerical and experimental results of a transverse compression test—punch test—on a woven composite specimen. The results were comparable in most cases.

Ladevaze and LeDantec introduced a continuum damage model for UD composite materials [30]. They wrote the strain energy based on the stress, stiffness, and damage variables of materials. Thereafter, driving forces, each of which being associated with a certain damage variable, was obtained by taking the derivative of strain energy with respect to damage variables. In fact, the damage evolution was based on such driving forces. In two subsequent investigations [31, 32], this approach was generalized for woven fabric materials. For instance, Johnson presented a 2D damage model that was able to predict the elastic failure in the warp and weft directions and the elastic-plastic in-plane shear failure for matrix [31]. Johnson used a linear relationship for the damage evolution based on the driving forces. In addition, that work employed a power law function to consider plastic hardening functions for cyclic loads.

The required parameters for the model were found using a tensile test. The damage model was implemented in an explicit finite element code in order to compare with the experimental results. In low velocity impact tests, in which there was considerable delamination failure, there was a substantial difference between numerical and experimental results, as shown in Figure 2.

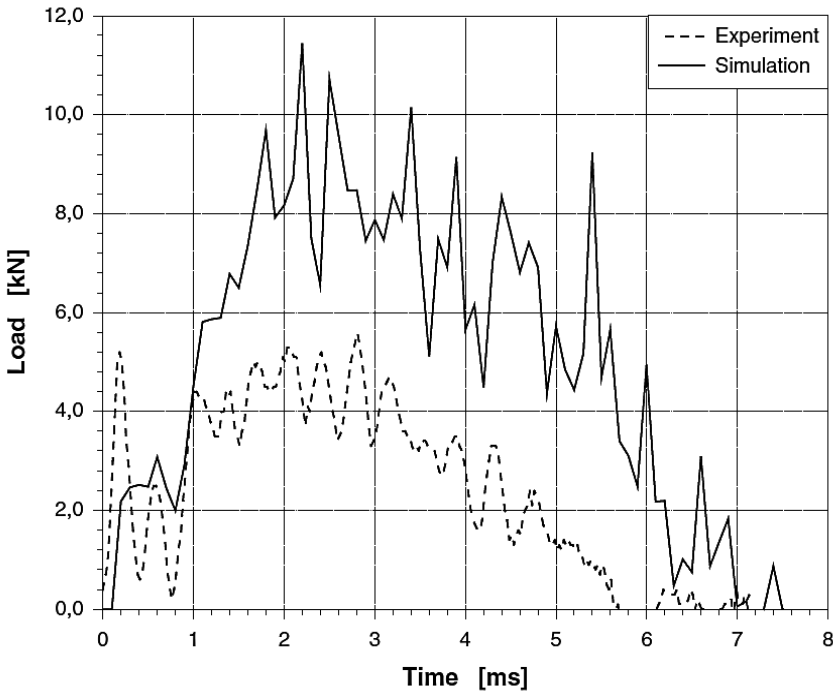


Figure 2. Comparison between numerical and experimental impact results [32].

Another research group introducing a damage model for woven composites is Iannucci and co-workers [33–35]. Iannucci et al. developed a progressive damage model for woven glass fiber-epoxy composite laminates and implemented it in a finite element code [33]. Their model was valid for shell elements with plain stress assumption. In addition, the proposed model was applicable to situations where there was no considerable damage, for example delamination, in the specimen. They postulated two unidirectional layers instead of one woven layer and found the Young’s modulus and other mechanical properties required for modeling. Damage parameters varying from 0 to 1 were allocated for two types of failure modes, including matrix cracking and fiber fracture. The employed failure criteria, however, had been originally developed for unidirectional composite laminates. They also eliminated the terms of shear stresses in the employed failure criteria. A significant point of their work was that they defined an advanced model for damage propagation and degradation mechanisms, in that the rate of damage growth was proportional to the extent of damage and the value of corresponding failure criterion. However, one of the drawbacks of the model was that the

damage growth rate could increase infinitely. The latter aspect of the model may not be reasonable on account of two facts:

- The maximum damage growth rate would be the stress wave speed in the material [33].
- Because of the crack growth saturation, as discussed before in section 2.1.2.2, the crack propagation cannot continue infinitely; it is restricted between the cells of weave architecture.

In the follow-up studies [34, 35], these authors introduced new failure modes in their originally developed model. Also, they made some efforts to distinguish between compression and tension failures. The presented damage model was rather accurate when the damage extent was not considerable. On the other hand, when there was a significant damage in the specimen, deviation between the model and experimental results was rather notable.

One of the latest research activities presenting a damage model for woven composites was performed by Cousigne et al. [36]. Employing LS-DYNA, they wrote a subroutine for woven fabric materials assuming a non-linear material behavior. Ramberg-Osgood equation [37] was exploited in different directions, covering longitudinal, transverse, and in-plane shear deformations. Effective macro-mechanical properties were determined based on tensile tests, and maximum stress failure criteria were chosen for damage initiation. Four post-damage models were considered as depicted in Figure 3. The force-displacement curves in Figure 4 demonstrate that the numerical results were not in a full agreement with the experimental data.

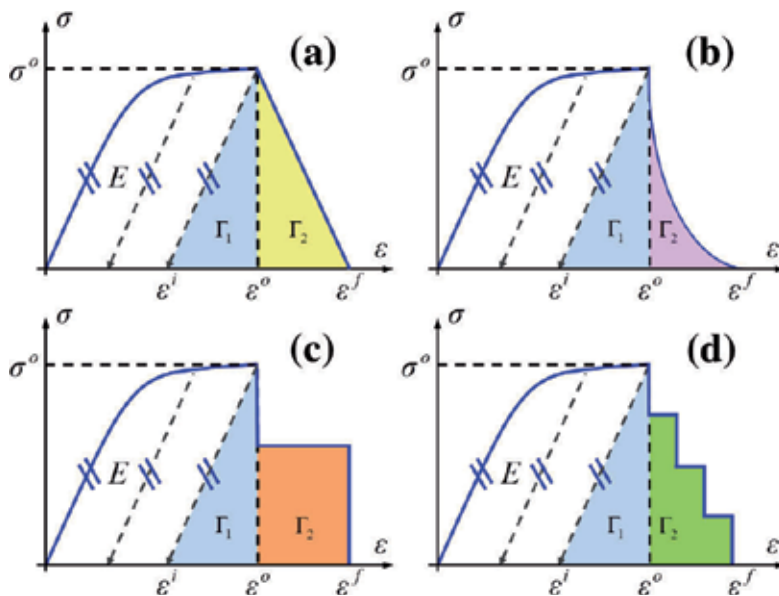


Figure 3. Four post-damage models for woven fabric materials: (a) linear damage, (b) non-linear damage, (c) constant stress level, (d) step-based material degradation [36].

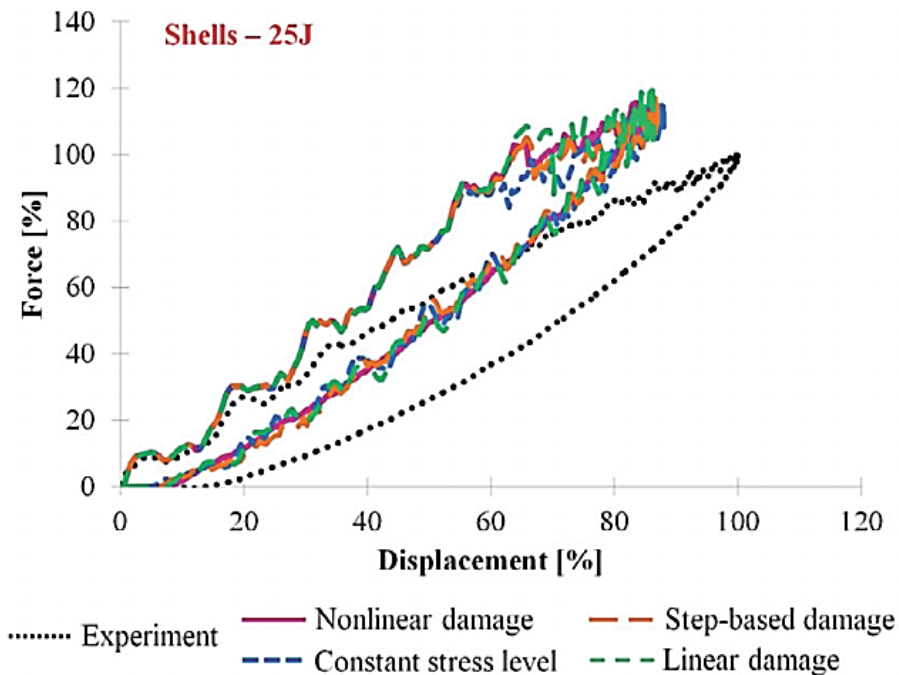


Figure 4. Force–displacement curves of 25J impact on a woven composite specimen [36].

Other researchers have aimed to use the pre-defined material models in commercial finite element programs to predict the macro-behavior of woven composite materials. A case in point is the study on low-velocity impact of thermoplastic woven composite specimens by Brown et al. [38]. They conducted an investigation into the applicability of MAT 162 of LS-DYNA material library—one of the most advanced material models for damage initiation and propagation in composite materials [14]—for the impact modeling of woven composite materials. At first, the parameters of MAT 162 were found using tensile tests on the woven specimens. Thereafter, the obtained parameters were used in impact simulations. Results showed that the identified damage model could not lead to highly accurate predictions against actual impact test data. In other words, the results again showed that the failure behavior of woven composite materials is more complicated than UDs and the original damage models need modifications.

2.1.3. Experimental studies

There have been several studies in the literature encompassing experimental research on woven composite materials. To illustrate a few, the compression behavior of woven fabric materials was investigated by Song et al. under quasi-static and high strain rate loading, employing a split Hopkinson bar [39]. The obtained results demonstrated that regardless of strain rate, the predominant failure mode was shear mode, while delamination happened only at high strain rates. Another category of most cited studies in this area links to the papers

presenting differences between unidirectional and woven fiber reinforced composites. For instance, Evci and Gulgec performed an experimental study to find the difference between the impact behavior of thermoplastic woven and unidirectional laminates with the same fiber/matrix materials and thickness [40]. They introduced plain weave composites as an outstanding replacement for UD in dynamics applications, owing to the fibers woven architecture that confines the damage. In addition, these materials were found to be more sensitive to strain rate, that is, their ultimate strength rises more substantially as compared with UD materials under high-strain rate loadings, mainly due to their higher visco-elasticity. Another article in this area is the study on the delamination modes I and II as well as impact resistance of woven fabric composite materials, performed by Kim and Sham [41]. Their results showed that woven composite materials are superior in comparison to UD composite materials under the above fracture modes and impact resistance criteria.

Mallikarachchi and Pellegrino endeavored to introduce the most elaborated failure criteria for symmetric two-ply woven carbon fiber reinforced plastics, by conducting numerous experiments [42]. In the first step, they used the Karkkainen relationship for failure occurrence including terms based on three forces and three moments applied to an element. This single equation is similar to the first presentation approach of failure criteria (section 2.1.2.1), which presents a surface for failure onset, and is not able to inform which type of failure arises in the sample. Tension, compression, shear, bending, and twist tests were performed with various lay-up configurations so as to find unknown constants of the utilized relationship/surface of failure. For example, [+45/-45] specimens were subjected to uniaxial testing and bending testing, separately, to induce shear and twisting modes, respectively. After identifying the unknown coefficients, they did several follow-up tests as combinations of five aforementioned loading types, in order to ensure that the presented model is reliable. However, the failure envelop relationship was not valid for some of the combined loading tests. Hence, instead of one equation for all the failure modes, they defined three failure modes, including in-plane, bending, and combined in-plane and bending, based on the three forces and three moments applied to the material element. The results showed that these failure criteria are valid for combined loadings. However, in the above approach, the final failure of woven composite was of interest and there was no identification of the first failure mode—matrix cracking—which decreases the stiffness of the material structure. In other words, such models are very reliable for prediction of catastrophic damage in textile composites but not for first-failure and progressive damage. In addition, although three relationships for failure of in-plane, bending, and combined loadings were considered, they cannot distinguish between individual failure modes under each type of deformation. Finally, the introduced relationships are based on the applied moments and forces, making the failure prediction analytics rather difficult for implementation in user-defined FE subroutines.

2.1.3.1. Effect of loading modes and yarns interaction

Generally speaking, among different deformation modes, the uniaxial behavior of materials has been investigated most. Woven composite materials are not an exception to this. However, the design of a targeted composite structure should not be based on the results of uniaxial tests

only. This is because in sensitive events, such as a crash, structures experience different loading modes *simultaneously*, including tension, compression, and shear, in different directions. As an illustration, in an impact testing on a rectangular composite specimen, the elements in upper and lower parts of the material system may undergo biaxial compression and tension, respectively. Although conventional materials which have the same properties in all the directions should have almost the same properties (e.g., Young's modulus) under uniaxial loading or combined loading, the properties of composite materials that are anisotropic is not necessarily similar under different types of loadings. The account of combined loading is specifically more critical for woven composites, resulting from the geometrical and mechanical interactions between warp and weft yarns. In general, in order to design any composite structure (woven or non-woven) with the highest performance reliability, it would be desired to characterize the mechanical behavior of the material under several combined loadings, rather than individual deformation modes. One common type of combined loadings is biaxial loading in which primarily a test specimen is subjected to equi-biaxial tension. However, providing facilities to apply such multi-axial tests is sometimes expensive and challenging. Moreover, creating a homogenous deformation in the zone of interest in biaxial specimens, normally far away from the loading jig, is crucial so as to obtain reliable characterization results. Furthermore, stress concentration in the specimen resulting from the sample shape in biaxial tests makes their analysis more complicated. In other words, a correct calculation of effective stress and strain either by analytical or numerical approaches should be considered next to the experimental testing. Currently, there is limited standard for biaxial testing of composites [43], whereas there are several standards for testing individual deformation modes, such as ASTM D3039 for the uniaxial tensile testing of composite materials. The biaxial testing of dry woven fabric materials using customized fixtures has substantiated the presence of severe coupling effects between warp and weft directions under different deformation modes [19]. In another recent study regarding a state-of-the-art combined biaxial-shear testing of dry carbon fabrics, Nosrat-Nazemi et al. conducted shear as well as biaxial tension-shear experiments [20]. Their results clearly demonstrated that there is another nonlinear coupling between the global shear behavior of the woven fabric specimens and the pre-tension applied to the samples.

The biaxial behavior of coated fabric materials has also shown that these materials behave substantially different by changing the ratio of applied stress in the warp direction to the applied stress in the weft direction. One of the first studies in this area, performed by Reinhardt, showed that the stiffness and ultimate strain of coated fabrics changes with different loading ratios between warp and weft [21]. In another study of coated fabric composites, Galliot and Luchsinger presented a simple model for non-linear unequi-biaxial tensile behavior of PVC-coated polyester fabrics based on experiments. In their model, the Young's modulus of different directions changed by changing the loading ratio [22]. Actually, this change resulted from the significant effect of interaction between warps and wefts. A linear relation between the Young's modulus and the loading ratio was also found in their investigation experimentally.

By refereeing to the above biaxial tests on dry and coated woven fabrics, the effect of interactions between warp and weft yarns under different modes has been well evidenced [19–22]. However, the influence of yarns' interaction in fully consolidated woven composites has not been explored in full. In three investigations [44–46], Welsh et al. studied the biaxial behavior of IM7-977-2 carbon-epoxy and E-glass vinyl plain weave composite laminates. Their results showed the existence of biaxial strengthening effect. However, the researchers of World Wide Failure Exercise recommended more experimental studies, as well as more attempts to advance the generalized set-ups of biaxial tests, on consolidated woven composites because of the scarcity of information in this area [3]. Regarding analytical studies on combined loading of consolidated textile composites, Welsh and co-workers [44–46] endeavored to predict the behavior of fabric composites using a multi-continuum theory (MCT). However, there was not sufficient agreement between the experimental and MCT results. In another study, Key et al. utilized multi-continuum theory in which warp and weft yarns as well as the matrix were considered as three model constituents [47]. Comparison between the analytical results and the experimental data obtained by Welsh et al. showed more compatibility because of employing a progressive damage model based on a continuous material property degradation state.

In conclusion, although the interweaved fiber architectures of woven composites bring assets such as out-of-plane impact resistance, ease of molding processes, and better resistance to damage growth, such complex material structures also cause difficulties for their analyses; three of which are in-plane as well as out-of-plane waviness and coupling effects between warp and weft yarns. In the modeling works reviewed above, researchers successfully took the advantage of some simplifications and assumptions in order to consider some of the aforementioned complexities. However, there is no explicit and practical damage model developed for woven composites yet, as also highlighted in the World Wide Failure Exercise [3]. It is believed that as the first step toward such comprehensive models under different deformation modes and different loading regimes (including loading–unloading and viscoelasticity), the underlying local damage mechanisms and their progression should be further explored under *individual* and *combined* failure modes via advanced experimental/numerical studies to understand their effects on the global stress-strain behavior of woven composites. Some preliminary results in this direction will be presented in Section 3.

2.2. Damage models for non-woven fabric composites

Several efforts have been put into research to accurately predict the mechanical behavior of non-woven fabric composites. As an example of such predictions, Cox assumed the paper material is composed of perfectly homogeneous plane of non-interactive long straight fibers which are oriented randomly. The material elastic modulus was calculated for small deformation regimes [48]. Applying an orthotropic model, Backer and Petterson investigated the tensile behavior of non-woven composites [49]. In an orthotropic model, stiffness coefficients in an arbitrary direction for small deformation can be estimated by knowing the stiffness constants in two main (principal) directions. There was a fair compatibility between the obtained initial elastic modulus from analytical and experimental analyses. However, non-

woven composites can be inherently random anisotropic materials due to the non-uniformity of oriented fibers. Non-uniform distribution of fibers was first taken into account in the studies [50–51]. In these works, the authors presumed that a non-woven fabric specimen is made of many layers of fibers with various orientations bonded to each other. However, fiber re-orientation was ignored on account of the bonding between fiber layers. Demirci et al. discussed the anisotropy of non-woven fabrics through continuum mechanics, based on the randomness of fiber orientation [52]. Utilizing image processing of data acquired by Scanning Electron Microscopy (SEM) and X-ray tomography, orientation distribution function (ODF) was measured as a representative of orientation randomness of fibers. Then, using the Fourier series, some parameters were defined to show the level of orthotropy. The analytical results which had good agreement with experimental results demonstrated a significant direction-dependence of nonwovens. In one of the other latest studies employing continuum mechanics [53], Ridruejo et al. presented a constitutive model for in-plane behavior of non-woven felts that included three parts: fibrous network, fibers, and damage. For modeling the fibers network, they followed Cox's model in which fibers do not have any interaction with each other. However, fiber orientation in large deformation was considered in the model. The damage of bonds and fibers were incorporated in the study in a phenomenological way. However, this method was not able to give a profound insight into the micro-level mechanical behavior of these materials which have more complex fibrous architecture than woven and UD composites. In other words, most of reported analytical works cannot precisely consider actual effects such as fibers reorientation, fibers sliding, and progressive damage propagation.

In order to arrive at a better understanding of the mechanical behavior of non-woven fabrics, representative unit cells (RUCs) can be employed based on numerical homogenization. The first study of this kind focusing on the micromechanics of non-woven composites was carried out by Petterson [54]. Straight fibers were modeled based on a specific statistical distribution within a unit cell. Another assumption in the simulation was a rigid bond between fibers. Thereafter, Hearle and Stevenson attempted to improve Peterson's fibrous network model by taking fiber curls into account [55]. The results demonstrated that fiber curl has a significant effect on the initial modulus of non-woven fabrics. The previous models were valid for in plane deformations. Narter et al. presented a 3D micro-mechanical model for prediction of elastic constants of non-woven composites, taking into account fiber elastic modulus, fiber linear density, and fabric bulk density [56]. Another extension of Petterson's work, considering the time-dependence behavior of felt composites, was performed by Kothari and Patel [57]. They investigated the creeping behavior of non-woven fabrics by considering the viscoelastic behavior of fibers. In another work, Silberstein et al. presented a micromechanical model for non-woven polymer fabrics that was able to implement an elasto-plastic behavior of fibers [58]. The obtained initial modulus and yield stress were based on fiber properties, network geometry, and network density. However, as similarly discussed for the RVE micromechanics of woven fabrics (section 2.1.1), this approach has several disadvantages, the main of which being lack of damage localization. Namely, this technique states that when damage initiates in a representative unit cell, it arises in the whole sample. However, this behavior could be contrasting with what is observed in reality where failure begins in a point of material medium, and then propagates to other points of the sample. Moreover, the RUC procedure may not able

to fully predict damage propagation of non-woven felts due to the presence of more randomness than, e.g., woven composites. Furthermore, on account of existence of voids, various fiber concentrations, and non-uniform fiber orientations at different points of a non-woven fabric, the homogenization rule may not be fully valid. In other words, the micro behavior of representative volume cells should be very cautiously extended to the macro behavior of non-woven felts. Therefore, some researchers decided to sacrifice computational time for accomplishing more reliable results by modeling the entire specimen at the micro/meso level instead of a single unit cell. Although this method is computationally expensive and may not be directly applied to large scale structures, small laboratory-scale specimens can be modeled and compared to experiments. In this type of modeling, however, simulation of bonding between fibers is controversial. In some studies, rigid contacts were defined between fibers. The first group of analyses that implemented this assumption was performed by Britton et al. [59–61]. Although they considered rigid contacts in bonds, they took into account bonding breakage. For the determination of bonding failure, they assumed when the force of a fiber exceeds a certain value, the fiber is debonded from the bond point. In another study, Wu and Dzenis considered the elastic behavior of planar fiber networks numerically [62]. In their simulations, slippage of fibers on each other and their angular displacement were overlooked. Constitutive equation was found based on the average of dissipated energy in each fiber. The numerical results were fairly comparable with analytical predictions. To make use of more advanced fiber contact models, Grindstaff and Hansen used springs to model bonds between fibers [63]. In order to determine the stiffness of springs, tensile tests were carried out on one single bond. One of the other advanced contact simulations was performed by Ridruejo et al. [64]. They simulated the behavior of glass fiber non-woven fabrics by explicitly introducing the fiber bundles using a random distribution. The implemented mechanical behavior and geometrical parameters of fibers were measured by removing a single fiber from the fabric and applying tensile test on it. In order to model a realistic contact, tiebreak contact was utilized in which fibers were jointed at their crossovers until bonding failure occurs. Although fibers do not move together after debonding, there was a pre-defined friction between them due to the use of this type of contact, which brought another capability of the model to consider fibers sliding. Experimental results of that study demonstrated that the main and first induced failure mode in non-woven fabrics under tension is bonding failure which propagates and creates a wide band. There was a good agreement between numerical and experimental results. Farukh et al. simulated thermally bonded nonwovens with a new insight into the bonding issue [65]. It has been reported that during the manufacturing process, high temperature and pressure at bond points can cause changes in molecular arrangement of fibers [66]. Additionally, stress concentration exists in fiber crossover points of nonwovens, similar to woven composites. As a result, the mechanical behavior of fibers in a fibrous network is different between an original fiber before the fabrication process and a fiber removed from the fabricated fabric sample. Hence, they extracted a fiber from the fabric sample in a way that the fiber was jointed to bonds at both ends. Their tensile tests showed that the ultimate strength and strain of fibers within fabrics are less, in comparison with those of unprocessed fibers. The numerical simulation was able to predict the general behavior of non-woven felts under tension with a reasonable accuracy.

3. Recent progress on further understanding of the damage behavior of woven composites

According to the aforementioned issues (section 2.1) for accurate damage modeling of woven composites, in light of their interwoven architectures—the main reason of superb behavior of these composites—there are several intrinsic distinctions that should be made between the mechanical behavior, particularly failure mechanism of long-fiber woven and UD composites. Before developing further enhanced and realistic damage models for woven composites, it is believed that the underlying sources of complexity need to be explored under various loading types. Among these, the impact of inherent in-plane waviness—misalignment—and out-of-plane waviness in yarns—crimping—on the damage mechanism of woven composites under tensile and bending modes has been recently investigated by the authors [67, 68], and is briefly reviewed here.

3.1. The in-plane waviness effect

A detailed experimental investigation was carried out into the mechanical behavior of a consolidated polypropylene/glass twill lamina under uniaxial tensile loading in warp and weft directions. Digital image correlation (DIC) and microscopy were employed in order to find the effect of in-plane waviness of fibers on the material response at each stage of tension. All the tests were performed based on ASTM D3039. Three test repeats were performed for each direction (warp and weft) in order to ensure the repetitiveness of results, as also confirmed by related statistical tests [67]. Figure 5 illustrates the presence of in-plane waviness in the studied specimens. In practice, in addition to out-of-plane waviness through the thickness of a woven specimen due to the interlacement of yarns in weaving process, the warp yarns of consolidated specimens through vacuum infusion technique were wavy in the plane of lamina, whereas the weft yarns were almost straight; this clearly indicated that the manufacturing/lamination process itself can add additional complexities to the mechanical behavior of woven composite structures.

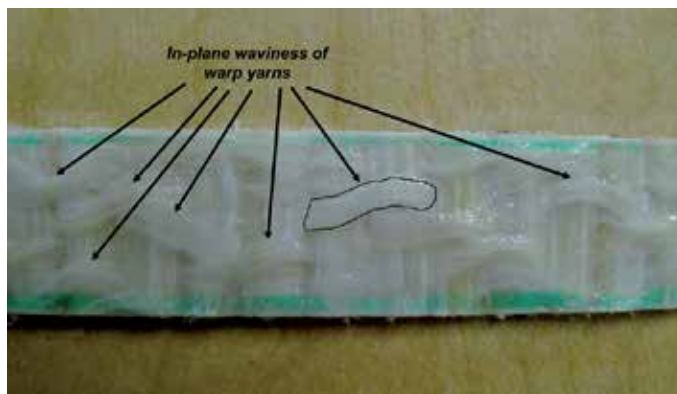


Figure 5. Example of in-plane waviness of warp yarns in a woven cured composite (notice that the weft yarns are nearly straight in the plane of fabric) [67].

Figure 6 shows the example of stress-strain behavior of the twill fabric samples obtained in the warp and weft directions. As depicted, the tensile behavior in the weft direction of the samples is almost linear up to the final failure with a sudden drop, which is analogous to that of most UD composites. On the other hand, the specimen responded non-linearly under the warp direction loading and then encountered failure in multiple steps with small falls at each. The results of DIC and microscopy pointed out that the main reason of such differences is the existence of in-plane waviness in the warp yarns. In fact, when the twill composite specimen was subjected to tension in the warp direction, the warp yarns which inherently had more in-plane waviness than weft (fill) yarns due to weaving process, moved similar to ‘snakes sliding’ on a ground of matrix, hence changing the global stiffness of the sample. Although matrix cracking followed by fiber breakage arose in the samples of both directions, as illustrated in Figure 7, performing analytical and statistical analyses on the obtained results from DIC, a high resolution stereotype microscope, and visual observations of tested samples demonstrated that the reason of matrix cracking is totally different between the warp and weft directions. Namely, the matrix experienced shear failure in warp direction whereas matrix tensile failure occurred in the weft direction. This difference in failure mode of matrix causes a sooner matrix crack initiation in specimens under tension in the warp direction. Not only does in-plane waviness affect the local damage behavior of woven composites in different directions, but also it can change the effective (global) mechanical properties such as Young’s modulus, ultimate strength, and ultimate strain.

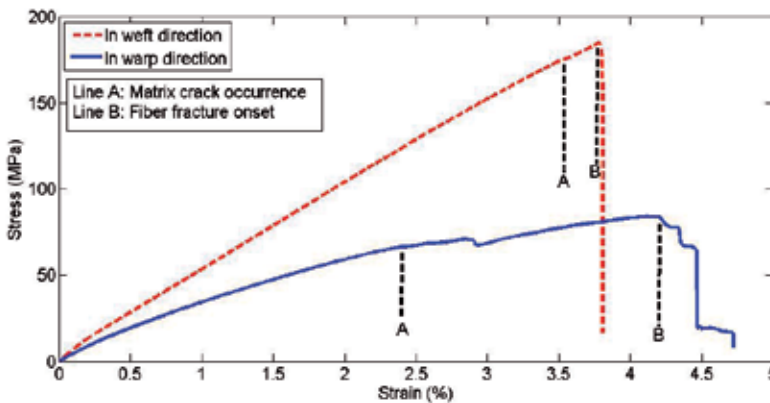


Figure 6. A comparison between the stress-strain behavior of the cured PP/glass twill lamina in the warp and weft directions: (A) Matrix cracking initiation, (B) Fiber fracture onset [67].

3.2. The out-of-plane waviness effect

In-plane waviness discussed in the previous section could mainly affect the tensile behavior of woven composites, rather than their bending behavior. On the other hand, undulation is the cause of less stiffness of woven composites in comparison with comparable UD composites with the same fiber/matrix constituents. Expectedly, fiber crimping should make the behavior

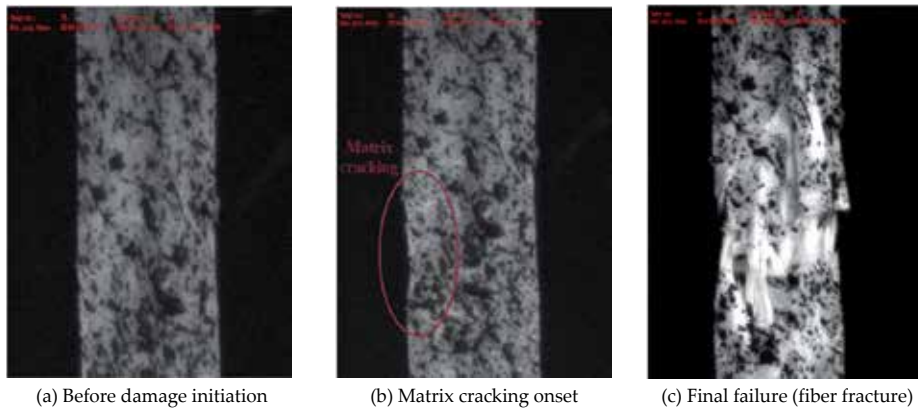


Figure 7. Different steps of mechanical behavior of twill composite specimen under warp tension (the white region in the red ellipse of panel (b) that does not exist in panel (a) points to the matrix cracking in macro level) [67].

of woven composites quite distinct from UD's under bending. To divulge this, the damage mechanism of oven-vacuum bagged twill glass/PP composite specimens under three-point bending was investigated [68]. The specimens were comprised of six twill layers with 6.18 mm of total thickness. Other dimensions of the specimens and deformation rate of loading were selected based on ASTM D7264. DIC was exploited to precisely observe the failure mechanisms of the woven composite samples step-by-step. The effect of surface quality was also examined in order to take into account the effect of the manufacturing process itself. In fact, due to the existence of crimping in woven composites, each studied specimen had two different surface conditions on its sides; one of which was almost flat as it was adjacent to the metallic mould during vacuum process. As a consequence, it was under more pressure, causing the undulation of the layer to fade. The other surface (open side) that was inherently not subject to the same processing pressure was wavy, with an average amplitude of 0.4 mm. Figure 8 demonstrates these two surfaces. As a result, two groups of samples were considered in the subsequent statistical analysis of the study. Namely, the specimens were subjected to loading in two conditions in which either the smooth or the curvy surface had direct contact with the loading nose.

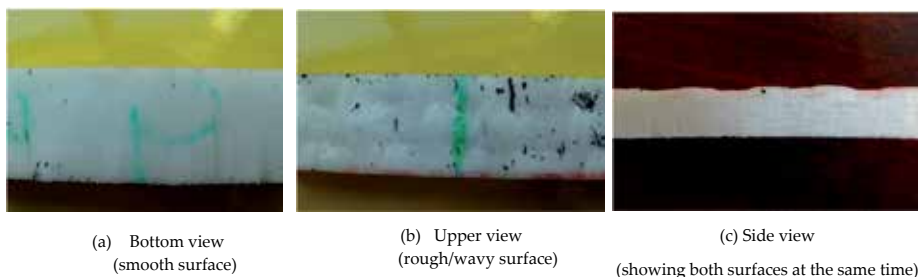


Figure 8. Different surfaces of an open-molded (oven vacuum bagged) twill specimen [68].

Typical bending responses of samples under the two surface conditions are presented in Figure 9. Although for both loaded surfaces, the bending response is linear until the first failure mode—fiber compression failure, significant differences can be observed between the two curves in Figure 9, proving the effect of surface quality (manufacturing) and eventually out-of-plane waviness of fibers on the bending behavior of woven composites.

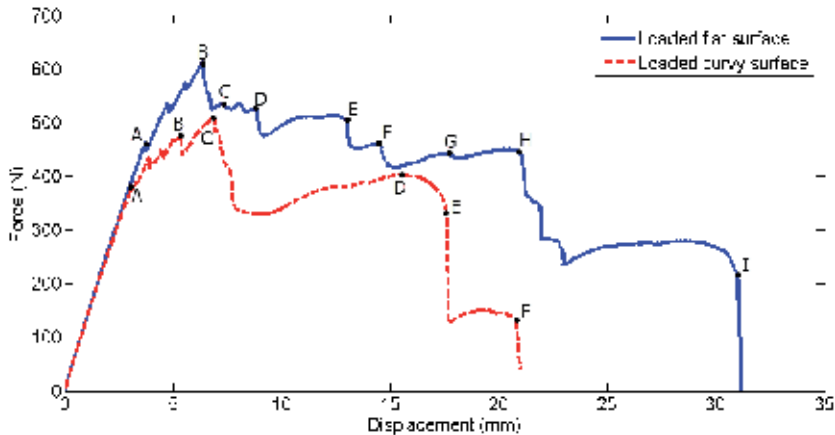


Figure 9. Comparison between the bending responses of two woven composite specimens with different loaded surfaces. For *flat surface loaded sample*: Point A: Initiation of fiber micro buckling in the first (top) layer, Point B: Completion of failure in the first layer, Point C: Delamination occurrence, Point D: Onset of fiber tensile failure in the lowest layer (6^{th}), Point E: Complete fiber breakage in 5^{th} layer. For *curvy surface loaded sample*: Point A: Initiation of fiber micro buckling in the first (top) layer, Point B: Completion of failure in the first layer, Point C: Complete compression failure in the second layer, Point D: Nucleation of fiber breakage in the lowest layer, Point E: Complete failure in the lowest layer, Point F: Complete fiber tensile failure in the 5^{th} layer [68].

Figure 10 further investigates the failure mechanisms of specimens in each loading condition. The DIC results informed that crimping can cause fiber compression failure not to occur exactly in the middle of the beam specimen where the applied (global) bending moment is maximum. In fact, due to the crimping, yarns in woven composites are comparable to sinusoidal beams with various amplitudes of waviness over their longitudinal axis, as illustrated in Figure 11. The higher the amplitude at a point, the less the buckling force of that location of yarn, and hence, a higher chance of failure initiation at that point. Consequently, the location in which fiber compression failure begins depends not only on the amount of applied bending moment, but also on the crimping amplitude of that point—which in effect changes the critical force of micro-buckling. However, delamination, the most common disadvantage of UD composites under bending due to the significant mismatch between layers of UD laminates, occurred only when the flat surface of the woven samples was under loading. However, concurrently taken photos by DIC and the force-displacement curves obtained by Instron machine divulged that delamination is not so influential to substantially drop the global force, point C and G in “loaded flat surface” curve as shown in Figure 9. The given interpretation for this observation may be that the debonded area is restricted between cells in woven composites, as shown in Figure 12(a). Hence, it cannot grow through the whole interface between the two layers, while the delamination area is much larger in UDs because it can propagate substantially [41].

Supporting this hypothesis, the actual micrograph in Figure 12(b) showed that matrix cracking has in the red regions of Figure 12 (a) where there is no fibers to resist the loading. These matrix cracks then resulted in debonding between the two layers. It is to note that along with the effect of out-of-plane waviness on the damage mechanism of woven composites, this type of waviness can affect the bending material parameters such as maximum force, ultimate deflection, and absorbed energy. For instance, the ultimate deflection was different by 37% between the two samples as seen in Figure 9.

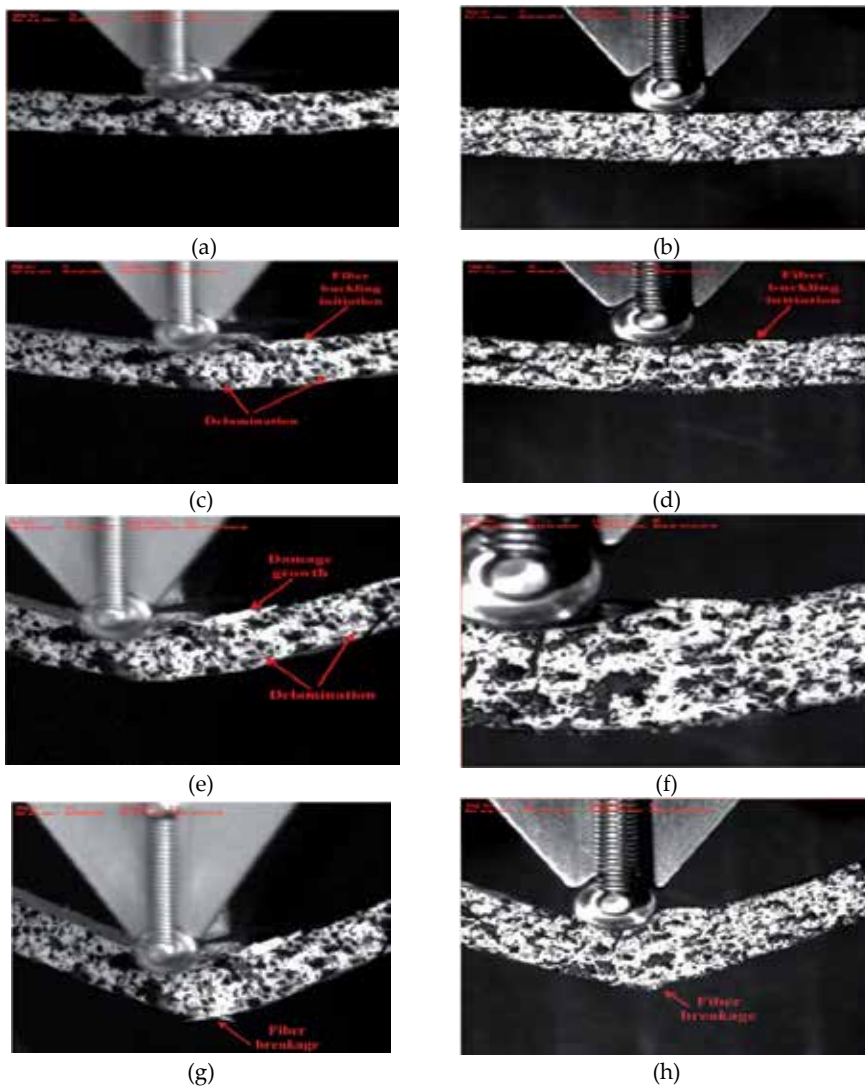


Figure 10. Damage mechanisms in two woven three-point bending specimens; left photos (a), (c), (e), and (g) correspond to the specimen loaded on a flat surface; right images (b), (d), (f), and (h) are for the specimen loaded on a curvy surface. (a) and (b): Specimens before any damage onset; (c) and (d): Initiation of fiber buckling; (e) and (f): Propagation of fiber buckling; (g) and (h): Fiber breakage initiation [68].

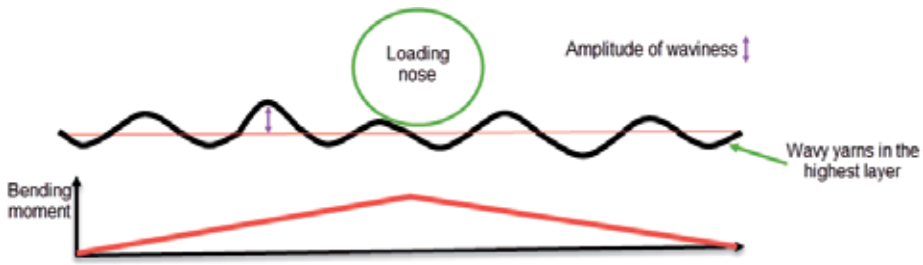


Figure 11. Schematic of varying bending moment and waviness amplitude in different locations of a yarn, especially in the open-side of the molded specimen (i.e., the highest layer of laminate).

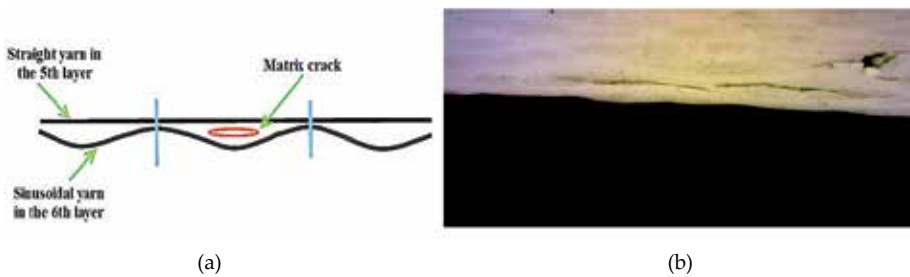


Figure 12. Restricted matrix crack in the woven composite specimen. (a) Schematic diagram; (b) Actual micro-image of cracks from the sample under three-point bending [68].

4. Conclusion and anticipated future developments

Based on the conducted review, the interlaced fiber architecture of woven composites, the main reason of their superb behavior, causes a series of complexities such as in-plane as well as out-of-plane misalignment effect in the laminated parts, along with a coupling between warp and weft yarns, all of which having a different effect under different deformation modes. As an example, recent experimental results show that not only the in-plane waviness inherited from the waving process is one of the reasons of non-linearity in uniaxial tensile behavior of woven composites, but it also leads to a significant unbalance in the damage tolerance measure in warp and weft directions. In effect, material properties such as Young's modulus, ultimate strength, and ultimate strain of the two principal directions of woven laminates should be expected to be statistically different in the presence of processing-induced in-plane waviness, despite the fact that as-received fabric preforms are often assumed balanced. In addition, evidence in the literature demonstrates that out-of-plane waviness can yield unusual failure modes in open-molded woven composites under three-point bending mode, similar to the propagation of "Plate Tectonics" in Geology. So dominant is the effect of yarn crimping that a change in the loaded surface of a sample can lead to a significant decrease in the bending resistance of the open-molded woven laminates. Moreover, it was observed that in converse

with UD composites, in which interlaminar failure grows instantly, delamination can be well confined between the cells of a weave architecture and not extended to the entire sample, hence inducing higher damage tolerance.

Owing to the aforementioned complexities in the response of woven fabrics, earlier micro, meso, and macro level damage models of UD composites may not be fully compatible to predict the behavior of woven structures under various loading regimes, while fulfilling high accuracy and minimum computational cost. To meet the two latter practical requirements, the most appropriate way to analyze woven composites and to predict their damage is believed to be the phenomenological approach, along with required experimental analyses. Currently, there is no comprehensive experimental study revealing the effect of woven architecture of fibers in a multitude of deformation modes, classifying the dominant failure modes specifically to these composites, and eventually presenting an explicit, short, and easy-to-implement phenomenological model for the damage nucleation stage and finally growth. Moreover, different stress-strain behaviors of textile composites with non-linear functions have been employed in the previous macro-level research investigations, while there have been no sufficient micro/meso level evidence on the roots of this non-linearity. As reviewed in this chapter, the determination of the sources behind material non-linearity is crucial to propose accurate damage models. Furthermore, with the exception of a few recent works, past researches have not paid close attention to combined loading effects—which are very likely in practical applications—on the behavior of woven composites. Recent experimental works reveal that the interaction between warp and weft yarns has a significant effect on both dry and coated fabrics under combined loadings; however, to the best of authors' knowledge, no detailed study of this kind has been reported for consolidated laminates. In addition, the characterization of loading-unloading behavior of woven composites in quasi-static and high strain rate regimes (e.g., for application in inflatable fabric tube, or impact design of structures), particularly after arising some first damage, have not received sufficient consideration.

Regarding the analysis of non-woven fabrics, in addition to the aforementioned complexities in woven composites, more complexities such as non-uniform fiber architecture, fiber sliding, and complex bonding behavior between fibers need to be addressed. As a consequence, the analysis of non-woven felts is deemed more complicated than woven composites, despite several general similarities seen in damage modeling approaches taken for both types of fabric materials.

Finally, it is noticed that statistical analysis has taken little part in the past characterization efforts on fabric reinforced composites. This is despite the fact that uncertainties underlying the soft reinforcing materials in the dry form [69], along with process-induced uncertainties and risk during matrix curing/manufacturing stages, may have an enormous effect on the variation of parameters needed for damage modeling. Subsequently, the application of hypothesis testing and black-box optimization methods in the field of damage modeling of composites is believed to be vital in future studies to ensure the reliability and applicability of the identified models.

Author details

Masoud Haghi Kashani and Abbas S. Milani

Composites Research Network-Okanagan Laboratory, School of Engineering, University of British Columbia, Canada

References

- [1] Dixit A, Mali HS. Modeling techniques for predicting the mechanical properties of woven-fabric textile composites: A review. *Mechanics of Composite Materials*. 2013;49(1):1-20.
- [2] Russell S. *Handbook of Nonwovens*. Woodhead Publishing. 2006.
- [3] Soden P, Kaddour A, Hinton M. Recommendations for designers and researchers resulting from the world-wide failure exercise. *Composites Science and Technology*. 2004;64(3):589-604.
- [4] Blackketter D, Walrath D, Hansen A. Modeling damage in a plain weave fabric-reinforced composite material. *Composite Technology and Research*. 1993;15(2):136-142.
- [5] Tang X, Whitcomb JD. Progressive failure behaviors of 2D woven composites. *Composite Materials*. 2003;37(14):1239-1259.
- [6] Jia X, Xia Z, Gu B. Micro/meso-scale damage analysis of three-dimensional orthogonal woven composites based on sub-repeating unit cells. *The Journal of Strain Analysis for Engineering Design*. 2012;47(5):313-328.
- [7] Jia X, Xia Z, Gu B. Numerical analyses of 3D orthogonal woven composite under three-point bending from multi-scale microstructure approach. *Computational Materials Science*. 2013;79:468-477.
- [8] Chandekar GS, Kelkar AD. Experimental and numerical investigations of textile hybrid composites subjected to low velocity impact loadings. *The Scientific World Journal*. 2014.
- [9] Ishikawa T, Chou T. Stiffness and strength behaviour of woven fabric composites. *Materials Science*. 1982;17(11):3211-3220.
- [10] Ganesh V, Naik N. Failure behavior of plain weave fabric laminates under on-axis uniaxial tensile loading: I—laminates geometry. *Composite Materials*. 1996;30(16):1748-1778.
- [11] Naik N, Ganesh V. Failure behavior of plain weave fabric laminates under on-axis uniaxial tensile loading: I—analytical predictions. *Composite Materials*. 1996;30(16):1779-1822.

- [12] Tabiei A, Song G, Jiang Y. Strength simulation of woven fabric composite materials with material nonlinearity using micromechanics based model. *Thermoplastic Composite Materials*. 2003;16(1):5-20.
- [13] Li J, Zhao M, Gao X, Wan X, Zhou J. Modeling the stiffness, strength, and progressive failure behavior of woven fabric-reinforced composites. *Composite Materials*. 2013;0021998313477171.
- [14] Manual LKU. Version R7. 0. Livermore Software Technology Corporation 2013.
- [15] Feng Z, Allen HG, Moy SS. Study of stress concentrations in woven composites. *Reinforced Plastic Composites*. 1999;18(3):198-214.
- [16] Tsai SW, Wu EM. A general theory of strength for anisotropic materials. *Composite Materials*. 1971;5(1):58-80.
- [17] Chang F, Chang K. A progressive damage model for laminated composites containing stress concentrations. *Composite Materials*. 1987;21(9):834-855.
- [18] Hashin Z. Failure criteria for unidirectional fiber composites. *Applied Mechanics* 1980;47(2):329-334.
- [19] Buet-Gautier K, Boisse P. Experimental analysis and modeling of biaxial mechanical behavior of woven composite reinforcements. *Experimental Mechanics*. 2001;41(3):260-269.
- [20] Nosrat-Nezami F, Gereke T, Eberdt C, Cherif C. Characterisation of the shear-tension coupling of carbon-fibre fabric under controlled membrane tensions for precise simulative predictions of industrial preforming processes. *Composites Part A: Applied Science and Manufacturing*. 2014;67:131-139.
- [21] Reinhardt HW. On the biaxial testing and strength of coated fabrics. *Experimental Mechanics*. 1976;16(2):71-74.
- [22] Galliot C, Luchsinger R. A simple model describing the non-linear biaxial tensile behaviour of PVC-coated polyester fabrics for use in finite element analysis. *Composite Structures*. 2009;90(4):438-447.
- [23] Hufner DR, Accorsi ML. A progressive failure theory for woven polymer-based composites subjected to dynamic loading. *Composite Structures*. 2009;89(2):177-185.
- [24] Hill R. A theory of the yielding and plastic flow of anisotropic metals. *Proceedings of the Royal Society of London. Series A, Mathematical and Physical Sciences*. 1948:281-297.
- [25] Vaziri R, Olson M, Anderson D. A plasticity-based constitutive model for fibre-reinforced composite laminates. *Composite Materials*. 1991;25(5):512-535.
- [26] Strong A. Brent. *Fundamentals of composites manufacturing: Materials, methods and applications*. Society of Manufacturing engineers. 2008.

- [27] Kachanov L. Time of the rupture process under creep conditions. *Isv. Akad. Nauk. SSR. Otd Tekh. Nauk.* 1958;8:26-31.
- [28] Frantziskonis G. Distributed damage in composites, theory and verification. *Composite structures.* 1988;10(2):165-184.
- [29] Feng Z, Allen HG, Moy SS. Theoretical and experimental investigation of progressive failure of woven composite panels. *Composite Materials.* 1999;33(11):1030-1047.
- [30] Ladeveze P, LeDantec E. Damage modelling of the elementary ply for laminated composites. *Composites Science and Technology.* 1992;43(3):257-267.
- [31] Johnson AF. Modelling fabric reinforced composites under impact loads. *Composites Part A: Applied Science and Manufacturing.* 2001;32(9):1197-1206.
- [32] Hochard C, Aubourg P, Charles J. Modelling of the mechanical behaviour of woven-fabric CFRP laminates up to failure. *Composites Science and Technology.* 2001;61(2): 221-230.
- [33] Iannucci L, Dechaene R, Willows M, Degrieck J. A failure model for the analysis of thin woven glass composite structures under impact loadings. *Computers and Structures.* 2001;79(8):785-799.
- [34] Iannucci L. Progressive failure modelling of woven carbon composite under impact. *Impact Engineering.* 2006;32(6):1013-1043.
- [35] Iannucci L, Willows M. An energy based damage mechanics approach to modelling impact onto woven composite materials—Part I: Numerical models. *Composites Part A: Applied Science and Manufacturing.* 2006;37(11):2041-2056.
- [36] Cousigné O, Moncayo D, Coutellier D, Camanho P, Naceur H. Numerical modeling of nonlinearity, plasticity and damage in CFRP-woven composites for crash simulations. *Composite Structures.* 2014;115:75-88.
- [37] Blacklock J, Richard R. Finite element analysis of inelastic structures. *AIAA.* 1969;7(3):432-438.
- [38] Brown K, Brooks R, Warrior N. Numerical simulation of damage in thermoplastic composite materials. In: *Proceedings of the 5th European LS-DYNA Users Conference; May 2005; Birmingham, UK*, p. 25-26.
- [39] Song Z, Wang Z, Ma H, Xuan H. Mechanical behavior and failure mode of woven carbon/epoxy laminate composites under dynamic compressive loading. *Composites Part B: Engineering.* 2014;60:531-536.
- [40] Evcı C, Gülgeç M. An experimental investigation on the impact response of composite materials. *Impact Engineering.* 2012;43:40-51.
- [41] Kim J, Sham M. Impact and delamination failure of woven-fabric composites. *Composites Science and Technology.* 2000;60(5):745-761.

- [42] Mallikarachchi H, Pellegrino S. Failure criterion for two-ply plain-weave CFRP laminates. *Composite Materials*. 2013;47(11):1357-1375.
- [43] Escárpita DAA, Cárdenas D, Elizalde H, Probst O, Ramirez R. Biaxial Tensile Strength Characterization of Textile Composite Materials. INTECH Open Access Publisher, 2012. P. 83-106.
- [44] Welsh JS, Mayes JS, Biskner AC. 2-D biaxial testing and failure predictions of IM7/977-2 carbon/epoxy quasi-isotropic laminates. *Composite Structures*. 2006;75(1):60-66.
- [45] Welsh JS, Mayes JS, Key CT, McLaughlin RN. Comparison of MCT failure prediction techniques and experimental verification for biaxially loaded glass fabric-reinforced composite laminates. *Composite Materials*. 2004;38(24):2165-2181.
- [46] Welsh JS, Adams DF. An experimental investigation of the biaxial strength of IM6/3501-6 carbon/epoxy cross-ply laminates using cruciform specimens. *Composites Part A: Applied Science and Manufacturing*. 2002;33(6):829-839.
- [47] Key CT, Schumacher SC, Hansen AC. Progressive failure modeling of woven fabric composite materials using multicontinuum theory. *Composites Part B: Engineering*. 2007;38(2):247-257.
- [48] Cox HL. The elasticity and strength of paper and other fibrous materials. *British Journal of Applied Physics*. 1952;3(3):72.
- [49] Backer S, Petterson DR. Some principles of nonwoven fabrics1. *Textile Research Journal*. 1960;30(9):704-711.
- [50] Bais-Singh S, Goswami BC. Theoretical determination of the mechanical response of spun-bonded nonwovens. *Journal of the Textile Institute*. 1995;86(2):271-288.
- [51] Liao T, Adanur S, Drean J. Predicting the mechanical properties of nonwoven geotextiles with the finite element method. *Textile Research*. 1997;67(10):753-760.
- [52] Demirci E, Acar M, Pourdeyhimi B, Silberschmidt VV. Computation of mechanical anisotropy in thermally bonded bicomponent fibre nonwovens. *Computational Materials Science*. 2012;52(1):157-163.
- [53] Ridruejo A, González C, LLorca J. A constitutive model for the in-plane mechanical behavior of nonwoven fabrics. *Solids Structures*. 2012;49(17):2215-2229.
- [54] Petterson DR. *On the Mechanics of Nonwoven Fabrics* [PhD Thesis]. Massachusetts Institute of Technology; 1959.
- [55] Hearle J, Stevenson P. *Studies in Nonwoven Fabrics Part IV: Prediction of Tensile Properties*1. *Textile Research*. 1964;34(3):181-191.

- [56] Narter MA, Batra SK, Buchanan DR, Micromechanics of three-dimensional fibre-webs: Constitutive equations. In: Proceedings of the Royal Society of London A: Mathematical, Physical and Engineering Sciences; 1999. p. 3543-3563.
- [57] Kothari V, Patel P. Theoretical model for predicting creep behaviour of nonwoven fabrics. *Indian Journal of Fibre and Rextile Research*. 2001;26(3):273-279.
- [58] Silberstein MN, Pai C, Rutledge GC, Boyce MC. Elastic-plastic behavior of non-woven fibrous mats. *Mechanics and Physics of Solids*. 2012;60(2):295-318.
- [59] Britton PN, Sampson AJ, Elliott C, Graben H, Gettys W. Computer Simulation of the Mechanical Properties of Nonwoven Fabrics Part I: The Method. *Text Research*. 1983;53(6):363-368.
- [60] Britton PN, Sampson AJ, Gettys WE. Computer Simulation of the Mechanical Properties of Nonwoven Fabrics Part II: Bond Breaking. *Textile Research*. 1984;54(1):1-5.
- [61] Britton PN, Sampson AJ, Gettys WE. Computer Simulation of the Mechanical Properties of Nonwoven Fabrics Part III: Fabric Failure. *Textile Research*. 1984;54(7):425-428.
- [62] Wu X, Dzenis YA. Elasticity of planar fiber networks. *Applied Physics*. 2005;98(9):093501.
- [63] Grindstaff T, Hansen S. Computer model for predicting point-bonded nonwoven fabric strength, Part I. *Textile Research*. 1986;56(6):383-388.
- [64] Ridruejo A, González C, LLorca J. Damage micromechanisms and notch sensitivity of glass-fiber non-woven felts: an experimental and numerical study. *Mechanics and Physics of Solids*. 2010;58(10):1628-1645.
- [65] Farukh F, Demirci E, Sabuncuoglu B, Acar M, Pourdeyhimi B, Silberschmidt VV. Numerical analysis of progressive damage in nonwoven fibrous networks under tension. *Solids Structures*. 2014;51(9):1670-1685.
- [66] Chidambaram A, Davis H, Batra SK. Strength loss in thermally bonded polypropylene fibers. In: *INTC 2000 Conference, Dallas, 2000*. p. 72-79.
- [67] Haghi Kashani M, Milani AS. Understanding the effect of in-plane waviness on damage behavior of cured woven composites. *Proceedings of 20th International Conference on Composite Materials; 19-24 July 2015; Copenhagen, Denmark*.
- [68] Haghi Kashani M, Milani AS. Understanding new damage mechanisms in woven composites: the effect of surface quality. *Proceedings of Canadian-International Conference on Composite Materials; 17-20 August 2015; Edmonton, Canada*.
- [69] Komeili M, Milani AS. *Meso-Level Analysis of Uncertainties in Woven Fabrics*. VDM Verlag, Berlin, Germany, 2010.

Technologies Involved in the Manufacture of Smart Nonwoven Fabrics

Izabella Krucińska, Ewa Skrzetuska, Beata Surma and Eulalia Gliścińska

Additional information is available at the end of the chapter

<http://dx.doi.org/10.5772/61587>

Abstract

Many methods can be used to protect humans against hazardous chemicals in the environment such as personal protective equipment and protective clothing. However, what matters most is prevention and early detection of threats. Detecting the presence of hazardous chemicals such as organic liquids and the vapours they give off is possible using sensors. Effective chemosensory properties are revealed by conductive polymers and carbon particles, where the electrical resistance of chemicals changes. Still open to debate is finding the optimum means of applying chemical sensors that would provide high sensitivity, durability, reliability, and resistance but at the same time would not be expensive. The authors propose introducing chemical sensors in the form of nonwoven fabrics produced by the melt-blown method and by electrospinning. The analysis takes account of melt-blown nonwoven fabric based on polylactide (PLA)-containing carbon nanotubes, nonwoven fabric made by electrospinning based on polyethylene oxide-containing carbon nanotubes and carbon nonwoven fabric from polyacrylonitrile submicron precursor fibres formed by electrospinning. Assessment of the effectiveness of the sensors to liquid vapours including methanol, acetone, benzene and toluene (concentration 200 ppm) has been carried out. The resulting nonwoven sensors are characterized by good electrical conductivity and altered electrical resistance as a result of the presence of vapours.

Keywords: Melt-blown method, electrospinning, vapour sensors, textile sensors, carbon nanotubes, submicrofibre-activated carbon

1. Introduction

Significant progress in the manufacture of composite materials has recently given rise to new opportunities for the use of nonwoven fabrics. The functionalization of composite materials involves the introduction of electrically conductive nanoadditives. It allows acquiring original polymer materials for possible use in smart products. There has been in recent years a growing

interest in technologies aimed at imparting specific properties to textile products (i.e. generating so-called “smart” nonwoven fabrics such as fabrics capable of changing their properties under the influence of external stimuli). Techniques used to produce nanocomposites or select nano and polymeric materials may be of use in the construction of various types of sensors. Smart textiles – also called “active”, “interactive” and “adaptive” textiles – can be produced using such solutions.

Smart textiles can be functionalized by incorporating active materials into fibre, or by modifying the surface of textiles to give them specific characteristics. Active materials can be stimulated by a number of factors such as stressing, temperature, humidity, ultraviolet radiation and chemical substances. Smart textiles react to these stimuli by changing various parameters such as dimension state, change in resistance or in the distribution of stresses [1–9]. The use of nanotechnology in the functionalization of materials made by classical textile techniques allows certain unique properties, such as sensory properties or electrical conductivity, to be achieved. Introducing different types of nanoparticles to fibres can drastically alter the properties of materials [10, 11]. Ongoing work is currently aimed not only at obtaining new polymers, but also at effectively modifying them with nanoadditives and finding new solutions in processing techniques, so as to obtain polymeric materials that can be used in the construction of sensors. Sensors are usually components of a larger system, often defined as devices that receive and respond to a signal or stimulus. Their task is to capture information from the environment or to test an object by recognizing and recording it. Sensors should enable fast, simple and continuous measurements of the value being measured. It is important that the impact of using sensors does not being about changes in the tested objects [12–15].

Innovative solutions of noncontact sensors, material processing and design have an important input in development of smart textiles. Such materials combine a number of features of sensors such as electronic data processing and the ability to send information to other devices (e.g. alarm systems, data loggers, and monitoring devices). This has resulted in a sharp increase in interest in specialized products for medicine, filtration and protective services. Sensors used in textiles such as clothes, carpets, upholstery, furniture, wallpaper and paint have the potential to radically change lifestyles, enabling monitoring and action at a distance [16–21]. Some electroactive polymers may be useful in the production of fibre sensors as a result of their intrinsic dielectric or conductive properties, light weight, flexibility and relatively low price [7–9, 22, 23]. This paper focusses on a new area of research undertaken by the authors, one that deals with transferring properties of electrical conductivity to nonwoven fabrics by incorporating carbon nanoparticles into their structure.

This work involves using carbon nanotubes to impart sensory properties. Melt-blown and electrospinning were the methods selected to form fibres. The characteristic properties of carbon nanotubes – such as thermal conductivity, electrical conductivity, high modulus, high strength and resistance to chemicals – make them widely used in nanotechnologies. The electrical properties of carbon nanotubes are typical of two-dimensional structures, and electrical conductivity varies depending on the structure of nanotubes (single or multi-walled) and chirality. The electrical conductivity of nanotubes is also sensitive to the influence of external factors such as electric fields, magnetic fields, mechanical properties, state of the

environment (temperature, vapour content of selected chemicals). Mechanical properties are characterized by high mechanical strength, elasticity, susceptibility to deformation as a result of bending, torsion or flexibility (e.g. during stretching the length of nanotubes may increase by up to 40% without changing their structure [24]). The peculiar properties of nanotubes are widely used in many fields of nanotechnology: for example, when creating nanocomposites using nanotubes as reinforcing material and functionalizing composites, when creating nanocontainers to store gases (like hydrogen) [24], when removing dioxins prior to medical waste incineration and from chemical products [24]. Nanotubes play important roles in environmental protection. However, the greatest hope for the peculiar electrical properties of nanotubes (e.g. in microelectronics [25]) lies in their potential to exceed the limits of silicon technology.

The electrical sensory properties of carbon nanotubes were used in this work to functionalize nonwoven fabrics produced using modern techniques. Melt blowing and electrospinning are often used to produce filter materials to protect against toxic molecules. Therefore, the manufacture of nonwoven fabrics that are sensitive to vapours for use in filtration materials represents an innovative approach to receiving signals about the concentration of toxic vapours in the air. A new generation of smart half-masks that protect the respiratory tracts of users can be developed using such fabrics.

2. Materials and methodology

2.1. Producing a nonwoven fabric of polylactide (PLA) using melt blowing and carbon nanotubes

The most suitable materials to produce nonwoven fabrics via melt blowing are those whose melt flow index is high. Most thermoplastic polymers can be used in this technique. However, as a result of very good processing properties and low price the most commonly used is polypropylene. Polycarbonate, polyester, polyamide and polystyrene are also frequently used to make nonwoven fabrics. When selecting an appropriate polymer for the construction of a chemical vapour sensor both the Hildebrandt and the Flory–Huggins theories should be followed [7, 26], especially when a compound is influenced by a solvent (swelling, dissolution). This happens when the solubility parameters of the polymer and solvent used are similar. The Flory–Huggins solubility parameter has been presented in previous work [7].

The polymeric sensor produced by melt blowing was assumed to have been manufactured from PLA to which multi-walled carbon nanotubes (MWCNT) were then introduced. Preliminary experiments made it possible to establish a percolation threshold for nonwovens produced by melt blowing. A conductive nonwoven containing 2% MWCNT was found to be adequate to produce a 4060D PLA polymer (98% PLA 4060D/2% MWCNT) [7]. Increasing the content of MWCNT to 4% was found to cause a linear increase in the conductivity of nonwovens, but a decline in the strength of the product.

Nonwoven fabrics made of PLA and MWCNT were produced in two stages. First, the polymer PLA 4060D (NatureWorks) had 4% MWCNT (Nanocyl® 7000, Nanocyl SA, Belgium) added

to it. A ready-made nanocomposite (PLA/4% MWCNT) was then mixed with pure PLA 4060D to obtain the final composition PLA/2% MWCNT. The two-step process was designed to ensure carbon nanotubes were uniformly distributed in the structure of the product and that the formation of undesirable agglomerates was reduced. The nanotubes were 90% pure, 9.5 nm in diameter and 1.5 μm in length. The polymer selected had a molar mass of up to 87 000 Da and a D-isomer content of 12% [7].

2.2. Producing a nonwoven fabric of polyethylene oxide using electrospinning and carbon nanotubes

Polyethylene oxide (PEO) with the addition of MWCNT was selected for the production of nonwovens using the electrospinning polymer solution technique [8]. The polymer had a molar mass of 400 000 Da. To produce nonwovens with this technique, a solution of PEO in distilled water at a concentration of 5 wt.% was prepared to which a homogeneous suspension of the MWCNT containing 3% by volume carbon nanotubes with respect to the polymer volume was added. Mixing the nanotube suspension was carried out using an ultrasonic homogenizer at 150 W and a frequency of 30–40 kHz. The nanotube suspension was then added to the polymer solution and mixed in an ultrasonic homogenizer at 150 W and a frequency of 3–40 kHz at a temperature of 20°C for 0.2 hours, followed by 24 hours in a magnetic stirrer. Electrospinning consisted of an electrostatic field made up of the polymer composition prepared. The electrostatic field was the result of the potential difference between the capillary feed polymer and a collecting drum. A supply voltage of 15 kV was applied to the capillary by a generator while the receiving drum was grounded. The distance between the capillary and the drum was 20 cm [8].

2.3. Carbon nonwoven fabric produced by polyacrylonitrile electrospinning

Another option presented in this paper is nonwoven fabrics made from submicron carbon fibres. The first step taken to produce carbon structures was to prepare a nonwoven precursor. The precursor was obtained by electrospinning fibres from a solution of polyacrylonitrile (PAN). A 15% spinning solution of PAN powder was prepared to obtain the nonwoven precursor. The solution was produced by Zoltek Zrt. (Hungary) in dimethyl sulfoxide (DMSO) manufactured by POCH (Gliwice, Poland). The intrinsic viscosity of the PAN was equal to 1.3 ± 0.02 dL/g [23, 27]. Electrospinning was performed on a large-size laboratory device large-size laboratory line for producing nonwovens from the solution electrospinning technique that had 32 capillaries at $22 \pm 10^\circ\text{C}$ and a relative humidity (RH) of 38% under normal atmospheric pressure [23]. Process parameters were: generator voltage 15 kV, distance between the feeding capillary and collecting drum 15 cm, capillary diameter 0.9 mm [23].

The precursor nonwoven fabric was first subjected to thermal stabilization, which consists in heating to a temperature of 200°C and thermosetting for 6 hours. It was then oxidized by heating to a temperature of 220°C and thermosetting for another 6 hours. The heating cycles were performed in a stream of air. After washing the nonwoven fabric in carbon dioxide, it was subjected to pyrolysis, which involved heating to a temperature of 600°C in an atmosphere of inert gas and annealing at the final temperature. The nonwoven fabric was then subjected

to chemical activation by impregnation with a solution of potassium hydroxide using a vacuum method, and kept under reduced pressure which was slowly increased to atmospheric pressure. This was followed by soaking the nonwoven fabric in an aqueous solution of potassium hydroxide, removing the excess hydroxide solution, leaving the nonwoven fabric at room temperature, drying to a constant weight and annealing in a stream of inert gas. Finally, the nonwoven fabric was cooled and extracted using an aqueous solution of hydrochloric acid and then distilled or deionized water [28].

2.4. Methods used for nonwoven fabric assessment

The cross-sectional shape and thickness of fibres comprising the nonwoven fabric were examined using a JEOL JSM-5200LV scanning electron microscope (SEM). Image processing and measurements were carried out using LUCIA G image analysis software. The results are shown in Table 1 and Figure 1.

The electrical conductivity of the nonwoven fabric produced was calculated by measuring surface resistance according to EN 1149-1:2008 – Protective clothing. The electrostatic properties of the nonwoven fabric were calculated using the surface resistivity test method. An electrometric direct method using a Keithley 610C solid-state electrometer was employed in the study. The voltage source was an RFT-4218 DC power supply with a voltage range of 0–3000 V. The electrodes and the test sample were placed in a Faraday cage. Constant conditions for conditioning and testing were: temperature 23°C, RH = 25%. The results are shown in Table 2.

Sensory tests for the presence of solvent vapours were carried out using a laboratory measurement system. Such a system allows for measurements of the humidity and temperature of the atmosphere prevailing in the system and the creation and introduction of a given concentration of liquid vapours to the measuring system. The sensory sensitivity of the nonwoven fabric produced was investigated with measuring apparatus constructed at the Department of Material, Commodity Sciences and Textile Metrology (Lodz University of Technology, Poland). This was equipped with a tank serving as a gas chamber, a pump for mixing gas fumes, and a measuring chamber containing the measuring electrodes connected to a Keithley multimeter. The gas chamber was used to evaporate the appropriate amount of solvent. The mass of solvent to be evaporated in the gas chamber to achieve a concentration of X ppm was calculated according to equations (1–2) [7]:

$$Y = (X \times M) / 22.4 \quad (1)$$

$$m = Y \times V \quad (2)$$

where Y is the density of solvent vapours (mg/m^3), X is parts per million ($1/10^6$, ppm), M is molecular weight (kg/kmol), m is mass of solvent to be evaporated (mg), V is volume of gas chamber (0.024 m^3).

The gas chamber houses a thermometer and humidity sensor that ensure tests are conducted under identical climate conditions (temperature 23°C and RH of 25%). After evaporation of the solvent in the gas chamber, the vapour is pumped to the measuring chamber in which a test sample 2 cm × 4 cm in size is placed on the measurement electrodes. The sensory properties of the nonwoven fabric were tested for vapours of various solvents, and changes in resistance were recorded. The liquids used were typed according to EN 14605+A1:2009. The sensory properties were also investigated for vapours of both polar and nonpolar organic liquids at a concentration of 200 ppm.

The sensory properties of samples for toxic vapour substances were characterized by defining a sensory factor S . This was defined by formula (3) [7, 29]:

$$S = |R_{rel}| * 100\% \quad (3)$$

where

$$R_{rel} = (R_i - R_0) / R_0 \quad (4)$$

R_{rel} is relative changes in electrical resistance, R_0 is initial sample resistance (Ω), R_i is final resistance of the sample (Ω) [7, 29].

3. Results and discussion

Table 1 shows the thickness of fibres forming the nonwoven fabrics.

Type of nonwoven fabric	Production technique	Thickness of fibre (μm)
98% PLA 4060D/2% MWCNT	Melt blowing	17.75
97% PEO/3% MWCNT	Electrospinning	0.24
Carbon (precursor 15% PAN/ 85% DMSO)	Electrospinning carbonization	0.78

Table 1. Thickness of fibres forming the nonwoven fabrics [7, 8, 23]

Figure 1 shows the structure of the nonwoven fabrics and the shape of constituent fibres.

The results show that fibres in the nonwoven fabric prepared by electrospinning a polymer solution of PEO have the lowest diameter. However, microscopic observation shows that the addition of carbon nanotubes has caused many beads, making the structure nonuniform. The carbon nonwoven fabric made of PAN has the highest fibre thickness uniformity. The melt-blown nonwoven fabric shows a high spread in fibre thickness – there are both fine fibres with

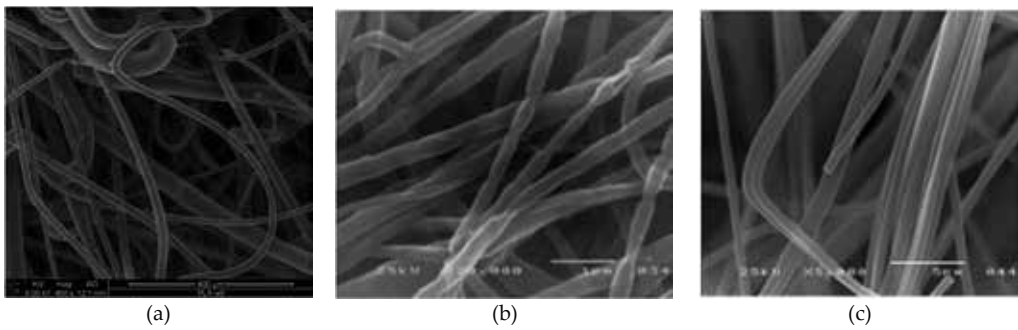


Figure 1. SEM images of fibres forming the nonwoven fabrics: a) 98% PLA 4060D/2% MWCNT, b) 97% PEO/3% MWCNT, c) carbon (precursor 15% PAN/85% DMSO) [7, 8, 23]

a diameter of approx. 5 μm and coarse fibres with a diameter of approx. 80 μm . Table 2 shows the results of the electrical conductivity test of the nonwoven fabrics.

Type of nonwoven fabric	Production technique	Surface resistivity (Ω)
98% PLA 4060D/2% MWCNT	Melt blowing	$5.63 * 10^7$
97% PEO/3% MWCNT	Electrospinning	$1.67 * 10^4$
Carbon (precursor 15% PAN/ 85% DMSO)	Electrospinning carbonization	$4.89 * 10^5$

Table 2. Electrical surface resistivity of the nonwoven fabrics

Table 2 shows that the best conductivity was observed for the PEO nonwoven fabric made by electrospinning the polymer solution, while the worst conductivity was observed for the PLA nonwoven fabric with carbon nanotubes formed using the melt-blown technique. According to EN 1149-1:2008, homogeneous materials are characterized by electrostatic properties when they show a surface resistivity of less than $2.5 \times 10^9 \Omega$. In other words, all three nonwoven fabrics have electrostatic properties.

Table 3 summarizes sensory test results for the presence of polar and nonpolar solvent vapours. The sensitivity threshold of solvent vapours was based on data about the toxic effects they have on the human body. The data suggest the minimum concentration of solvent vapours having a toxic effect on the human body is 200 ppm for toluene, 300 ppm for methanol and 500 ppm for benzene and acetone [7]. Research into all three types of nonwoven fabrics was carried out at 200 ppm.

Table 3 shows average test results calculated from sensory measurements of the three nonwoven fabrics. Figures 2–5 illustrate changes in relative electrical resistance calculated by formula (4) in terms of the influence of different solvent vapours.

Solvent	Sensory factor (%)		
	98% PLA 4060D/2% MWCNT	97% PEO/3% MWCNT	Carbon (precursor 15% PAN/85% DMSO)
	Melt blowing	Electrospinning	Electrospinning + carbonization
Methanol	15	98	18
Acetone	40	67	19
Toluene	35	106	14
Benzene	60	102	13

Table 3. Sensory test results for the presence of solvent vapours in the three nonwoven fabrics [7, 23]

Sensory phenomena occurred in all three types of nonwoven fabrics. Comparison of the nonwoven fabrics presented in Table 3 shows that the nonwoven fabric manufactured by electrospinning a polymer solution containing nanotubes (97% PEO/3% MWCNT) has the higher sensitivity to vapour sensing of all the solvents (at 200 ppm concentration) than the nonwoven fabric constructed with carbon fibres carbonized from a nonwoven precursor (15% PAN/85% DMSO). This may result from the characteristics of polymer and carbon fibres. Fibre thickness may also be significant. Reducing fibre thickness increases specific surface area, which allows greater surface diffusion of solvent molecules to fibres. Furthermore, PEO/MWCNT-penetrating molecules are known to bring about further separation of nanotubes in percolation paths that were originally formed by nanotubes separating as a result of stretching.

Results from the nonwoven fabric made of 98% PLA 4060D/2% MWCNT show that sensor response to methanol vapours is relatively low (15%), while responses to benzene, acetone and toluene vapours reach 60%, 40% and 35%, respectively. Relative changes in electrical resistance R_{rel} coincide with the Flory–Huggins parameter $\kappa_{PLA/benzene} < \kappa_{PLA/acetone} < \kappa_{PLA/toluene} < \kappa_{PLA/methanol}$.

Looked at from a technological viewpoint, this research demonstrates that all of the process parameters evaluated affect the properties of the manufactured products. Comparison of the response plots of produced nonwoven fabrics with chemical stimuli shows that the melt-blown nonwoven fabric made of polymer (98% PLA 4060D/2% MWCNT) respond differently than the nonwoven fabric made of polymer solution (97% PEO/3% MWCNT) and the carbon nonwoven fabric made of the precursor formed using a 15% PAN/85% DMSO solution.

Analysis has shown that differences in both the intensity and directivity of sensory properties are likely caused by the use of different technological parameters. This phenomenon may result from the structural arrangement of macromolecules and nanotubes affecting the formation of electroconductive tracks directed along the fibre axis. Too large a distance between one nanotube and another may cause a rapid increase in resistance. Finding the optimum draw ratio imposed during nonwoven fabric formation can lead to better positioning of them in the conductive network formed by well-oriented MWCNT. This implies that dispersed nanotubes can be combined or separated for such nano and submicron-composite structures.

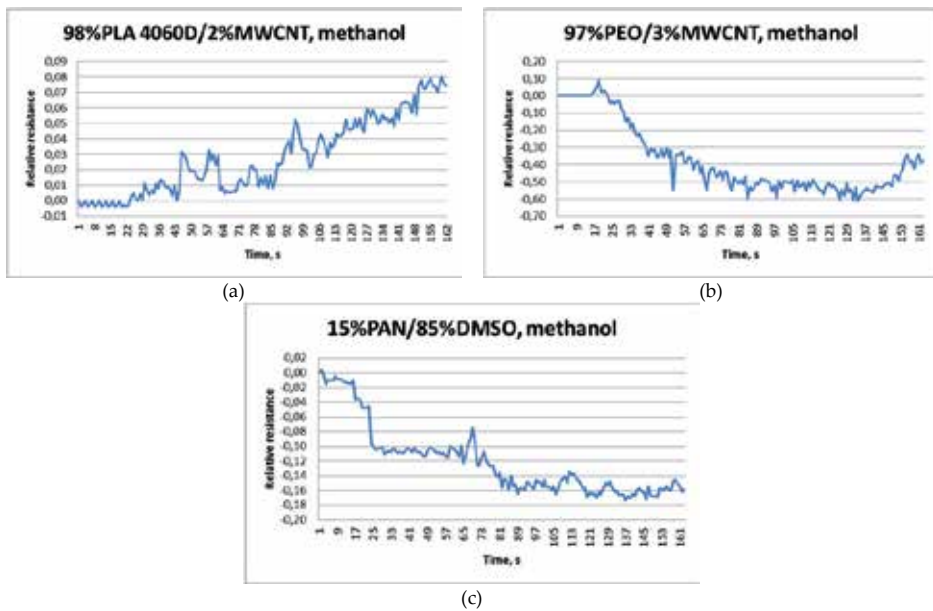


Figure 2. Changes in relative electrical resistance of nonwoven fabrics subjected to methanol vapours at 200 ppm: a) 98% PLA 4060D/2% MWCNT, b) 97% PEO/3% MWCNT, c) carbon (precursor 15% PAN/85% DMSO)

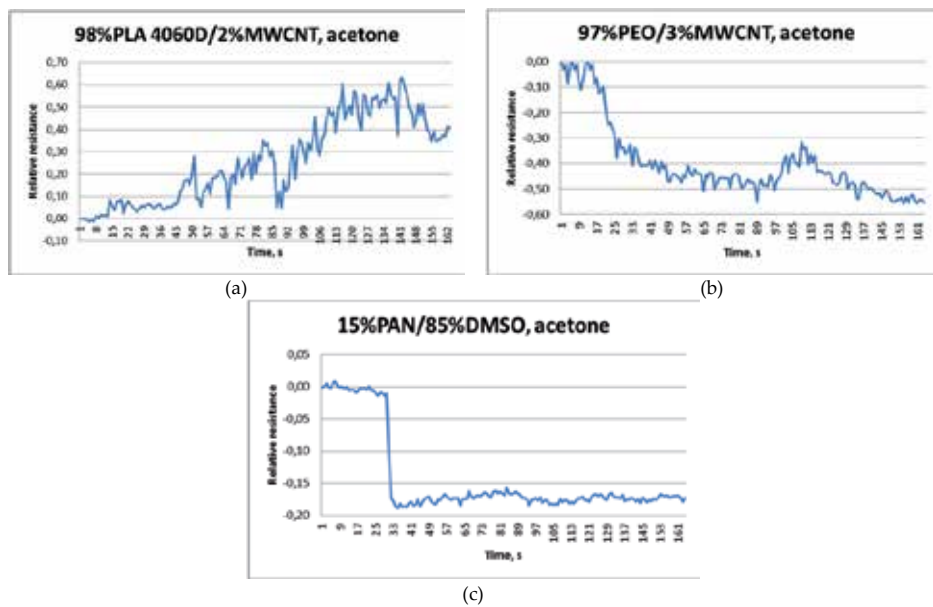


Figure 3. Changes in relative electrical resistance of nonwoven fabrics subjected to acetone vapours at 200 ppm: a) 98% PLA 4060D/2% MWCNT, b) 97% PEO/3% MWCNT, c) carbon (precursor 15% PAN/85% DMSO)

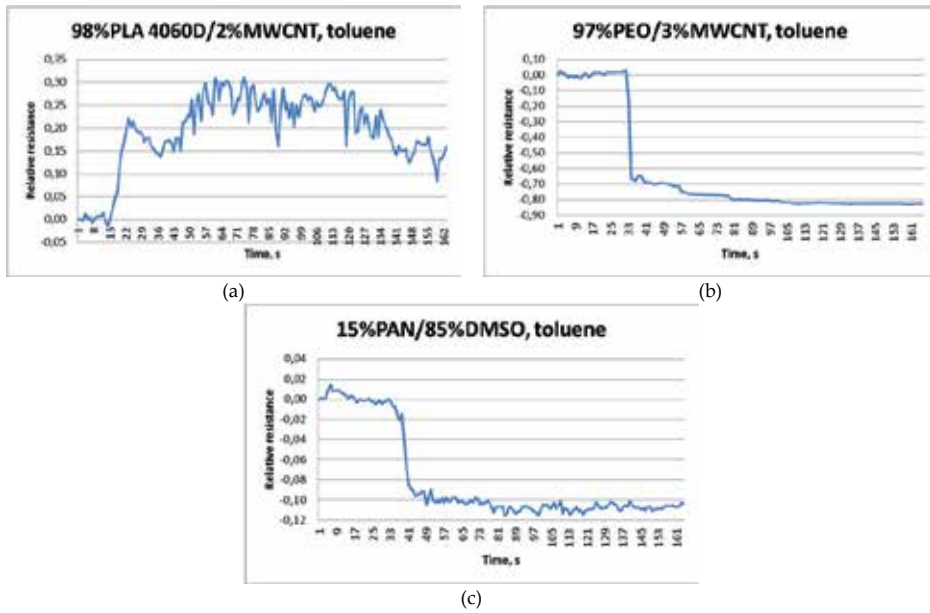


Figure 4. Changes in relative electrical resistance of nonwoven fabrics subject to toluene vapours at 200 ppm: a) 98% PLA 4060D/2% MWCNT, b) 97% PEO/3% MWCNT, c) carbon (precursor 15% PAN/85% DMSO)

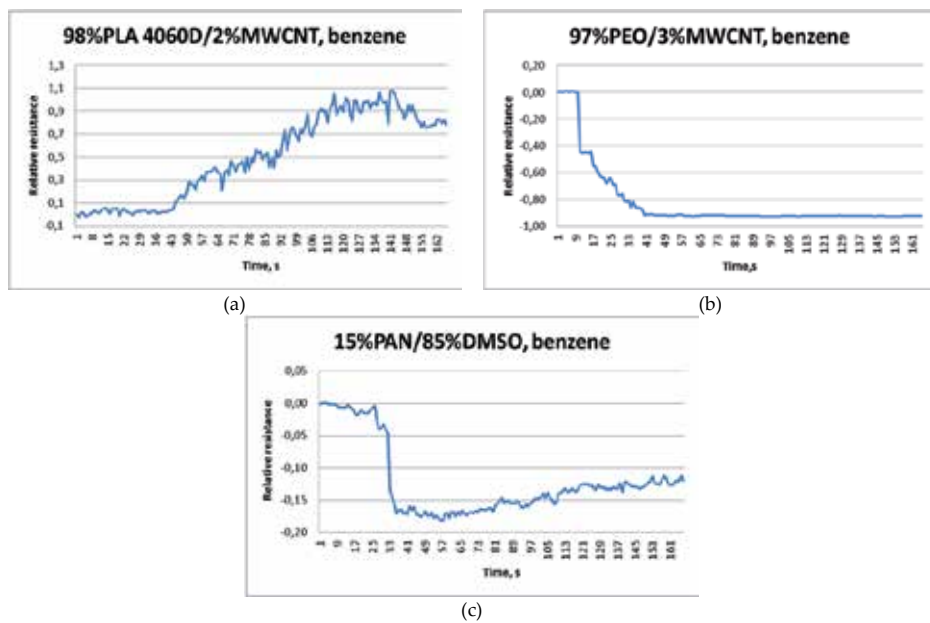


Figure 5. Changes in relative electrical resistance of nonwoven fabrics subject to benzene vapours at 200 ppm: a) 98% PLA 4060D/2% MWCNT, b) 97% PEO/3% MWCNT, c) carbon (precursor 15% PAN/85% DMSO)

4. Conclusions

This paper has shown the possibility of using nonwoven fabrics as sensors to detect organic vapours. The results show that electrospinning and melt blowing for nonwoven fabric formation comprising a composite system made of a polymer matrix reinforced with MWCNT (98% PLA 4060D/2% MWCNT, 97% PEO/3% MWCNT) can be used to produce nonwoven fabrics whose resistance changes under the influence of solvent vapours. This is equally true of submicron carbon fibres made from a precursor using a 15% PAN/85% DMSO solution. All three nonwoven fabrics revealed an electrical response on contact with methanol, acetone, benzene and toluene vapours at a concentration of 200 ppm. Samples in direct contact with vapours show high sensitivity and very short response times, no longer than 20 seconds after exposure.

Nonwoven sensors show good electrical conductivity and, in the presence of vapours, they change their resistance. Such sensors are very light as a result of their high porosity. This also provides them with high sensory capacity. They show high sensitivity for substances that are widely used in industry and/or are highly toxic. What is more, sensors produced in this way can be easily shaped and adapted to the surface on which they are to be placed.

Author details

Izabella Krucińska*, Ewa Skrzetuska, Beata Surma and Eulalia Gliścińska

*Address all correspondence to: izabella.krucinska@p.lodz.pl

Department of Material and Commodity Sciences and Textile Metrology, Technical University of Lodz, Lodz, Poland

References

- [1] Michalak M., Krucińska I., Surma B., *Textronic Textile Product, Fibres & Textiles in Eastern Europe*, 5 (59), (2006), 54–59.
- [2] Coyle S., Morris D., Lau K.-T., Diamond D., Moyna N., *Textile-based wearable sensors for assisting sports performance. Wearable and Implantable Body Sensor Networks, International Workshop*, (2009), 307–311.
- [3] Schwarz A. et al., *Electro-conductive and elastic hybrid yarns – The effects of stretching, cyclic straining and washing on their electro-conductive properties, Materials and Design*, 32 (2011), 4247–4256.

- [4] De Rossi D. et al., Electroactive fabrics and wearable biomonitoring devices, *Autex Research Journal*, 3 (4), (2003), 180–185.
- [5] Chiolerio A. et al., Inkjet printing and lower power laser annealing of silver nanoparticle traces for the realization of low resistivity lines for flexible electronics, *Microelectronic Engineering*, 88, (2011), 2481–2483.
- [6] Krucińska I., Skrzetuska E., Urbaniak-Domagala W., Prototypes of Carbon Nanotube-Based Textile Sensors Manufactured by the Screen Printing Method, *Fibres & Textiles in Eastern Europe*, 2(91), (2012), 79–83.
- [7] Krucinska I., Surma B., Chrzanowski M., Skrzetuska E., Puchalski M., Application of melt-blown technology in the manufacturing of a solvent vapor-sensitive, non-woven fabric composed of poly(lactic acid) loaded with multi-walled carbon nanotubes, *Textile Research Journal*, 83 (8), (2013), 859–870.
- [8] Krucinska I., Surma B., Chrzanowski M., Study on Sensing Properties of Electro-spun PEO/MWNT Non-woven Fabric, *Research Journal of Textile and Apparel*, 14 (4), (2010), 89–96.
- [9] Krucinska I., Surma B., Chrzanowski M., Skrzetuska E., Puchalski M. Application of melt-blown technology for the manufacture of a temperature-sensitive non-woven fabrics composed of polymer blends PP/PCL loaded with multi-wall carbon nanotubes, *Journal of Applied Polymer Science*, 127, (2013), 869–878.
- [10] Li Ch., Thostenson E.T., Chou T.-W., Sensors and actuators based on carbon nanotubes and their composites: A review, *Composites Sciences and Technology*, 68, (2008), 1227–1249.
- [11] Wong Y.W.H., Yuen C.W.M., Leung M.Y.S., Ku S.K.A., Lam H.L.I., Selected applications of nanotechnology in textiles, *Autex Research Journal*, 6, (2006), 1–8.
- [12] Meijer, G.C.M., *Smart Sensor Systems*, John Wiley & Sons, Ltd., United Kingdom, (2008), 23–54, ISBN: 978-0-470-86691-7.
- [13] Fraden J., *Handbook of Modern Sensors: Physics, Design and Applications*, Springer, New York, (2004), 13–33, ISBN 0-387-00750-4.
- [14] Gopd W., Hesse J., Zemel J.N., *Sensors – A Comprehensive Survey*, Volume 2, VCH, Weinheim, (1994), 208–267, ISBN 3-527-26173-5.
- [15] Di Renzo M., Rizzo F., Meriggi P., Applications of a textile-based wearable system for vital signs monitoring. *Conference Proceedings of the Annual International Conference of the IEEE Engineering in Medicine and Biology Society*, 1, (2006), 2223–2226.
- [16] Wilson P., Buechley H., Buechley L., Making Textile Sensors from Scratch, *TEI'10, Proceedings of the 4th International Conference on Tangible, Embedded and Embodied Interaction*, (2010), 25–27, MIT Media Lab, Cambridge.

- [17] Buechley L., Eisenberg M., Fabric PCBs, Electronic Sequins, and Socket Buttons: Techniques for E-textile Craft, *Journal of Personal and Ubiquitous Computing*, 13(2), (2009), 133–150.
- [18] Buechley L., Eisenberg M., Catchen J., Crockett A., The LilyPad Arduino: Using Computational Textiles to Investigate Engagement, Aesthetics, and Diversity in Computer Science Education, in *Proceedings of the SIGCHI conference on Human factors in Computing Systems (CHI)*, (2008), 423–432.
- [19] Enokibori Y., Suzuki A., Mizuno H., Shimakami Y., Mase K., E-Textile Pressure Sensor Based on Conductive Fiber and Its Structure, *UbiComp'13*, September (2013), 8–12, Zurich, Switzerland.
- [20] Guinovart T., Parrilla M., Crespo G.A., Rius X., Andrade F.J., Potentiometric sensors using cotton yarns, carbon nanotubes and polymeric membranes, *Analyst*, 138, (2013), 5208–5215.
- [21] Cherenack K., van Pieterse L., Smart textiles: Challenges and opportunities, *Journal of Applied Physics*, 112, (2012), 290–302.
- [22] Yang Y.L., Chuang M.C., Lou S.L., Wang J., Thick-film textile-based amperometric sensors and biosensors, *Analyst*, 135, (2010), 1230–1234.
- [23] Gliścińska E., Solvent Vapour-Sensitive Activated Carbon Submicrofibres Based on Electrospun Polyacrylonitrile Fibre Mat, *Fibres & Textiles in Eastern Europe*, 4(112), (2015), 23, 14–24, DOI: 10.5604/12303666.1152737.
- [24] Huczko A., *Nanorurki Węglowe. Czarne diamenty XXI wieku*, WNT Warszawa, Polska, (2004), ISBN: 8388442864.
- [25] Graham A.G., Duesberg G.S., Seidel R.V., Liebau M., Unger E., Pamler W., Kreupl F., Hoenlein W., Carbon Nanotubes for Microelectronics?, *Small*, 1 (4), (2005), 382–390.
- [26] Kobashi K., Villmow T., Andres T., Häußler L., Pötschke P., Investigation of liquid sensing mechanism of poly(lactic acid)/multi-walled carbon nanotube composite films, *Smart Materials and Structures*, 18, (2009), 15–18.
- [27] Gliścińska E., Babel K., Krucińska I., Sposób wytwarzania aktywnych nanowłókien węglowych, *Zgłoszenie patentowe nr P. 391137*, (2009).
- [28] Gliścińska E., Babel K., Preparation of Activated Carbon Fibres from Electrospun Polyacrylonitrile Fibre Mat and Characterisation of Their Chemical and Structural Properties, *Fibres & Textiles in Eastern Europe*, 3(99), (2013), 42–47.
- [29] Krucińska I., Skrzetuska E., Urbaniak-Domagala W., Printed Textiles with Chemical Sensor Properties, *Fibres & Textiles in Eastern Europe*, 4(106), (2014), 68–72.

Design, Development, Characterization, and Application of Jute-based Needle-Punched Nonwoven

Sanjoy Debnath

Additional information is available at the end of the chapter

<http://dx.doi.org/10.5772/61705>

Abstract

Out of different technical textiles, needle-punched nonwoven is one of the promising technical textiles which has wide ranges of applications. This present chapter deals with jute and synthetic fibre-based needle-punched nonwoven. The design and manufacturing of such nonwoven and proper characterization of the developed fabrics based on the end use has been covered. Jute and jute-based material has some added advantages in certain technical applications like composites, agro-textiles, geotextiles, etc. Various machine parameters as well as processing parameters have been varied to design the fabrics for certain end uses. Applications of advanced modelling techniques like statistical and artificial neural network modelling have also been considered to achieve optimum properties in the fabric for certain end uses. Hence, the overall aspects of designing to end uses of the fabrics, considering its development and characterization, have been covered in this chapter.

Keywords: Jute, natural fibre, technical textiles, properties of nonwoven, designing of needle-punched nonwoven

1. Introduction

Jute fibre is one of the best fibres grown majorly in Bangladesh, India, Nepal, and China. The British introduced jute processing in India and Bangladesh. Initially, jute processing was made through flax machinery and found unsuitable. This forced the development of jute processing machinery, which was developed in Dundee, Scotland, and then the processing started in that country. Later the industry started in Bengal and India by the East India Company in the year 1856. Those days, jute fibre was imported from these Asian countries and products were developed in Europe (Dundee, Scotland). With the development and diversification of jute products from its conventional jute sacks as packaging material and carpet backing, the jute

nonwoven products are developed. These jute fibres are comparatively coarse in nature and have wide variation in fineness apart from its mesh-like structure. Its high moisture regain also places its suitability in certain applications. These properties make it more popular in the development of needle-punched nonwoven rather than the other nonwoven like thermal bonded and adhesive bonded nonwoven structures. Apart from these properties, the jute fibre is one of the cheapest natural fibre available commercially in countable amount.

Jute includes good insulating and antistatic properties, as well as having low thermal conductivity and a moderate moisture regain. It includes acoustic insulating properties and are manufacture with no skin irritations. Jute has the ability to be blended with other fibres, both synthetic and natural and accepts cellulosic dye classes such as natural, basic, vat, sulphur, reactive, and pigment dyes. Jute can also be blended with wool. By treating jute with caustic soda, crimp, softness, pliability, and appearance are improved, aiding in its ability to be spun with wool. Liquid ammonia has a similar effect on jute, as well as the added characteristic of improving flame resistance when treated with flame proofing agents.

Jute has a long history of use in the sackings, carpets, wrapping fabrics (cotton bale), and construction fabric manufacturing industry. However, the major breakthrough came when the automobile, pulp and paper, and the furniture and bedding industries started to use jute and its allied fibres with their nonwoven and composite technology to manufacture nonwovens, technical textiles, composite production of sheet moulding compound, resin transfer moulding, vacuum pressing techniques, and injection. In this chapter, the emphasis has been made on the design and development of jute-needle-punched nonwoven and their characterization in specific applications. Also, different important applications of jute and jute-based needle punched nonwovens have been covered.

2. Design and development of jute-based needle-punched nonwoven

Designing of needle-punched nonwoven from jute and its blend plays a very important role as far as the end product is concerned. The variation on fabric properties changes on various factors, like fabric weight, needling density, depth of needle penetration, needle gauge, blending of jute with other fibres, type of jute fibre used, pre-treatment of jute fibre, etc. Out of these various factors, the most influencing parameters are fabric weight, needling density, depth of needle penetration, and blending of jute with other fibres. Thus, the designing and development of jute needle-punched nonwoven neural network modelling approach holds good for designing, modelling, and the prediction of important properties. The following discussions describe these aspects.

2.1. Artificial neural networks modelling

The physiology of neurons present in biological neural system such as human nervous system was the fundamental idea behind developing the artificial neural networks ANNs. This computational model was trained to capture a nonlinear relationship between input and output variables with scientific and mathematical basis. In recent days, a commonly used

model is layered feed-forward neural network with multilayer perceptions and back propagation learning algorithms [1-4].

The ANNs are computing systems composed of a number of highly interconnected layers of simple neuron-like processing elements, which process information by their dynamic response to external inputs. The information passes through the complete network by linear connection with linear or nonlinear transformations. The weights were determined by training the neural nets. Once the ANN was trained, it was used for predicting new sets of inputs. Multi-layer feed-forward neural network architecture (Figure 1) was used for predicting the tenacity, initial modulus, air permeability, initial thickness, percentage compression, thickness loss, and compression resilience properties of fabrics [5-8]. The circle in Figure 3.5 represents the neurons arranged in five layers as one input, one output and three hidden layers. Three neurons in the input layer, three hidden layers, each layer consisting of three neurons and one neuron in the output layer. HL-1, HL-2, and HL-3 are the first, second, and third hidden layers, respectively, whereas i and j are two different neurons in two different layers. The neuron (i) in one layer was connected with the neuron (j) in next layer with weights (W_{ij}) as presented in Figure 1.

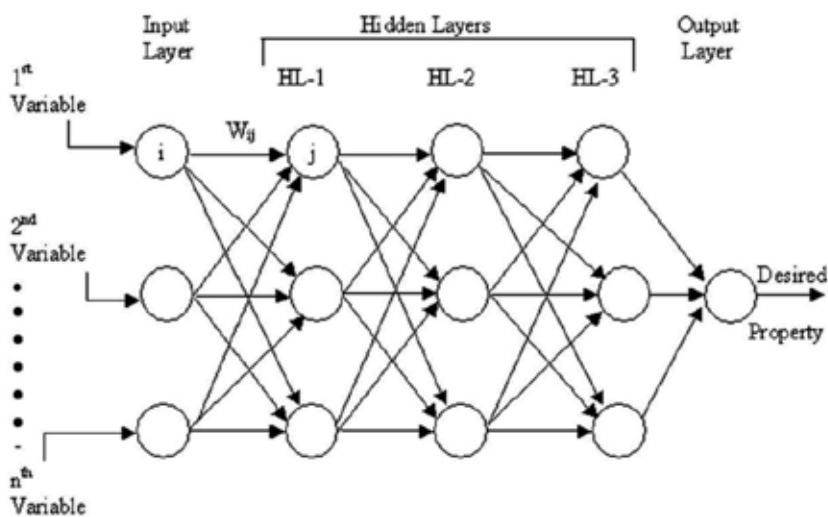


Figure 1. Neural architecture of the fabric property [8]

The data were scaled down between 0 and 1 by normalizing them with their respective values. The ANN was trained with known sets of input-output data pairs.

3. Characterization of jute-based needle-punched nonwoven

Unlike other fibre-based needle-punched nonwoven, jute needle-punched also requires specific tests to be evaluated to match its suitability in specific applications. This is because the

jute fibre has some of the unique features which others do not have, like high moisture regain, coarseness, biodegradability, high surface roughness, etc. Following are some of the important tests to be carried out to suit its suitability in some of those application areas.

3.1. Measurement of tensile property

Tensile is one of the most important properties to be evaluated for any textile material. To evaluate this property, all the samples are tested for tensile strip test on Universal Tensile Tester (UTM) following the standard test method ASTM D1682-64 under standard atmospheric condition ($65 \pm 2\%$ relative humidity and $27 \pm 2^\circ\text{C}$ temperature). For needle-punched nonwoven, the sample specimen width is 25.4 mm and the gauge length is to be set at 75 mm. The strain rate has to be set in such a way that the failure of the samples occurs between a time-span of 20 ± 3 seconds, depending on the type of fabric samples. Maximum load (in terms of Newton unit) breaking extension in percentage have to be recorded. From the value of breaking load, the tenacity values are calculated by the following formula [9]:

$$T = \frac{BL}{SW \times FW} \times 100$$

where, T – fabric tenacity (cN/tex); BL – breaking load (N); SW – specimen width (mm); and FW – fabric weight (g/m^2).

The initial modulus and secant modulus have also been calculated from the respective stress-strain curves.

3.2. Measurement of air permeability

The jute needle-punched nonwoven fabrics are porous in nature and hence they are permeable. To study the air permeability property, this test is carried out. Evaluation of air permeability nonwoven fabric samples can be done using any reliable air permeability tester (Shirley Air Permeability Tester). The results are expressed as the units of volume of air in cubic-centimetre, passed per second, through one square centimetre of fabric at a pressure difference of 10 mm or 1 cm head of water. But in some cases, the range of flow metre available in the instrument may not achieve the high flow rate required for this specific pressure difference. In such a case, superimposed layers of fabric on one another have been tested at a time and the flow rate reading for a single layer was calculated by multiplying the result by number of layers. Air permeability value was calculated by dividing the flow rate reading in cc/sec at 1 cm pressure head of water by the test area, which is in this instrument 5.07 cm^2 (1 inch²). Sectional air permeability (SAP) value was used to compare the permeability of different fabric samples. The SAP values of all the samples were determined from the following formula [10]:

$$SAP = AP \times T_0$$

where, SAP is the sectional air permeability in $\text{cm}^3/\text{s}/\text{cm}$; AP, the air permeability in $\text{cm}^3/\text{cm}^2/\text{s}$; and T_0 , the mean thickness in meter at 1.55 kPa pressure of the fabric sample. This test is

recommended to carry out at $65 \pm 2\%$ relative humidity and 27 ± 2 °C temperature after conditioning the sample for 24 hrs. For each sample 10 tests were performed.

3.3. Measurement of bending property

The stiffness of the jute needle-punched nonwoven textile fabric is used for technical textile, and samples are investigated by examining different bending parameters, for example, flexural rigidity and bending modulus, at $65 \pm 2\%$ relative humidity and 27 ± 2 °C temperature after conditioning the sample for 24 hours. The flexural rigidity of the fabric samples was determined by measuring the bending length following the standard cantilever principle by using the stiffness tester. The average value was calculated from 10 specimens in both warp and weft directions of the woven fabrics. Similarly for nonwoven samples both machine and cross directions of the fabric specimens were considered. The specimen size of each sample was 150 mm x 25 mm for higher flexible fabrics. The bending length was measured directly from the instrument. Flexural rigidity was calculated from the following formula [9]:

$$FR = \frac{WC^3}{10^4} \times 9.81$$

where FR = flexural rigidity in Newton in Newton-cm; W = fabric area density (g/m^2); and C = bending length in cm.

For bending modulus, the thickness of each sample was measured under the pressure of 1 lb/in² by using a thickness tester (ASTM D5199-91⁷). The bending modulus of the samples was determined from the following formula:

$$BM = \frac{12G}{g^3}$$

where BM= bending modulus in Newton/cm²; G= g = thickness (cm) of sample at 1 lb/in².

In case of thick and rigid fabric, the above method of measurement of bending length is not valid. In such a case, a loop method is suggested [11].

3.4. Design measurement of water imbibition property

For the measurement of water retention characteristics, the samples were cut into equal size of 4 cm x 4 cm and weight under the following natural atmospheric conditions, for example, dry bulb temperature 87°F, wet bulb temperature 81°F, and relative humidity 77%.

The samples are soaked in distilled water for about 48 hours. Later, all these samples are hung in free air for about 40 minutes to drip out the excess water absorbed by the samples. These samples are then kept on a blotting paper for 5 minutes to absorb further excess water present on the surface of the samples. Now, the weight of the wet samples is taken to find the absorbency of water by using the following formula [9]:

$$WA = \frac{W_{wet} - W_{dry}}{W_{dry}} \times 100$$

where WA is water absorbency in percentage, W_{wet} is the weight of fabric in wet condition, and W_{dry} is the weight of the fabric in dry condition.

Release of moisture with respect to time are determined for all samples unit they achieved the constant weight.

3.5. Compression

Compression is one of the important properties to be measured to evaluate the performance of the needle-punched nonwoven jute fabric for some specific application point of view like carpet, geotextile, etc. The initial thickness, compression, thickness loss, and compression resilience can be calculated from the compression and decompression curves. For measuring these properties, a thickness tester is required. The pressure foot area is 5.067 cm^2 (diameter = $\phi 2.54 \text{ cm}$). The dial gauge with a least count of 0.01 mm and maximum displacement of 10.5 mm is attached to the thickness tester. The compression properties are studied under a pressure range between 1.55 kPa and 51.89 kPa .

The initial thickness of the needle-punched fabrics is observed under the pressure of 1.55 kPa . The corresponding thickness values are observed from the dial gauge for each corresponding load of 1.962 N . A delay of 30 seconds is given between the previous and next load applied. Similarly, 30 seconds delay was also allowed during the decompression cycle at every individual load of 1.962 N . These compression and recovery thickness values for corresponding pressure values are used to plot the compression–recovery curves.

The percentage compression, percentage thickness loss, and percentage compression resilience are estimated using the following three relationships [12]:

$$C = \frac{T_0 - T_1}{T_0} \times 100$$

$$TL = \frac{T_0 - T_{21}}{T_0} \times 100$$

$$CR = \frac{W'_c}{W_c} \times 100$$

where C is the compression in percentage, TL is the thickness loss in percentage, CR is the compression resilience in percentage, T_0 is the initial thickness, T_1 is the thickness at maximum pressure, T_2 is the recovered thickness, W_c is the work done during compression, and W'_c is the work done during the recovery process.

The average of 10 readings from different places for each sample need to be considered. The coefficient of variation should be within 6%, if not a greater number of readings is necessary.

All these tests must be carried out in the standard atmospheric condition of $65 \pm 2\%$ RH and $20 \pm 2^\circ\text{C}$. The fabrics are conditioned for 24 hours in the above mentioned atmospheric conditions before testing.

3.5.1. Compression in wet condition

In some specific applications like geotextile, the jute and jute-based needle-punched nonwoven fabrics require special conditioning to test the fabrics under wet condition. To study the compression behaviour of needle-punched nonwoven fabric under wet condition [13-15], samples have to be cut into pieces of 25 cm x 25 cm and soaked in distilled water for a period of 24 hours before conducting the experiment. After 24 hours of soaking in distilled water the samples are passed through a pair of padding mangle with a uniform pressure exerted upon them by applying a constant load on either side of the top roller. The pressure between the padding mangles and their speed are constant. Under this condition, it can be assumed that the water pickup of the sample remained constant. Then, the sample is tested immediately for its compression property. The initial thickness, compression, thickness loss, and compression resilience were calculated from the compression and decompression curves. The compression, thickness loss, and compression resilience can be calculated from the above relationship mentioned above in Section 3.5.

3.6. Compression creep

There are some instances where the jute-based needle-punched nonwoven fabrics are used for floor mat and carpet applications. In such applications, the compression creep is one of the essential parameters required to be carried out to evaluate the compression deformation over a period of time. An instrument has been suggested as shown in Figures 2, to measure the compression creep of the needle-punched nonwoven fabrics [16-17].

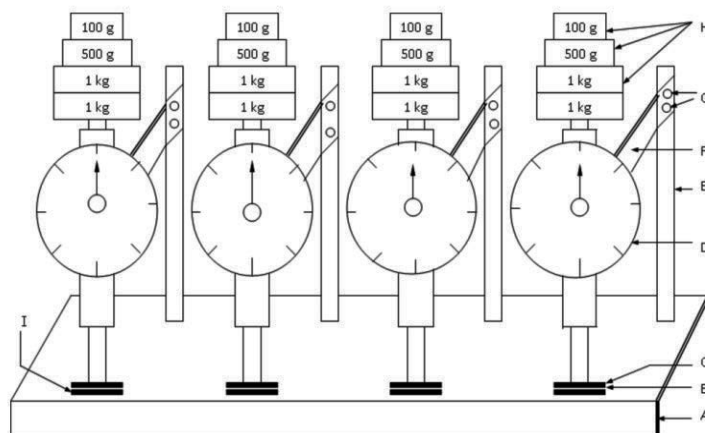


Figure 2. Instrument for measurement of compression creep [16-17]

The instrument is capable enough to measure the compression creep for four samples at a time. The fabric samples are mounted under a known compression load with a dial gauge (D) to measure the thickness under the compression. The pressure foot (C) diameter was chosen as 25.4 mm (1 inch) for all samples. The least count of the dial gauge (D) was 0.01mm. The nonwoven sample is placed between the pressure foot (C) and anvil (I). The initial thickness can be noted without adding any additional load. The instant deformation (T_0) is noted from the dial gauge after applying the compression load (H) of 25.51 N (2.6 kg) at the top of the weight pan (J) of the dial gauge (D). The selection of this pressure foot diameter of 25.4 mm and compression load of 2.6 kg is to simulate the area of the foot of a normal chair and the weight of a normal empty chair comes on the carpet surface through each leg of the chair, respectively. To study the compression creep, each sample is allowed to remain under this compression load for 168 hours (7 days). This compression creep time was selected because it was found from previous study that all the fabric's compression creep reaches equilibrium within 168 hours. The compression creep (%) is evaluated from the thickness deformation values, which are measured using the following relation:

$$CR = \frac{T_0 - T_t}{T_0} \times 100$$

where CR is a compression creep in percentage, T_0 is the instant thickness after applying the maximum load, and T_t is the thickness after 7 days.

The average of 10 readings from different places for each sample is considered. The coefficient of variation should be less than 6% in all the cases. The fabrics required conditioning for 72 hours in the above-mentioned condition before carrying out the experiment.

3.7. Thermal resistance

The thermal resistance of a textile material is usually defined by the ratio of the temperature difference between the two faces of the fabric material to the rate of flow of heat per unit area normal to the faces. It is analogous to the electrical resistance in case of current flow through an electrical conductor. Disc method, an application of Lee's disc apparatus to textiles, was employed to evaluate thermal resistance of polyester needle-punched nonwoven fabric samples. In this method, the material under test is held between two metal discs of which one has known thermal resistance. In steady condition, the temperature drop across the metal disc with known thermal resistance and across the material under test is measured, and from the values obtained the thermal resistance of the specimen is determined by the following techniques.

Let TR_k and TR_s be the thermal resistance of the known disc and the sample under test, respectively. Let t_1 be the temperature registered by the lower surface of the known disc, t_2 be the temperature registered by the lower surface of the sample under, and t_3 be the upper surface of the sample under test. Assuming constant rate of flow of heat at steady state condition, the TR_s is computed from the following formula in degrees Kelvin square metre per Watt:

$$\frac{t_1 - t_2}{TR_k} = \frac{t_2 - t_3}{TR_s}, \text{ or } TR_s = TR_k \times \frac{t_2 - t_3}{t_1 - t_2} \quad (1)$$

In this experiment, a guarded two-plate thermal resistance instrument has been used to measure the thermal resistance of jute-based needle-punched fabrics [18-19]. The thermal resistant instrument is based on a microprocessor and provides automatic results of thermal resistance value in ‘tog’. The area of the test specimen used is 706.85 cm² (diameter 30 cm). The test is non-destructive and the process of preparation of sample is free from human error. Thermal insulation of each fabric sample is measured randomly at five different places under a pressure of 0.3352 kPa. The average of five readings was considered and the coefficient of variation of readings was < 2%.



Figure 3. Instrument for measuring the thermal resistance of fabrics [19]

The specific thermal resistance (STR_s) value is used to compare the thermal resistance of different fabric samples. STR_s values of all the samples are determined using the following equation:

$$STR_s = \frac{TR_s}{T_0}$$

where STR_s is the specific thermal resistance in K m²/W; TR_s , the thermal resistance value of fabric in K m²/W; and T_0 , the mean thickness in meter at 1.55 kPa pressure of the fabric sample.

3.8. Evaluation of water absorbency

The fabric samples were cut into equal size of 4 cm x 4 cm, and conditioning in the standard atmospheric condition of $65 \pm 2\%$ RH and $20 \pm 2^\circ\text{C}$. The fabrics were conditioned for 24 hours in the above-mentioned atmospheric conditions and the dry weight (W_D) was measured. To study the water absorbency, samples were dipped in distilled water for 24 hours to ensure uniform soaking of water and then wet samples were hung in free air for about 30 minutes to drip out the excess water absorbed by the samples. Now, the weight (W_W) of wet samples was measured. The water absorbency [20] was calculated using following relationship:

$$WA(\%) = \frac{(W_W - W_D)}{W_D} \times 100$$

The average of 10 results was considered.

3.9. Evaluation of soil moisture control

The soil moisture can be efficiently controlled by the jute agro-textile. This is very essential to maintain the soil moisture for longer duration and thereby the water requirement during irrigation can be minimized. Suitable jute agro-textile can be used as mulching material. To find the efficacy of the performance of the jute-based mulching material for controlling the soil moisture, two simulated methods are recommended, namely, non-contact method and contact method. The importance of these two different methods is that during application of the agro-textile the fabrics are not assured to touch the contours of the soil surface uniformly both in lengthwise as well as widthwise directions of the fabrics. Following are the two methods recommend to measure the soil moisture control using jute needle-punched nonwoven fabrics [21].

3.9.1. Non-contact method

Some place of the mulching needle-punched nonwoven agro-textile will not come in contact with the soil surface due to the contours of the soil. To study the moisture of soil on those non-contact areas of the fabric, this method is considered [21]. In this measurement, six beakers of 100 ml are taken containing 25 ml of water in each beaker. Among them, the mouths of five beakers are tightly covered with the fabric samples and the rest are kept as control without any fabric cover. These beakers containing water and samples were weighed initially and weights were repeatedly taken at certain time interval until they reached a constant weight. This experiment is conducted under normal atmospheric conditions. At each time interval, the percentage evaporation loss is calculated from the weight difference of the individual beaker assembly at that point of time with respect to its initial weight. The results are plotted as a time versus cumulative evaporation loss to compare the performance of various agro-textile fabrics of different fabric weight.

3.9.2. Contact method

In this test, six similar size petri dishes have to be taken containing 90 gm of standard alluvial soil with saturated moisture in each pretty dish. The five petri dishes are covered with fabric samples in such a way that the fabrics have direct contact with the moist soil. The control dish is not covered with any sample fabric. To determine the moisture barrier property, the weight of each dish with soil and sample is measured initially. These weights are further taken at certain time intervals until all the dishes reach a constant weight. The cumulative evaporation loss is calculated in a similar method like non-contact process [21]. The results are plotted as a time versus cumulative evaporation loss to compare the performance of various geotextile fabrics of different fabric weight. This experiment is replicated five times and the average of five readings for each sample was calculated.

3.10. Evaluation of soil temperature control

The application of jute agro-textile mulch has influence on the control of soil temperature. This factor depends on various aspects of jute needle-punched nonwoven fabric design and parameters selected during manufacture of the fabrics. In this test, jute needle-punched nonwoven and commercial plastic mulch (black polyethylene sheet 50 g/m² and thickness 20 µm) materials are compared with respect to control soil (without any mulch). A plot is made to determine soil temperature behaviour with respect to time against control [21].

Three earthen pots of the same size and shape were taken and the same quantity of alluvial soil is filled in each pot. The same quantity of water is poured in all the pots till saturation level is achieved and excess water is poured out. Under this condition, the surface water is allowed to evaporate for 24 hours so that the same ambient conditions are attained in all the pots. Needle-punched jute nonwoven and commercial black polyethylene sheets of 50 g/m² microns are laid on the top of the soil on each pot. Utmost care is to be taken to see to it that no part of the soil surface is left exposed/uncovered by the agro-textiles/experimental materials. Before covering with the mulching materials, the soil temperature is measured in each pot. The temperature is measured approximately 1 inch below the soil surface at five different spots and averaged to determine the mean temperature. Soil temperatures are determined identically as above at a fixed interval of two hours. This study needs to be continued for four days and temperatures recorded for all the three pots including control and can be represented graphically.

3.11. Measurement of sound insulation

An unwanted noise, a part of sound is irritating and which caused many problem of human related to mental and psychological aspects. Jute needle-punched nonwoven textile materials have good property to control sound if they are properly designed for this purpose. A simple design of such an instrument to measure the sound insulation of the textile nonwoven materials has been explained by Sengupta, 2010 [22]. It consists of a sound insulating box which is made out of 12 mm thick rigid plastic (acrylic sheet) and has a provision of removable top lid. Inside one vertical wall of this box, a sound source and a decibel meter (s) are fixed. In

another movable (to adjust the distance between sound source and receiver) vertical wall, a decibel meter (R) is fixed coaxially opposite to the sound generator to measure the sound intensity. In between these two decibel meters, a sliding (to adjust the distance between sound source and fabric) arrangement is there to fix the fabric sample vertically. An electrical panel has been used to control the sound intensity. Figure 4 shows the schematic diagram of the sound insulation tester as described above [22].

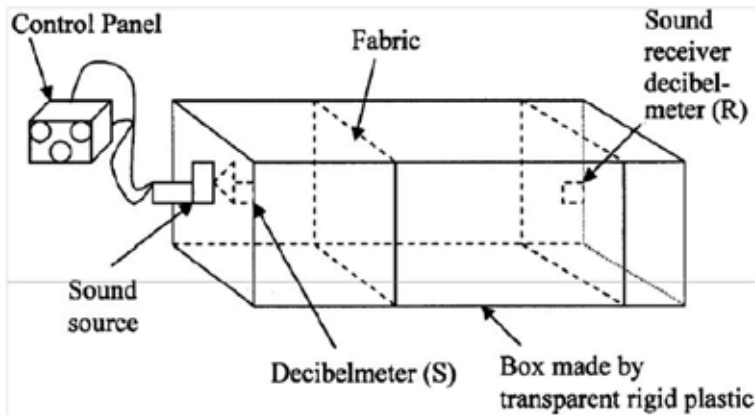


Figure 4. Schematic diagram of sound insulator tester [22]

Operating the control panel, a sound of particular decibel sound is created. The source decibel and the receipt decibel are measured by two-decibel metres S and R, respectively, without and with fabric samples. The sound reduction responsible for fabric, where sound insulation is expressed as the difference between the decibel reduction with sample and decibel reduction without sample, is shown below:

$$db_F = (dB_S - dB_R)_{WS} - (dB_S - dB_R)_{WOS}$$

where db_F is the sound reduction responsible for fabric; dB_S is the sound intensity at source; db_R is the sound intensity at receiver; WS is with sample; and WOS is without sample.

3.12. Measurement of electrical resistance

Textile materials have good electrical insulation property provided they are in dry condition. There are many such applications where the textile materials (fibre/yarn/fabric) are used as electrical insulation purposed. The electrical insulation application of the textile materials are used in medium voltage ranges (within 415 V). To measure the electrical insulation a circuit is necessary which measures the current-voltage (V-I) characteristics of textile material as shown in Figure 5 [23-24].

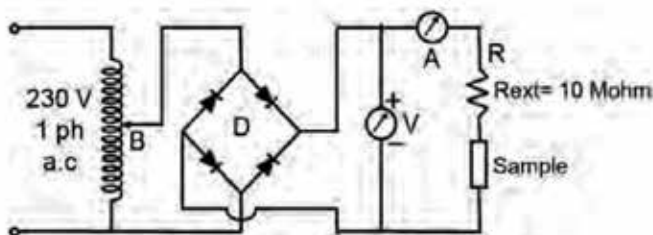


Figure 5. Circuit for electrical resistance of nonwoven [23]

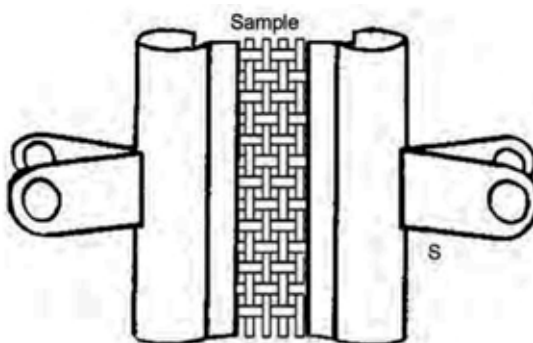


Figure 6. Sample holder

This circuit consists of sample holder (S), variac (B), rectifier unit (D), ammeter (A), voltmeter (V), and $10 \text{ M}\Omega$ discrete resistance (R). Two bulldog-clips are used between which the sample is placed (Fig. 6) with gauge lengths 2.54, 5.08, and 10.16 cm. The sample is in series with a known resistance ($10 \text{ M}\Omega$) and is connected to a D.C. power supply. The voltage is varied from 80V to 220V in 5 steps and corresponding current through the sample is measured after 10s to calculate the resistance [25-26]. The measurement is done at 27°C and 65% relative humidity. Five sets of voltage-current readings are taken for plotting V-I characteristic curves. The slope (voltage/current) or resistance for each V-I characteristic is determined. The specific resistance has been calculated normalizing the resistance by thickness [multiplying/dividing the resistance (Mega ohm) by thickness (cm)].

4. Application of jute-based needle-punched nonwoven

Needle punched nonwoven are mostly used in various applications. Jute itself is popular for application in the packaging industry and in carpet industry as carpet backing material. However, the jute-based needle-punched nonwoven find its application in geotextile, agro-textile, composite reinforcing material, sound insulating material, air filter, carpet, thermal

insulating material, etc. as per as the agricultural application is concerned; it is mostly used as mulching material, thermal insulating material for control soil temperature, soil moisture control material, cannel lining material, horticultural nursery pot, etc. some of the promising applications and case studies are covered below.

4.1. Application for mulching application

Efficient management of soil moisture by jute needle-punched nonwoven for cultivation of horticultural crops in red lateritic zone has been attempted at West Medinapur District of West Bengal, India. The experiments on vegetable cultivation were laid out in randomized block design (RBD) with three vegetables – cauliflower, tomato, and beans – and four types of jute nonwoven mulch of fabric densities 150 g/m², 200 g/m², 250 g/m², and 300 g/m² excluding control. There is evidence that mulching with jute geotextiles increased the yield of cauliflower substantially and that of tomato to a lesser extent. It had practically insignificant effect in the yield of beans. Maximum yield of 73.66 t/ha of cauliflower was obtained with jute nonwoven fabric of 250 g/m² (control 49.08 t/ha) whereas tomato's increased yield was 110.39 t/ha with 150 g/m² fabric as compared to 83.39 t/ha achieved under controlled conditions. However, beans had negative effect with mulching by jute nonwoven. The results also confirm that mulching with jute nonwoven of 300 g/m² fabric density increased the yield of sweet lime fruits substantially, that is, more than 100 fruits per plant per year as compared to only 34 fruits per plant per year obtained under traditional cultivation method [27-28].

Nonwoven fabric samples were selected as mulch materials at the experimental field of tea plantation, situated at Gopali village (near IIT, Kharagpur, West Bengal). In the first phase, these fabric samples were laid in between the two rows of tea plants (Tocklai of Assam variety) where the spacing between the two rows was 1 metre and between the two plants in a row was 0.7 metre. The length of each row was 16 metres. For each sample two rows were used for mulching experiment. Jute nonwoven samples (150, 200, and 250 g/m²) each of 32 metres in length were used for the continuous row mulching process. Two separate rows were kept for control/without any mulching material. Uniform amount of water was spread over the tea plantation in both the control and mulched area using standard sprinkler at the rate of 5hours/day. The mulch performance was studied by measuring the biomass in 2-month intervals. Some critical observations regarding the types of weeds grown were also reported. This experiment was replicated five times for test of significance.

4.2. Application for cannel lining

Four trapezoidal channels of 50 metre length each were constructed with zero bed slope and were lined with jute geotextile (nonwoven geotextile coated with polythene sheet either on single side or double sides) of 1 metre width and different fabric densities. Final dimensions of the channels were measured at different sections of each of the channels and average dimensions were determined as shown in Table 1 [29]. The experiment was undertaken in field channels laid out in the experimental farms of BCKV, Mohanpur, Nadia, West Bengal.

The weather data consisting of daily maximum and minimum temperatures, evaporation, rainfall, and maximum and minimum relative humidity were collected from the weather

station located in the farm. From the difference in water depths and water level widths between two consecutive days, the total loss of water from the channel was calculated. Total loss consists of evaporation and seepage losses from the channel as shown in Table 2. Evaporation loss was estimated by daily evaporation and channel dimensions. The seepage volume was calculated by adjusting the evaporation loss that occurred from the average surface area of water level during the period. The rate of seepage was determined by dividing the seepage volume by average wetted area of the channel. The observations and results noted and statistical analysis of the daily seepage values have been done on one factor randomized complete block design and the analysis of variance.

Both ends of the channels were blocked so that water can be retained in them. The channels were filled with water and depth and top width of water in the channels were recorded every day at 8 A.M. till the water levels reached about half of the initial level.

Various lining materials such as precast channel, brick masonry, bituminous mixture, soil cement, polythene sheets, etc., have so far been used for controlling seepage in irrigation channels. Some are too costly to be locally used while others have short life and are not much effective. Keeping it in view, this work was taken up to find out a viable alternative to these traditional materials. In this project, jute nonwoven geotextile of 250 g/m² and 300 g/m² fabric weight were coated with polyethylene sheet on one side and both sides and were experimented to assess the seepage loss through open channels. 300 g/m² fabric with both sides coated controlled seepage most efficiently. Single side coated sheets also performed well in seepage control, but allowed more water to seep compared to double side coated sheets. However, 250 g/m² fabric with both sides laminated yielded optimum performance.

Water losses in watercourses and field channels may occur by seepage, breaches along the channels through rat holes, and ponding of water in depressions and channel sections. Unlined irrigation channels account for overall seepage losses between 20% and 30%. Geotextile fabrics are very effective in controlling seepage from open channels. Jute nonwoven fabric of 300 g/m² (double sides coated) controlled seepage losses most efficiently. However, considering the permissible limit of seepage and cost factors, 250 g/m² fabric (both sides coated) may be recommended.

4.3. Application for horticultural nursery pot

Horticulture pot of 3' × 8' has been made from jute needle punched fabric for use in nursery in place of conventionally used plastic bag. The jute needle punched nonwoven is made from TD3 jute and waste jute. In both cases, scrim cloth reinforcement has been given at the back to avoid the damage during use and to retain dimensional stability [30].

4.4. Application for jute geotextile application

Jute needle-punched nonwoven has been successfully used as reinforcing material in the construction of rural road in Guptipara, Hooghly, West Bengal, India. There are also examples of using jute geotextile on river bank protection. The bank was first cut to a suitable slope of 30°, approximately same as the angle of internal friction of the bank soil. The surface was levelled and made free from angular projections, undulations, soil slurry, and mud. JGT rolls

were unrolled and placed along the slope from top down to the lowest water level. Care was taken to see that JGT was laid with the overlapping in the direction of water flow. More rolls were rolled along the length of the bank and two layers of same area/fabric density were placed one upon the other with sufficient overlap. JGT was fixed to the bank with the help of bamboo pegs in either direction. Care was taken to ensure that JGT does not suffer damage due to puncture, tear, and similar operational stresses and it touches the bank slope at all points (proper drapability). Suitable grass seeds were then spread on the treated bank for better stabilization. The growth of grass was observed at 15-day intervals by determining the average number of seedlings per unit area and the average length of grass [31].

4.5. Application for jute-based needle-punched nonwoven in garment

In the manufacturing of warm garments like jackets, very fine jute-polypropylene fibre-blended needle-punched nonwoven of 90 g/m² as inner lining material can produce good thermal insulating property. Due to very poor strength of 90 g/m² reinforced cotton gauge cloth of 20g/m², produce sufficient strength for easy handling during manufacturing process of the garment. The five repetitive washing of jacket made of jute-polypropylene fibre blended needle-punched nonwoven used as inner lining material and outer material is of jute-polyester and cotton blended union fabric shows no significant change on its performances.

5. Conclusions

Jute needle-punched nonwoven has vast application in different industrial sectors. Proper designing and development of material is needed for particular application. Selection of jute fibre and blended material in specific application makes the needle-punched nonwoven product more useful. Apart from the applications mentioned, there exists ample scope in the development of specific product for air filtration, sound insulation materials, etc., for which specific tests have been recommended. Overall jute-needle-punched nonwoven has wide scope in future industries due to its sustainability in product development. Moreover, nonwoven from jute-based materials has added advantage of environment friendly disposal. This gives jute-based nonwoven a priority over synthetic fibre-based nonwovens.

Author details

Sanjoy Debnath*

Address all correspondence to: sanjoydebnath@yahoo.com

ICAR-National Institute of Research on Jute & Allied Fibre Technology, Kolkata –West Bengal, India

References

- [1] Vangheluwe L., Sette S., and Pynckels F. Assessment of set marks by means of neural nets. *Textile Research Journal*, 1993:63(4):244-246. ISSN 0040-5175
- [2] Rajamanickam R., Hansen S. M., and Jayaraman S. Analysis of the modelling methodologies for predicting the strength of air-jet spun yarns. *Textile Research Journal*, 1997:67(1):39-44. ISSN 0040-5175
- [3] Zhu R., and Ethridge M. D. Predicting hairiness for ring and rotor spun yarns and analysing the impact of fibre properties. *Textile Research Journal*, 1997:67(9):694-698. ISSN 0040-5175
- [4] Wen Chen P., Chun Liang T., Fai You H., Li Sun W., Chueh Wang N., Chyilin H., and Cherng Lien R. Classifying textile faults with a back propagation neural network using power spectra. *Textile Research Journal*, 1998:68(2):121-126. ISSN 0040-5175
- [5] Debnath S., Madhusoothanan M., and Srinivasmoorthy V. R. Modelling of tensile properties of needle-punched nonwovens using artificial neural networks. *Indian Journal of Fibre & Textile Research*, 2000a:25(1):31-36. ISSN 0971-0426
- [6] Debnath S., Madhusoothanan M., and Srinivasmoorthy V. R. Prediction of air permeability of needle-punched nonwoven fabrics using artificial neural network and empirical models. *Indian Journal of Fibre and Textile Research*, 2000b:25(4):251-255. ISSN 0971-0426
- [7] Debnath S., and Madhusoothanan M. Modeling of compression properties of needle-punched nonwoven fabrics using artificial neural network. *Indian Journal of Fibre & Textile Research*, 2008:33(4):392-399. ISSN 0971-0426
- [8] Debnath S. Chapter 3: Modelling of needle-punched nonwoven fabric properties using artificial neural network. In: Kenji Suzuki, editor. *Artificial Neural Networks - Industrial and Control Engineering Applications*. Rijeka, Croatia: InTech; 2011, p. 65-88. ISBN: 978-953-307-220-3
- [9] Debnath S., Nag D., De S. S., Ganguly P. K., and Ghosh S. K. Studies on mechanical and hydraulic properties of JGT for geo-technical applications. *Journal of The Institution of Engineers (India)*, 2006:TX86(2):46-49. ISSN 0257-4438
- [10] Debnath S., and Madhusoothanan M. Thermal insulation, compression and air permeability of polyester needle-punched nonwoven. *Indian Journal of Fibre & Textile Research*, 2010:35(1):38-44.
- [11] Debnath S., Kane C. D., Kadole P. V., and Patil C. A. Needle-punched non-woven blankets from polyesters. *Indian Textile Journal*, 1994:105(3):72-80.
- [12] Debnath S., and Madhusoothanan M. Compression behaviour of jute-polypropylene blended needle-punched nonwoven fabrics. *Indian Journal of Fibre and Textile Research*, 2007:32(4):427-433. ISSN 0971-0426

- [13] Debnath S., and Madhusoothanan M. Studies on compression properties of polyester needle-punched nonwoven fabrics under dry and wet conditions. *Journal of Industrial Textiles*, 2012a:41(4):292-308. DOI: 10.1177/1528083711416394
- [14] Debnath S., and Madhusoothanan M. Compression behaviour of jute-polypropylene blended needle-punched nonwoven under wet condition. *The Journal of The Textile Institute*, 2012b:103(06):583-594. DOI: 10.1080/00405000.2011.592662
- [15] Debnath S., and Madhusoothanan M. Studies on compression behaviour of polypropylene needle punched nonwoven fabrics under wet condition. *Fibres and Polymers*, 2013:14(5):854-859.
- [16] Debnath S., and Madhusoothanan M. Compression creep behaviour of polyester needle-punched nonwoven fabrics. *Journal of The Textile Institute*, 2012a: 103(12): 1328-1334. DOI: 10.1080/00405000.2012.680696
- [17] Debnath S., and Madhusoothanan M. Compression creep behaviour of jute-polypropylene blended needle-punched nonwoven, *Textile Research Journal*, 2012b:82(20): 2097-2108. DOI: 10.1177/0040517512445336
- [18] Debnath S., and Madhusoothanan M. Thermal resistance behaviour of polyester needle-punched nonwoven. *Journal of The Institution of Engineers (India)*, 2011a: 91TX(2):27-33.
- [19] Debnath S., and Madhusoothanan M. Thermal resistance and air permeability of jute-polypropylene blended needle-punched nonwoven. *Indian Journal of Fibre & Textile Research*, 2011b:36(2):122-131.
- [20] Debnath S., and Madhusoothanan M. Water absorbency of jute-polypropylene blended needle-punched nonwoven. *Journal of Industrial Textiles*, 2010a:39(3):215-231. DOI: 10.1177/1528083709347121
- [21] Debnath S., Ganguly P. K., De S. S., and Nag D., Control of soil moisture and temperature by light weight jute fabrics. *Journal of The Institution of Engineers (India)*, 2010:90TX(2):16-19.
- [22] Sengupta S. Sound reduction by needle-punched nonwoven fabric. *Indian Journal of Fibre & Textile Research*, 2010:35(3)237-242.
- [23] Sengupta S., and Sengupta A. Electrical resistance of jute fabric. *Indian Journal of Fibre & Textile Research*, 2013a:37(1):55-59.
- [24] Sengupta S., and Sengupta A. Electrical resistance of jute needle-punched non-woven fabric – Effect of punch density, needle penetration and area density. *Journal of the Textile Institute*, 2013b:104(2):132-139.
- [25] Sengupta S., and Debnath S. A system for measuring electrical behaviour of textile material, Indian Patent File no. 1188/KOL/2014, dated Nov 17, 2014a.

- [26] Annual Report 2013-14, National Institute of Research on Jute & allied Fibre Technology Kolkata, India, 2014b:24-26.
- [27] Nag D., Choudhury T. K., Debnath S., Ganguly P. K., and Ghosh S. K. Efficient management of soil moisture with jute non-woven as mulch for cultivation of sweetlime and turmeric in red lateritic zone. *Journal of Agricultural Engineering (India)*, 2008:46(3):59-62. Print ISSN 0256-6524
- [28] Nag D., Debnath S., Ganguly P. K., and Ghosh S. K. Efficient management of soil moisture by jute geotextile for cultivation of horticultural crops in red lateritic zone. *Journal of The Institution of Engineers (India)*, 2010:AG 91(1):21-24.
- [29] Choudhury M. R., Chatterjee P., Dey P., Nag D., Debnath D., Ghosh S. K., and Ganguly P. K. Lining of open channel with jute geotextile and its performance in seepage control. *Journal of Agricultural Engineering*, 2008:45(4):83-86. Print ISSN 0256-6524
- [30] Anonymous. NIRJAFT Annual report 2011-2012. 2012:72-73.
- [31] Ghosh S. K., Debnath S., Nag D., and Ganguly P. K. Geo-jute for river bank protection – a case study. *Journal of Agricultural Engineering (India)*, 2006:43(3):62-65.
- [32] Debnath C. R., and Roy A. N. Mechanical behaviour of needle punched textiles of jute nonwovens. *Indian Textile Journal*, 1999:110(3):50-53. ISSN 0019-6436
- [33] Sengupta S., and Debnath D. Agro-textile: use of jute nonwoven. In: Nag D. et al., editor. *Jute and Allied Fibres: Issues and Strategies*. New Delhi, India: The Indian Natural Fibre Society, Kolkata; 2014, p. 409-401.

Nanotechnology Formulations and Modeling of Hydraulic Permeability Improvement for Nonwoven Geotextiles

Han-Yong Jeon

Additional information is available at the end of the chapter

<http://dx.doi.org/10.5772/61997>

Abstract

First, the general concept of nanotechnology formulations used to manufacture geotextiles (GT) is introduced. Separation and filtration functions using geotextiles from nanoclay formulations are introduced as important concepts. Yellow clay was added as nanoparticles to make a polyester formulation in turn to make nonwoven geotextiles to improve the removal effects of toxic and organic components of leachate solutions. Engineering behavior was evaluated to confirm the effects of adding yellow clay. There is a possibility of nanocomposite formulations for geosynthetics in the future. Second, sustainable laminar geotextile composites with different fiber-packing densities were made, and the effects of laminar structures were examined on water permeability. To fabricate these materials, the fiber-packing densities of laminar geotextile composites were discriminated correspondingly. The experimental values of water permeability by permittivity test were smaller than those of the theoretical values due to the loss of hydraulic pressure at the interface between geotextiles. To interpret the water permeability behaviors, structural model of tubes with different fiber-packing densities was applied. Finally, the inlet forms – bell mouth and soft tube structures – of laminar geotextile composite pores were estimated from the loss rates of hydraulic pressure.

Keywords: Nanotechnology formulations, yellow clay, nanoparticles, leachate solution, nanocomposites, laminar geotextile composites, permeability, structural model of tubes, inlet forms, loss rates of hydraulic pressure

1. Introduction

1.1. Nanotechnology to fibers

Nanotechnology is a new technology which can make an ultimately fine material such as a fiber (see Figure 1) by controlling atoms and molecules as small as 10^{-9} m in size, and this technology can be widely used in many industrial situations. Among the many possible nanoproducts, nanofibers could be controlled for fiber length, diameter, surface properties, pore distribution, fiber evenness, cross-sectional shapes, etc.

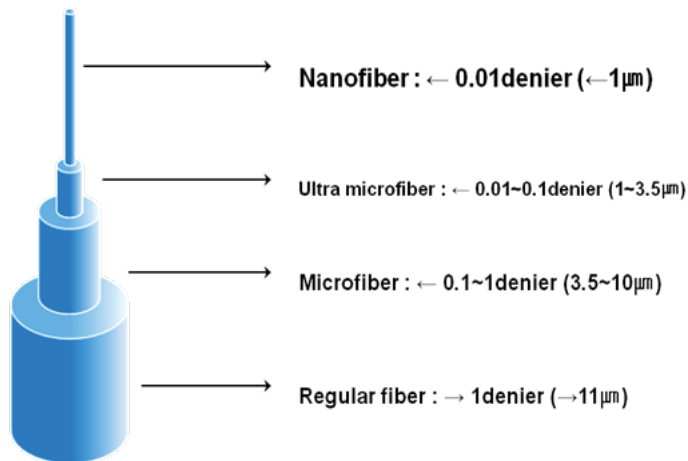


Figure 1. Comparison of nanofibers to conventional standard fibers.

Nanofibers are one of the most advanced materials which can be easily designed with high-performance materials having distinctive properties. New geosynthetic materials which have separation, filtration, and absorption functions and are specifically made could be developed in the field of geoenvironmental applications. (Koerner, R. M., 2005) In addition to fibers, nanoparticles (such as nanoclay) can be used to make unique formulations, which can, in turn, be used to make conventional fibers for geotextiles and yarn-type geogrids. As an example of nanocomposite geosynthetics in geoenvironmental applications, it is very important to eliminate the toxic and organic components of various waste leachate solutions. Such capability is not found in the standard manufactured nonwoven geotextiles and hence the functional nonwoven geotextiles need to be manufactured which can absorb the toxic and organic components that may be harmful to personal health and the environment.

It is possible to manufacture these types of functional nonwoven geotextiles by using nanotechnology. Section 2 describes nanofiber technology to gain insight into extremely small-scale manufacturing. Section 3 describes the objective of this study that introduces nanoclay into a polymeric formulation to manufacture a geotextile for use in geoenvironmental applications. Section 4 provides commentary for future applications.

1.2. Nanofiber application methods

Figure 2 shows various aspects of nanofiber manufacturing technology and productivity of nanofibers where it is seen that mass production of nanofibers is possible by modified electrospinning. Electrospinning is the general method used to manufacture nanofibers, which is similar to the melt-blown method, but the current problem is to increase mass productivity.

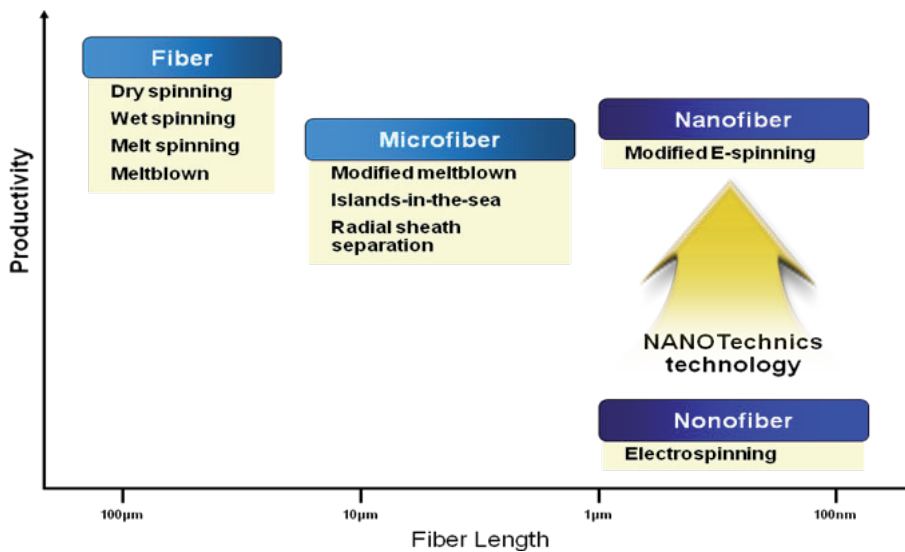


Figure 2. Fiber manufacturing technology and productivity.

In general, regular fibers are widely used to manufacture geotextiles and yarn-type geogrids, but filtration efficiency of microfibers and nanofiber geotextiles would be better than the standard fiber used to manufacture conventional geotextiles. To be considered, it is expected that nanofiber geosynthetics could provide the sustainable filtration function in geoenvironmental applications by their composition structure as shown in Figure 3. If the numbers of filled fibers per unit area increases, the pore size among nanofibers is decreased. Therefore, fine pollutants cannot pass through pores made by nanofibers and the filtration efficiency will be improved. This means that ultrathin geosynthetic filters can be manufactured having a high-quality filtration function to absorb fine impurities and toxic components in both polluted water media and polluted air media (Figure 4). Figure 5 shows the separation concept of a nanofiber air filter by pressure. To optimize this air filter, a higher particle collection and dust retention rate are required. Therefore, hybrid-type air filters must be the optimum, and Figure 6 shows such fiber materials versus fiber length. For hybrid membrane technology (HMT) and expanded PTFE materials, nanofiber layers are accumulated above the general fiber materials as a hybrid material. This is the important result of larger specific adsorption area in the surface of geosynthetics. Figure 7 shows the relationship between separation fields and separation membranes using fiber-related nanotechnology.

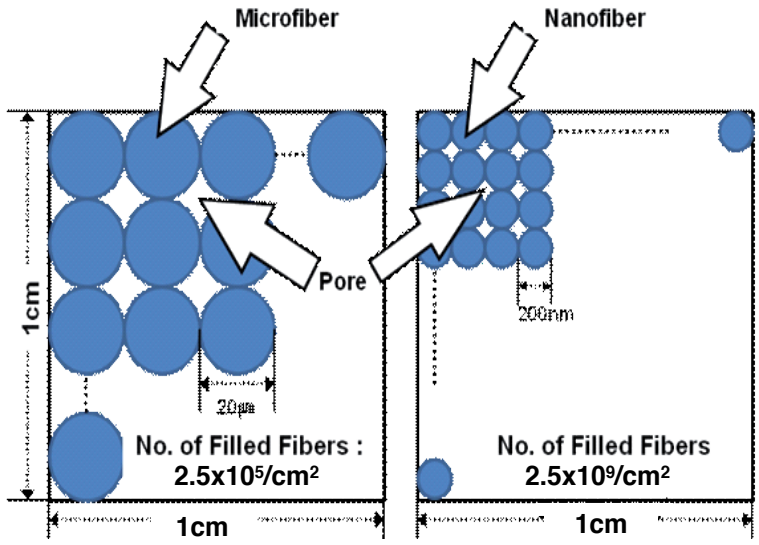


Figure 3. Fiber filling between microfiber and nanofiber per unit area.

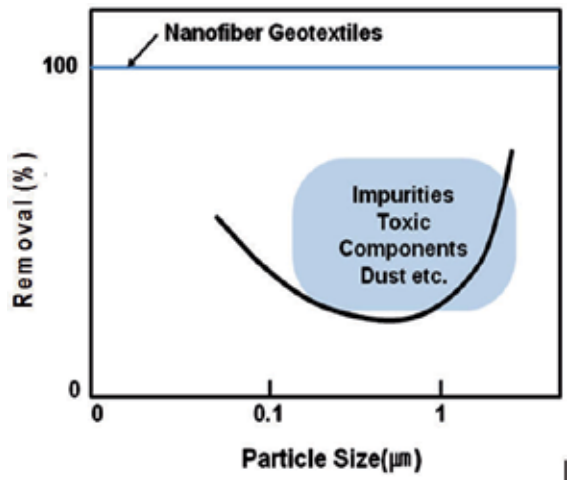


Figure 4. Effect of using a nanofiber geotextile filter.

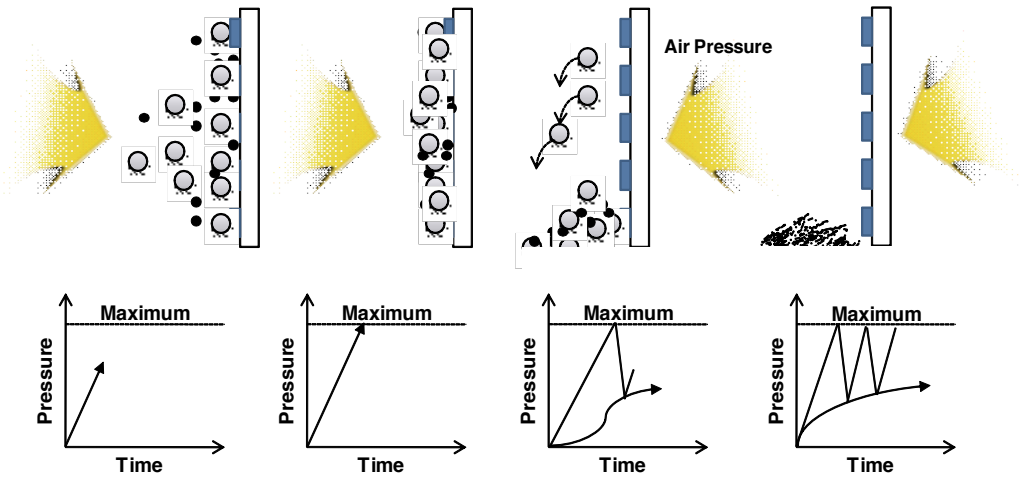


Figure 5. Maintenance of filtration efficiency for nanofiber filters.

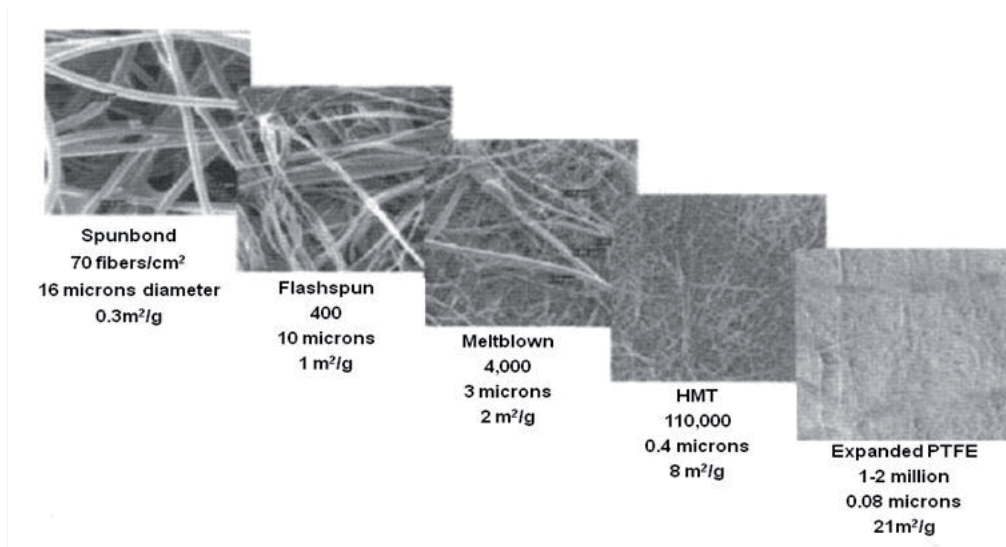


Figure 6. Comparison of fiber diameter and surface area using nanofiber and other fibers.

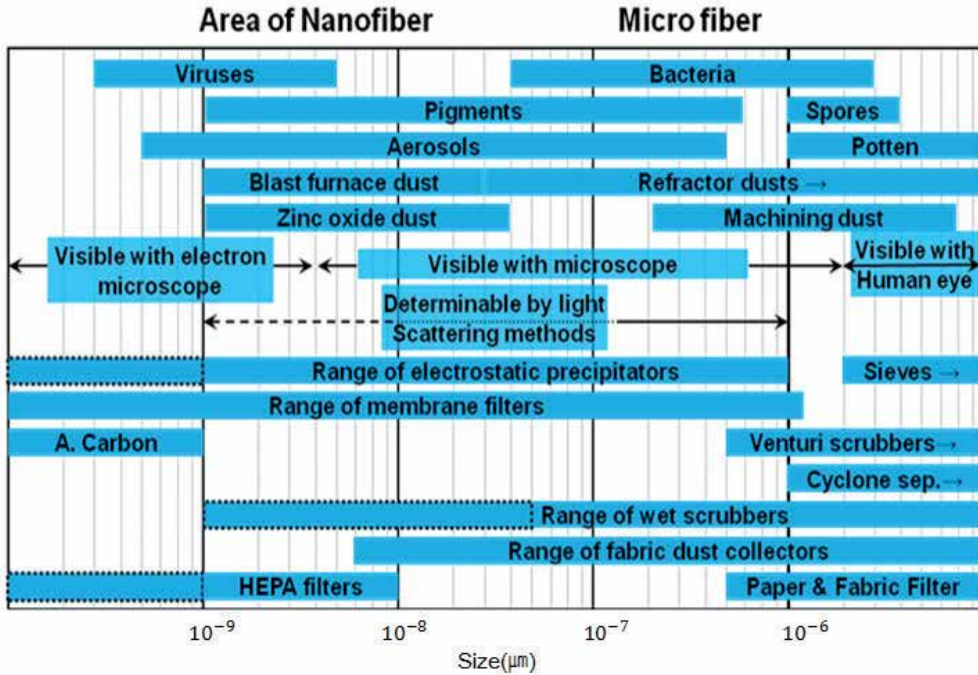


Figure 7. Relationship between separation fields and separation membranes using nanotechnology.

1.3. Nonwoven geotextiles by nanotechnology formulations

1.3.1. Nano clay fibers geotextiles

A related aspect of nanotechnology is to use one or more components of a blending formulation in the nanoscale so as to create a nanocomposite formulation. Having pellets made from such a formulation, standard manufacturing processes can be used to manufacture any type of geosynthetic material. Two to three percent yellow clay nanoparticles have been added to make a formulation in order to manufacture polyester geotextiles. Table 1 shows the specifications of the two types of geotextiles in this study: one with nanoclay (the formulated geotextile (FGT) series) and one without (the GT series). The standard polyester geotextiles were used to compare the performance difference against those with the clay nanoparticle blending formulation.

Table 2 shows the properties of the nanoclay blended to the virgin polyester resin formulation from which it is known that the amount to be added is 2–3%.

Composition	Geotextile Type	Weight (g/m ²)	Clay Content (%)
Nanoclay-Formulated Nonwoven Geotextiles	FGT-1	272	2-3
	FGT-2	463	
	FGT-3	784	
	FGT-4	1514	
Traditional Nonwoven Geotextiles	GT-1	284	None
	GT-2	480	
	GT-3	756	
	GT-4	1546	

Table 1. Specifications of the two types of polyester geotextiles.

Component	Loss	SiO ₂	Al ₂ O ₃	Fe ₂ O ₃	TiO ₂	CaO	MgO	Na ₂ O	K ₂ O
Content (%)	97.54	1.80	0.07	0.11	0.13	0.01	0.01	0.02	0.01

Table 2. Components of the added yellow clay particles.

1.3.2. Testing protocols used to evaluate engineering performance

Tensile properties of nonwoven geotextiles were tested using ISO 10319 to minimize the deviation between index and performance tests. The modified EPA 9090 Test Method that was proposed by United States Environmental Protection Agency (EPA) was adapted to test the chemical resistance of the geotextiles. The chemical resistance of nonwoven geotextiles in waste leachate solution was evaluated by comparing the strength retention before/after immersion at 25°C, 50°C, 80°C, and for 180 days using ASTM (American Society for Testing and Materials) D 4632. AATCC (American Association of Textile Chemists and Colorists) 30 was used to estimate the biological resistance in the waste landfill leachate. Similar to chemical resistance, the biological resistance of nonwoven geotextiles was evaluated by comparing the strength retention before/after immersion. ASTM D4751-99a was used to compare the apparent opening size (AOS), and ASTM D1987-95(2002) was used to examine the permittivity of nonwoven geotextiles before/after immersion in the waste landfill leachate. (ASTM D 35 Committee, 2015) Finally, the adsorption efficiency was estimated to obtain the amounts of toxic and organic components that remained within the nonwoven geotextiles through inductively coupled analysis (ICP) analysis. An actual field leachate was used from the Woonjung-Dong waste landfill site in Gwangju, Korea (Rep.), where food wastes were mainly disposed of. It was seen that the pH value of the leachate solution indicated a weak-alkaline state and the presence of toxic components, for example, Cd and Pb, etc., and many kinds of organic components were included.

1.3.3. Tensile properties

Figure 8 shows the tensile strength of both the nanoclay-blended and traditional polyester nonwoven geotextiles. For the two types (i.e., FGTs and GTs), tensile strengths in both directions (machine direction (MD) and cross machine direction (CMD)) increased with weight but tensile strains decreased with weight. This is a very common trend in tensile properties of nonwoven geotextiles. (Jewell, R. A., 1996; Holtz, R. D. et al. 1995)

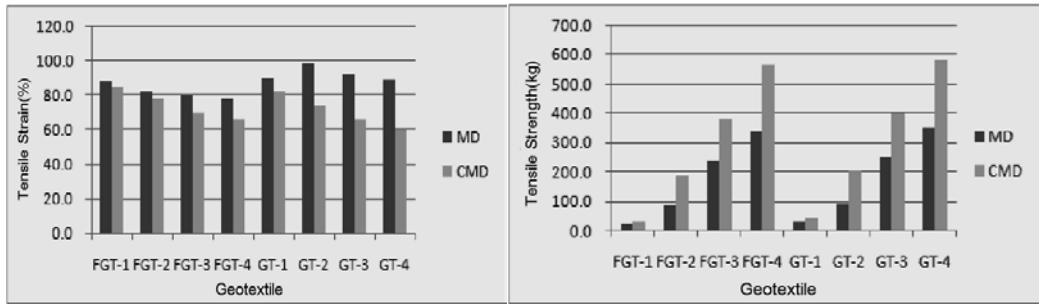


Figure 8. Tensile properties of nanoclay-blended and traditional polyester nonwoven geotextiles (where MD, CMD mean the machine and cross machine directions, respectively).

1.3.4. Effects of chemical and biological degradation

Figure 9 shows the tensile strength retention of both the nanoclay-blended and traditional polyester nonwoven geotextiles before/after immersion in the leachate solution. Tensile strength and strain retention of both types of polyester nonwoven geotextiles (FGTs and GTs) show the similar tensile property and decrease with temperature. These phenomena are shown very clearly at 80°C, and this result would be due to the hydrolysis effect of both polyesters under high temperature in the alkaline state. (Gugumus, F., 1996) In addition, the strength retention of polyester nonwoven geotextiles before/after leachate immersion state in the waste landfill site was examined. Figure 10 shows the tensile strength retention in order to explain the biological resistance.

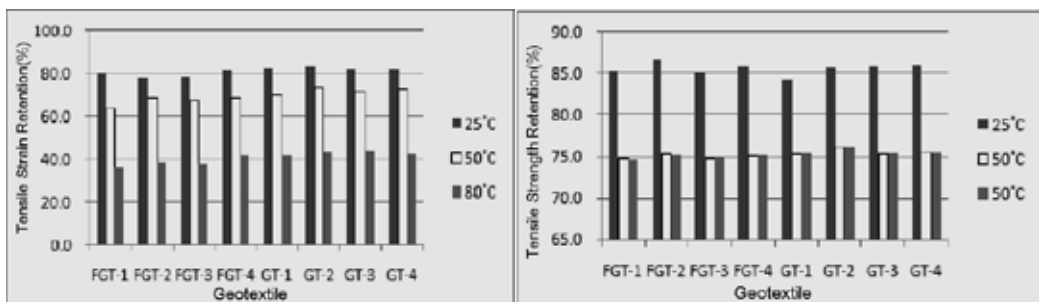


Figure 9. Chemical resistance by tensile property retention of nanoclay-blended and traditional polyester nonwoven geotextiles.

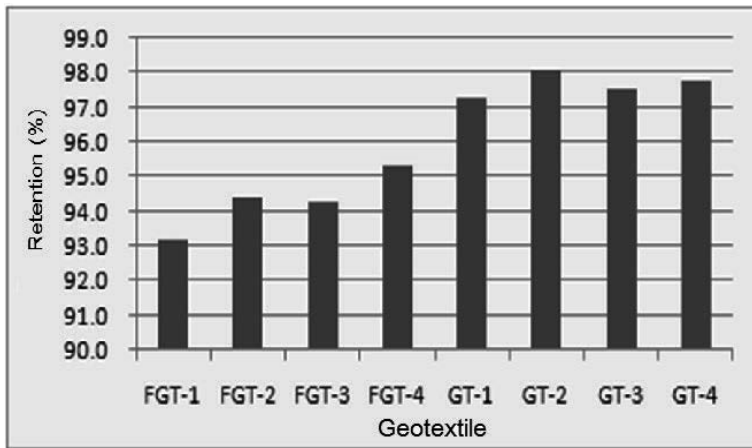


Figure 10. Biological resistance by tensile strength retention of nanoclay-blended and traditional polyester nonwoven geotextiles.

The nanoclay-blended polyester nonwoven geotextiles (i.e., the FGTs) show lower tensile strength retention than the traditional polyester nonwoven geotextiles (i.e., GTs). It is assumed that this means the FGTs were influenced by the components of the leachate solutions in a greater or less amount because of the nanoclay component. However, this does not mean that fungi and bacteria can attack these geotextiles. Figure 11 shows the values of cumulative reduction factors and the allowable tensile strengths of all of these nonwoven geotextiles.

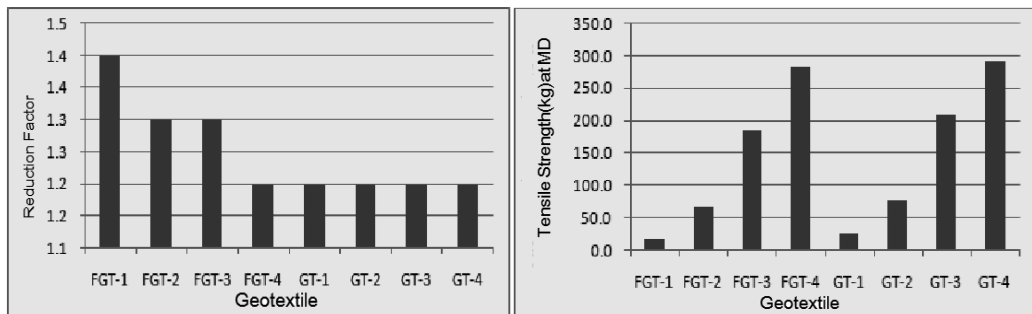


Figure 11. Allowable tensile strength of nanoclay-blended and traditional polyester nonwoven geotextiles.

1.3.5. Hydraulic properties due to clogging phenomena

Clogging means a channel blocking in the nonwoven geotextiles and this is an important cause of decreasing water permeability among soil particles. Usually, AOS does not decrease while clogging has not occurred in the nonwoven geotextiles. Figure 12 shows AOS values of polyester nonwoven geotextiles before/after immersion in the waste landfill site. The nanoclay-blended polyester nonwoven geotextiles (the FGTs) showed relatively small AOS values than

the traditional polyester nonwoven geotextiles, which indicates that a significant clogging was formed in the FGTs. Hence, toxic, organic, and floating components in the leachate solution could be simply adsorbed to the nanoclay-blended polyester nonwoven geotextiles.

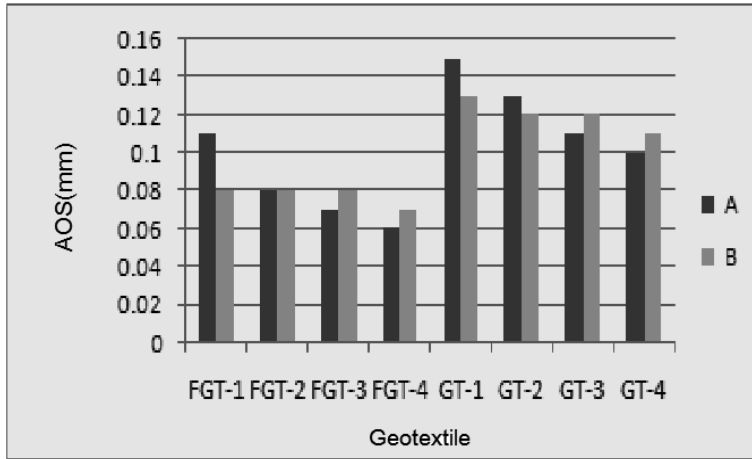


Figure 12. AOS of nanoclay-blended and traditional polyester nonwoven geotextiles before/after immersion (where A, B mean before and after immersion, respectively).

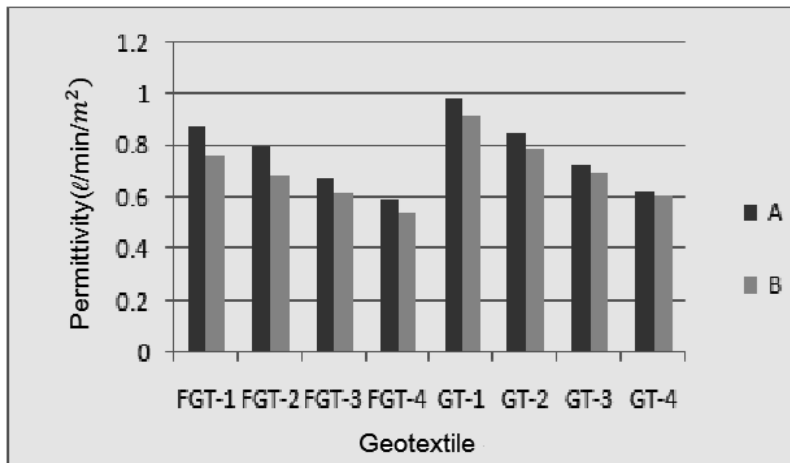


Figure 13. Permittivity of nanoclay-blended and traditional polyester nonwoven geotextiles before/after immersion (where A, B mean before and after immersion, respectively).

Figure 13 shows the permittivity of the polyester nonwoven geotextiles before/after leachate solution in the waste landfill site. As shown in the case of biological resistance, AOS, and permittivity, the FGTs showed smaller permittivity values than traditional polyester nonwoven geotextiles because of clogging effects of FGTs. Figure 14 shows strength retention of the

polyester nonwoven geotextiles before/after clogging and the same result was observed. The nanoclay-blended polyester nonwoven geotextiles (the FGTs) show smaller tensile strength retention than the traditional polyester nonwoven geotextiles (the GTs). Figure 15 shows the values of cumulative reduction factors and the allowable permittivity of all of these nonwoven geotextiles.

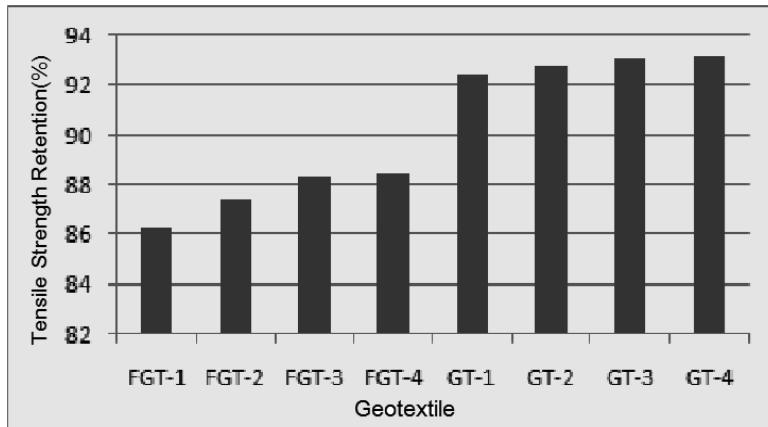


Figure 14. Tensile Strength retention of nanoclay-blended and traditional polyester nonwoven geotextiles after clogging.

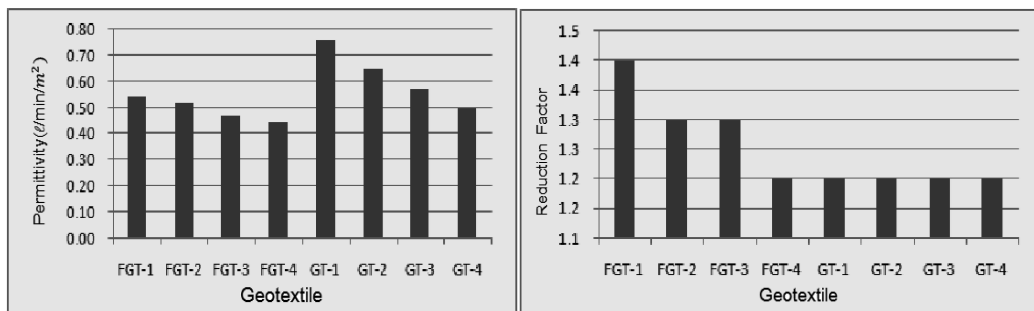


Figure 15. Allowable permittivity of nanoclay-blended and traditional polyester nonwoven geotextiles after clogging.

1.3.6. Adsorption efficiency

Figure 16 shows the adsorption efficiency of hazardous and heavy metal components of nanoclay-blended polyester nonwoven geotextiles. Here, FGTs showed excellent adsorption efficiency compared to the traditional polyester nonwoven geotextiles.

Finally, further study must be conducted to generate a detailed, clear, and quantitative adsorption effect with various nonwoven geotextiles, which have different fiber compositions.

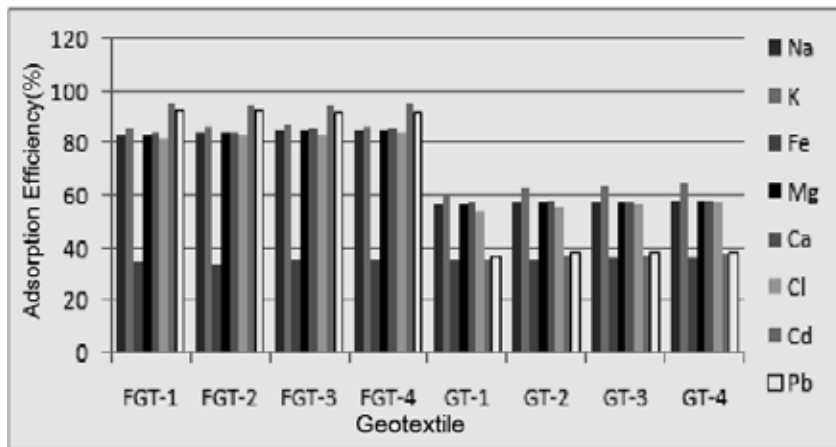


Figure 16. Component adsorption of nanoclay-blended and traditional polyester nonwoven geotextiles.

1.4. Future of nanotechnology applications in geoenvironmental engineering

The following was suggested by Dr. Ian D. Peggs in his article "The Future of Geosynthetics – One Opinion" regarding the manufacturing capabilities for use by the geosynthetics community: (Peggs, I. D., 2008)

- Nanoclays and nanofibers already exist for use in the geosynthetics technology
- Carbon and graphite are also related to geosynthetics in that they can be generated from polymers
- Geomembrane manufacturers have three-layer extruders and a few have five-layer extruders suited for the technology
- Multilayer-extruded barrier products are not new, so there exists a technology base
- Geogrids can be made stronger
- Geonets can be made less compressible
- Geocells can be made more rigid
- Stress cracking and oxidation resistances can be increased
- New materials will be involved in bringing new participants and new applications to the industry
- Five-layer geomembranes offer a better opportunity to customize colors (for example) for owners and for better awareness
- Color-coding can also be related to performance characteristics
- Color can be marketed – it was done successfully in HDPE gas pipe and PVC water pipe

- The technology presents an opportunity to make a significant step (not just a small one) toward more specialty products that will be accepted and utilized accordingly

1.5. Conclusion

Though the above list represents a suggestion and recommendation of a geosynthetic expert for nanotechnology geosynthetics in geoenvironmental engineering, it is very important to extend and set up this new application field for advanced geosynthetics. To develop the typical performance of regular geosynthetics, it is very natural and necessary to manufacture nanoparticle formulations and nanofiber geosynthetics as advanced materials and search/extend the new applications to the geoenvironmental engineering fields in the near future. (Jeon, H. - Y. *et al.*, 2008)

2. Modeling for hydraulic permeability improvement

2.1. Introduction

Geosynthetics as special functional materials have played very important roles in developing and improving the utilities of geotechnical, environmental, and transportation fields in recent times. Especially among them, woven and nonwoven geotextiles are widely used in 120 specific application areas as described earlier because of their various application functions, such as separation, reinforcement, filtration, drainage functions, etc. (Ingold, T. S., 1994) Needle-punched nonwoven geotextiles for subgrade reinforcement do not have a great difference in mechanical properties between machine and cross directions due to the randomly entangled structure of staple fibers at any directions. In addition, nonwoven geotextiles have excellent drainage and filtration functions and pass the liquid and retain the soil on the upstream side for civil and geotechnical applications. (Holtz, R. D. *et al.*, 1997; Van Zanten, R. V., 1986) Water permeability of nonwoven geotextiles is influenced by the entangled state of fibers, fiber composition, thickness, etc. For the case of fiber assemblies, such as nonwoven geotextiles, water permeability is influenced by the morphological structure of these in macroscopic viewpoints. In this study, laminar geotextile composites with different fiber-packing densities were made and the effects of laminar structures were examined on water permeability.

2.2. Theory of normal permeability on laminar geotextile composites

Nonwoven geotextiles are a kind of materials with high porosity and have the three-dimensional structure with different fiber orientations. It is assumed that the pore shapes of geotextiles are very narrow and tube typed, and therefore, the permeability of geotextiles depends on the pore-size distribution. The structural model of laminar geotextile composites is considered as an assembly of narrow tubes, which join each other with different fiber-packing densities. Figure 17 shows the two schematic diagrams of laminar geotextile composites and the assembly to have the different fiber-packing densities. From Darcy's law, water permeability of laminar geotextile systems could be written as follows:

$$\frac{Q}{A} = \frac{h}{\frac{T_1 \cdot K_2 + T_2 \cdot K_1}{K_1 \cdot K_2}} \tag{1}$$

where Q = quantity of flow, mm^3

A = cross-sectional area of geotextile, mm^2

h = head of water on the geotextile, mm

T = the thickness of geotextile, mm

K_1, K_2 = the coefficient of cross-plane permeability of upper- and lower-layer geotextiles, respectively, cm/sec

The coefficient of cross-plane permeability of laminar geotextile composites, K , could be calculated by:

$$K = \frac{T_1 + T_2}{\frac{T_1 \cdot K_2 + T_2 \cdot K_1}{K_1 \cdot K_2}} \tag{2}$$

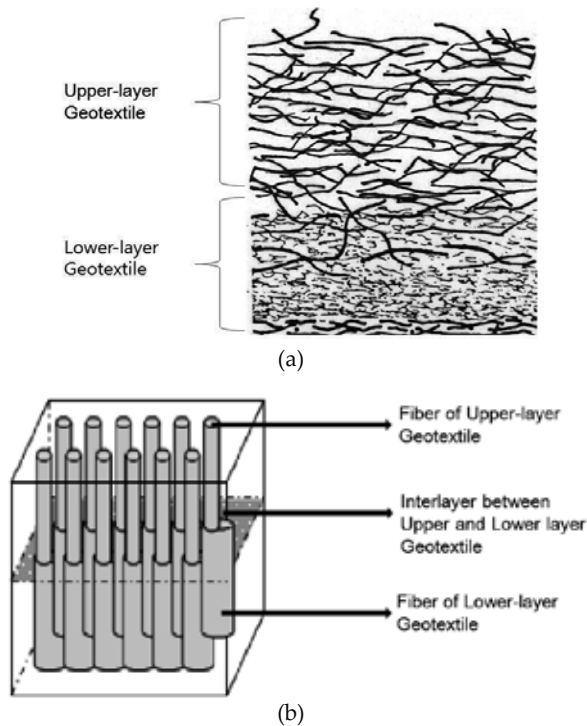


Figure 17. Schematic diagrams of (a) laminar geotextile composites and (b) structural model of tubes with different fiber-packing densities.

Permittivity, Ψ , could be written as

$$\frac{1}{\Psi} = \frac{\Psi_1 + \Psi_2}{\Psi_1 \cdot \Psi_2} \quad (3)$$

where Ψ_1, Ψ_2 = permittivity of the upper/the lower geotextile

If the loss rate of hydraulic pressure, f_i , is considered at the interface between geotextiles, permittivity, Ψ' , could be calculated as follows:

$$\frac{1}{\Psi'} = \frac{1}{\Psi_1} + \frac{1}{(1 - f_i) \cdot \Psi_2} \quad (4)$$

For convenience, equation (4) could be rewritten as:

$$f_i = 1 - \frac{1}{\Psi_2 \cdot \left(\frac{1}{\Psi'} - \frac{1}{\Psi_1} \right)} \quad (5)$$

2.3. Experimental

2.3.1. Sample preparation

To fabricate laminar geotextile composites, fiber-packing densities of geotextiles were discriminated respectively. Six types of fibers were used to manufacture the laminar geotextile composites. The characteristics of these specimens are shown in Table 3.

Specimens	Type of Yarn	Weight (g/m ²)	Thickness (mm)
A	Staple fiber	510	4.14
B	"	240	1.88
C	"	390	2.86
D	"	535	3.96
E	Slit-film yarn	700	1.15
F	"	220	0.68

Table 3. Characteristics of specimens for manufacturing laminar geotextile composites.

2.3.2. Manufacturing of laminar geotextile composites

Laminar geotextile composites having different fiber-packing densities were manufactured by needle-punching process. The fiber-packing densities of upper parts were smaller than those of lower parts, and specifications of six laminar geotextile composites are represented in Table 4.

Geotextile Composite	A-B	A-C	A/E	A-F	D/A	D/C
Thickness (mm)	6.02	7.00	5.29	4.82	8.10	6.82
Weight (g/m ²)	750	800	1,210	730	1,050	830

Table 4. Specifications of laminar geotextile composites.

2.3.3. Water permeability test

The hydraulic conductivity of laminar geotextile composites was determined in terms of permittivity under the constant head method and falling head method in accordance with ASTM D 4491 test method. The permeability coefficient was determined by multiplication of permittivity and thickness of geotextile. (Fluet Jr, J. E., 1985; ASTM D 35 Committee, 2015)

2.4. Results and discussion

2.4.1. Hydraulic permeability

Table 5 shows the values of permittivity and coefficients of cross-plane permeability for six laminar geotextile composites by the cross-plane permeability test and theoretical values obtained by equations (2) and (3). Figure 18 shows the inverse of permittivity and coefficients of cross-plane permeability. To interpret permeable phenomena, it is more convenient to determine the water permeability by using the permittivity than the coefficient of cross-plane permeability. Therefore, theoretical values of water permeability of laminar geotextile composites are larger than those of experimental values. It was considered that this was due to the effects of loss rate of hydraulic pressure as a result of changes of porous areas at the inner interface of geotextile composites.

Laminar Geotextile Composite	Permeability Coefficient (cm/sec)				Permittivity (sec ⁻¹)			
	Upper Layer	Lower Layer	Composite	Eq. (2)	Upper Layer	Lower Layer	Composite	Eq. (3)
A/B	4.951	2.364	3.576	3.757	1.173	1.258	0.578	0.607
A/C	4.441	2.125	2.828	3.039	1.086	0.743	0.411	0.441
A/E	4.914	0.023	0.096	0.105	1.193	0.020	0.018	0.020
E/A	0.023	4.914	0.091	0.106	0.020	1.193	0.017	0.020
A/F	5.033	0.029	0.185	0.199	1.193	0.042	0.038	0.041
D/A	3.487	3.956	3.513	3.712	0.881	0.956	0.434	0.458
D/C	4.427	2.042	2.812	2.972	1.118	0.714	0.412	0.436
C/D	2.042	4.427	2.860	2.972	0.714	1.118	0.419	0.436

Table 5. Permeability coefficient and permittivity of laminar geotextile composites.

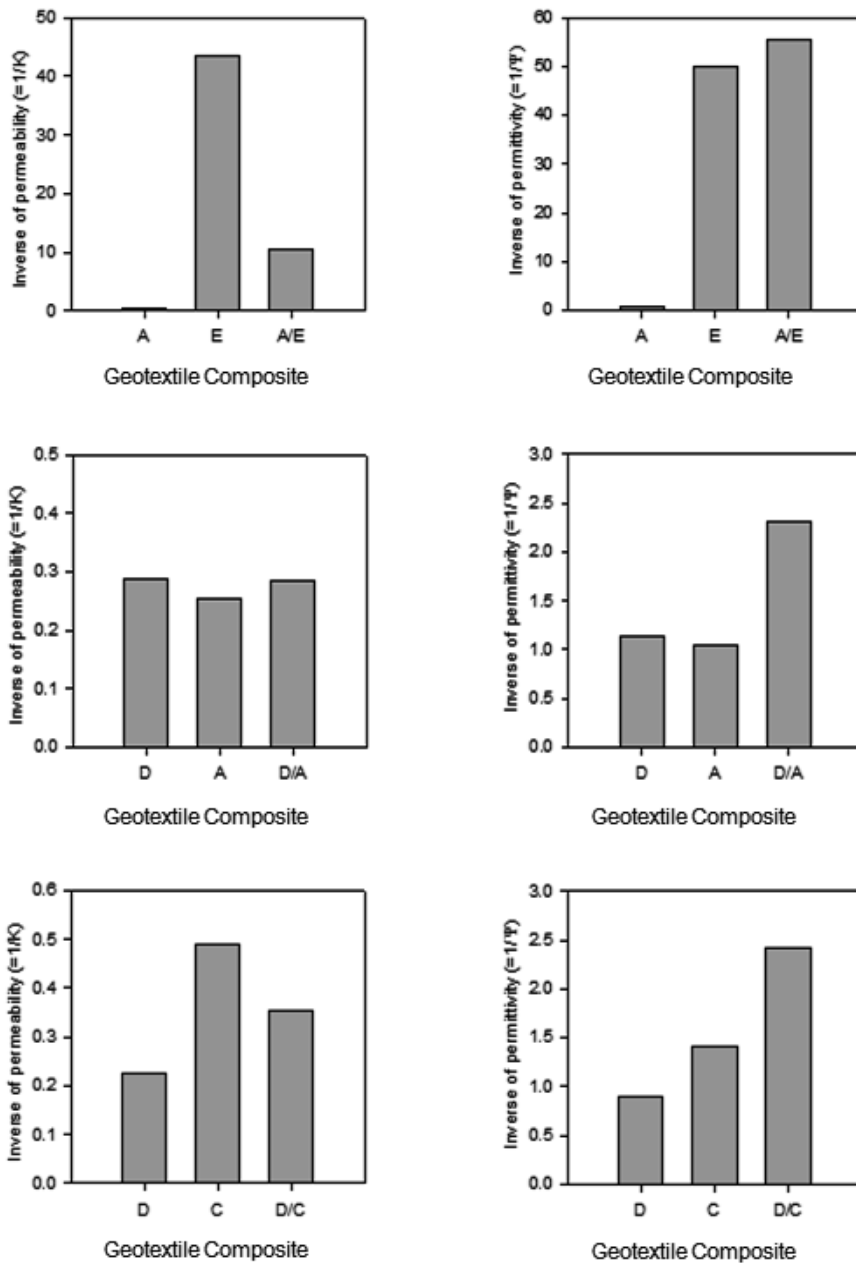


Figure 18. Inverse values of normal permeability and permittivity for several samples of nonwoven geotextiles.

2.4.2. Modeling by inlet forms

The inlet forms of inner interface of laminar geotextile composites to be related to the loss rate of hydraulic pressure are shown in Figure 19. In case of various porous areas of laminar

geotextile composites, the permittivity and loss rates of hydraulic pressure are represented in Table 6. The lower the coefficient values of cross-plane permeability and permittivity, the larger the loss rate of hydraulic pressure. This was why the inlet forms of inner interface of laminar geotextile composites were bell mouth or soft tube structures.

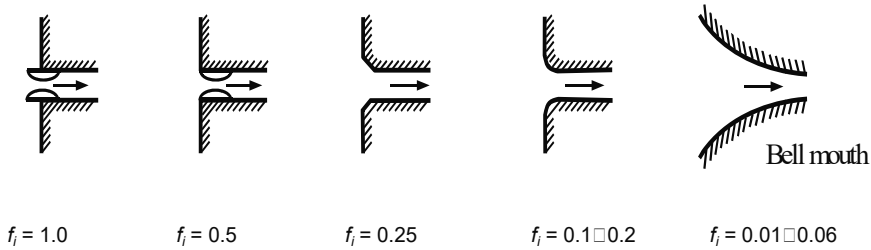


Figure 19. Inlet forms of inner interface of laminar geotextile composites.

Laminar Geotextile Composite		Permittivity (sec ⁻¹)		Loss Rate of Hydraulic Pressure (f _i)
Upper Layer	Lower Layer	Composite		
A-B	1.173	1.258	0.578	0.095
A-C	1.086	0.743	0.411	0.111
A-E	1.193	0.020	0.018	0.087
E-A	0.020	1.193	0.017	0.144
A-F	1.193	0.042	0.038	0.066
D-A	0.881	0.956	0.434	0.105
D-C	1.118	0.714	0.412	0.085
C-D	0.714	1.118	0.419	0.091

Table 6. Loss rate of hydraulic pressure of laminar geotextile composites.

2.5. Conclusion

For laminar geotextile composites having different fiber-packing densities, water permeability was decreased with the smaller fiber-packing densities and this was due to the more bulky and less compacted structure of fibers. It was reasonable to apply the permittivity to interpret the water permeability of laminar geotextile composites instead of the coefficient of cross-plane permeability. The experimental values of water permeability exhibited the smaller values than theoretical values due to the loss rate of hydraulic pressure and inlet forms of inner interface. From these results, it was known that the hybrid structure of geotextiles to perform the smart drainage function could be manufactured by the variation of the fiber-packing density.

Author details

Han-Yong Jeon*

Address all correspondence to: hyjeon@inha.ac.kr

Department of Applied Organic Materials Engineering, Inha University, Incheon, South Korea

References

- [1] Koerner, R. M. (2005), *Designing with Geosynthetics*, Fifth Edition, Pearson Prentice Hall, Inc., Upper Saddle River, New Jersey, USA, pp. 1-75.
- [2] Jewell, R. A. (1996), *Soil Reinforcement with Geotextiles*, Chapter 5, CIRLA Special Publication, Thomas Telford, Westminster, London. UK.
- [3] Gugumus, F. (1996), Thermooxidative degradation of polyolefins in the solid state: Part 1. Experimental kinetics of functional group formation, *Polymer Degradation and Stability*, 52, pp. 131-144.
- [4] Holtz, R. D. et al. (1995), *Geosynthetic Design and Construction Guidelines*, Publication No. FHWA HI-95-038, pp. 27-105.
- [5] Peggs, I. D. (2008), *The Future of Geosynthetics – One Opinion*, <http://www.geosynthetics.net>
- [6] Jeon, H. -Y. et al. (2008), *Evaluation of Clay Added Nonwovens as Filter in Waste Landfill, Molecular Crystals and Liquid Crystals*, 484, pp. 185-194.
- [7] Ingold, T. S. (1994). *The Geotextiles and Geomembranes Manual*, First Edition, Elsevier Advanced Technology, Oxford, pp. 299-474.
- [8] Holtz, R. D. et al. (1997). *Geosynthetic Engineering*, BiTech Publishers Ltd., British Columbia, pp. 29-68.
- [9] Van Zanten, R. V. (1986). *Geotextiles and Geomembranes in Civil Engineering*, John Wiley & Sons, New York, pp. 9-36.
- [10] Fluet Jr, J. E. (1985). *Geotextile Testing and the Design Engineer*, ASTM Committee D-35, Philadelphia, pp. 7-56.
- [11] ASTM D 35 Committee (2015). *ASTM Standards on Geosynthetics*, ASTM International, West Conshohocken, PA, USA.

Edited by Han-Yong Jeon

Non-woven Fabrics is differentiated text which covers overall stream from raw fibers to final products and includes features of manufacturing and finish process with specialized application end use. Application range of non-woven fabrics is extended to all the industrial fields needless to say apparel, such as ICT (information and communication technology), bio- and medicals, automobiles, architectures, construction and environmental. Every chapter is related to the important and convergent fields with the technical application purpose from downstream to upstream fields. Also, applicability of non-woven fabrics is introduced to be based on the structural analysis of dimensional concept and various non-woven fabrics as a state-of-art embedded convergent material are emphasized in all industry fields by using nanofibers and carbon fibers.

Photo by sss615 / DollarPhotoClub

IntechOpen

